12-1-2012

Studies on spreading depolarization in healthy and metabolically compromised brain tissues

Isamu Aiba

Isamu Aiba
Candidate

Department of Neurosciences
Department

This dissertation is approved, and it is acceptable in quality and form for publication:

Approved by the Dissertation Committee:

C. William Shuttleworth , Chairperson

Tom Resta

Donald Partridge

Fernando Varenzuela

STUDIES ON SPREADING DEPOLARIZATION IN HEALTHY

AND METABOLICALLY COMPROMISED BRAIN TISSUES

by

ISAMU AIBA

DISSERTATION

Submitted in Partial Fulfillment of the
Requirements for the Degree of

Ph.D. in Biomedical Sciences

The University of New Mexico
Albuquerque, New Mexico

December 2012

Studies on Spreading Depolarization in Healthy and Metabolically Compromised Brain Tissues

By

Isamu Aiba

B.S., Biochemistry, Hiroshima University, 2003

M.S., Biochemistry, Hiroshima University, 2005

Ph.D., Biomedical Sciences, University of New Mexico, 2012

Abstract

Spreading depolarization (SD) is a slowly propagating wave of depolarization of neurons and glia. Since its original discovery in 1944, SD has been observed in various experimental settings, both *in vitro* and *in vivo*. SD has recently been detected in brains of human patients with various injuries, and a contribution of SD to deleterious consequences of acute brain injury is increasingly accepted.

The present dissertation work focus mainly on the characterization of SD and cellular events associated with it. Main interests of these studies are on underlying mechanisms that convert non-injurious factors into mediators of acute neuronal injury.

One of the major findings is an important role of NMDA-type glutamate receptors (NMDAR) in the injurious consequences of SD. Prior to my work, contributions of NMDARs to the initiation and propagation of SD were well acknowledged, however there was little evidence regarding NMDAR contributions to injurious consequences of SD. My studies have identified a brief period of sustained glutamate release and concomitant NMDAR activation following the onset of SD, and demonstrate a significant contribution of this excitatory phase to neuronal injury in the setting of metabolic compromise. Selective block of this later excitatory phase was sufficient to prevent Ca^{2+} deregulation and membrane damage in metabolically compromised tissue. These glutamate-dependent injury processes suggest a novel link between SD and previous studies of acute excitotoxic neuronal injury.

Another important focus of the present dissertation is Zn^{2+} physiology and its contribution to SD. In the mammalian brain, Zn^{2+} is enriched in synaptic vesicles of many glutamergic neurons and is released as a neuromodulator. Importantly Zn^{2+} is well known as a potent antagonist of NMDARs. Based on the significant contribution of NMDAR activation to SDs, Zn^{2+} could potentially play a protective role in brain injury by reducing the number of SD occurring in the injured brain. However Zn^{2+} is also often considered as a neurotoxic factor. In

fact, it is suggested that synaptically released Zn^{2+} can translocate in postsynaptic neurons and contribute to neuronal death. My studies have evaluated roles of synaptic Zn^{2+} release in regulation of SD as well as the contribution to potentially toxic intracellular Zn^{2+} accumulation as a consequence of transmembrane Zn^{2+} flux.

My studies revealed that extracellular actions of Zn^{2+} indeed inhibit SD initiation and propagation in healthy tissue. However the inhibitory effects of Zn^{2+} were highly sensitive to oxygen concentration, such that in severe hypoxia or anoxic conditions, Zn^{2+} antagonisms of NMDARs and SD were profoundly reduced. Studies on potential mechanism revealed that this was partly due to redox potential shit and resultant modification of the receptors. Interestingly, such redox modulation mechanism could partly contribute to ineffectiveness of other NMDAR antagonists. Thus loss of oxygen supply in metabolic compromised tissue could be important modulator of the effects of Zn^{2+} on SD.

Another line of study examined potential use of intracellular dialysis for detection of Zn^{2+} influx to postsynaptic neurons. One of the confounds for studying intracellular Zn^{2+} responses was how to distinguish contributions from transmembrane Zn^{2+} influx and Zn^{2+} release from intracellular sites. A Key finding of this part of studies is that intracellular dialysis significantly disrupt intracellular Zn^{2+} homeostasis mechanisms and enabled to selective detect transmembrane Zn^{2+} influx over intracellular Zn^{2+} release. Development of the new detection method significantly improved understanding of intracellular Zn^{2+} signal sources in SD and related events.

In summary, these studies show that the metabolic state of tissue can significantly influence regulation of NMDAR activation and synaptic Zn^{2+} release. These findings should be of value for developing novel interventions to minimize the deleterious consequences of SD in acute brain injury.

Table of Contents

1. Introduction

Brain information is carried by depolarization and hyperpolarization of single neurons and intercellular communication via chemical synapses. These processes involve tightly regulated ion fluxes across the plasma membrane. The continuous maintenance of transmembrane ionic gradients throughout the network of ~100 billion neurons in the brain (Azevedo et al., 2009) demand a very large amount of energy. The energy demand is particularly pronounced in the human. It was estimated that adult human brain accounts for ~20-25% of total resting metabolic rate, significantly higher than other primates (8-10%), and far higher than in non-primate mammals (3-5%) (Leonard et al., 2007). The high energy demand makes the brain significantly vulnerability to injury following loss of cerebral blood flow. In a study published in 1943, occlusion of the cerebral blood supply in human subjects (using a cervical pressure cuff) resulted in fixation of eye movement within 5-6 seconds, followed by immediate loss of consciousness (Rossen et al., 1943). Further prolongation of ischemia is critical for viability of neurons, and even 4-10 minutes losses of cardiac function has been reported to cause irrecoverable loss of brain activity (Grenell, 1946; Cole and Corday, 1956).

The high vulnerability of brain tissue to ischemia results in very short time-windows for reperfusion therapy of ischemic stroke patients. Currently the only available pharmacological intervention for thrombotic stroke is thrombolysis with tPA, but the time-window of the treatment is only within 3-4 hours after stroke

onset (Hacke et al., 2004). In a large scale study, it was shown that only 23.5% (88/374) patients could arrive at the hospital within 3 hours and only 4.3% (16/374) of them could receive thrombolytic treatment (CASPR Investigators, 2005). There are some successful clinical studies showing a small extension of successful treatment time-windows (up to 4.5 hours) and improve diagnosis methods (e.g. mobile stroke unit) that could also increase the numbers of patients receiving tPA therapy (e.g. Stemer and Lyden, 2010; Walter et al., 2012). However, the treatment window is still very short and most ongoing research is focused on the later deleterious events.

Following the initial onset of acute brain injury, a slow progressive enlargement of infarction or development of neurological deficits often occurs for days (Dirnagl et al., 1999). Such delayed aggravation of brain injury is often called “secondary injury”. The incidence of secondary injury is not restricted to ischemic stroke, but also occurs in other acute brain injuries such as intracranial hemorrhage and brain trauma (Aronowski and Zhao, 2011; Haddad and Arabi, 2012). Because of difficulties in treatment of initial acute injuries, prevention of secondary injury has been actively studied, because of the much longer time window for potential intervention. While multiple mechanisms underlying the secondary injury have been proposed (Dirnagl et al., 1999), currently no effective pharmacological intervention is available. Development of effective therapeutics would undoubtedly be of benefit to a large number of patients. The present dissertation work has studied exclusively the mechanisms underlying the delayed

injury process, with a main focus on the events termed “spreading depolarization” (SD).

1.1 Spreading depolarization

1.1.1 SD initiation and propagation

SD is a propagating wave of near complete depolarization of a volume of tissue, including both neurons and glia. SD is generally initiated by a harsh stimulation (e.g. potassium, ischemia) that severely depolarizes local brain tissue and rapidly depletes intracellular ATP. This initiating depolarization results in loss of transmembrane ionic gradients, significant cellular swelling, continuous potassium efflux and release of neurotransmitters including glutamate (Somjen, 2001). Together with release of these mediators, concomitant shrinkage of the extracellular space steeply elevates local glutamate and potassium concentrations. Extracellular accumulation and diffusion of these excitatory solutes trigger severe depolarization of neurons and glia in the surrounding tissue, resulting in a feed-forward depolarization that slowly spreads across brain tissue at a rate of 2-5 mm/min (Somjen, 2001).

Both potassium and glutamate can contribute to feed-forward depolarization, however their relative contributions vary significantly depending on the specific SD model tested. Thus when SD is generated by severe hypoxia or oxygen glucose deprivation, potassium appears to play a predominant role in maintaining propagation throughout tissues. This potassium-dependent model

was originally proposed by Grafstein (Grafstein, 1956). Based on her model, a ramp increase of local potassium ion concentration occurs at the wavefront of SD and is alone sufficient to mediate feed-forward depolarization. Consistent with this hypothesis, a brief excitatory period has been observed to precede the large depolarization of SD (termed prodromal excitation, Herreras et al., 1994; Larrosa et al., 2006). Such prodromal discharge may contribute to the ramp potassium elevation observed ahead of SD propagation. However, potassium elevations do not appear to be absolutely required for all forms of SD, as prodromal K^+ elevations have not been observed in some forms of SD (such as SD generated with local KCl injection).

An alternative, glutamate-dependent SD propagation model was proposed by van Harreveld (Van Harreveld, 1959). In his model, glutamate (or a related excitatory neurotransmitter) is proposed as the critical component of SD propagation. During SD, extracellular glutamate concentration is generally elevated to ~30-100 μM (Fabricius et al., 1993; Iijima et al., 1998; Rossi et al., 2007) and most subtypes of ionotropic glutamate receptors are expected to be activated. Virtually all of the ionotropic glutamate receptors in the brain are non-selective cation channels and receptor activation at the severely depolarized membrane potential leads to potassium efflux (Yu et al., 1999). Thus glutamate receptor activation can contribute to elevated local potassium concentrations, thereby depolarizing non-neuronal cells and priming feed-forward depolarization. The specific sources of glutamate accumulation can be variable depending on the model used to generate SD. Thus release from presynaptic terminals may

contribute to most of SD, while glutamate release from astrocytes via volume-sensitive anion channels significantly contributes to glutamate accumulation in the SD generated by the Na^+/K^+ ATPase inhibitor ouabain (Basarsky et al., 1999). Under conditions of extreme severe metabolic stress, glutamate can accumulate due to the reverse action of glutamate transporters (Rossi et al., 2000). The indispensable role of glutamate receptor activation in some form of SD initiation/propagation has been supported by full block of SD with glutamate receptor antagonists (discussed below, section 1.3.3).

However, similar to the potassium hypothesis, the glutamate hypothesis is not always valid, as some forms of SD are insensitive to glutamate receptor antagonists. Thus currently the most widely-accepted model is a dual hypothesis which states both glutamate and potassium contribute to SD, but the relative contribution can vary significantly between forms of SD (Somjen, 2001). While mechanisms determining the relative contributions of glutamate and potassium are not clearly established, regulation of extracellular solute concentrations should be an important determinant. As will be discussed below (section 1.3) , SD is a significant contributor to some forms of brain injury, and thus understanding propagation mechanisms of SD should be important for development of pharmacological interventions, for a range of conditions.

1.1.2 Terminology of spreading depolarization

A famous consequence of spreading depolarization was originally described by Leao in 1944 as “spreading depression”, a propagation of

suppression of local brain activity. However spreading depression of brain activity is only one of the important consequences of spreading depolarization. In fact, spreading depolarization triggers multiple consequences, and multiple "spreading" events have been described (e.g. spreading ischemia, spreading hyperemia, spreading convultions)(Dreier, 2011). In order to clarify the underlying mechanisms, a suggestion was made to use "spreading depolarization (hereafter SD)" to specifically describe depolarization events (Dreier, 2011), and the present study follows the suggestion. However the use of SD is sometimes confusing especially when discussing mechanisms of SD. This is due to the fact that SD has been studied by multiple groups, generated by different stimuli in different recording conditions and in different brain tissues. In order to make this introduction most relevant to my dissertation studies, most of reference studies cited in this introduction are limited to SD recorded in similar experimental system and preparations used in the present studies, otherwise difference will be appropriately explained. Terms such as anoxic depolarization (AD) and periinfarct depolarization (PID) also describe specific spreading depolarization events, but will be used to emphasize their contributions to brain injury.

1.1.3 Ionic deregulation and tissue swelling during SD

The large ion fluxes associated with SD result in modulation of extracellular ionic concentrations and cause large shifts in extracellular field potential (Martins-Ferreira et al., 2000). The wavefront of SD is thus electrically

detected as a steep extracellular DC potential shift. This sharp potential shift coincides with a steep drop in the extracellular sodium concentration (to ~55 mM) and increase in extracellular potassium concentration (~30 mM). Ca^{2+} concentration also severely decreased to 10% of basal level. Given that the extracellular space occupies only ~20% of total brain volume at rest (Sykova and Nicholson, 2008), local transmembrane ionic gradients are severely destroyed. During SD generated in brain slice, severe neuronal depolarization continues for ~1 minute. Brain tissue is surprisingly effective at restoring these ionic gradients and neurons promptly repolarize in the presence of sufficient energy supplies. Restoration of ionic deregulation is mediated mainly by activities of ATP dependent pumps (e.g. Na^+/K^+ ATPase, Ca^{2+}-ATPase)(Somjen, 2001). Intracellular Na^+ and Ca^{2+} loads serve as a trigger for mitochondrial biogenesis and the tissue oxygen consumption rate increases (Galeffi et al., 2011). In fact, tissue oxygen concentration declines steeply for ~10 minutes after SD in brain slice (Galeffi et al., 2011) and *in vivo* (Takano et al., 2007).

The massive fluxes and tissue swelling make SD easily detectable. However these same features also provide technical challenges for mechanistic studies. For example, tissue swelling is a significant problem for imaging study because the volume changes associated with SD significantly modulate the transparency and reflectance of brain tissue, and influence interpretation of fluorescence responses. The tissue volume changes also make it challenging to obtain stable single-cell electrophysiological recordings during SD. Finally, large changes in extracellular potential require correction of membrane potential during

SD, and make it difficult to accurately measure absolute potential changes associated with SD. In fact many recent SD studies use extracellular recording or computer modeling, rather than single cell recordings, for SD characterization. However most of cation fluxes can be masked in extracellular recordings during SD because of the near complete depolarization during SD. In order to characterize conductance changes associated with SD, voltage clamp recording is required. There have been very few voltage-clamp recordings of SD (Czeh et al., 1993; Zhou et al., 2010a), and these studies have only characterized the large current during SD and have not characterized synaptic activity change associated with these events. Fine electrophysiological recordings of SD may enable detailed characterization of events ongoing during SD, and provide new insights into mechanisms involved in injury following SD in metabolically compromised tissues.

1.2 SD and brain injury

1.2.1 Hypothetical mechanism for SD induced injury

As described above, the large ionic deregulation during SD impose a significant metabolic burden to the neurons. However SD generated in healthy tissue is normally a non-injurious event. In brain slice studies, this can be attributed to the presence of a continuous supply of high concentrations of oxygen and glucose. When SD is generated *in vivo*, the large energy demand is compensated for by massive recruitment of blood flow to the depolarized brain tissue (i.e. spreading hyperemia) (Dreier, 2011). The hyperemia is chiefly

mediated by dilation of arterioles and passive dilation of capillaries (Fernandez-Klett et al., 2010). Although the signaling pathway(s) responsible for functional hyperemia during SD is not well established, contributions of NO generated in parenchyma, acetyl-choline release from parasympathetic nerves, and calcitonin gene-related peptide release from trigeminal nerves have been demonstrated during SD (Busija et al., 2008). Such hyperemia could facilitate restoration of ionic homeostasis by providing energy substrates as well as increasing clearance rates of extracellular solutes. These observations suggest that failure to recruit blood flow during SD could lead to injurious consequences in ischemic injury.

The significance of SD to brain injury in ischemic stroke models has been consistently reported. SD generated *in vivo* by global ischemia without reperfusion, or *in vitro* by oxygen glucose deprivation can immediately cause irrecoverable damage to brain tissue (Jarvis et al., 2001; Takano et al., 2007). Such depolarization is often termed anoxic depolarization (AD) and this is likely an underlying mechanism for irrecoverable brain damage formed during initial injury. In a focal ischemia model *in vivo*, AD also occurs after focal ischemia and creates ischemic core. Neurons in the tissue surrounding ischemic core are continuously experiencing severe metabolic stress, but still maintain their membrane potential based on the collateral blood supply from vessels in healthy brain tissue. These vulnerable tissues are often termed penumbra tissue and considered to be a volume of tissue that undergoes progressive degeneration. Studies have revealed that SD can propagate in penumbral tissues and contribute to secondary injury. SD propagating within penumbral tissue is usually

termed peri-infarct depolarization (PID). Recurrent PIDs were observed days after stroke onset and the incidence significantly contributed to delayed infarct enlargement in rodents (Gill et al., 1992; Iijima et al., 1992; Nedergaard and Hansen, 1993; Hartings et al., 2003), cats (Ohta et al., 2001) and non-human primates (Strong et al., 2000). Pharmacological studies confirmed significant contribution of PID to infarct enlargement as intervention of PID correlatively decreased numbers of PID and infarct size (Gill et al., 1992; Hartings et al., 2003; Lu et al., 2005). While PIDs can occur in recurrent form, recent imaging studies revealed that some PID clusters can be explained by multiple detection of single PID circulating around the ischemic core (Nakamura et al., 2010). These PIDs selectively depolarize hypoperfused brain tissue (penumbra) that surrounds the ischemic core and produce large metabolic burdens to the already compromised tissue. It appears very likely that such a repetitive metabolic challenge contributes to irrecoverable brain damage.

While it is widely assumed that SD generated in metabolically compromised tissue sets up an additional metabolic burden that contributes to neuronal damage, very little is known at cellular level about how energy-depleted neurons are damaged following SD. Duration of extracellular potential shift during SD is generally prolonged in metabolically compromised tissue and correlated with poor outcomes (Takano et al., 2007; Oliveira-Ferreira et al., 2010; Hartings et al., 2011b). This suggests that events during the late-SD phase may contribute to brain injury. Identification of cellular mechanisms of SD dependent

neuronal injury may help in the development of approaches to save neurons at risk of injury following SD in compromised tissues.

1.2.2 SD in human patients

The significance of SD in human brain injury had not been well appreciated by clinical researchers until a recent series of studies, which convincingly demonstrated SD in human patients (Strong et al., 2002; Fabricius et al., 2006; Dohmen et al., 2008; Dreier et al., 2009; Bosche et al., 2010; Hartings et al., 2011c; Hartings et al., 2011b; Dreier et al., 2012; Drenckhahn et al., 2012; Hertle et al., 2012a; Woitzik et al., 2012). In 2008, the COSBID (Cooperative Studies of Brain Injury Depolarization) group first recorded cortical activity in human stroke patients with electrode strips placed directly on the cortical surface (electro-corticography; ECoG) (Dohmen et al., 2008). This study detected SD in virtually all stroke patients. SD was detected days after stroke onset. In some patients SD triggered irrecoverable loss of local brain activity and radiographic evidence of infarct growth, strongly suggesting that SD can contribute to secondary injury in human stroke patients. Subsequently, large numbers of clinical recordings made with similar approaches have detected SD in multiple brain pathology (e.g. subarachnoid hemorrhage, brain trauma). A recent prospective study confirmed that the incidence of SD was a significant risk factor that predicted outcomes in patients with head trauma (Hartings et al., 2011c). Based on the incidence of SD during days after initial treatments in the

ICU, it has now been suggested that SD is an important target to prevent progression of injury (Strong et al., 2007; Lauritzen et al., 2011).

An additional noteworthy finding from these recent clinical studies is the confirmation of the significance of earlier findings from preclinical studies of SD in small animals. For example seizure-like excitatory phases associated with SD seen in brain slice *in vitro* and rodent brain *in vivo* (Van Harreveld and Stamm, 1953; Hablitz and Heinemann, 1989) were recently detected in human patients (Dreier et al., 2012). In addition, SD-induced ischemia (spreading ischemia Dreier et al., 1998), which once was considered to be an artifact of harsh stimuli in animal studies, has been observed in patients with subarachnoid hemorrhage (SAH) and is now considered to be a significant contributor to the onset of delayed ischemic neurological deficit (DIND) (Dreier et al., 2009; Strong and Macdonald, 2012). Thus these clinical observations validate the potential utility of data obtained from small animals (e.g. rabbits, rodents) for understanding important aspects of SD and subsequent injury in human subjects.

1.2.3 Sensitivity of SD to NMDAR antagonists

Based on its significant contribution to brain injury, there has been long standing interest in the pharmacological intervention of initiation and propagation of SD. Currently the most studied pharmacological compounds to inhibit SD are antagonists of NMDA-type glutamate receptors (NMDAR).

The efficacy of NMDA antagonists to inhibit initiation and propagation of SD are variable depending on the model used. It has been consistently shown

that SD generated in healthy tissue is effectively prevented by NMADR antagonists both *in vitro* and *in vivo* (Anderson and Andrew, 2002; Faria and Mody, 2004; Peeters et al., 2007).

In contrast, the efficacy of NMDAR antagonists to prevent SD induced in stroke models is variable and likely sensitive to local tissue metabolism. SD (or AD) generated by either global ischemia or oxygen glucose deprivation (OGD) is highly resistant to NMDAR antagonists (e.g. Jarvis et al., 2001; Murphy et al., 2008). Thus initial SD events that contribute to formation of initial ischemic core do not appear to require NMDAR activity for propagation (Jarvis et al., 2001; Murphy et al., 2008). In contrast to these initial events, subsequent PIDs occurring days after stroke onset seems to have a higher sensitivity to NMDAR antagonist. Thus NMDAR antagonists significantly decreased the incidence of PIDs generated following focal ischemia and reduced infarct volumes (Gill et al., 1992; Ohta et al., 2001; Hartings et al., 2003). While PIDs were not recorded, a number of studies also reported that NMDAR antagonists significantly reduced the infarct volume following focal stroke (Takamatsu et al., 1998; Li et al., 2004; Woitzik and Schilling, 2007; Eikermann-Haerter et al., 2012). Because PIDs appear to contribute to delayed injury formation, NMDAR antagonist may be useful for limiting PIDs that contribute to progressive infarct enlargement. The mechanisms underlying differential NMDAR antagonist sensitivity of SD events involved in ischemic infarct development are not well understood. One potential explanation is a differential capacity of ischemic tissues to clear extracellular potassium. In severe ischemia, mechanisms required to decrease extracellular

potassium can be impaired (e.g. by loss of clearance by local blood flow, or due to astrocyte depolarization). Under such conditions, tissue depolarization during SD could readily elevate extracellular potassium concentrations ahead of the propagating wave, allowing SD propagation without NMDAR activation. However because of profound changes in the extracellular environment during ischemia, it is also possible that other factors related to differences in extracellular redox potential and modification of NMDAR sensitivity could also contribute.

Recently, there has been a growing interest in utilizing NMDAR antagonists for clinical intervention for SD. The most widely studied antagonist is ketamine, because this is already used as a sedative for human patients (Sinner and Graf, 2008). A preliminary clinical report has shown a reduced number of SDs with ketamine administration (Sakowitz et al., 2009), and a retrospective clinical study has also demonstrated a significant reduction of SD incidence by ketamine (Hertle et al., 2012a). These preliminary clinical studies support the potential usefulness of NMDAR antagonist for preventing SD in human patients.

1.3 Roles of NMDAR in SD

1.3.1 NMDA-type glutamate receptor

As noted above (section 1.2.1) extracellular glutamate concentration reach ~30-100 μM during SD (Fabricius et al., 1993; Iijima et al., 1998; Rossi et al., 2007) and most glutamate receptors are expected to be in an activated state. Three classes of ionotropic glutamate receptors, (AMPA, kainate and NMDA) are

expressed in the brain. Among these three receptor types, the NMDAR has unique biophysical properties suitable for mediating charge transfer during SD.

The NMDAR is ubiquitously expressed in the mammalian brain and its activity is involved in multiple brain functions. NMDARs are formed as tetramers of GluN subunits. A pair of GluN1 subunits is mandatory for channel formation and formation of the coagonist (D-serine, glycine) binding sites. Most NMDARs contain an additional two GluN2 (A-D) subunits to form a functional tetramer. GluN3A/B subunits can also contribute to formation of functional NMDAR tetramers with significantly reduced open probability and less Ca^{2+} permeability when expressed as GluN1/2/3 heterotetramers (Ciabarra et al., 1995). GluN3 subunits can also form excitatory glycine receptors as GluN1/GluN3 tetramers (Chatterton et al., 2002). However the physiological relevance of GluN3 containing NMDA receptor in adult brain is not well established (Pachernegg et al., 2012) and will not be further discussed. GluN2 subunit composition significantly alters the kinetics of NMDAR currents. GluN2A containing receptors have higher open probabilities than GluN2B-containing receptors, whereas GluN2B containing receptors usually show slower currents than GluN2A-containing receptors (Erreger et al., 2005). Such different kinetics predicted stimulation-dependent activation of different GluN2 containing receptors. Thus low frequency stimulation preferentially activates GluN2B containing receptors, whereas high frequency stimulation evokes more GluN2A- containing NMDAR current.

The biophysical properties of NMDARs are unique when compared with other glutamate receptors. The NMDAR has an extraordinarily large charge transfer capacity compared with other glutamate receptors. One study reported that, in single nucleated (out-side-out) patches obtained from dendrites of CA1 pyramidal neurons, NMDAR currents showed >40 pS unitary conductance with a ~3 sec total deactivation time constant. In contrast, AMPA currents in the same preparation had ~10 pS unitary conductance with ~10 ms deactivation kinetics (Spruston et al., 1995). The fast kinetics of non-NMDAR glutamate receptors are partly due to the presence of auxiliary subunits. For example, AMPAR requires transmembrane AMPA receptor regulatory proteins (TARPs) for surface expression and antagonist sensitivity (Nicoll et al., 2006; Maclean and Bowie, 2011), and kainate receptor interaction with Neto1 is also important for shaping kinetics of kainate receptor currents (Straub et al., 2011). It is not yet known whether similar auxiliary subunits are present for NMDARs.

While the NMDAR has extremely slow deactivation kinetics and large conductance, NMDAR current is limited by endogenous inhibitors. In fact, gating of NMDARs is strongly inhibited by cations such as Mg^{2+}, Zn^{2+} and H^{+}, which may important for compensating for the slow channel desensitization. Among endogenous inhibitors, voltage dependent channel block by Mg^{2+} is highly effective and almost completely eliminates NMDAR current at resting membrane potentials. When neurons are severely depolarized, voltage sensitive ion channels are rapidly inactivated. In contrast severe depolarization relieves Mg^{2+}

block and rather potentiate NMDAR current. Thus during the severe depolarization of SD, NMDAR is suitable for generating ionic deregulation.

Another important property of NMDARs is their high permeability for Ca^{2+}, compared with very poor Ca^{2+} permeability in the most of other glutamate receptors expressed in adult (while some AMPA/kainate receptors exhibit considerable Ca^{2+} permeability (Liu and Zukin, 2007; Perrais et al., 2010)). However the importance of Ca^{2+} permeability of NMDAR to SD propagation is not well defined. While Ca^{2+} influx is critical for propagation some SD, such a Ca^{2+} requirement seems to be due to essential role of P/Q type calcium channels in transmitter release during some SD. In fact, inhibition of P/Q channels can prevent generation of some forms of SD (Kunkler and Kraig, 2004), and a mutation in P/Q type channel gene (Cav2.1) that enhances channel function resulted in higher susceptibility to SD (Tottene et al., 2009). As will be discussed later, the Ca^{2+} permeability of NMDAR is often discussed in the context of intracellular signaling in excitotoxicity (see section). SD involves profound Ca^{2+} deregulation which invades proximal dendrites to soma (Dietz et al., 2008). However it was not determined whether NMDAR activation contributes to the Ca^{2+} deregulation and neuronal injury during SD.

1.3.2 Evolution of interest in excitotoxicity and NMDAR

While the discussion of NMDARs has so far centered on SD, there has long been interest in NMDAR contribution to ischemic brain injury. This is because aberrant glutamate signaling plays critical roles in the neuronal injury

induced by hypocxia or ischemia *in vitro*. The neuronal damage due to excitatory amino acid is generally called excitotoxicity. The concept of excitotoxicity was initially developed based on the vulnerability of retinal neurons to glutamate, and the subsequent demonstration of vulnerability of large parts of the brain to high concentrations of glutamate (Olney, 1969). It was later shown that exposure to 100-500 µM glutamate reliably triggered neuronal death in cortical cultures (e.g. Choi et al., 1987). The link between excitotoxicity and ischemic neuronal death was concluded based on a large numbers of studies using neuronal cultures system. In neuronal culture, ischemia is simulated with oxygen and/or glucose deprivation (OGD) and/or by the addition of metabolic inhibitors (e.g. chemical ischemia), and these stimuli reliably cause neuronal death (e.g. Rothman, 1983; Rothman, 1984; Goldberg et al., 1986). One of the most important observations made from these early studies was that neuronal cultures studied early after plating (~2 days) were far more resistant to simulated ischemia than neurons which had been maintained in culture long enough to develop large numbers of synaptic connections (>14 days) (Rothman, 1983). It was hypothesized that aberrant excitatory synaptic activation is an important contributor to ischemic neuronal death. Supporting a role for glutamate excitotoxicity *in vivo*, extremely high extracellular glutamate concentrations (100-300 µM) were recorded in brain following experimental stroke in rat and rabbit (Benveniste et al., 1984; Hagberg et al., 1985).

Efforts to evaluate the contribution of excitotoxicity to ischemic neuronal death were greatly facilitated by development of selective glutamate receptor

antagonists (Beal, 1992). A series of *in vivo* stroke studies revealed that glutamate receptor antagonists are effective (Simon et al., 1984; Faden et al., 1989). Based on increased understanding of mechanism underlying excitotoxicity, glutamate receptor antagonists, especially those targeting the NMDAR became attractive as potential therapies (Choi and Rothman, 1990). However clinical trials of NMDAR antagonists for acute stroke treatment failed miserably. The reasons for these failures have not been clearly identified, however poor clinical study designs and differences in evaluation standards between basic research (e.g. infarct size) and clinical studies (e.g. neurological deficit) have often been raised as key issues (see reviews in Ikonomidou and Turski, 2002; Hoyte et al., 2004). NMDAR activation is involved in regeneration of brain function following injury and continuous suppression may decrease infarct volume but would hinder recovery of neurological function. Thus continuous suppression of NMDAR activity may be protective by decreasing infarct size, but may worsen clinical outcomes. As described above, SD has now emerged as a novel and clinically relevant target for many acute brain injuries. The prevention of SD by NMDAR antagonist can be designed quite differently from previously failed idea of simply reducing NMDAR activity. Thus prevention of SD generally would require much higher concentration of NMDAR antagonists but NMDAR antagonism can be limited to a very short time window if SD incidence can be monitored at the intensive care unit. Based on failures of large number of clinical trials on NMDAR antagonists, it is important to carefully determine how NMDARs contribute to SD and consequent brain injury.

1.4 Intracellular Ca^{2+} deregulation in neuronal injury

1.4.1 Intracellular Ca^{2+} signaling

One of the most important mediators of excitotoxicity is intracellular Ca^{2+} influx. The contribution of Ca^{2+} to excitotoxic neuronal death has been repeatedly confirmed by significant prevention of neuronal death by removal of extracellular Ca^{2+} or intracellular loading of a Ca^{2+} chelator (Goldberg et al., 1986; Choi, 1987; Manev et al., 1989; Tymianski et al., 1993b). In the 1970 and 1980s, Ca^{2+} sensitive fluorescence probes became available for neurophysiological experiments (Tsien, 1980), allowing direct evaluation of intracellular Ca^{2+} responses to physiological stimulation as well as Ca^{2+} deregulation in excitotoxicity. These studies revealed that strong glutamate exposure generates rapid initial Ca^{2+} increase and that neurons subsequently develop larger secondary Ca^{2+} deregulation (Manev et al., 1989). Importantly development of such a secondary Ca^{2+} response significantly correlates with reactivity to vital staining (e.g. trypan blue, ethidium bromide)(Tymianski et al., 1993a), indicating that secondary Ca^{2+} deregulation can represent early sign of neuronal degeneration.

Ratiometric indicators allowed estimation of intracellular Ca^{2+} concentration by using optical methods. Studies revealed that synaptic stimulation can raise dendritic Ca^{2+} concentration from 100 nM to above 1 µM (Petrozzino et al., 1995), which is a good range to control Ca^{2+} sensitive channels and signaling molecules (e.g. EC_{50} for Ca^{2+}: SK channels: 0.4-5 µM

(Pedarzani et al., 2001), BK channels 1-10 µM (at -50mV) (Vergara et al., 1998), soluble adenylcyclase: 0.3-4 µM and 100 µM (Jaiswal and Conti, 2003), PKCs (conventional): 0.7-1.4 µM (Kohout et al., 2002)). Cytoplasmic Ca^{2+} at this range can be effectively cleared, by the activities of Ca^{2+} exchangers, Ca^{2+} ATPase and mitochondria. In contrast, during the secondary Ca^{2+} deregulation in excitotoxicity models, intracellular Ca^{2+} concentrations often remain elevated to higher levels (above 30 µM) and for longer periods (Abele et al., 1990; Vander Jagt et al., 2008). As will be discussed later, excitotoxic Ca^{2+} elevations are not always recoverable or may take substantially more time to be cleared, likely because buffering and clearance mechanisms are impaired. For example, Ca^{2+} activated calpain has been shown to cleave Na^{+}/Ca^{2+} exchangers and hinder cytoplasmic Ca^{2+} clearance (Bano et al., 2005). In addition, excessive Ca^{2+} uptake by mitochondria results in opening of a large conductance pore in mitochondria, called the permeability transition pore (mPTP). mPTP opening impairs mitochondrial Ca^{2+} buffer functions, and also limits ATP production needed to fuel Ca^{2+} ATPase activity. The release of cytochrome *c* following mPTP formation can also serve as an important trigger for apoptotic signaling.

1.4.2 Dendritic Ca^{2+} deregulation in excitotoxicity

Most first generation Ca^{2+} probes had affinities that were too high to accurately assess Ca^{2+} signals during excitotoxicity, and the indicators were often saturated in ischemia or glutamate exposure studies. When lower affinity Ca^{2+} probes were developed, highly localized Ca^{2+} responses became better

resolved. Thus the secondary Ca^{2+} deregulation seen in excitotoxicity studies are originated in distal dendritic, thus suggested an important concept that dendritic compartments serve as the origin of Ca^{2+} deregulation in excitotoxicity. When isolated neurons were briefly stimulated with glutamate, most of initial glutamate application cause recoverable transient Ca^{2+} increase, while repetitive stimulations generate sustained and sometimes irrecoverable elevation of dendritic Ca^{2+} deregulation (Connor et al., 1988; Wadman and Connor, 1992). In the studies in acute brain slice preparations, repetitive glutamate microapplication or kainate application resulted in similar secondary Ca^{2+} deregulation originated in distal dendrite which slowly progress toward soma (Connor and Cormier, 2000; Shuttleworth and Connor, 2001). In this model, the latter study confirmed that secondary Ca^{2+} deregulation is due to sustained Ca^{2+} influx and prevented by NMDAR antagonist. In a study using bath NMDA application (Vander Jagt et al., 2008), transient intracellular Ca^{2+} increase occurred immediately after NMDA application, followed by a slowly propagating secondary Ca^{2+} deregulation originated in distal dendrite. This study also showed that delayed application of NMDAR antagonist (MK801) could prevent progressing Ca^{2+} deregulation (Vander Jagt et al., 2008). These results strongly suggest NMDAR contribution to secondary Ca^{2+} deregulation in various models. In addition to significant correlation between secondary Ca^{2+} deregulation and neuronal viability (Tymianski et al., 1993a), these studies suggest a dendritic origin of neurotoxic Ca^{2+} signaling in excitotoxicity.

The dendritic origin of neuronal damage is consistent with the vulnerability of these small compartments to ischemic challenge. When neurons in culture or in brain slices were exposed to oxygen glucose deprivation, or a high concentration of an excitatory amino acid, dramatic structural changes have been observed in dendrites (Joshi and Andrew, 2001; Zeng et al., 2007). This is characterized by obvious swellings interspersed by dramatic thinning of dendritic shafts. This morphology is often termed “dendritic beading” as the structure appears quite similar to beads on a string (Park et al., 1996). While dendritic beading is a characteristic of injured neurons, beading itself could be a neuronal defense system against excitotoxicity to limit conductance in the stressed compartments.

The large surface/volume ratio and high ion channel density reasonably suggest dendritic origin of injurious signal. During SD, dendritic Ca^{2+} concentrations are sustained at very high levels for a relatively long period of time (minutes) following the passage of SD (Dietz et al., 2008). In addition, SD generated with oxygen glucose deprivation or ischemia *in vivo* triggers dendritic beading of pyramidal neurons (Jarvis et al., 1999; Murphy et al., 2008). The massive glutamate release during SD and Ca^{2+} deregulation suggest that SD may trigger neuronal injury similar to those seen in excitotoxicity studies. However the relationship between excitotoxicity and SD has not been well explored. As noted above, extracellular glutamate concentrations are highly elevated during SD propagation and massive NMDAR activation is expected. However whether or not NMDAR activation during SD can contribute to the

injurious consequences of SD in metabolically compromised tissues is not well established.

1.5 Zn^{2+} deregulation in ischemic injury

1.5.1 Zn^{2+} toxicity

Roles of Zn^{2+} in ischemic brain injury and SD are another major interest in the present study. The currently most widely accepted hypothesis in the Zn^{2+} field is that Zn^{2+} accumulates in the injured brain and contributes to neuronal death. The concept of neuronal Zn^{2+} toxicity was developed by a series of studies by Choi and Koh. In their first study, exogenous Zn^{2+} was shown to ameliorate some forms of excitotoxicity in neuronal cultures (Koh and Choi, 1988). The Zn^{2+} toxicity was quite different from NMDAR mediated excitotoxicity, in that it was not mainly due to toxic Ca^{2+} overload. In fact Zn^{2+} toxicity was enhanced by AMPA receptor activation and augmented by removal of extracellular Ca^{2+} in neuronal culture (Weiss et al., 1993). Subsequent works showed that Ca^{2+}-permeable GluR2 lacking AMPA receptors are important contributor to toxic Zn^{2+} influx in these preparations. The significance of Zn^{2+} toxicity was later tested in a global ischemia model. The study revealed significantly high intracellular labile Zn^{2+} concentration in damaged neurons and demonstrated that delayed administration of a Zn^{2+} chelator (CaEDTA) could provide a significant neuroprotection (Koh et al., 1996). Because CaEDTA is membrane impermeable, this early study suggested that transmembrane Zn^{2+} influx to the damaged neurons contributed to ischemic neuronal death. A similar

protective effect of CaEDTA was later reproduced in several studies using different stroke models (Lee et al., 2002; Calderone et al., 2004)

While many pathways are proposed, one of the well established toxic mechanisms of intracellular Zn^{2+} is inhibition of cellular energy metabolisms. One of the most profound toxic Zn^{2+} activities is opening of mPTP and release of cytochrome c from isolated mitochondria which can be elicited by 10-100 nM extramitochondrial Zn^{2+} (Jiang et al., 2001). In addition to its mitochondrial effect, Zn^{2+} can also inhibit glycolytic enzymes such as GAPDH while concentration required for inhibition was not strictly determined (Sheline et al., 2000). In addition to these pathways, Zn^{2+} is now implicated in autophagy and necrotic cell death (Hwang et al., 2008; Sensi et al., 2009).

In addition to direct Zn^{2+} toxicity, intracellular Zn^{2+} accumulation significantly contributes to the onset of secondary Ca^{2+} deregulation in excitotoxicity and initiation of some SD. Intracellular Zn^{2+} concentrations increase during NMDA challenge in an acute brain slice and removal of Zn^{2+} with a membrane permeable Zn^{2+} chelator (TPEN) significantly delayed onset of secondary Ca^{2+} response in neuronal dendrites (Vander Jagt et al., 2009). In addition, stimuli used to generate SD (ouabain, oxygen glucose deprivation) also elevate intracellular Zn^{2+} concentration and removal of intracellular Zn^{2+} with TPEN significantly delayed or abolished SD (Dietz et al., 2008; Medvedeva et al., 2009). These results suggested that intracellular Zn^{2+} accumulation contributes to acute neuronal injury by facilitating neurotoxic events, rather than intracellular Zn^{2+} by itself. It is important to note that (unlike *in vivo* stroke studies) membrane

impermeable Zn^{2+} chelator CaEDTA did not show any protective effects in these models. This suggests that intracellular Zn^{2+} accumulation in these *in vitro* models could be mediated by mechanism(s) distinct from Zn^{2+} accumulation seen in experimental stroke studies. However mechanisms underlying intracellular Zn^{2+} accumulation occurring prior to acute excitotoxic injury and SD have not been clarified.

1.5.2 Synaptic Zn^{2+} release and its intracellular accumulation

One important hypothesis in ischemic Zn^{2+} toxicity is that toxic intracellular Zn^{2+} accumulation occurs by uptake of synaptically released Zn^{2+} (hereafter synaptic Zn^{2+} translocation) (Koh et al., 1996; Koh, 2001). Activity dependent Zn^{2+} release from mammalian brain tissue was originally discovered in 1984 (Assaf and Chung, 1984; Howell et al., 1984), and one of these studies estimated that extracellular Zn^{2+} concentrations in synaptic clefts can reach ~300 μM. Histological detection of brain free Zn^{2+} revealed high concentration of Zn^{2+} present in synaptic vesicles of many glutamergic neurons and Zn^{2+} was proposed to be a modulator of synaptic functions (Frederickson et al., 1992). Evidence for the indispensable roles of the ZnT3 transporter for establishing the vesicular Zn^{2+} pool was demonstrated in transgenic animal with *ZnT3* gene deletion (Cole et al., 1999). Later studies by applying high affinity fluorescence indicator, FluoZin3, in the bath medium revealed strong correlation between extracellular Zn^{2+} concentration and local presynaptic activity (Qian and Noebels, 2005, 2006). The contribution of synaptic Zn^{2+} release to intracellular Zn^{2+}

accumulation was established by an imaging study using bulk loading of low affinity Zn^{2+} indicator which revealed extremely slow intracellular Zn^{2+} accumulation which became evident ~5 minutes after brief synaptic stimulation (Suh, 2009).

The significance of synaptic Zn^{2+} translocation is better supported by functional studies. In the mammalian brain vesicular Zn^{2+} content is highest in mossy fiber synaptic vesicles and mossyfiber-CA3 synapses provides a good model to study the significance of Zn^{2+} release and translocation to postsynaptic neurons (Lee et al., 2011). One such study showed that high concentrations of CaEDTA (10 mM) could prevent uptake of synaptically released Zn^{2+} by CA3 neurons, and also block induction of long term potentiation (Li et al., 2001a). Later studies have suggested that Zn^{2+} influx activates Src kinase, potentiation of TrkB receptor and potentiates these synapses (Huang et al., 2008). ZnT3 KO animals lack virtually all vesicular Zn^{2+} (Cole et al., 1999) and the phenotype of these animals can be useful for examining roles of vesicular Zn^{2+}. In an early report, young ZnT-3 KO animals did not show any behavioral deficits (Cole et al., 2001), however a later study showed impaired spatial memory in 6-month old ZnT3 KO animals, with associated decrease in AMPA and NMDAR subunit expression (Adlard et al., 2010). ZnT3 expression generally decreases in older animals and the latter study proposed that vesicular Zn^{2+} is important for maintaining neuronal function in aged animals. However data obtained from ZnT3 animal need to be analyzed carefully because ZnT3 KO animals could develop significant adaptive mechanism to compensate for lack of vesicular Zn^{2+}.

In fact, these animals express mossy fiber-CA3 LTP independent of postsynaptic Zn^{2+} accumulation (Pan et al., 2011).

In contrast to functional significances of synaptic Zn^{2+} translocation in synaptic physiology, evidence for deleterious role of synaptic Zn^{2+} translocation is rather weak in pathological situations. The toxicity of Zn^{2+} influx is supported by the protective effect of membrane impermeable Zn^{2+} chelator CaEDTA. However Zn^{2+} chelation by CaEDTA requires prior dissociation from Ca^{2+} to capture Zn^{2+} and this significantly limits its ability to chelate rapid Zn^{2+} transient. In fact, CaEDTA at lower concentration (1 mM) cannot eliminate synaptically released Zn^{2+} (Qian and Noebels, 2005, 2006). Together with a short functional half-life of CaEDTA *in vivo* (90 miniutes Frederickson et al., 2002), it is unlikely that CaEDTA could effectively block synaptic Zn^{2+} translocation.

Instead of targeting synaptically released Zn^{2+}, protective effect of CaEDTA is also considered as a consequence of intracellular Zn^{2+} chelation. While mechanism is not conclusive, high concentration of CaEDTA (~150 mM, estimated from Lavoie et al., 2007) significantly reduced intracellular Zn^{2+} concentration *in vivo* (Frederickson et al., 2002; Calderone et al., 2004; Lavoie et al., 2007). Contribution of intracellular Zn^{2+} chelation by CaEDFTA was supported by a study that showed that Zn^{2+} can be released from an intracellular pool following exposure to oxidative stress and the resultant intracellular Zn^{2+} accumulation was sufficient to trigger neuronal death (Aizenman et al., 2000; Aras and Aizenman, 2011). The non-essential role of synaptic Zn^{2+} release in intracellular Zn^{2+} accumulatoin following seizure was also demonstrated, in which

study intracellular Zn^{2+} accumulation was observed in ZnT3 KO animals (Lee et al., 2000). These evidences indicate that synaptically released Zn^{2+} is not always required for histologically detectable Zn^{2+} accumulation seen in ischemic brain injury. Excessive Zn^{2+} chelation is generally toxic (Hyun et al., 2000; Maclean et al., 2001) and identification and selective targeting of intracellular Zn^{2+} accumulation mechanism is important.

1.5.3 Intracellular Zn^{2+} homeostasis

As described above, excessive intracellular Zn^{2+} accumulation can significantly contribute to neuronal death. However intracellular Zn^{2+} is also an essential component of cellular physiology. In fact Zn^{2+} is required for catalytic centers of enzymes (e.g. catalase, superoxide dismutase and matrix metalloproteinases) as well as for structural component (e.g. Zn^{2+} fingers). In order to minimize Zn^{2+} toxicity, while keeping Zn^{2+} available for essential functions, neurons have a finely-tuned Zn^{2+} homeostasis mechanism. In mammalian neurons, the total intracellular Zn^{2+} content is at range between 100-200 μM (Colvin et al., 2010). However cytoplasmic Zn^{2+} concentrations are considered to be extremely low or even absent because of the tightly-regulated activity of Zn^{2+} transporters and buffer molecules.

There are two classes of Zn^{2+} transporter family; Zn^{2+} transporters (ZnTs) and Zn^{2+} importer proteins (ZIPs). ZnTs either extrude or sequester Zn^{2+} from the cytoplasm. ZnT1 is expressed in cortical neurons and its gene expression level is regulated in feedback manner. When cytoplasmic metal ion

concentrations elevate, metal ions bind to the transcription factor MTF-1 and transactivates ZnT1 gene expression (Langmade et al., 2000). Upregulation of ZnT1 expression may thus be important for extruding intracellular Zn^{2+} concentrations. ZnT1 gene expression is upregulated by transient ischemia and such mechanism may contribute to limiting Zn^{2+} toxicity in brain after stroke (Tsuda et al., 1997). Cytoplasmic Zn^{2+} is also sequestered in lysosomes and mitochondria by activities potentially involving ZnT2, 4 and 5 (Sensi et al., 2009). In contrast to ZnT transporters, ZIP transporters drive Zn^{2+} into the cytoplasmic fraction. ZIP activity may be important for maintaining intracellular Zn^{2+} content needed for essential functions, however excessive activity of ZIPs can be neurotoxic. In fact knock-out of ZIP1,3 significantly reduced Zn^{2+} uptake into hippocampal neurons and reduce seizure-induced neuronal degeneration (Qian et al., 2011).

In addition to the Zn^{2+} transporter systems, Zn^{2+} binding molecules contribute to maintenance of extremely low intracellular Zn^{2+} concentrations. Intracellular Zn^{2+} binding molecules such as glutathione, thionein and metallothionein (MT) are considered to be important for buffering intracellular Zn^{2+}. MT generally is involved in a defense mechanism against metalotoxicity. Mammalian genomes encode MT1, -2, -3 and -4 genese, while significant numbers of subtypes (e.g. MT2A, MT2B) can present in each gene family (Moleirinho et al., 2011). Similar to ZnT1, MT1 and 2 are upregulated by MTF-1 transcription factor activation in response to increased intracellular metal concentrations, and plays protective roles against metalotoxicity in ubiquities cell

types (Heuchel et al., 1994). In contrast, Metallothionein 3 (MT3) is the predominantly expressed MT isoform in brain. MT3 was originally purified from neuroblastoma as a Growth Inhibitory Factor (GIF) and inclusion of MT3 in culture medium significantly inhibited outgrowth of cortical neurons (Uchida et al., 1991). Such inhibitory activity is not shared by MT1 and MT2, and it was proposed that high Cu^{2+} binding of MT3 due to its unique N-terminal amino acid sequence contribute to the inhibitory effects (Faller and Vasak, 1997). MT3 KO mice develop behavioral abnormalities (Koumura et al., 2009) and such growth inhibitory effect may play role in proprer brain development.

MT3 is constitutively expressed (unlike MT1 and MT2) and considered to play physiological roles in intracellular Zn^{2+} homeostasis. Biophysical characterization revealed that different Zn^{2+} binding sites of MT3 have different Zn^{2+} affinities and one of the weakest Zn^{2+} binding sites has an estimated 10^{-8} M affinity for Zn^{2+} (Krezel and Maret, 2007). The presence of multiple Zn^{2+} affinities in a MT3 molecule explain why MT1 or 2 usually equilibrate in a 7-Zn^{2+} bound complex when incubated with high $ZnCl_2$, while MT3 can equilibrate in multiple Zn^{2+} binding states multiple complexes of up to 10 Zn^{2+}-bound forms (Palumaa et al., 2005). Such dynamic binding characteristics predict effective transfer of Zn^{2+} to other high affinity Zn^{2+} binding sites. Thus Zn^{2+} binding to MT3 is not the terminal equilibrate state, rather serves as an intermediate hub to control distribution of intracellular Zn^{2+} throughout a neuron. Zn^{2+} binding to MT3 is mediated by thiol groups and is highly sensitive to oxidation and acidification (Toriumi et al., 2005). These sensitivities of MT3-Zn^{2+} binding should be

important for controlled Zn^{2+} release from MT3 to distribute Zn^{2+} to transporters or high affinity Zn^{2+} binding proteins. However intracellular oxidation and acidosis occur in injured tissue and Zn^{2+} release from MT may also contribute to the toxic intracellular Zn^{2+} accumulation.

While these Zn^{2+} homeostasis mechanisms are important for cellular physiology, it becomes a significant confound when measuring the intracellular Zn^{2+} dynamics.

1.5.4 Extracellular action of synaptically released Zn^{2+}

Discussion so far concentrated on intracellular Zn^{2+} actions, howewver extracellular Zn^{2+} also plays significant roles in the modulation of neuronal excitability. Accumulating evidence suggests that virtually almost all ion channels or receptors have some sensitivity to inhibition by extracellular Zn^{2+} (Frederickson et al., 2005), while it is likely that the degree of inhibition significantly differs between experimental models (further discussed in Discussion section). Among many Zn^{2+}-sensitive ion channels, the NMDAR is one of the most well-studied and most sensitive to Zn^{2+} (Westbrook and Mayer, 1987). High sensitivity of NMDAR was subsequently characterized in detail (Paoletti et al., 1997). This work not only demonstrated inhibition of NMDAR by nanomolar Zn^{2+}, but also suggested that NMDAR potentiation seen with reducing agents (e.g. DTT) is mediated by removal of contaminating Zn^{2+}, rather than by redox modulation of the channel itself. (Tauck, 1992) Prior work had shown that reducing agents such as DTT potentiate NMDAR currents (Reynolds et al., 1990;

Kohr et al., 1994), and redox modulation had been shown to potentiate NMDAR current and was implicated to some injurious processes (Hammond et al., 1994; Sanchez et al., 2000). Given the high affinity for NMDAR and extracellular Zn^{2+} concentration at synaptic cleft, Zn^{2+} release should be able to play roles in NMDAR inhibition in physiological conditions. In fact it was shown that at mossy fiber CA3 synapses, synaptic Zn^{2+} release limits postsynaptic NMDAR current (Vogt et al., 2000; Pan et al., 2011). It is thus of considerable interest that Zn^{2+} inhibition of NMDAR may be a central mechanism of these effects.

Because excessive NMDAR activation contributes to neuronal injury, extracellular Zn^{2+} potentially suppress some forms of excitotoxic injury. In seizure studies some reported that ZnT3 KO animals and Zn^{2+} deficient animals (which had decreased Zn^{2+} content) have a lower threshold for seizure (Cole et al., 2000; Lee et al., 2000; Dominguez et al., 2003; Takeda et al., 2003; but see also Qian et al., 2011). In addition one study revealed higher vulnerability of ZnT3 KO to brain trauma (Doering et al., 2010). Even in some ischemia models, low concentration of CaEDTA has been shown to accelerate infarct enlargement (Kitamura et al., 2006), whereas significant neuroprotection was observed following Zn^{2+} administration (Zhao et al., 1996). While Zn^{2+} toxicity in ischemia model is well developed, these suggest that Zn^{2+} can play a protective role in certain circumstances. However the question still remains whether endogenous synaptically released Zn^{2+} can limit NMDAR dependent toxic events and what factors determine the relative contribution of synaptically released Zn^{2+} to

potentially neurotoxic intracellular Zn^{2+} accumulation and potential protective extracellular Zn^{2+} functions.

1.6 Summary

The primarily goal of the present studies was to elucidate mechanisms converting non-injurious event to events that bring harmful consequences in metabolically compromised brain tissue. NMDA receptor mechanisms and complex roles of extracellular and intracellular Zn^{2+} in SD were examined in both healthy and metabolically compromised condition.

Studies in Chapter 1 examined mechanisms underlying neuronal injury caused by SD induced with potassium chloride microinjection. These studies tested the hypothesis that NMDA receptor activation occurring after the onset of SD is responsible for initiating excitotoxic injury in neuronal dendrites. This work provided the first detailed characterization of an excitatory phase during the late-SD phase and revealed that NMDAR activation during this phase can be sufficient to convert a recoverable SD into an irrecoverable event in metabolically compromised neurons.

Studies in Chapter 2 were driven by the hypothesis that Zn^{2+} released from synaptic vesicles can limit SD by inhibiting NMDARs. The results of this study generally supported the hypothesis in a model of potassium induced SD *in vitro* and *in vivo*, and revealed potentially protective roles of extracellular Zn^{2+}.

Chapter 3 contains studies promoted by results in Chapter 2, and examined whether inhibitory effects of extracellular Zn^{2+} were effective in ischemic tissues. These studies showed a dramatic difference in sensitivity that appeared to be due extracellular redox modulation.

Experiments in Chapter 4 focused on an important technical aspect of intracellular Zn^{2+} measurements from single neurons. This study tested and supported the hypothesis that intracellular dialysis removes neuronal MT3 and greatly distorts analysis of intracellular Zn^{2+} accumulation. These findings were then exploited to provide the first evidence that both intracellular and extracellular sources of Zn^{2+} contribute to postsynaptic accumulation of Zn^{2+} after synaptic activation.

2. Sustained NMDAR Activation by Spreading Depolarizations Can Initiate Excitotoxic Injury in Metabolically Compromised Neurons

Isamu Aiba & C. William Shuttleworth

Department of Neurosciences, University of New Mexico, Albuquerque, NM, USA

(In Press: “Journal of Physiology”)

2.1 ABSTRACT

Spreading depolarizations (SD) are slowly propagating waves of near-complete neuronal and glial depolarization. SD have been recorded in patients with brain injury and the incidence of SD significantly correlates with outcome severity. Although it is well-accepted that the ionic dyshomeostasis of SD presents a severe metabolic burden, there is currently limited understanding of SD-induced injury processes at a cellular level. In the current study we characterized events accompanying SD in the hippocampal CA1 region of murine brain slices, using whole-cell recordings and single-cell Ca^{2+} imaging. We identified an excitatory phase that persisted for approximately 2 min following SD onset, and accompanied with delayed dendritic ionic dyshomeostasis. The excitatory phase coincided with a significant increase in presynaptic glutamate release, evidenced by a transient increase in spontaneous EPSC frequency and paired-pulse depression of evoked EPSCs. Activation of NMDA receptors (NMDARs) during this late excitatory phase contributed to the duration of individual neuronal depolarizations and delayed recovery of extracellular slow potential changes. Selectively targeting the NMDAR activation following SD onset (by delayed pressure application of a competitive NMDAR antagonist) significantly decreased the duration of cellular depolarizations. Recovery of dendritic Ca^{2+} elevations following SD were also sensitive to delayed NMDA antagonist application. Partial inhibition of neuronal energy metabolism converted SD into an irrecoverable event with persistent Ca^{2+} overload and membrane compromise. Delayed NMDAR block was sufficient to prevent these acute injurious events in

metabolically-compromised neurons. These results identify a significant contribution of a late component of SD that could underlie neuronal injury in pathologic circumstances.

2.2 INTRODUCTION

Spreading depression (SD) was originally described as a slowly propagating suppression of electrocorticographic (ECoG) activity (Leao, 1944) and was subsequently characterized as a slowly propagating wave of near-complete cellular depolarization of neurons and glia (Somjen, 2001). Stimuli such as elevated potassium or ischemia can cause localized depolarization of a volume of neurons and glia sufficient to trigger a propagating event, and result in a characteristic large slow field potential shift. Accumulation of extracellular potassium and glutamate mediates the feed-forward depolarization event as it spreads slowly (2-4 mm/min) through gray matter (Somjen, 2001). Because suppression of ECoG activity is a consequence of the depolarizing event, the general term spreading depolarization (SD) is used in the current study to emphasize the underlying mechanism (see Dreier, 2011).

Recent clinical recordings confirm a relatively high incidence of SD in injured brain and it is hypothesized that the cumulative metabolic burden of recovery from long lasting depolarizations underlies neuronal injury in metabolically-compromised tissue (Dreier, 2011; Lauritzen et al., 2011). Thus SDs recorded from these tissue regions often show prolonged slow potential shifts (Shin et al., 2006; Oliveira-Ferreira et al., 2010; Takeda et al., 2011), the

duration of which is correlated with the severity of injury (Oliveira-Ferreira et al., 2010; Hartings et al., 2011b) and considered to be a useful parameter to assess damaging effects of SD. However, the cellular event(s) that contribute to pathologically long-lasting slow extracellular potential changes are not fully understood.

Previous studies have shown a significant contribution of NMDA-type glutamate receptors (NMDARs) to SD. Thus NMDAR antagonists have been shown to inhibit initiation and/or propagation of SD in experimental models (Gill et al., 1992; Anderson and Andrew, 2002; Hartings et al., 2003; Faria and Mody, 2004; Peeters et al., 2007; Aiba et al., 2012) and a preliminary clinical study has suggested prevention of SD in injured brain with ketamine, a nonspecific NMDAR antagonist (Sakowitz et al., 2009; Hertle et al., 2012b). NMDAR antagonists have also been shown to reduce the duration of slow extracellular potential shifts, both *in vitro* and *in vivo.* The fact that NMDAR antagonists could selectively reduce the secondary phase of DC shifts without significantly affecting the initial phase has implied a role for NMDAR activation during the late SD period (Marrannes et al., 1988; Herreras and Somjen, 1993b; Larrosa et al., 2006) but such activation has not been directly demonstrated.

Coordinated glutamate release and intracellular Ca^{2+} loading as a consequence of SD may be similar in many ways to excitotoxic events mediated by NMDAR stimulation. SD results in substantial intracellular neuronal Ca^{2+} transients, which recover fully in healthy tissue, but are irrecoverable when metabolic substrates are lacking (Kunkler and Kraig, 2004; Dietz et al., 2008;

Gniel and Martin, 2010). However, the cellular events and Ca^{2+} sources responsible for conversion from recoverable to irrecoverable Ca^{2+} loading are not known. Previous studies identified dendritic compartments as likely initiation sites for excitotoxic injury in CA1 neurons (Connor et al., 1988; Wadman and Connor, 1992; Shuttleworth and Connor, 2001; Vander Jagt et al., 2008) and we examine here whether Ca^{2+} deregulation in dendrites may also be responsible for triggering NMDAR-dependent injury associated with SD.

In the current study we utilized whole-cell recordings to characterize a significant excitatory event following the initial depolarization of SD, generated in hippocampal area CA1 of murine brain slices. This excitatory period resulted in sustained NMDAR activation, and was responsible for prolonged Ca^{2+} elevations in dendrites. Suppression of this activity during the late phase of SD was sufficient to prevent neuronal injury in metabolically compromised neurons.

2.3 METHODS

2.3.1 Ethical approval

All experimental protocols were approved by the institutional animal care and use committee (IACUC) of the University of New Mexico.

2.3.2 Slice preparation

Brain slices were prepared from 53 adult (4-10 week old) male C57BL/6 mice. For all experiments that involved pharmacological interventions, control and drug-treated slices from the same experimental animals were interleaved throughout the study. Animals were deeply anesthetized by an injection (0.2 ml s.c.) of a ketamine/xylazine mixture (85 and 15 mg/ml, respectively) and decapitated. Brains were quickly extracted into ice cold cutting solution (in mM): 3 KCl, 1.25 NaH_2PO_4, 6 $MgSO_4$, 26 $NaHCO_3$, 0.2 $CaCl_2$, 10 glucose, 220 sucrose, equilibrated with 95% O_2/5% CO_2), hemisected, and then 350 µm coronal corticohippocampal slices were prepared by using a vibratome. Slices were allowed to recover in artificial cerebrospinal fluid (ACSF, containing (in mM): 126 NaCl, 3 KCl, 1.25 NaH_2PO_4, 1 $MgSO_4$, 26 $NaHCO_3$, 2 $CaCl_2$, and 10 glucose, equilibrated with 95% O_2/5% CO_2) at 35ºC for 1 hour and then maintained in ACSF at room temperature until transfer to the recording chamber.

2.3.3 Generation of SD

Slices were maintained in a submerged chamber superfused with ACSF at 2 ml/min at 31-33ºC. SD was generated in the hippocampal CA1 stratum radiatum subfield by local pressure ejection of 1 M KCl via micropipettes (1-5 µm tip diameter, 10-40 ms, 40psi) using a picospritzer (Parker Hannifin, OH). The ejection volume was estimated at ~10 nl, based on CCD imaging and diameter measurements of ejected drops onto a glass coverslip. Such measurements could be reliably made from drops generated by 10 ejection pulses and comparison with a 1 µl standard. Electrophysiological recordings of SD were made from single CA1 pyramidal neurons and/or stratum radiatum for extracellular potentials, at locations >200 µm from the KCl ejection site. Recording at this distance avoided contamination from the KCl micro-injection, and ensured that recordings were of SD-associated events occurring >3 seconds after propagation from the application site. In some experiments (Figure 3) the effects of SD were assessed on responses evoked by stimulating Schaffer collateral inputs (0.1-0.4 mA, 70 µs) with a concentric bipolar electrode placed in stratum radiatum. Test stimuli that generated 30% of maximal amplitude responses were selected from input output curves.

2.3.4 General recordings

Extracellular recordings were made from CA1 stratum radiatum, using glass microelectrodes filled with ACSF (0.5-1.0 MΩ) slowly advanced 50 µm below the slice surface. Extracellular DC potential was acquired at 2-10 kHz

using a Multiclamp 700A amplifier, digitized (Digidata 1332) and analyzed using pClamp 9.2 software (Molecular Devices, Foster City, CA).

Single-cell loading of fluorescent indicators and electrophysiological recordings were made using whole-cell clamp techniques and a Multiclamp 700A amplifier with CV-7B headstage (Molecular Devices, Foster City, CA). Single CA1 pyramidal neurons were visually identified and whole-cell access was established with low resistance patch pipettes (1-2 MΩ) filled with a potassium gluconate-based internal solution containing (in mM): 135 potassium gluconate, 8 NaCl, 1 $MgCl_2$, 2 Na_2ATP, 0.3 NaGTP, 10 Hepes, 0.05 EGTA, pH 7.2 adjusted with KOH. Fluorescence indicators or blockers were supplemented to this standard solution depending on the specific experiments, as described in appropriate Methods and Results sections below. The quality of recordings was assessed by using the membrane test command of Clampex (Molecular Devices, Foster City, CA). Recorded CA1 pyramidal neurons had characteristic low input resistances (120.9 ± 6.6 MΩ), high capacitances (190.8 ± 8.3 pF) and I_h currents in response to hyperpolarizing voltage-steps (n=30).

2.3.5 Fluorescence imaging

Intracellular Ca^{2+} measurements were made from single CA1 pyramidal neurons as described previously with minor modifications (Vander Jagt et al., 2008). Indicator loading was via whole-cell pipettes filled with standard internal solution supplemented with low affinity Ca^{2+} indicator, Fura-6F (0.5 mM, Life technologies, Grand Island, NY). Dialysis duration was strictly limited to either 3

or 5 min depending on the experiments (see Results), and electrodes were then carefully removed. The combination of high pipette indicator concentration and brief dialysis time typically resulted in a final intracellular indicator concentration of ~100 µM, as determined by comparison with neurons extensively dialyzed with test indicator concentrations. Because of its low affinity, the temporal and spatial dynamics of intracellular Ca^{2+} were unlikely perturbed by Fura-6F at this final intracellular concentration (Neher, 1995). Following indicator loading, neurons were allowed to recover for 10 min. During SD, Fura-6F fluorescence was monitored at its isobestic wavelength (360 nm), and focus was adjusted to maintain a segment of proximal apical dendrite in the focal plane. Fura-6F fluorescence also excited at 350, 380 nm for Ca^{2+} measurements, with the three excitation wavelengths each being delivered at 1 Hz from a monochromator (Polychrome V, Till Photonics GmbH, NY). Emission signals passed through a dichroic mirror (400 nm LP), band pass emission filter (510/35 nm) and were collected with a CCD camera (Till Imago), controlled by Till Vision software (Version 4.00). Intracellular Ca^{2+} dynamics were evaluated after generation of background-subtracted ratio images (350 nm/380 nm) and Ca^{2+} concentrations estimated by comparison with *in vitro* calibration standards (Life Technologies, Grand Island, NY) and calculation using the equations described in (Grynkiewicz et al., 1985). Pseudo-color images of estimated intracellular Ca^{2+} were prepared by applying a mask generated from filtered 380 or 350 nm fluorescence images to the raw pseudocolored ratio image. The kinetics of intracellular Ca^{2+} dynamics

were obtained from regions of interest set within the soma and proximal apical dendrite (50-100 µm from soma).

In some experiments, neuronal morphology after SD was assessed in neurons loaded with Lucifer yellow (Life Technologies, NY). Internal solution was supplemented with 0.2% Lucifer yellow, and fluorescence was excited at 410 nm excitation and long-pass filtered emission signals (>420 nm) collected by CCD camera at 0.67 Hz. Loss of indicator was estimated by the relative change in fluorescence intensity from region within cell bodies.

2.3.6 Whole-cell electrophysiological recordings

Voltage-clamp recordings were made at -50 mV after liquid junction potential correction. The sodium channel blocker QX314 (5 mM) was included in the internal solution for all voltage-clamp recordings. A holding voltage of -50 mV (after 10 mV liquid junction potential correction) was chosen in order to enable simultaneous detection of spontaneous EPSCs and SD currents. Spontaneous EPSCs were detected with Mini analysis software (version 6.0.3, Synaptosoft Inc., NJ), using a high threshold (10 pA) in order to minimize detection of false positives. We excluded EPSCs detected during the initial 20 seconds following the onset of large SD currents, because input resistance and capacitance currents decreased to less than 10% of baseline levels, preventing reliable monitoring of recording quality. Except for this period, series resistance was maintained (<20% variance) in successful recordings (see Figure 3C). Recordings with >20% changes in series resistance or apparent voltage error

during SD (as determined by readout of holding voltage and distortion of SD current waveform) were excluded from analysis.

All current-clamp recordings were made without any holding current applied (voltage-follower mode). In some recordings, test current pulses (-200 pA, 500 ms) were manually injected to monitor recovery of input resistance following SD. Current-clamp recordings with >20% changes in bridge balance or input resistance following recovery from SD were discarded.

Successful whole-cell recordings of SD required electrodes with relatively large tip diameters (>3 μm) and initial series resistances less than 20 MΩ as determined by the membrane test in Clampex (Molecular Devices, CA). SD involves tissue swelling, and therefore continuous fine adjustment of electrode position was needed throughout the whole-cell recordings. On the criteria described above, we obtained an overall success rate ~50% for these whole-cell studies.

Extracellular potential changes during SD in our submerged slices (5-10 mV) were substantially smaller compared with previous reports from recordings from interface chambers, and were highly sensitive to the depth of electrodes. Thus we did not apply any voltage correction to our recordings (whole-cell current and membrane potential) and acknowledge that cellular responses may be under-estimated (Somjen, 2001). In addition, some voltage error also occurs during the large SD current (Hamann et al., 2002), and complicates absolute measurements of whole-cell currents. However, interpretation of the present

data does not rely on absolute current and voltage changes, and series resistance and cellular capacitance measurements were similar between neurons throughout the study. For these reasons we did not apply any arithmetic corrections of data, and possible confounds are discussed in the appropriate results section.

2.3.7 Drugs

All chemicals were obtained from Sigma-Aldrich (St Louis, MO) unless otherwise noted. DL-AP5 was prepared as a 10 mM stock in water and stored at -20^{o}C and used within 1 week of preparation.

2.3.8 Data analysis

Unless otherwise described, statistical analyses were made with Mann-Whitney *U*-tests for two-group comparisons and Kruskal-Wallis tests with post-hoc Dunn's multiple comparison test for additional group comparisons using GraphPad Prism version 4.03 (GraphPad Software, La Jolla, CA) software. Individual data points are shown as dots together with bar graph presenting mean ± SEM. In experiments with repetitive measurement, corresponding data points are connected with a dash line. A *p*-value <0.05 was considered statistically significant.

2.4 RESULTS

2.4.1 NMDAR activation contributes to prolonged dendritic Ca^{2+} elevations following SD

Figure 1 shows intracellular Ca^{2+} dynamics in CA1 pyramidal neurons during and after SD. Single neurons were loaded with a low affinity ratiometric Ca^{2+} indicator (Fura-6F, K_D~5 µM) via patch pipettes (final concentration approximately 100 µM following the brief loading period, see Methods). Following SD, large rises in intracellular Ca^{2+} concentration occurred initially in distal dendrites and then propagated toward the soma (Figures 1A-C). Intracellular Ca^{2+} concentration returned first to baseline levels in soma, but Ca^{2+} remained at levels estimated above 10 µM in dendrites for significantly longer periods of time (~2 min), before recovering to baseline levels (Figures 1A&B show a representative example, and Figure 1C shows mean data from 8 neurons).

The sustained dendritic Ca^{2+} elevations were highly sensitive to the competitive NMDA receptor antagonist DL-AP5. Figures 1D-F show effects of bath application of a low concentration of DL-AP5 (20 µM). This concentration was chosen as it did not prevent the initiation and propagation of SD under these conditions (Aiba et al., 2012; see also Figure 4). With bath application of DL-AP5, initial Ca^{2+} concentration increases at the soma were indistinguishable from those observed in control experiments (peak Ca^{2+} concentration, Control: 11.5 ± 0.8 µM (n=8), DL-AP5: 12.5 ± 1.0 µM (n=7), $p>0.1$, Figures 1C *vs.* 1F), however

the duration of dendritic Ca^{2+} elevations were markedly shortened such that dendritic recovery was almost coincident with recovery in soma in the presence of DL-AP5 (Figures 1E&F).

2.4.2 Increased glutamate release during the repolarization phase of SD

To investigate mechanism(s) underlying NMDAR-dependent dendritic Ca^{2+} loading, we first characterized excitatory synaptic inputs during the course of SD (**Figure 2**). The baseline frequency of spontaneous excitatory postsynaptic currents (sEPSCs) was low (0.9 ± 0.16 Hz, n=9, Figure 2Aa), and application of the SD stimulus resulted in an immediate increase in the frequency of sEPSCs that persisted until the arrival of SD at the recording electrode (20.4 ± 3.5 Hz, mean duration of prodromal period: 4.6 ± 0.9 s, n=9, Figure 2Ab). The arrival of SD was then detected as a large monophasic inward whole-cell current ~3 seconds after stimulus application, with an accompanying initial rapid extracellular potential change. Input resistance decreased to ~10% of baseline levels during the large inward current, preventing reliable measurements of sEPSCs during the early phase of SD.

sEPSCs reappeared during the decay of the SD current (Figure 2Ac) and Figure 2B emphasizes that the mean sEPSC frequency during the recovery from the large SD current was invariably greatly increased, before declining back to baseline levels. Figures 1B, C show quantitative analyses of sEPSC frequency and amplitude during the late SD phase. The increased sEPSC frequency was not due to the fact that sEPSC amplitudes were increased and allowed

previously sub-threshold events to be detected. In fact, the amplitudes of sEPSC were significantly decreased compared to baseline during the late SD phase (baseline: 32.0 ± 3.6 pA, late-SD phase: 22.8 ± 2.8 pA, n=9, $p<0.001$), suggesting that the increased apparent EPSC frequency is largely attributable to increased presynaptic release.

In addition to increased sEPSC frequencies, we occasionally observed large (>1 nA) inward sEPSCs during the late SD phase (data not shown). These events may be related to burst discharges reported following SD (see Discussion), however these events were not reproducibly detected in the current study and were excluded from analysis.

Action potential dependent release made a contribution to increased sEPSC frequencies. In a separate set of experiments, block of voltage-gated sodium channels with tetrodotoxin (TTX, 1 µM) prevented sEPSC frequency increases during the prodromal excitation phase (n=12) and significantly reduced the frequency of events recorded immediately following the large SD current (Figure 2B), with less effect on subsequent recovery to baseline. Activation of presynaptic NMDARs has been shown to increase release probability (Larsen et al., 2011; McGuinness et al., 2011), however addition of DL-AP5 (20 µM) together with TTX did not significantly affect sEPSC frequency in the present study (Figure 2B). TTX and DL-AP5 also had no significant effect on sEPSC amplitudes (Figure 2C, $p=0.09$). Thus, glutamate release during the late SD phase appeared to be mediated by both action potential-dependent and -independent release mechanisms. The effect of DL-AP5 alone on sEPSC

frequency was also analyzed in a different set of experiments (used also to generate Figures 4F&G, below) and was without effect (n=6, p>0.1). The lack of effect of DL-AP5 on sEPSC frequency also suggests that activation of postsynaptic NMDAR, rather than presynaptic NMDAR are responsible for prolonged dendritic Ca^{2+} loading after SD.

2.4.3 Increased evoked release during the late-SD phase

Increased release probability following SD was confirmed from changes in paired pulse ratio (PPR) of evoked EPSCs (**Figure 3**). EPSCs could not be evoked during the SD inward current, but reappeared with greatly decreased PPR only after full recovery of the current (Figures 3A&B). During this period, membrane responses to test pulses had recovered to control levels, but the rise times and decay time constants of evoked EPSCs were significantly increased (Figure 3C, time to peak: 388.4 ± 33.5%, decay tau: 204.7 ± 20.0% of baseline, n=8). Traces in the late SD period were heavily contaminated with sEPSCs as discussed above (Figure 3C). Bath application of DL-AP5 (20 μM) partially normalized the slow decay time constants of EPSCs during this period (151.7 ± 38.2%, n=8, p<0.05 *vs.* control), implying a role for NMDAR activation. Similar to lack of effects on sEPSC frequency, DL-AP5 did not affect changes in PPR associated with SD (Figure 3B). Taken together with results of Figure 2, these results suggest that both action potential-dependent and -independent release mechanisms can be enhanced during the late SD phase.

Following the period of excitation, a prominent suppression of evoked activity occurred after SD (mean duration 5.14 ± 0.71 min, measured using 70% recovery as a threshold, n=8). This secondary suppression is likely due to activation of adenosine A_1 receptors (Lindquist and Shuttleworth, 2011). The present report concentrates only on consequences of increased NMDAR activation that occur earlier, immediately following the onset of SD.

2.4.4 NMDAR activation contributes to the duration of SD depolarizations

The relationship between single cell membrane potential changes and extracellular DC potential shifts is shown in **Figure 4A.** Similar to previous recordings with sharp electrodes (Canals et al., 2005), whole-cell recordings of KCl-induced SD in CA1 pyramidal neurons showed complete depolarization and full recovery took ~1 min. The secondary phase of extracellular DC signals (i.e. the second maximum of the inverted saddle-like waveform) coincided with the slow single-neuron repolarization. Because no correction for extracellular voltage shifts was applied to single cell recordings, neuronal depolarizations are likely underestimated (see Methods). Thus during the late SD phase, depolarization is expected to be sufficient to relieve Mg^{2+} block of NMDARs and, when coupled with increased glutamate release described above, should result in substantial NMDAR activation. This was confirmed in studies showing that bath application of DL-AP5 significantly decreased the duration of neuronal depolarization (Figures 4B&C), without affecting peak depolarization (peak amplitudes: 0.79 ± 5.7 mV *vs.* -2.06 ± 6.6 mV, control and DL-AP5, respectively

p>0.5, n=7). Full washout of DL-AP5 effects was confirmed in two experiments where whole-cell recordings were maintained through three consecutive SDs. Furthermore, the duration of the secondary phase of extracellular DC shifts was also reversibly decreased by DL-AP5 application (Figures 4D&E). Finally, the duration of the large inward current during SD was also significantly reduced by DL-AP5 (Figures 4F&G). These experiments imply that NMDAR activation during the late SD phase is an important contributor to the long lasting neuronal depolarization.

2.4.5 Delayed antagonist applications confirmed a contribution of NMDAR activation during the late-SD phase

The results above suggested that increased release and consequent activation of NMDARs following the onset of SD could contribute to prolonged ionic deregulation. This possibility was first examined by testing the effects of localized application of DL-AP5 selectively in the period immediately following the onset of SD onset, when recording extracellular DC shifts (**Figure 5A-C**). The antagonist was delivered with pressure pulses from glass micropipettes (5-10 µm diameter) placed close (<20 µm) to the recording electrode. High pipette concentrations of NMDAR antagonists were used (500 µM DL-AP5 or 200 µM MK801) to obtain rapid onset and localized block, and in the first set of experiments the pulse application was initiated immediately following onset of the initial potential shift (Figure 5A&B). In each experiment, a single SD (SD1) was first generated in the presence of the delivery electrode, but without drug

ejection, and this was followed by a second SD (SD2) in which the antagonist was delivered with pressure pulses (20 ms, 10-15 repetitions at 1.5 Hz). Selective application of DL-AP5 immediately following SD significantly decreased the duration of extracellular potential changes and similar results were obtained with MK801 (200 µM, duration SD2/SD1: 0.745 ± 0.004, $p<0.05$ *vs.* vehicle, n=5). Pressure pulses of vehicle solution (ACSF with 0.1% DMSO) showed no significant effect (Figure 5A&C), indicating that any mechanical stress induced by the pressure pulses did not contribute to these effects. These results imply that NMDAR activation during the late-SD phase is a significant contributor to the secondary extracellular potential change.

We next tested the possibility that prolonged Ca^{2+} elevations described in Figure 1 could be a consequence of NMDAR activation following SD, using the same localized DL-AP5 applications described above. This possibility was tested by localized pressure application of DL-AP5 only during the period of dendritic Ca^{2+} overload immediately following the onset of SD. As shown in Figure 5D-F, sustained dendritic Ca^{2+} elevations were completely prevented by this approach. No effect was observed in control studies with ACSF-filled ejection electrodes (n=3). These data suggest that NMDAR activation during the late-SD phase could underlie sustained dendritic Ca^{2+} loading.

2.4.6 NMDAR inhibition during the late-SD phase is protective against SD in energy- depleted neurons

We have previously reported that sustained dendritic Ca^{2+} elevations can be a key contributor to excitotoxic injury of neurons in slice (Shuttleworth and Connor, 2001), and in a model of NMDAR overactivation this can be due to energy depletion in these vulnerable compartments (Vander Jagt et al., 2008). We tested here whether the late-SD NMDAR activation could cause neuronal injury by a similar mechanism. We tested this hypothesis by increasing the vulnerability to SD-induced injury in single cells without changing the population response (and thereby the initiation or propagation of SD). This was done by dialyzing single neurons with an internal solution containing an inhibitor of mitochondrial respiration (NaN_3, sodium azide, in dialysis pipette) and reduced ATP. The composition of the pipette solution and dialysis duration was determined from a series of pilot experiments modifying both ATP and sodium azide concentrations during brief (3-5 min) application, to obtain conditions that induced metabolic stress, but did not alone cause acute injury. Dialysis (5 min) with internal solution containing 1 mM sodium azide and lacking any added ATP resulted in a significantly decreased input resistance (% change; -40.4 ± 5.0% *vs.* +1.1 ± 5.2%, azide *vs.* control, n=5, $p<0.01$), likely due to the activation of ATP sensitive potassium currents (Sun et al., 2006). It is noted that equilibration of the pipette content and the cytosol would be incomplete with these short dialysis periods. No progressive depolarization or action potential bursts were observed with this dialysis and in addition, basal Ca^{2+} concentrations were maintained at

physiological levels until SD challenge (estimated Ca^{2+} concentration in soma: 0.170 ± 0.041 µM, n=10).

Dialysis with the metabolic inhibitor greatly impaired recoverability from Ca^{2+} elevations after SD **(Figure 6)**. Thus in control experiments, dendritic Ca^{2+} concentrations were sustained at high levels following initial Ca^{2+} increases (Figure 6A&B), with no signs of recovery throughout the duration of recordings. Ca^{2+} levels in the soma showed some transient recovery after SD, but invariably increased again to very prolonged Ca^{2+} elevations above 10 µM (Figure 6A&B). Under these conditions, 4 out of 5 neurons showed no recovery of soma or dendrite Ca^{2+} levels within 10 min (Figure 6E). It is emphasized here that such prolonged Ca^{2+} deregulation was never observed in the neurons dialyzed with a control internal solution (see Figure 1A-C above). Delayed application of DL-AP5 was very effective at preventing loss of Ca^{2+} homeostasis in these metabolically compromised neurons (Figure 6C-E). Thus in neurons dialyzed with the metabolic inhibitor, late DL-AP5 exposure resulted in prompt and complete recovery of Ca^{2+} levels in both soma and dendrites (n=5). When the same neurons were then challenged with another SD following DL-AP5 washout (>15 min), all cells generated sustained Ca^{2+} overloading similar to the pressure controls (n=5).

Ca^{2+} deregulation following SD was associated with significant loss of the Ca^{2+} indicator, (Fura-6F), and this was suggestive of acute injury as discussed previously (Vander Jagt et al., 2008). However reliable analyses of membrane permeability were difficult because of poor signal-noise ratio with the low Fura-6F

concentrations used here, and background autofluorescence changes during SD. Therefore a parallel set of studies was conducted with neurons loaded with the membrane impermeable fluorescent indicator Lucifer Yellow (0.2% in NaN_3 containing internal solution, hereafter termed LY). Indictor leak was assessed from fluorescence intensity in soma, and showed that profound loss of intracellular LY always occurred after SD in metabolically-compromised neurons (**Figure 7A&C**). This fluorescence loss was attributable to acute increase in membrane permeability, caused by NMDAR activation during the late-SD phase, rather than photobleaching or other detection artifact. Thus indicator levels were well-maintained by delayed NMDAR block after SD (localized pressure application of DL-AP5, as described above, Figure 7B&C) and profound indicator loss was then observed in the same neurons after DL-AP5 washout and subsequent challenge with a second SD (Figure 7C). These results suggest that the NMDAR activation that occurs specifically in the late phase of SD contributed to the development of Ca^{2+} overload and decreased membrane integrity in metabolically-compromised neurons.

2.4.7 NMDAR activation contributes to extended depolarization of SD in energy-depleted preparations

We first examined the effect of partial metabolic inhibition on the duration of extracellular DC shifts and sensitivity to delayed NMDAR block. In each experiment, a pair of SDs was generated and slices were exposed to sodium azide prior to the second SD. The effects of delayed DL-AP5 application (or

saline control) were tested on the second SD, using the localized pressure application method described above (Figure 5). A series of pilot experiments was conducted and determined that exposure to 1 mM sodium azide for 5 min prior to SD (and maintained throughout the experiment) was the maximum that could be tolerated without disrupting the initiation of SD. Under these conditions, the duration of extracellular potential shift was increased by sodium azide pre-exposure in all preparations tested with the saline control pulse (n=5, 32.6 ± 3.6% increase from control, $p<0.005$, paired *t*-test, **Figure 8A&B**). In contrast, delayed DL-AP5 pressure application prevented the prolongation of DC duration in sodium azide. The smaller effect of NaN_3 on the duration of extracellular potential (compared with Ca^{2+} deregulation in Figure 6) may be due in part to less severe metabolic inhibition compared with direct intracellular dialysis of azide without added ATP.

We next examined the effects of metabolic compromise and NMDAR activation on the duration of single neuron depolarizations. We used a similar intracellular dialysis approach as described above (Figures 6&7) but with lower sodium azide concentrations so that whole-cell configuration could be maintained during dialysis and subsequent SD challenge (total ~30min recording). The composition of the pipette solution was determined from a series of pilot experiments modifying sodium azide concentrations (20 µM-1 mM) in ATP-free internal solution. From these studies, 300 µM was the maximal sodium azide concentration that could be used. Under these conditions, the durations of single cell depolarizations were significantly increased (Figures 8C&D). Delayed

applications of high DL-AP5 concentrations could not be tested in these experiments, because of sensitivity to movement caused by pressure pulses. However bath application of a moderate concentration of DL-AP5 (20 µM, 10 min, which was not sufficient to prevent SD; see above) significantly reduced the prolongation of depolarization in energy-depleted neurons (Figures 8C&D). Together, these data are consistent with a role for NMDAR activation in prolonged depolarization and extracellular DC shifts in the context of metabolic compromise.

2.5 DISCUSSION

2.5.1 General

The present study characterized an excitatory event during the recovery phase of SD that could contribute to neuronal injury. Our recordings of sEPSC frequency and PPR suggest that presynaptic glutamate release is enhanced during the late-SD phase, while neurons are still repolarizing. Both action potential-dependent and -independent mechanisms can contribute to enhanced release, and NMDAR activation during late-SD phase contributed to extended neuronal depolarization. This excitatory event during the late-SD phase contributed to prolonged intracellular Ca^{2+} elevations in neuronal dendrites and (when combined with metabolic compromise) was sufficient to lead to neuronal injury. These findings identify a link between SD and excitotoxic signaling at the cellular level, and could suggest novel approaches to prevent conversion of SD to a damaging event in metabolically compromised tissue.

2.5.2 Characterization of a late excitatory phase of SD

Spontaneous EPSC frequency was initially elevated during the brief prodromal excitation phase. During the large inward current of SD, a large reduction in membrane resistance hindered EPSC detection, but enhanced EPSCs were detected as soon as membrane resistance recovered (Figure 2A). Thus although not directly tested, these data leave open the possibility that presynaptic release probability was continuously elevated throughout the SD

event. Significant NMDAR-dependent cation loading should be dependent on both release probability and the level of postsynaptic depolarization, and a substantial contribution would be expected during the late SD phase when neurons remain partly depolarized and with significant gradients for ion influx.

The recorded increases in EPSC frequency likely reflect increased presynaptic release, rather than increased sensitivity of event detection due to changes in either input resistance or extracellular glutamate accumulation. Thus in addition to increased EPSC frequencies observed after complete recovery of membrane resistance (see Figure 3C) significant decreases in PPR (consistent with increased initial presynaptic release probability) were also demonstrated throughout the late-SD phase. It is noted that that evoked synaptic transmission (requiring TTX-sensitive channels) was beginning to recover at an early time point (~35s in the example shown in 3A), when postsynaptic repolarizations was likely incomplete (see Figure 3&4, see also Canal *et al.*, 2005). This early presynaptic recovery likely underlies the TTX-sensitivity of sEPSCs seen in Figure 2B. The mechanism(s) underlying increased release probability will be important to identify, and could include a combination of factors including presynaptic Ca^{2+} elevations and saturation of presynaptic Ca^{2+} buffers, as well as changes in extracellular osmolarity and potassium concentrations (Sara et al., 2002; Somjen, 2002; Blatow et al., 2003).

There have been several prior voltage-clamp recordings of SD, but none appear to report an increase in release during the late SD phase (Czeh et al., 1993; Zhou et al., 2010a). It is possible that different experimental methods

(including age of animals, and the use of local microinjection of KCl rather than bath applications to generate SD) might have made it easier to detect excitation during the late-SD phase in the present study**.** In addition, the lower recording temperatures required for these whole-cell recordings (31-33^{o}C) may have made SD less intense, and thus facilitated recording of the late excitatory phase.

Spiking activity in the late-SD period has been observed in previous recordings using either extracellular or intracellular sharp microelectrode recordings from brain slices (e.g. Pomper et al., 2006), and also *in vivo*. Indeed, in his initial description of spreading depression of cortical activity, Leao (1944) noted a "burst of spikes following a slow negative wave" and a burst of high frequency electrical activity was also illustrated during the decay of extracellular potential in an study of cortical spreading depression in rodents (Takano et al., 2007). Bursting activity during the late-SD phase was also reported in a recent clinical study, detected as epileptic discharges occurring on the slow extracellular potential shift (Dreier et al., 2011). Residual postsynaptic depolarization alone could facilitate conversion of subthreshold postsynaptic potentials into spikes in the late-SD phase, however coincident increases in presynaptic release probability could be a significant contributor in these other studies.

2.5.3 Prolonged NMDAR receptor activation during the late- SD phase

NMDAR activation is well-established to contribute to the initiation and/or spread of SD (see Introduction), however, it has not previously been clarified whether ongoing NMDAR activation can also contribute significantly to

consequences of SD. This was investigated in the present study by using two approaches; 1) bath applications of a low concentration of NMDAR antagonist, that itself had no effect on SD initiation and propagation (see Aiba et al., 2012), and 2) focal delivery of NMDA antagonists, applied by pressure pulses only after the passage of SD past the recording site. These present studies revealed a brief (~2 min), but important, period of NMDAR activation during the late-SD phase.

A persistent phase of NMDAR activation was also demonstrated during anoxic depolarizations generated by simulated ischemia in hippocampal slices, although in that case reverse transport of glutamate under anoxic conditions appeared to be a major contributor (Rossi et al., 2000), rather than the increased synaptic glutamate release observed here with normoxic SD.

Recent work has shown that extended duration of DC shifts correlates with poor outcomes of brain trauma patients (Hartings et al., 2011b). The present studies raise the possibility that NMDAR activation during the late SD phase could contribute to these long events, based on the sensitivity to delayed antagonist application of secondary extracellular potential shifts Interestingly, in the clinical recordings, it was noted that long duration events were often accompanied by saddle-like waveforms, (Hartings et al., 2011b). The present results are consistent with the idea that activation of NMDARs during the late-SD phase could underlie saddle-like waveforms (see also Introduction). The simultaneous measurements of extracellular potential shifts and membrane potential (see Figure 4A) suggest that the secondary phase of slow potential

changes occurs during the repolarization phase of neuronal membrane potentials. Due to its nonselective-cationic nature and voltage-dependent magnesium block (Spruston et al., 1995), charge transfer through NMDARs is expected to be minimal during complete depolarizations immediately following the arrival of SD, and then increase as neurons begin to repolarize (see Figure 4A).

Extracellular potential shifts of SD are larger and are also more sensitive to NMDAR antagonists when recorded in hippocampal dendritic fields, when compared with recordings from the cell body layer (Herreras and Somjen, 1993a). Thus NMDAR contributions to DC recordings in neocortex may be complicated by the complexity of signal sources. Further studies are therefore needed to address the association of injurious NMDAR activation with extracellular potential durations and waveforms in clinical recordings.

2.5.4 Cellular Mechanisms of Injury

Large intracellular Ca^{2+} elevations during SD have been inferred from extracellular measurements of Ca^{2+} decreases following SD (Somjen, 2001), and are confirmed by more recent intracellular measurements (Kunkler and Kraig, 2004; Dietz et al., 2008; Gniel and Martin, 2010). Using the low affinity indicator Fura-6F, it was shown that under normoxic conditions, recovery of intracellular Ca^{2+} elevations in CA1 neurons took substantially longer in dendritic compartments than in somata (Dietz et al., 2008). In the present work, it is

shown that these sustained Ca^{2+} elevations are due to persistent NMDAR activation in the late SD period.

Excessive cytosolic Ca^{2+} elevations are well established to lead to some forms of neuronal death, and small dendritic compartments may be important injury initiation sites (Connor et al., 1988, Shuttleworth & Connor 2001). Brief intensive glutamate receptor activation has been shown to trigger dendritic Ca^{2+} deregulation that propagates from dendrites, even in the absence of continued agonist stimulation (Wadman and Connor, 1992; Shuttleworth and Connor, 2001). A dendritic initiation site for excitotoxic injury was also observed with continuous NMDA exposures (Vander Jagt et al., 2008) and in that case propagation of dendritic Ca^{2+} overload was due to depletion of metabolic reserves and reversed by delayed NMDA receptor block (Vander Jagt et al., 2008). In other studies with glutamate microstimulation, a transition was observed between rapid recovery of dendritic Ca^{2+} elevations with single stimuli, and very prolonged or irrecoverable increases following repetitive stimulation (Connor and Cormier, 2000). SD shares some similarities with these prior excitotoxicity studies, as there was substantial glutamate release during the late SD period, resulting in NMDAR activation and sustained dendritic Ca^{2+} elevations. These sustained dendritic Ca^{2+} elevations peaked ~1 min following the onset of SD (Figure 1A-C), during the period of neuronal repolarization.

When metabolic capacity was selectively reduced in a single cell (while permitting normal SD propagation), dendritic Ca^{2+} and somatic Ca^{2+} levels remained very high following SD, and neurons showed signs of acute neuronal

injury (Figure 6&7). Severe increases in membrane permeability were verified by loss of the fluorophore Lucifer yellow, and were almost completely prevented by selective application of an NMDA receptor antagonist during the late-SD phase. At least part of the effect is likely due to extended depolarization and additional Ca^{2+} influx, since metabolic inhibition also prolonged depolarization in an NMDA-dependent manner (Figure 8). However it is noteworthy that the durations of Ca^{2+} elevations were more severely prolonged than were the neuronal and extracellular depolarizations (compare Figures 6&8). Part of the reason for this mismatch could be a technical limitation, since it was not possible to achieve the same level of metabolic inhibition in the experiments in Figure 8 (see Results). However the duration of sustained Ca^{2+} elevations is also determined by Ca^{2+} extrusion rates. Reduction of extrusion rates is expected in metabolically compromised tissues, and this may contribute significantly to the duration of Ca^{2+} deregulation and neuronal injury demonstrated in Figures 6&7. These results suggest that consequences of NMDAR activation during the late-SD period could be a significant contributor to conversion of normally irrecoverable SD to irrecoverable injury observed in metabolically compromised tissue.

2.5.5 Conclusions

The present study provides a link between SD and cellular mechanisms of excitotoxic neuronal injury. Characterization of enhanced glutamate release during a period of postsynaptic vulnerability suggests temporal NMDAR targeting

and/or approaches other than NMDAR antagonists (e.g. targeting presynaptic release) may be considered to limit deleterious effects of SD in the injured brain.

2.6 FIGURE LEGENDS:

Figure 2.1: NMDAR activation contributes to prolonged dendritic Ca^{2+} loading after SD.

A-C: Intracellular Ca^{2+} dynamics during SD monitored in single neurons loaded with Fura-6F in control conditions (n=8). SD was generated by local microinjection of KCl (>200 µm from recorded neurons) and Fura-6F ratios were determined at 1 Hz. **A:** Raw image of Fura-6F fluorescence (380 nm excitation, left panel, scale bar: 20 µm) and selected pseudocolored images representing intracellular Ca^{2+} levels at times indicated in minutes. Calculated Ca^{2+} concentrations from this neuron are shown in **B** (soma values in blue, dendrite values determined from region indicated by arrows are in red). **C:** Mean data from 8 such control experiments. **D-F:** As described above, except that slices were pre-exposed to 20 µM DL-AP5 for 10 min prior to SD (n=7 for panel F). Note the rapid recovery of dendritic Ca^{2+} levels in AP5, despite the similar initial Ca^{2+} loading in soma and dendritic compartments.

Figure 2.2: Increased spontaneous EPSP frequency following the initial depolarization of SD. **A:** Representative traces of simultaneous whole-cell current (I_m: voltage clamped at -50 mV) and extracellular DC potential recordings. SD was generated by local microinjection of KCl (>200 µm from recording site,

application time indicated by *) and was recorded from single pyramidal neuron and corresponding dendritic field. The image shows locations of the whole-cell patch pipette, extracellular DC recording electrode and KCl ejection pipette (highlighted by dashed lines). Traces in a-c show recordings from baseline (a), prodromal (b) and late-SD (c) phases of the whole-cell current at an expanded time base to show increases in sEPSC frequency associated with SD. Membrane responses to test pulses are marked by #. **B:** Plot showing mean increases in sEPSC frequency associated with SD. In control conditions (diamonds, n=6), sEPSC frequency to >30 Hz, and slowly recovered over the subsequent minute. Time was adjusted to the onset of SD (t=0, indicated by arrow head) and mean sEPSC frequency is shown in 10 second bins. sEPSC frequencies during the first 20 seconds after SD onset were excluded, because the quality of voltage-clamp could not be verified during the initial phase of the large SD current. Tetrodotoxin (TTX, open squares, n=12) significantly reduced sEPSC frequency at time points indicated by asterisks ($p<0.05$ compared with controls), but co-application of with DL-AP5 did not further affect sEPSC frequency (triangles, n=6, $p>0.20$). **C**. sEPSC mean amplitudes were not significantly altered, when tested at the first time point shown after SD (asterisk in Figure 2B).

Figure 2.3: Increased release probability during the late-SD phase as assessed from paired-pulse ratios (PPR). A: Representative trace of voltage-clamp recording during SD. Whole-cell current was recorded at -50 mV with

bipolar stimulation of Shaffer-collaterals. Paired stimulation (100 ms interpulse interval) was delivered at 0.2 Hz, and evoked EPSCs appear as sharp vertical lines and are expanded in the insets (a-c). Note the reversed PPR and slow EPSC kinetics during the late-SD phase (b). **B:** Quantitative analysis of PPR changes in control conditions (n=8) and in the presence of DL-AP5 (20 μM, 10 min, n=8). Data during the late-SD phase were collected from the initial 3-5 responses. DL-AP5 did not show any significant effects on PPR throughout the recordings. **C:** Representative traces showing membrane responses to test pulses (-10 mV, 200 ms) and the waveform of single evoked EPSCs during baseline and in the late-SD phase. Note that the membrane response to the test pulse shows almost full recovery. On the other hand, kinetics of evoked EPSC was significantly slowed in the late-SD phase (see Results). Spontaneous EPSCs occurring during the late-SD phase are indicated by arrow heads.

Figure 2.4: NMDAR antagonism accelerated repolarization and current decay of SD. **A:** Simultaneous recording of membrane potential (V_m) and extracellular DC potential changes associated with SD, demonstrating the extended neuronal depolarization during the late SD phase. Test current pulses (-200 pA, 500 ms, downward deflections in V_m) were applied periodically throughout the recordings to monitor seal quality and assess input resistance changes. **B:** Example traces from a single neuron, showing membrane depolarizations during a control SD and then during a second SD generated in DL-AP5 (20 μM, 10 min exposure, 20 min interval between SDs). DL-AP5

significantly decreased the duration of depolarization and this effect was completely reversed following DL-AP5 washout in recordings from this neuron. **C:** Mean data from similar experiments where the effects of DL-AP5 were tested in separate populations of control and AP5-treated preparations. Mean durations of 10-90% repolarization are presented (data pooled to give total of 7 recordings for each bar; 2 where repetitive SDs could be recorded from single neurons, and 5 from single SDs in each condition, *p<0.05). **D:** Example traces from a single slice, showing extracellular DC potential changes during a control SD and then during a second SD generated in DL-AP5 (20 µM, 10 min exposure, 20 min interval between SDs). **E:** Mean data from 5 such experiments and showing reversibility after DL-AP5 washout. Duration was determined from the time to 70% recovery from the initial peak. * p<0.05. **F:** DL-AP5 (20 µM, 10 min) also decreased duration of large inward current during SD. SD currents were normalized to peak responses, and average waveforms from control (solid line, n=6) and DL-AP5 (dashed line, n=6) are shown. Data pooled to give a total of 6 recordings for each trace; 3 where repetitive SDs could be recorded from single neurons, and 3 from single SDs in each condition). **G**: Mean data showing the time to 50% recovery from peak currents, in the population of neurons shown in F. *p<0.05

Figure 2.5: NMDAR activation during the late-SD period underlies prolonged ionic loads. A-C: Delayed pressure application of DL-AP5 (after the passage of SD) significantly decreased the duration of extracellular DC

potentials. A: Time control showing that the duration of DC shifts was reproducible when repetitive SDs were generated in a single slice. Localized pressure application of vehicle (0.1% DMSO, during time indicated by horizontal bar) during the second SD (gray trace) did not cause any reduction on DC response compared with the initial SD (black trace). **B:** In contrast, delayed DL-AP5 application significantly decreased the duration of the DC shift (gray trace), compared with the initial control response in the same slice (black trace). **C:** Mean data from 5 such vehicle and AP5 studies (**p<0.01) **D-F:** Delayed NMDAR block prevented prolonged dendritic Ca^{2+} loading after SD. D**:** Raw image of Fura-6F fluorescence (380 nm excitation, left panel, scale bar: 20 μm) and selected pseudocolored images representing intracellular Ca^{2+} levels at times indicated in minutes. Calculated Ca^{2+} concentrations from this neuron are shown in **E (**soma values in blue, dendrite values determined from region indicated by arrows are in red). **F:** Mean data from 5 such experiments. Horizontal bars indicate the duration of localized DL-AP5 applications.

Figure 2.6: Prolonged NMDAR activation contributes to neuronal injury in metabolically compromised neurons. Energy metabolism of single neurons was partially inhibited by brief dialysis with sodium azide-containing internal solution and Ca^{2+} responses during SD were then evaluated. **A:** Raw image of Fura-6F fluorescence (380 nm excitation, left panel, scale bar: 20 μm) and selected pseudocolored images representing intracellular Ca^{2+} levels at times indicated in minutes. Calculated Ca^{2+} concentrations from this neuron are shown

in **B** (soma values in blue, dendrite values determined from region indicated by arrows are in red). Note that even though there was an initial transient recovery of somatic Ca^{2+} responses after the initial peak, sustained Ca^{2+} deregulation rapidly developed throughout the neuron after SD. **C&D:** Same as described above for A&B, with the exception that DL-AP5 was applied locally to this selectively vulnerable neuron after the passage of SD. Note the prompt recovery of Ca^{2+} levels throughout the neuron. **E:** Population data from control (Gray traces, n=5) and DL-AP5-treated preparations (red traces, n=5), showing effectiveness of delayed DL-AP5 applications on neuronal Ca^{2+} overload, measured in somatic compartments of sodium azide-loaded neurons. Arrow head indicates SD onset and the horizontal bar indicates the duration of vehicle (ACSF) or DL-AP5 pressure pulse applications.

Figure 2.7: Prolonged NMDAR activation triggered significant membrane compromise in metabolically stressed neurons. Single neurons were loaded with 0.2% Lucifer yellow (LY) in sodium azide-containing internal solution, prior to SD challenge. These neurons showed profound loss of intracellular LY following SD (**A**), but such loss was almost completely prevented by delayed DL-AP5 application (**B**). Localized DL-AP5 applications were as described above in Figures 5&6. A&B show representative fluorescence images from single neurons. **C** shows mean indicator loss measured 10 min after SD. Responses of 4 control neurons (white bar) are compared with 4 neurons which were protected with delayed DL-AP5 pulses, and then subjected to a second SD after DL-AP5 washout (gray bars, **$p<0.01$ vs. control).

Figure 2.8: ***NMDAR activation contributes to extended depolarization of SD in energy-depleted preparations*** **A-B:** Effects on extracellular DC potential shifts. **A:** In each panel, a pair of SDs was generated in a single slice. The first SD was without drug applications (black trace) and the second was in the presence of sodium azide (1 mM, 5 min pre-exposure, gray trace) and also included localized pressure application of either saline or DL-AP5 (indicated by the horizontal bar). **B:** Summary data of DC durations (70% recovery) from 5 sets of each experiment shown in **A**. ***p<0.005, paired *t*-test between control SD and second SD with NaN_3 and pressure applications. **C-D:** Effects on single cell depolarizations. **C:** Representative traces under control conditions (top), in a neuron dialyzed with sodium azide (middle; 300 µM, NaN_3 in intracellular solution lacking ATP) and in an azide-loaded neuron with DL-AP5 bath application (bottom; 20 µM, 10 min exposure). Responses in each panel are from different preparations, recorded in consecutive experiments. **D:** Mean durations of neuronal depolarization (10-90% repolarization) from experiments shown in C. The duration of neuronal depolarization was significantly extended by sodium azide-dialysis (n=5) compared with control (n=4), and the effect was reversed by DL-AP5 (n=4). **p<0.01, *p<0.05, one way ANOVA with post hoc Turkey's multiple comparison test.

Figure 2.1

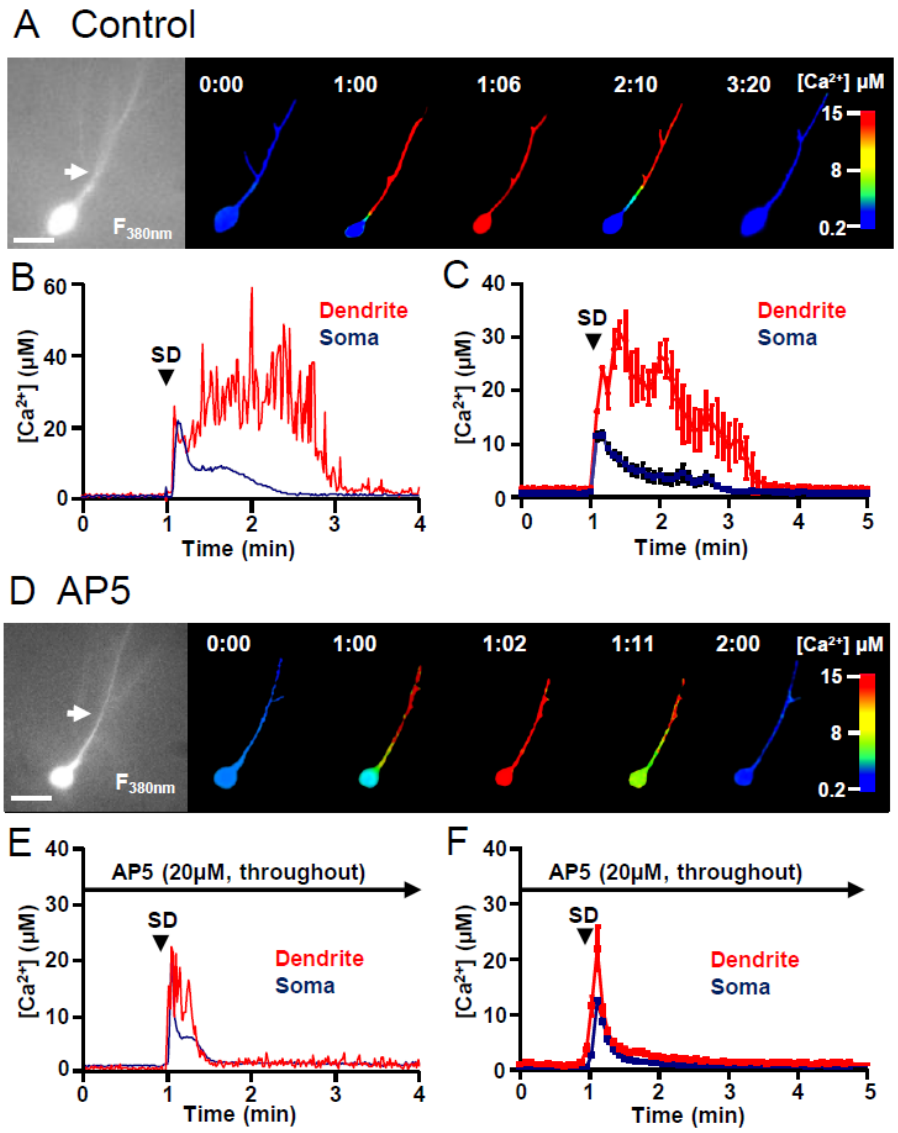
A Control
0:00
1:00
1:06
2:10
3:20
[Ca²⁺] µM
15
8
0.2
F380nm
B
C
[Ca²⁺] (µM)
SD
Dendrite
Soma
Time (min)
D AP5
0:00
1:00
1:02
1:11
2:00
E
F
AP5 (20µM, throughout)

Figure 2.2

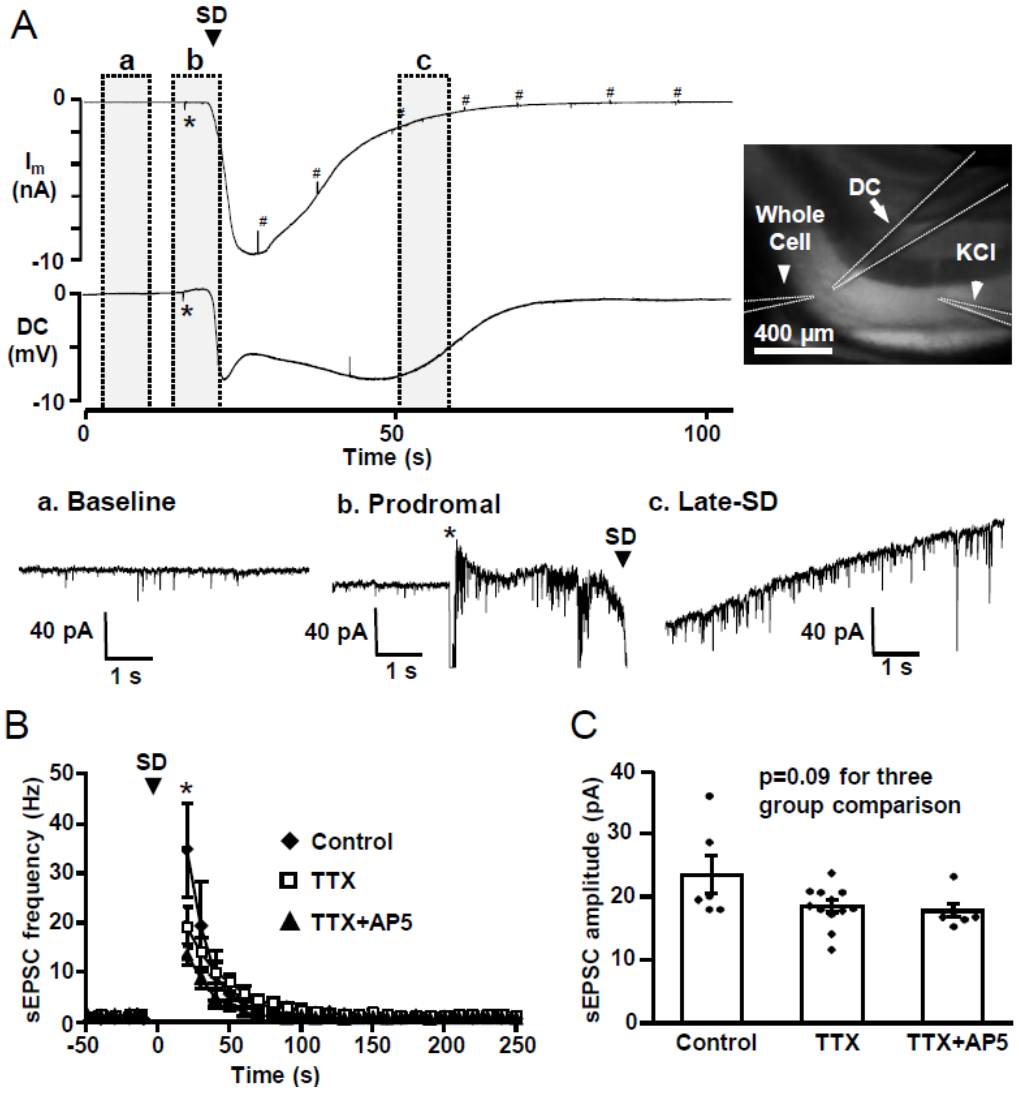
A
SD
a
b
c
0
-10
I_m (nA)
DC (mV)
0
50
100
Time (s)
Whole Cell
DC
KCl
400 µm
a. Baseline
b. Prodromal
c. Late-SD
40 pA
1 s
B
sEPSC frequency (Hz)
Control
TTX
TTX+AP5
Time (s)
C
sEPSC amplitude (pA)
p=0.09 for three group comparison
Control
TTX
TTX+AP5

Figure 2.3

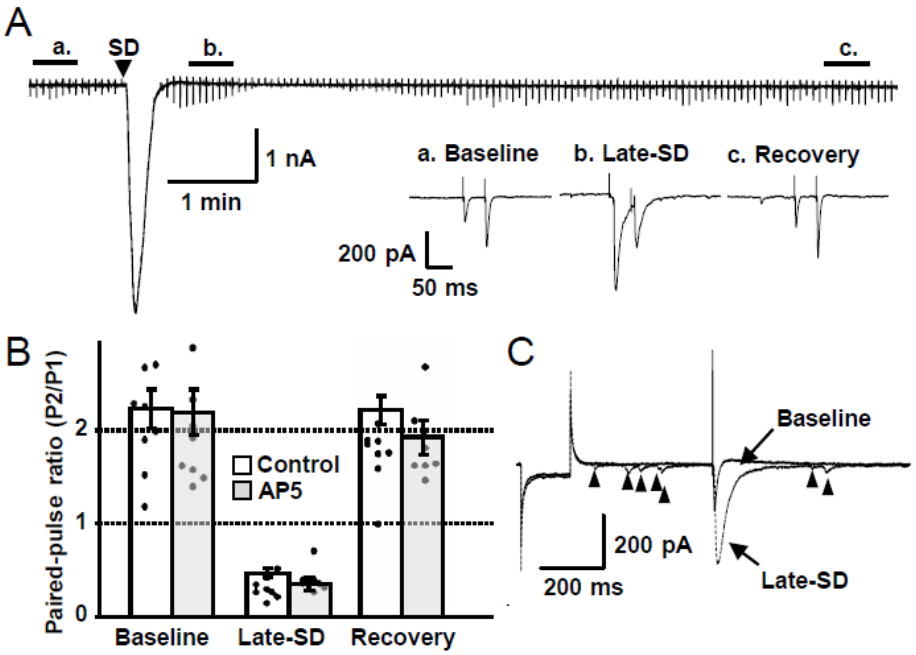
A
a.
SD
b.
c.
1 nA
1 min
a. Baseline
b. Late-SD
c. Recovery
200 pA
50 ms
B
Paired-pulse ratio (P2/P1)
2
1
0
Control
AP5
Baseline
Late-SD
Recovery
C
Baseline
200 pA
200 ms
Late-SD

Figure 2.4

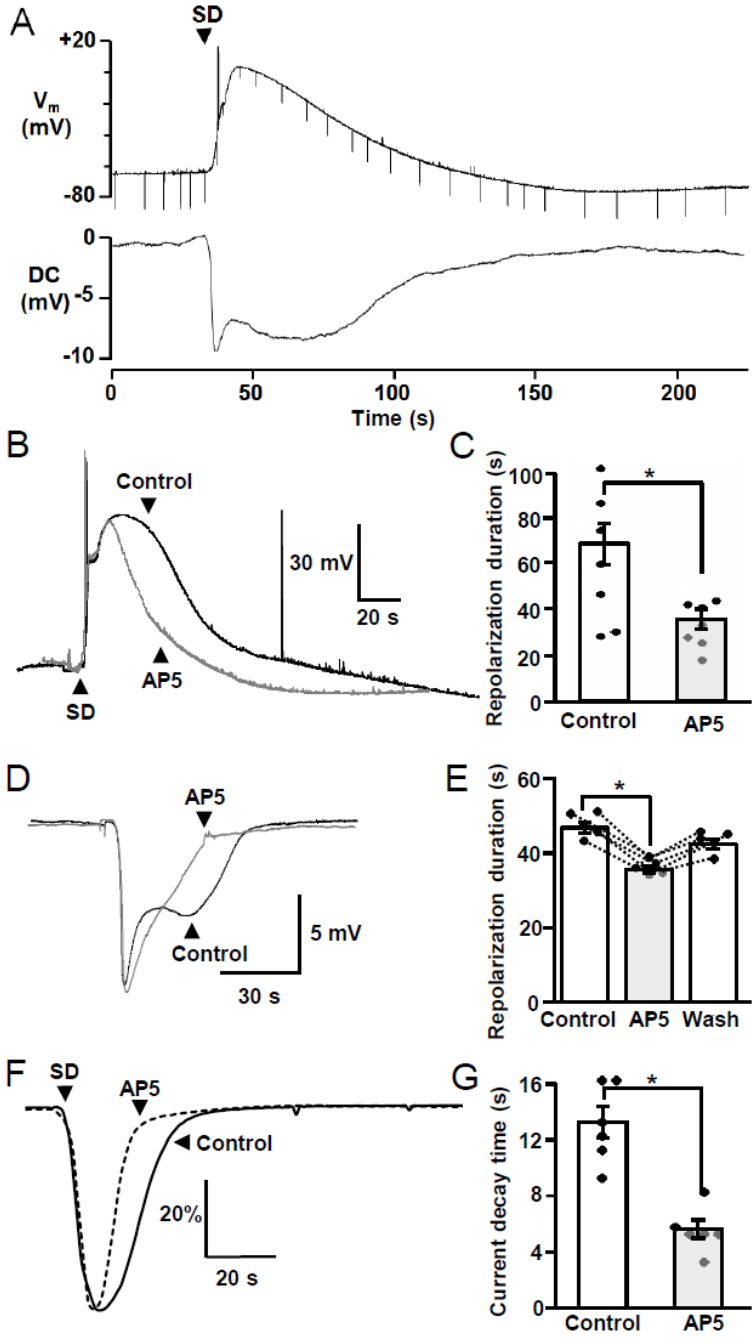
A
SD
+20
V_m (mV)
-80
0
DC (mV)
-5
-10
0
50
100
150
200
Time (s)
B
Control
30 mV
20 s
AP5
SD
C
Repolarization duration (s)
100
80
60
40
20
0
*
Control
AP5
D
AP5
Control
5 mV
30 s
E
Repolarization duration (s)
60
40
20
0
*
Control
AP5
Wash
F
SD
AP5
Control
20%
20 s
G
Current decay time (s)
16
12
8
4
0
*
Control
AP5

Figure 2.5

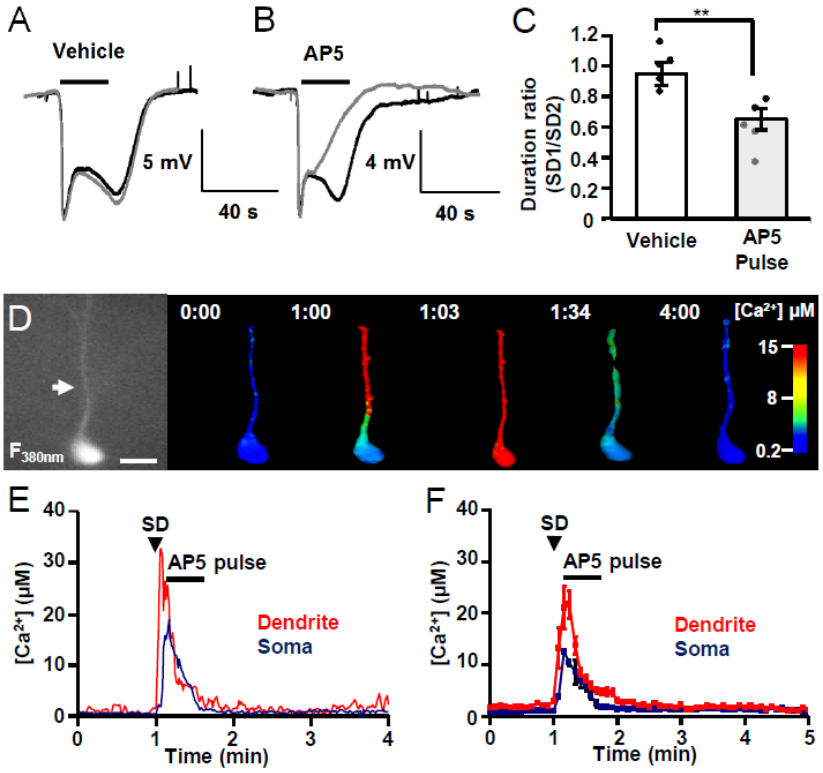
A
Vehicle
5 mV
40 s
B
AP5
4 mV
40 s
C
**
Duration ratio (SD1/SD2)
1.2
1.0
0.8
0.6
0.4
0.2
0
Vehicle
AP5 Pulse
D
0:00
1:00
1:03
1:34
4:00
[Ca²⁺] µM
15
8
0.2
F380nm
E
SD
AP5 pulse
Dendrite
Soma
[Ca²⁺] (µM)
Time (min)
F
SD
AP5 pulse
Dendrite
Soma
[Ca²⁺] (µM)
Time (min)

Figure 2.6

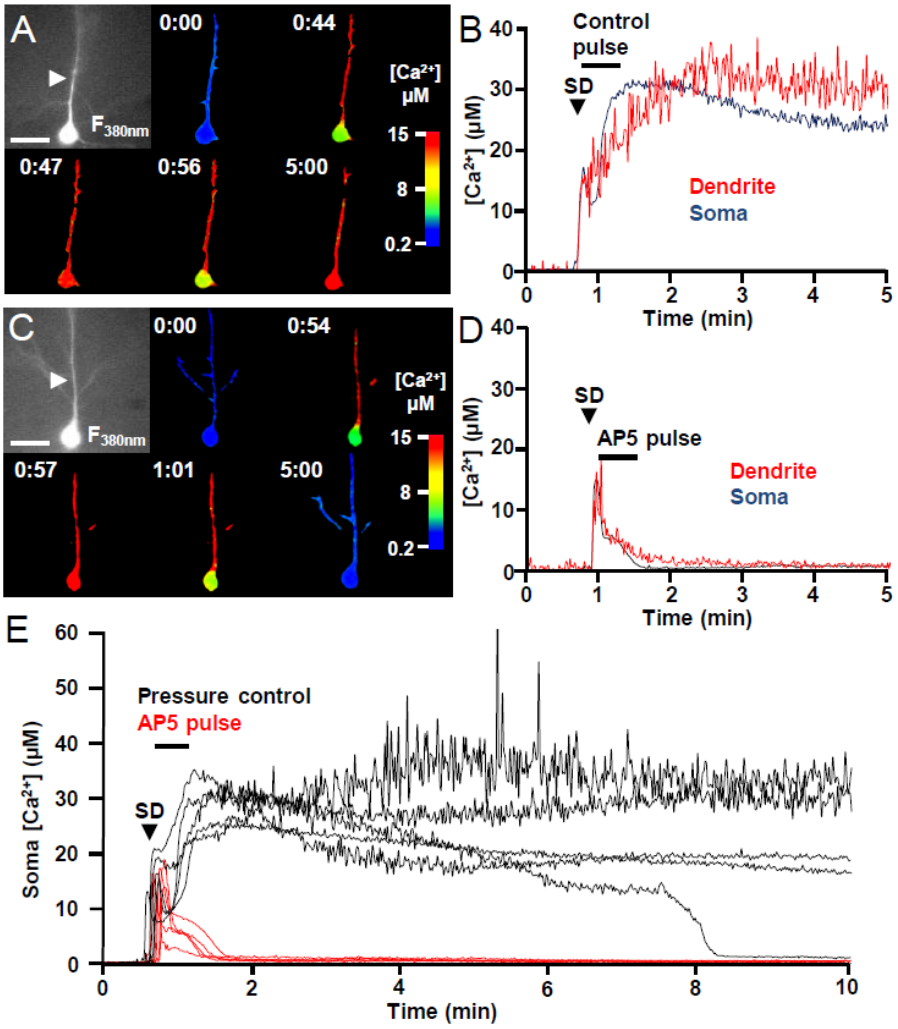
A
0:00
0:44
0:47
0:56
5:00
F380nm
[Ca2+] µM
15
8
0.2
B
Control pulse
SD
Dendrite
Soma
[Ca2+] (µM)
Time (min)
C
0:00
0:54
0:57
1:01
5:00
F380nm
[Ca2+] µM
15
8
0.2
D
SD
AP5 pulse
Dendrite
Soma
[Ca2+] (µM)
Time (min)
E
Pressure control
AP5 pulse
SD
Soma [Ca2+] (µM)
Time (min)

Figure 2.7

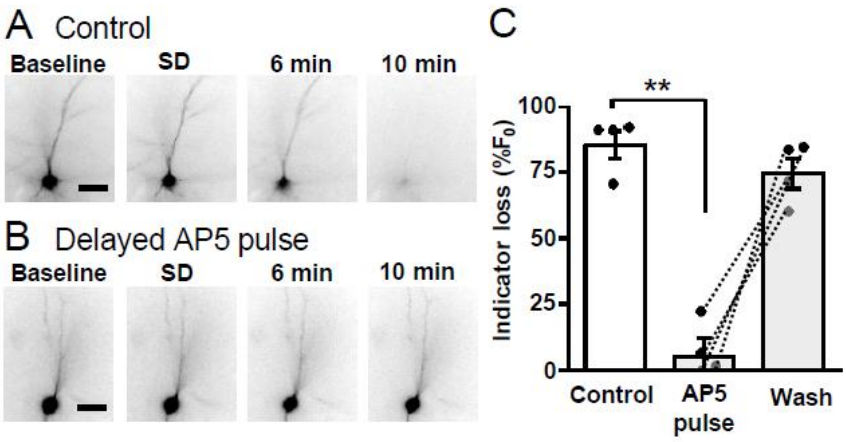
A Control
Baseline
SD
6 min
10 min
B Delayed AP5 pulse
Baseline
SD
6 min
10 min
C
**
Indicator loss (%F0)
100
75
50
25
0
Control
AP5 pulse
Wash

Figure 2.8

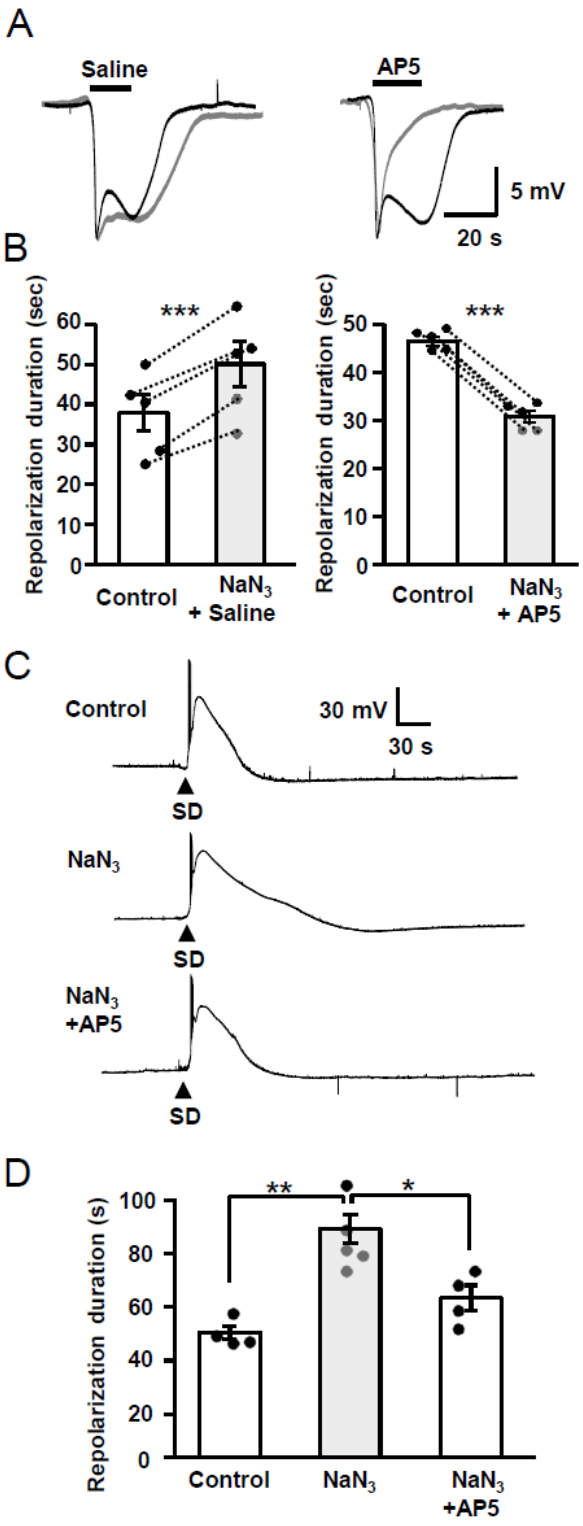
A
Saline
AP5
5 mV
20 s
B
Repolarization duration (sec)
***
Control
NaN3 + Saline
Repolarization duration (sec)
***
Control
NaN3 + AP5
C
Control
30 mV
30 s
SD
NaN3
SD
NaN3 +AP5
SD
D
Repolarization duration (s)
**
*
Control
NaN3
NaN3 +AP5

3. Synaptic Release and Extracellular Actions of Zn^{2+} Limit Propagation of Spreading Depression and Related Events *in vitro* and *in vivo*.

Isamu Aiba[1], Andrew P. Carlson[2], Christian T. Sheline[3] and C. William Shuttleworth[1]

[1] Department of Neurosciences, University of New Mexico, Albuquerque, NM

[2] Department of Neurosurgery, University of New Mexico, Albuquerque, NM

[3] Department of Ophthalmology and the Neuroscience Center of Excellence LSU Health Sciences Center, New Orleans, LA

(Published in Journal of Neurophysiology 107(3):1032-41.)

3.1 ABSTRACT

Cortical spreading depression (CSD) is a consequence of a slowly-propagating wave of neuronal and glial depolarization (spreading depolarization; SD). Massive release of glutamate contributes to SD propagation, and it was recently shown that Zn^{2+} is also released from synaptic vesicles during SD. The present study examined consequences of extracellular Zn^{2+} accumulation on the propagation of SD. SD mechanisms were studied first in murine brain slices, using focal KCl applications as stimuli and making electrical and optical recordings in hippocampal area CA1. Elevating extracellular Zn^{2+} concentrations with exogenous $ZnCl_2$ reduced SD propagation rates. Selective chelation of endogenous Zn^{2+} (using TPEN or CaEDTA) increased SD propagation rates, and these effects appeared due to chelation of Zn^{2+} derived from synaptic vesicles. Thus in tissues where synaptic Zn^{2+} release was absent (knockout of vesicular Zn^{2+} transporter ZnT-3), SD propagation rates were increased, and no additional increase was observed following chelation of endogenous Zn^{2+} in these tissues. The role of synaptic Zn^{2+} was then examined on CSD *in vivo.* ZnT-3 KO animals had higher susceptibility to CSD than wild-type controls as evidenced by significantly higher propagation rates and frequencies. Candidate mechanisms were explored in brain slices and suggested a potential role of Zn^{2+} inhibition of NMDA-Rs. These results suggest the extracellular accumulation of synaptically-released Zn^{2+} can serve as an intrinsic inhibitor to limits SD event. The inhibitory action of extracellular Zn^{2+} on SD may counteract to some extent the neurotoxic effects of intracellular Zn^{2+} accumulation in acute brain injury models.

3.2 INTRODUCTION

Cortical spreading depression (CSD) was discovered as a slowly propagating suppression of electrocorticographic (ECoG) activity (Leao, 1944) and subsequently characterized as a regenerative, severe depolarization of neurons and glia (Somjen, 2001). CSD is thought to underlie aspects of migraine and events very similar to CSD have recently been recorded with relatively high frequencies in patients with ischemic stroke, subarachnoid hemorrhage, traumatic brain injury and intracerebral hemorrhage (Dreier, 2011; Lauritzen et al., 2011). Because suppression of ECoG activity may not be readily apparent during propagation of these events in injured brain, the general term spreading depolarization (SD) has been used to emphasize the important underlying mechanism. Recovery from SD places a substantial metabolic burden on tissues, and it is very likely that failure of ionic homeostasis caused by repetitive SD events contributes to infarct enlargement in injured brain. Thus prevention of SD is considered a promising target for reducing the progression of acute brain injuries (Dreier, 2011; Hartings et al., 2011a; Lauritzen et al., 2011).

The propagation of SD is associated with increased extracellular glutamate concentrations (Fabricius et al., 1993) and activation of NMDA-type glutamate receptors (NMDA-Rs) contributes to SD progression in many experimental situations. Thus NMDA-R antagonists inhibit SD and related events both *in vitro* and *in vivo* (Gill et al., 1992; Anderson and Andrew, 2002; Hartings et al., 2003; Faria and Mody, 2004; Peeters et al., 2007). The divalent cation Zn^{2+} is enriched in synaptic vesicles at many glutamatergic synapses, due

to the activity of a specific transporter termed ZnT-3 (Cole et al., 1999). A range of studies have concluded that Zn^{2+} can be co-released with glutamate following vesicle fusion at some synapses (Assaf and Chung, 1984; Howell et al., 1984; Qian and Noebels, 2005), and can potentially modify synaptic function by altering the activity of ion channels, receptors and transporters (Frederickson et al., 2005). NMDA-Rs are among the most well studied molecular targets for extracellular Zn^{2+} actions. Structural studies have identified high and low affinity Zn^{2+} binding sites in the amino-terminals of NR2A and NR2B subunits, and interaction with Zn^{2+} causes suppression of channel activity in an allosteric manner (Gielen et al., 2009). In addition to allosteric inhibition, lower sensitivity (IC_{50}>20μM) voltage-dependent inhibition by Zn^{2+} has also been described (Paoletti et al., 1997). Because Zn^{2+} and glutamate are expected to be co-released at synapses where NMDA-R are present, Zn^{2+} could potentially serve to limit excessive activation of NMDA-R in many forms of brain pathology (Paoletti et al., 2009). In addition to NMDA-Rs, Zn^{2+} has been shown to attenuate inhibitory synaptic transmission mediated by ionotropic GABA receptors, with substantially different sensitivities depending on subunit composition (Smart et al., 2004). These interactions could potentially lead to complex effects of Zn^{2+} on SD.

We recently reported that intracellular accumulation of Zn^{2+} contributed to initiation of some forms of SD in brain slices, including events generated by ischemia-like conditions (Dietz et al., 2008). In addition, SD propagation was shown to involve substantial release of vesicular Zn^{2+} into the extracellular

space, in a wavelike manner that accompanied the SD wavefront (Carter et al., 2011b). We found that Zn^{2+} from this source accumulated post-synaptically, and speculated that this intracellular accumulation may contribute to further SD initiation, or possibly injury. However, in the current study we tested whether extracellular Zn^{2+} accumulation during SD could also have a self-limiting effect on SD propagation. The current results show that extracellular Zn^{2+} does serve to limit SD propagation, and suggest dual roles for Zn^{2+} in SD and injury progression.

3.3 MATERIALS and METHODS

3.3.1 1. Animals

All experimental procedures using animals were reviewed and approved by the Institutional Animal Care and Use Committee (IACUC) of the University of New Mexico. For *in vitro* characterization of $ZnCl_2$, inhibitor and chelator effects, 4-10week old mice (FVBN or C57Bl/6) animals of either sex were used, and drug effects compared with control SD responses generated in the same slices. For *in vitro* studies of effects of ZnT-3 deletion, tissues from age-matched wild type C57BL/6 animals and ZnT-3 KO animals were compared. The ZnT-3 KO mice were originally generated as described previously (Cole et al., 1999), and were backcrossed onto C57BL/6 for more than 13 generations. Experiments between

genotypes were alternated. For *in vivo* CSD studies, 11-16 week old male animals were used, alternating between age-matched C57BL/6 and ZnT-3 KO.

3.3.2 Drugs

Unless otherwise stated, reagents were obtained from Sigma Aldrich (St Louis. MO). Histidine (200μM) was included in all solutions used for $ZnCl_2$ studies (including for studies of control responses) in order to increase Zn^{2+} solubility in the phosphate containing recording solutions (Rumschik et al., 2009).

3.3.3 Statistical analysis

All results are presented as mean ± SEM, and were analyzed by Student's *t*-tests or one-way ANOVA with appropriate post hoc *t*-tests, unless otherwise mentioned. Throughout the study, events >2 standard deviations from the mean were excluded as outliers.

3.3.4 In vitro SD recordings

Murine brain slices were prepared as previously described (Carter et al., 2011b). Briefly, mice were deeply anesthetized, decapitated and brains extracted into ice cold cutting solution. 350μm coronal slices were prepared with a vibratome and transferred to ACSF. Brain slices were allowed to recover at 35°C for one hour, and then maintained in ACSF at room temperature until transferred to the recording chamber (RC27-L, Warner Instruments). Slices were continuously superfused with artificial cerebrospinal fluid (ACSF, containing (in

mM) 126 NaCl, 3 KCl, 1.25 NaH_2PO_4, 1 $MgSO_4$, 26 $NaHCO_3$, 2 $CaCl_2$, and 10 glucose, equilibrated with 95% O_2/5% CO_2) at 32°C.

SD was generated in the hippocampal CA1 region by localized microinjection of 1M KCl from a conventional patch micropipette (tip diameter 10-20μm), by using a pressure ejection controller (Parker Picospritzer III, General Valve Corp, 40psi). The stimulus threshold was determined by incrementally increasing pulse duration (10-100ms), and all experiments were conducted using pulse durations 50-100% longer than the threshold (typically 50-150ms). Drug challenges were compared with control responses generated in the same slices.

As a control for osmotic effects of KCl microinjection, we confirmed that local injection of equimolar NaCl (1M) did not mimic the responses to localized KCl microinjections, when tested in the same slices. Thus NaCl pulses did not generate propagating SD-like events, as determined from propagating light transmission increases, or DC potential shifts at the recording site (n=3).

SD propagation through the CA1 region was detected electrically and optically. DC potential shifts were recorded with extracellular electrodes (0.5-1 MΩ) placed in stratum radiatum, 50μm below the slice surface. Signals were amplified with a MultiClamp 700A amplifier, and acquired using pClamp 9.2 software (Axon Instruments) Intrinsic optical signals were assessed from transmitted light from a halogen source (>575nm) and collected by a CCD camera (Till Imago, controlled by TillVision v4.0 software, Till Photonics). SD

propagation rates were determined by tracking the wavefront of intrinsic optical signals, following image acquisition at 0.33Hz (Fig. 1A).

3.3.5 Slice electrophysiology

Single cell recordings were obtained from hippocampal CA1 pyramidal neurons. Neurons were visually identified and whole cell clamp was made with 1-2MΩ glass pipettes. Intrinsic excitability and EPSCs were recorded with potassium-gluconate based internal solution (10mM Hepes, 135mM potassium-gluconate, 8mM NaCl, 1mM $MgCl_2$, 2mM ATP-Na_2 and 0.3mM GTP-Na_3) in ACSF. Intrinsic excitability was examined by voltage responses to ±200pA current pulses with no holding current applied. Prolonged recording (>10min) often resulted in rundown of action potential frequency and therefore intrinsic excitability was measured 2-3min after establishment of whole-cell configuration from neurons pre-exposed to $ZnCl_2$ for at least 10min.

Field excitatory postsynaptic potentials (fEPSPs) were evoked by stimulation of Schaffer collateral inputs using a concentric bipolar electrode and detected using glass electrodes in the CA1 subfield. After input output curves were determined, stimulation intensity was set at ~50% of maximal for subsequent pharmacological analysis. For isolation of NMDA-R components of fEPSP, slices were first incubated in low magnesium ACSF (50µM Mg^{2+} balanced with increased Ca^{2+} (3mM)) for 20min, and then 10µM DNQX and 10µM bicuculline were added.

3.3.6 Intracellular and Extracellular Imaging of FluoZin-3 fluorescence

Intracellular Zn^{2+} was measured from single CA1 neurons loaded with FluoZin-3 as described previously (Vander Jagt et al., 2009). Patch pipettes contained 10mM Hepes, 135mM potassium-gluconate, 8mM NaCl, 1mM $MgCl_2$, 2mM ATP-Na_2 and 0.3mM GTP-Na_3, 500µM FluoZin3. Dialysis was strictly limited to 3min, which limited final intracellular indicator concentration to levels <100µM. Electrodes were then slowly removed and neurons allowed to recover for 15min. FluoZin3 fluorescence was excited at 495nm (80ms, 0.2Hz) and band-pass filtered (535±25nm) emission fluorescence was collected with the CCD system. Neurons were exposed with either ZnPyr (1µM Zn^{2+}, 100nM pyrithione) or $ZnCl_2$ (100µM) for 10min and then were washed with ACSF. FluoZin3 signals were background corrected using regions of interest from adjacent non-loaded neurons, and expressed as $\Delta F/F_0$.

Extracellular Zn^{2+} accumulation was imaged as described previously (Carter et al., 2011b). Slices were superfused with 1µM FluoZin3 containing ACSF. In order to enhance signal to noise ratio, 1mM CaEDTA was included (Qian and Noebels, 2005; Carter et al., 2011b). FluoZin-3 signals were monitored with the CCD system at 1Hz. To correct for autofluorescence changes, signals were background subtracted using recordings made in the same slices, but without FluoZin3 addition.

3.3.7 In vivo cortical spreading depression (CSD)

Mice were anesthetized with isofluorane (3% induction, 1-1.25% maintenance) and nitrous oxide (70%) in oxygen (30%), and positioned in a stereotaxic frame. The depth of anesthesia was monitored throughout the experiments and the isofluorane concentration was adjusted to maintain depth sufficient to prevent reflex responses. The scalp was opened and anterior and posterior burr holes were made approximately 1mm apart bilaterally in the parietal bone, and the distance between them measured for calculation of CSD propagation rates. Craniotomies anterior to the burr holes were made for either electrical or KCl stimulation (see Fig. 4A). When windows were not used for experiments, saline filled cotton pads were set on the brain surface. In all experiments, glass electrodes were placed through ipsilateral burr holes, ~300µm below the cortical surface, and electrical activity was amplified by using an Axoprobe 1A amplifier (Axon Instruments) and digitized by using a Powerlab 8/16 system (AD Instruments). The digital data was segregated and filtered via AC coupling and DC coupling for ECoG and extracellular DC recording, respectively. CSD propagation rates were calculated from the latency of CSD and the measured distance between the recording electrodes.

Durations of ECoG suppression were calculated after CSD elicited by bipolar electrical stimulation. CSD propagation rates and frequencies were calculated from repetitive CSDs generated by KCl applications. A gelatin sponge (Gelfoam®, Ethicon 360) soaked with 0.3M KCl was used to apply KCl on the anterior cranial widow and electrical responses were recorded for 30min. During

the 30min trial, KCl was reapplied to prevent drying, either immediately after detection of each SD event, or after 10min in the absence of significant electrical responses. To be included in the analysis, events must have propagated in an anterior to posterior direction, with less than 50% decreased in amplitude between electrodes. Repetitive SDs were tested in both hemispheres and the data from each animal were averaged.

After completion of the study, mice were euthanized by intraperitoneal injection of a barbiturate overdose.

3.4 RESULTS

3.4.1 Extracellular Zn^{2+} inhibits SD propagation

We first examined the effects of elevating extracellular Zn^{2+} on the propagation of SD events generated in brain slice preparations. SD was triggered by brief microinjection of KCl into stratum radiatum of area CA1, and SD was detected by a combination of optical (intrinsic optical signals, IOS) and extracellular DC recording (see Methods). The experimental setup and representative recordings are shown in Figures 1A&B. Under control conditions, SD was visualized as a wave of increased light transmittance that propagated at ~2.5 mm/min, in both directions from the site of KCl application. Opposite to optical responses to KCl, local microinjection of NaCl caused localized non-propagating decrease of light transmission, likely due to tissue constriction following increased osmolarity (data not shown). A biphasic DC potential shift characteristic of SD was recorded coincident with arrival of the optical signal at the extracellular recording electrode site (Fig. 1B). These baseline responses are consistent with a large body of prior literature of SD in hippocampal slices (Somjen, 2001).

The effects of elevating extracellular Zn^{2+} concentrations were tested following bath application of $ZnCl_2$. For all experiments testing effects of exogenous $ZnCl_2$, 200µM histidine was included in recording solutions in order to increase its solubility in phosphate-containing solutions (Rumschik et al., 2009). Histidine alone had no significant effect on SD propagation (Fig. 1D, discussed

below), and was included in control and test recording solutions for all studies involving $ZnCl_2$. $ZnCl_2$ exposures were kept brief (10 min), to maximize the contribution of effects on extracellular sites, and reduce possible intracellular accumulation. Under these conditions, the propagation rates of SD were concentration-dependently decreased by Zn^{2+}, with significant inhibitory effects at 50 and 100µM (Fig. 1C). The observed Zn^{2+} effect was completely reversed by brief co-incubation with the membrane impermeable Zn^{2+} chelator CaEDTA (1mM, 10min, n=5).

The suitability of this approach with histidine supplementation to increase availability of Zn^{2+} in ACSF was confirmed in a set of pilot studies comparing $ZnCl_2$ additions in 1) normal ACSF, 2) ACSF supplemented with histidine, and 3) modified ACSF lacking added phosphates. Without $ZnCl_2$ additions, SD propagation in all three solutions was identical ($p>0.05$). When 100µM $ZnCl_2$ was applied in normal ACSF, there was an obvious visible precipitate likely due to formation of zinc phosphate complexes. This was not observed in histidine or phosphate-free solutions. Further comparisons between the three solutions were therefore made using 50µM $ZnCl_2$. Figure 1D shows that this concentration caused similar inhibition of SD propagation rate effective in both Pi free and histidine (Pi-free 33.6±0.01%, histidine 42.0±0.05%), but significantly less effective in ACSF, (17.3 ±0.09%, $p<0.01$ compared with Pi-free and histidine, n=5) consistent with greater extracellular availability (Fig. 1D). Superfusion in phosphate-free solution often led to significant tissue swelling (as assessed by light transmission increases) and thus in order to avoid potential effect of

phosphate removal on cellular metabolism, we chose histidine supplementation rather than phosphate-free ACSF for the remaining studies (Rumschik et al., 2009).

Single cell Zn^{2+} imaging (following intracellular FluoZin-3 loading, see Methods) revealed relatively slow, but significant intracellular Zn^{2+} accumulation following brief exposures to $ZnCl_2$ (100µM $ZnCl_2$, 48.7 ±10.0% $\Delta F/F_0$ increase after 10 min exposure, n=3, Fig. 1E). Because intracellular Zn^{2+} accumulation is known to modulate neuronal excitability (Frederickson et al., 2005), we next tested whether intracellular accumulation of Zn^{2+} could contribute to inhibition of SD propagation. An approach to selectively increase intracellular Zn^{2+} loading was carried out by exposure of slices to a low concentration of a Zn^{2+}-ionophore complex (1µM $ZnCl_2$ together with 100nM sodium pyrithione for 10min, hereafter referred to as Znpyr) and followed by brief wash (3 min) to minimize extracellular Zn^{2+} levels. This Zn^{2+} loading protocol resulted in rapid intracellular Zn^{2+} accumulation, that reached significantly higher levels than observed with the $ZnCl_2$ exposures (Fig 1E; 1µM Znpyr: 123.8±12.5% after 10 min loading and 3 min wash, $p<0.01$ vs. 100µM $ZnCl_2$ 10min, t-test n=3). Figure 1F shows that preferentially increasing intracellular Zn^{2+} loading with ZnPyr did not have any effect on SD propagation rate.

As a control, we evaluated other effects of pyrithione. Pyrithione itself is a membrane permeable chelator and it is possible that presence of pyrithione depleted synaptic vesicle Zn^{2+} pools and thereby modulated SD propagation. The content of the available synaptic vesicle Zn^{2+} pool was analyzed by

recording extracellular Zn^{2+} accumulation during SD, utilizing extracellular FluoZin3 (Carter et al., 2011b). Exposure to Napyr (100nM, 15min) did not significantly reduce extracellular Zn^{2+} transients attributed to release from synaptic vesicles (control 111.4±23.9% vs. Napyr 105.1±15.7%, peak $\Delta F/F_0$, p=0.84, n=3). Consistent with these results, Napyr did not affect SD propagation rate (Fig. 1F, Napyr).

Taken together, these results imply that extracellular, rather than intracellular actions of Zn^{2+} most likely explain the inhibitory effects of $ZnCl_2$ on SD shown in Figure 1C.

3.4.2 Vesicular Zn^{2+} limits SD propagation

We next tested whether basal levels of Zn^{2+} present in the slices or Zn^{2+} released endogenously during SD may serve to inhibit SD propagation. Zn^{2+} levels in the extracellular space could be contributed to by multiple sources, including contamination of recording solutions (Kay, 2004), or release from synaptic vesicles (Frederickson et al., 2005) and other endogenous sources (Frederickson et al., 2005; Sensi et al., 2009). Figure 2A shows that pre-exposure to a membrane permeable Zn^{2+} chelator (TPEN, 50µM, 10 min pre-exposure), significantly increased SD propagation rate. In a second different set of preparations, slices were pre-exposed to CaEDTA (1mM), a Zn^{2+} chelator with poor membrane permeability. CaEDTA exposures were kept short (10 min), to minimize potential depletion of intracellular Zn^{2+} pools (Frederickson et al., 2002). Under these conditions, CaEDTA also significantly increased rate of SD

propagation (Fig. 2B). These results suggest that extracellular Zn^{2+} that is present within slices inhibits SD propagation rate.

Zn^{2+} is highly enriched in glutamergic synaptic vesicles and is released at high levels during SD at the propagating wavefront (Carter et al., 2011b). To evaluate a possible contribution of this source of endogenous Zn^{2+} to inhibition of SD propagation, we compared SD propagation rates in brain slices from WT and ZnT-3 KO animals. ZnT-3 is a vesicular Zn^{2+} transporter and thus genetic deletion of ZnT-3 results in loss of synaptic Zn^{2+} (Cole et al., 1999) and abolished extracellular accumulation of Zn^{2+} following SD (Carter et al., 2011b). As shown in Fig. 2C, ZnT-3 KO preparations showed significantly faster SD propagation rates than those in WT preparations (WT: 2.78±0.15 mm/min, ZnT-3 KO: 4.12±0.47 mm/min, $p<0.001$, $n=5$). In addition, unlike WT preparations, pretreatment with the Zn^{2+} chelator CaEDTA did not increase propagation rates in ZnT-3 KO slices.

In a different set of experiments, the effects of exogenous $ZnCl_2$ applications were also compared between WT and ZnT-3 KO slices. As shown in Fig. 2D, $ZnCl_2$ (100μM) decreased SD propagation rates in both WT and ZnT-3 KO preparations to a similar degree. These data support the idea that higher propagation rates in ZnT-3 KO is likely due to lack of vesicular Zn^{2+} release and action, rather than changes in Zn^{2+} sensitivity.

Together, these results suggest that Zn^{2+} released from synaptic vesicles during SD inhibits propagation of the advancing SD wavefront.

3.4.3 Vesicular Zn^{2+} inhibits CSD propagation in vivo

We next tested the significance of the *in vitro* results for cortical spreading depression (CSD) *in vivo*. Electrical recordings were made from the parietal cortex of anesthetized mice, and CSD was generated by stimulation of the cortical surface in an anterior cranial window, by using either a bipolar stimulating electrode or repetitive KCl applications (see Methods, Fig. 3A). Fig. 3B shows a representative CSD generated by electrical stimulation in a WT animal. The top panel shows a characteristic DC deflection that lasts for ~1min. This was accompanied by a longer-lasting (~5min) depression of electrocorticographic (ECoG) activity (Fig. 3B middle and bottom).

CSD was reliably generated by both electrical and KCl stimuli in all WT and ZnT-3 KO animals studied, with no differences in electrical properties of single CSD episodes. Figs 3C&D compare the amplitudes and durations of DC deflections in both genotypes, generated by electrical stimuli. No differences were observed in any of these parameters. The durations of ECoG depression were analyzed from the recovery of the power of band-passed ECoG activity (Fig. 3B middle). We did not observe any significant difference in the depression period (50% recovery) of ECoG following CSD (Fig. 3E).

Fig. 4A shows representative CSDs generated by repetitive KCl applications. CSD propagation rates were significantly faster in ZnT-3 KO animals compared with WT controls (Fig. 5B. WT and ZnT-3 KO, 2.38±0.21 mm/min and 3.08±0.22 mm/min, respectively, p=0.045, n=6). In addition, ZnT-3

KO animals showed markedly higher CSD frequencies than WT animals (Fig. 4C). Thus ZnT-3 KO animals showed significantly higher numbers of CSDs in a 30 min recording period (WT and ZnT-3 KO, 3.3±0.28 and 4.2±0.33, respectively, p=0.011, n=6), associated with shorter inter SD intervals (Fig. 4C, WT and ZnT-3 KO, 9.5±1.4 min and 6.9±0.5 min, respectively, p=0.0053, n=6). In normal brain, ECoG suppression is usually significantly shorter than the duration of the inter-SD interval, and thus CSDs rarely invade at-risk tissue where ECoG is still suppressed. However in ZnT3-KO animals, the significant decrease in inter-SD interval (without a concomitant decrease in ECoG suppression duration (compare 4C, & 3E)) increased the incidence of CSD propagating into ECoG-suppressed brain. This observation suggests that extracellular Zn^{2+} could play a role in preventing CSD propagation into the unrecovered brain tissue (see Discussion). These results are consistent with the hypothesis that synaptic Zn^{2+} release inhibits CSD propagation rate and frequency *in vivo*.

3.4.4 Potential extracellular Zn^{2+} targets that could contribute to modulation of SD propagation

As described above (Introduction), NMDA-Rs are a candidate target to explain the inhibitory effect of extracellular Zn^{2+} on SD propagation. Previous work has shown that $ZnCl_2$ inhibits NMDA-R at the hippocampal CA1 synapse (Vogt et al., 2000; Izumi et al., 2006) and Figures 5A&B confirm that $ZnCl_2$ concentration-dependently decreased isolated NMDA-R components of evoked fEPSPs evoked by single stimuli (see Methods). Comparing Figures 1C and 5B

shows that $ZnCl_2$ was more effective against $fEPSP_{NMDA}$ than against SD propagation. These mismatches could be due to the different pools of NMDA-R (subunit compositions or synaptic/extrasynaptic localization) were activated in these different tests (see Discussion). Figures 5C-E demonstrates that a similar mismatch in effectiveness was also observed with the synthetic NMDAR antagonist D-AP5. Thus low concentrations of D-AP5 (2-20µM) readily inhibit or block $fEPSP_{NMDA}$ (Fig 5C&D), while higher concentrations are required to either slow SD propagation (20-50µM) or block the response completely (100µM, n=4). Mismatch in sensitivity to NMDAR antagonism could be due to much higher levels of extracellular glutamate accumulating during SD, compared with EPSPs generated by single electrical stimuli.

The similarity between effects of D-AP5 and $ZnCl_2$ on $fEPSP_{NMDA}$ and SD inhibition is consistent with a role for NMDA-R in the actions of Zn^{2+} to inhibit SD propagation, but does not provide a direct test of the hypothesis. One approach would be to fully block NMDA-Rs involved in SD with D-AP5, and then determine whether $ZnCl_2$ lost the ability to slow the event. However, because high concentrations of D-AP5 completely prevented initiation and propagation of SD (Fig. 5E), this type of test was not possible. Figure 5F shows a different study, where inhibitory effects of endogenous Zn^{2+} were removed by using the ZnT-3KO, and then the effectiveness of AP-5 was tested. In this case baseline SD propagation rates were elevated by synaptic Zn^{2+} removal (as in Figure 2C), but D-AP5 retained the same degree of block as was observed in WT tissues (WT vs. Control: 22.9±0.04% vs. 23.9±0.02% inhibition with 25µM D-AP5;

40.9±0.05% vs. 39.5±0.04% for 50μM D-AP5). This suggests that there was no significant cooperativity between Zn^{2+} and D-AP5 in inhibiting SD, and this could be due to either to different sites of action of these inhibitors on the NMDA receptor (Paoletti and Neyton, 2007) and/or because Zn^{2+} interacts with other extracellular targets to reduce excitability and inhibit SD.

Figure 6 shows that incubation with $ZnCl_2$ (100μM) did not result in significant changes in resting potential, action potential number or input resistance of single CA1 pyramidal neurons (Fig. 6A-D). Furthermore, consistent with a previous report (Izumi et al., 2006) $ZnCl_2$ had no significant effect on a measure of presynaptic release probability - paired pulse ratio (PPR) of evoked field excitatory postsynaptic potentials (fEPSP; Fig. 6E&F, $p>0.5$, $n=4$). $ZnCl_2$ also had no effect the amplitudes of evoked fEPSPs (100 μM $ZnCl_2$: 98.5 ±13% of control, $p>0.1$, $n=4$,). Similarly, no obvious difference in the evoked responses between WT and ZnT-3 KO preparations were observed (input-output curve (range: 0.2-0.6mA), PPR (interpulse interval: 20, 50 and 100ms), $p>0.1$ in both tests, $n=5$). These data imply that there was no significant Zn^{2+} inhibition of evoked presynaptic Ca^{2+} influx and glutamate release, or of AMPA receptors that might contribute to decreased SD propagation rates (Kunkler and Kraig, 2004; Pietrobon, 2010).

Figure 6G shows that $GABA_A$-R activation contributes significantly to limiting the rate of SD, since full block of these channels with gabazine significantly enhanced SD propagation rate. Since $GABA_A$–Rs are known to be inhibited by Zn^{2+} (Weiss et al., 2000; Frederickson et al., 2005; Sensi et al.,

2009), actions on these channels cannot be directly responsible for inhibitory effects of SD on propagation rate. Furthermore, when GABAA-Rs were fully blocked with gabazine, $ZnCl_2$ was not more effective than in control conditions (mean inhibitory effect of $ZnCl_2$; control 28.9%, gabazine 29.3% Fig 6G, *$p<0.01$).

3.5 DISCUSSION

3.5.1 General

The current study demonstrates that Zn^{2+} released during SD can serve to limit progression of the event. This conclusion is supported by consequences of exogenous Zn^{2+} applications, increased SD propagation rates following extracellular Zn^{2+} chelation and higher SD propagation rates in ZnT-3 KO preparations. The significance of results in brain slices was confirmed in an *in vivo* CSD model, in which ZnT-3 KO animals had higher CSD propagation rates and frequencies than WT animals. Previous work has emphasized a neurotoxic role of intracellular Zn^{2+} accumulation (Weiss et al., 2000; Sensi et al., 2009). However, our current study raises the possibility that the synaptic Zn^{2+} released during SD may be beneficial in some contexts by limiting SD.

3.5.2 Zn^{2+} released from synaptic vesicles inhibits SD propagation

Zn^{2+} is capable of interacting with a large number of ion channels, receptors and intracellular signaling pathways (Weiss et al., 2000; Frederickson et al., 2005; Sensi et al., 2009), however the inhibitory actions of Zn^{2+} on SD propagation appear to be due to extracellular actions rather than intracellular accumulation. Thus, approaches to selectively increase intracellular Zn^{2+} (with zinc pyrithione) did not retard SD, and the inhibitory effects of brief $ZnCl_2$ exposures were readily reversible. Both these observations are compatible with interaction of an extracellular target.

The fact that brief exposures to Zn^{2+}-selective chelators significantly increased SD propagation rates implies that there is sufficient extracellular Zn^{2+} within the slice to inhibit SD propagation. Two main sources of Zn^{2+} need to be considered; contamination of Zn^{2+} from a variety of exogenous sources (Kay, 2004), and endogenous sources including synaptic vesicles. Results from tissues lacking Zn^{2+} in synaptic vesicles (ZnT-3 KO) show that release from vesicles underlies these effects. Thus SD generated in ZnT-3 KO preparations was significantly faster than in wild type tissues, both measured *in vitro* in hippocampal slices and *in vivo* during CSD. Importantly, the potentiating effects of CaEDTA were abolished in ZnT-3 KO slices, demonstrating no additional effect of contaminating Zn^{2+}.

We recently showed that a large release of Zn^{2+} from synaptic vesicles accompanies the advancing SD wave front (Carter et al. 2011), and it seems likely that such release is responsible for retarding progression of the event. If this is the case, then release should occur just prior to the complete depolarization that characterizes SD. It is noted that SD propagation is preceded by a episodic transient hyperexcitation (Herreras et al. 1994; Larrosa et al. 2006) which is associated with increase of spontaneous EPSC frequencies (unpublished observations). The exact extracellular Zn^{2+} concentrations achieved during and after SD are not yet clear. However, extracellular Zn^{2+} transients generated by SD were ~10-times higher than those produced by trains of electrical stimulation, and from comparison with prior work (Assaf and Chung 1984; Howell et al. 1984), it seems likely that Zn^{2+} concentrations can reach at

least 100 μM in synaptic clefts following SD. However estimates of extracellular Zn^{2+} concentrations are controversial and need to be consolidated (Frederickson et al. 2005; Kay 2003).

3.5.3 Potential mechanisms contributing to Zn^{2+} inhibition of SD

We did not observe effects of $ZnCl_2$ on intrinsic excitability or synaptic function that could explain the decrease in SD propagation rate. A marked increase in extracellular GABA concentration has been reported during SD (Molchanova et al., 2004) and Zn^{2+} can inhibit $GABA_A$ receptors (Smart et al., 2004), but based on the effects of $GABA_A$-receptors block with gabazine (Fig 6), such an action of Zn^{2+} would be expected to accelerate (rather than inhibit) SD propagation.

One candidate for decreases in SD propagation is inhibition of NMDA-Rs. As described above (Introduction) and demonstrated in the present work, NMDA-R antagonists can completely abolish some forms of SD, presumably by substantially increased threshold for initiation. Activation of NMDA-R at the advancing wave front also appears to contribute significantly to setting the SD propagation rate. Previous work showed that CPP slowed SD propagation in brain slice (Larrosa et al., 2006) and the present study extends these observations by showing that with partial inhibition of NMDA-R, SD could still be generated, but propagated substantially more slowly than in control conditions.

In the present study, we confirmed effective inhibition of NMDA-R by exogenous application of $ZnCl_2$, but it was not possible to completely inhibit

evoked NMDA potentials with $ZnCl_2$. A similar partial block of NMDA-R components of fEPSPs was reported previously (Izumi et al., 2006). At least two factors could contribute to the partial nature of this block. First, Zn^{2+} preferentially inhibits NMDA receptors containing NR2A subunits and significantly higher concentrations are required to inhibit NR2B containing receptors (Paoletti and Neyton, 2007; Gielen et al., 2009). It is important to note that Zn^{2+} sensitive NR2A containing receptors appear more predominantly localized to synaptic sites, whereas extrasynaptic regions express more NR2B-containing receptors (Hardingham and Bading, 2010). Thus a potentially greater involvement of extrasynaptic receptors during massive glutamate at the SD wavefront might explain the weaker inhibitory effects of Zn^{2+} on SD, as compared with evoked synaptic potentials. Second, the effective concentration of Zn^{2+} that can be achieved in brain slice studies is limited by solubility in the ACSF-based recording solutions. Zn^{2+} interacts with and precipitate with phosphate and thus decrease activity of Zn^{2+}, and for this reason histidine was included in recording solutions to increase availability (Rumschik et al., 2009). However it is likely that the effects were still underestimated. Some combination of these two factors is expected to explain why SD was slowed, but not abolished by the concentrations of $ZnCl_2$ we could test in this study.

The similarity between effects of D-AP5 and $ZnCl_2$ on $fEPSP_{NMDA}$ and SD inhibition is consistent with a role for NMDA-R in the actions of Zn^{2+} to inhibit SD propagation but (as noted above in Results), direct tests of this hypothesis were not possible due to the essential requirement of NMDAR for generation of the SD

event. Thus it is not yet known whether inhibition of NMDAR might be sufficient to explain decreased SD propagation rate, and/or whether other targets of Zn^{2+}, including the recently described Zn sensing metabotropic receptor (Chorin et al., 2011) could also contribute.

3.5.4 Implications for Zn^{2+}-based interventions to limit brain injury

Important studies have shown that Zn^{2+} chelation can be neuroprotective in rodent stroke models and a large body of work has identified multiple intracellular pathways linking intracellular Zn^{2+} accumulation to injury (Koh et al., 1996; Sheline et al., 2000; Weiss et al., 2000; Sensi et al., 2009). However on the other hand, several studies have suggested opposite (neuroprotective) roles of Zn^{2+} in ischemic injury (Galasso and Dyck, 2007). Thus administration of exogenous Zn^{2+} decreased ischemic lesion size (Zhao et al., 1996) and pretreatment with CaEDTA has been shown to accelerate early ischemic infarct formation in a rat stroke model (Kitamura et al., 2006). In addition, ZnT-3 KO animals have been shown to have higher susceptibility to some other forms of brain injury (Cole et al., 2000; Doering et al., 2010).

Recent work has consolidated the idea that SD can contribute significantly to the expansion of ischemic injuries (Dreier, 2011; Lauritzen et al., 2011), and it is possible that divergent effects of Zn^{2+} on SD explains the apparently contradictory effects of Zn^{2+} chelation in different injury models. Thus we recently provided evidence that Zn^{2+} chelation increased the threshold for initiation of some forms of SD in brain slices. This was attributed to intracellular

Zn^{2+} accumulation, which likely contributed to metabolic failure in an *in vitro* ischemia model (Dietz et al. 2008). Substantial synaptic Zn^{2+} release also accompanies SD and leads to postsynaptic uptake (Carter et al. 2011) raising the possibility that Zn^{2+} released during repetitive SDs in ischemia can prime injured tissues by lowering SD threshold and/or activating other intracellular cell death pathways. However Zn^{2+} chelation did not prevent initiation of SD under normoxic conditions (Dietz et al., 2008, and present study), presumably because the initiation of these events was determined by localized accumulation of K^+, rather than progressive depletion of metabolites.

The current study reveals an additional important complexity to the actions of Zn^{2+} in SD, by describing significant extracellular actions. By slowing the progression of recurrent SD events through peri-infarct regions, synaptic release of Zn^{2+} could limit the deleterious invasion of SDs into tissue that has not fully recovered from previous depolarizations. It will be of interest to determine the relationship between extracellular Zn^{2+} accumulation and the durations of DC shifts and ECoG recovery in rodent models of focal ischemia, to evaluate this possibility.

The idea of opposing intracellular and extracellular actions of Zn^{2+} may emerge as a common theme in Zn^{2+} pathophysiology, as a recent report showed that while intracellular Zn^{2+} accumulation contributes to neuronal excitability due to KCC2 downregulation, binding of Zn^{2+} to an extracellular receptor leads to activation of KCC2 (Chorin et al., 2011). These considerations further strengthen the idea that strategies that specifically target intracellular Zn^{2+} accumulation

(while maintaining potentially beneficial effects of extracellular Zn^{2+}) could be more effective interventions for ischemic stroke.

3.6 FiGURE LEGENDS

Figure 3.1: Extracellular Zn^{2+} inhibits SD propagation. A: Images showing electrode placement and propagation of SD through the hippocampal CA1 subregion. SD was generated by local microinjection of KCl (10ms pulse) from a stimulation pipette (*Stim*), and was detected using an extracellular recording electrode (*Rec*). SD was also tracked from propagating intrinsic optical signal increases (>575nm transmission, *arrows*). Scale bar = 250µm. **B:** Time courses of intrinsic optical (IOS) and electrical signals (DC) generated from the preparation illustrated in A. **C:** Brief $ZnCl_2$ pre-exposures (10 min in histidine-supplemented ACSF) resulted in concentration-dependent reductions in SD propagation rate (*p<0.05, **p<0.01, n=5). **D:** Comparison of buffer composition on effectiveness of $ZnCl_2$ applications. $ZnCl_2$ (50µM; 10min) was more effective in phosphate free ACSF (Pi free) and histidine supplemented ACSF (200µM histidine) than in control ACSF (* p<0.05, n=5). **E:** Intracellular Zn^{2+} accumulation assessed in single neurons loaded with FluoZin3. $ZnCl_2$ exposures (100µM) resulted in slow intracellular accumulation, and more rapid increases were observed with Znpyr (1µM $ZnCl_2$ with 100nM pyrithione). **F:** Preferentially loading intracellular Zn^{2+} had no effect on SD propagation rate. Exposure to Znpyr (as in 1E, followed by brief wash) did not reduce SD propagation rate, and no effects were observed with a control for non-specific effects of pyrithione (sodium pyrithione, Napyr 100nM) influenced SD propagation rate (n=5).

Figure 3.2: SD propagation rate in WT and ZnT-3 KO animals *in vitro*. A&B: Effects of Zn^{2+} chelation on SD propagation rate. Slices were pre-incubated with one of two Zn^{2+} chelators prior to SD initiation; TPEN (50μM, **A**) or CaEDTA (1mM, **B**). Both chelators significantly increased SD propagation rates (*p<0.01 n=5). **C:** In slices from ZnT-3 KO animals (*filled bars*), control SD propagation rates were significantly higher than those observed in WT slices. In addition, Zn^{2+} chelation with CaEDTA did not further increase SD propagation rates in ZnT3-KO slices (*p<0.01, **p<0.05, n=5). **D:** $ZnCl_2$ (100μM 10min) effectively decreased SD propagation rate in both WT and ZnT-3 KO preparation. Experiments were interleaved between WT and ZnT-3 KO (*p<0.01, n=5).

Figure 3.3: CSD threshold and propagation rate in WT and ZnT-3 KO animals. A: Arrangement of craniotomies and burr holes for CSD recording. **B:** Representative responses showing extracellular DC recording (*top*), ECoG (*middle*) and relative ECoG power (*bottom,* 10sec bins) following a single CSD generated by electrical stimulation. CSD was recorded as large, long-lasting negative DC potential shift, coupled with transient suppression of ECoG activity. **C-E:** Lack of difference in the DC shift duration (**C**), DC shift amplitude (**D**), or duration of ECoG suppression (**E**, measured as 50% recovery time). n=6 for each.

Figure 3.4: ZnT-3 KO animals showed higher CSD incidence. Increased CSD propagation rates and frequencies in ZnT-3 KO animals. A: Representative traces of repetitive CSD generated by topical KCl applications in WT and ZnT-3 KO. *Arrowheads* indicate onset of CSD and recording artifacts

generated by re-application of KCl are denoted by *asterisks*. **B:** Propagation rates of CSD in WT and ZnT-3 KO. Mean SD propagation rates were determined for each animal, from the time-offset between CSDs detected with a pair of electrodes. (* $p<0.05$ n=6). **C:** Inter-CSD intervals were significantly lower of ZnT-3 KO animals. (* $p<0.001$, n=6)

Figure 3.5: Partial inhibition of NMDA-R could contribute to effects of $ZnCl_2$ on SD propagation rate. **A&B:** $ZnCl_2$ partially inhibits NMDA-R. Isolated NMDA-R components of evoked fEPSP (see Methods) were reduced by $ZnCl_2$ in a concentration-dependent manner (10-100µM, 10min). **C-F:** NMDAR block with D-AP-5 concentration dependently inhibits SD propagation. C&D show concentration dependent inhibition of $fEPSP_{NMDA}$ (**$p<0.01$, n=3). E shows that D-AP5 at 100µM reversibly prevented SD generation. SD incidences are shown in the numbers in bar graphs. Intermediate concentration of D-AP5 shows decreased SD propagation rates in both WT and ZnT-3 KO preparations (F). Recovery was evaluated after at least 30min washout of D-AP5 (** $P<0.01$ vs. WT control, ##$p<0.01$ vs. ZnT-3 KO control, n=5).

Figure 3.6: Lack of effect on intrinsic excitability, presynaptic release or $GABA_A$-R mechanisms. **A-D:** Lack of effect on intrinsic excitability of CA1 pyramidal neurons tested by recording responses to intracellular current injection (representative traces in A). $ZnCl_2$ (100µM, 10-30min, n=8 each) had no effect on resting potential (B), action potential frequency (C) or input resistance (D). **E&F:** No significant effect of $ZnCl_2$ (100µM, 10min) on paired pulse ratios determined from fEPSP recordings ($p=0.50$, n=4). **G.** $GABA_A$-R block by gabazine (10µM)

significantly increased SD propagation rate. The degree of SD acceleration by gabazine was unaffected by $ZnCl_2$ (100µM, 10min; *$p<0.01$, $n=4$)

Figure 3.1

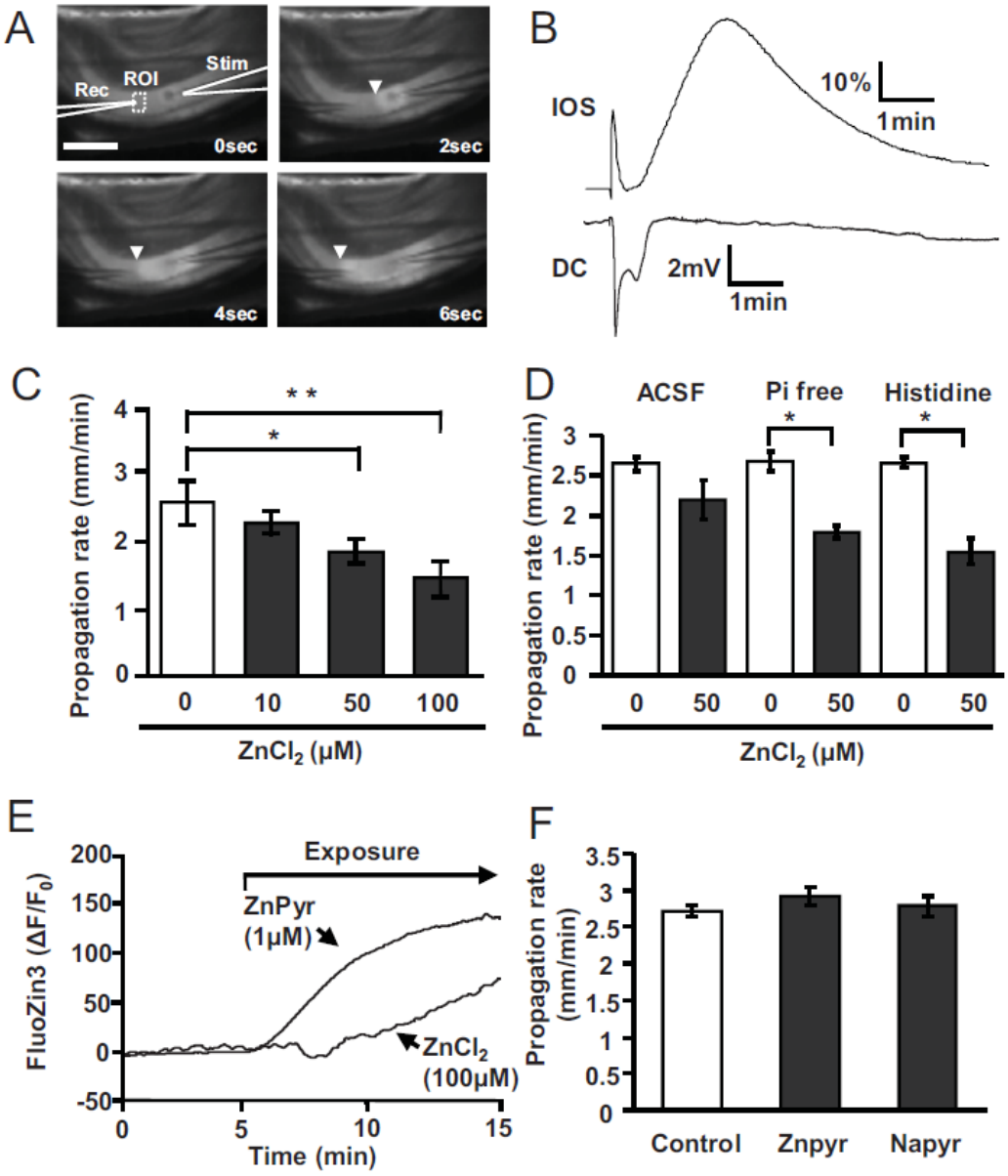
A
Rec
ROI
Stim
0sec
2sec
4sec
6sec
B
IOS
10%
1min
DC
2mV
1min
C
Propagation rate (mm/min)
* *
*
0
10
50
100
ZnCl2 (μM)
D
ACSF
Pi free
Histidine
Propagation rate (mm/min)
0
50
0
50
0
50
ZnCl2 (μM)
E
FluoZin3 (ΔF/F0)
Exposure
ZnPyr
(1μM)
ZnCl2
(100μM)
Time (min)
F
Propagation rate
(mm/min)
Control
Znpyr
Napyr

Figure 3.2

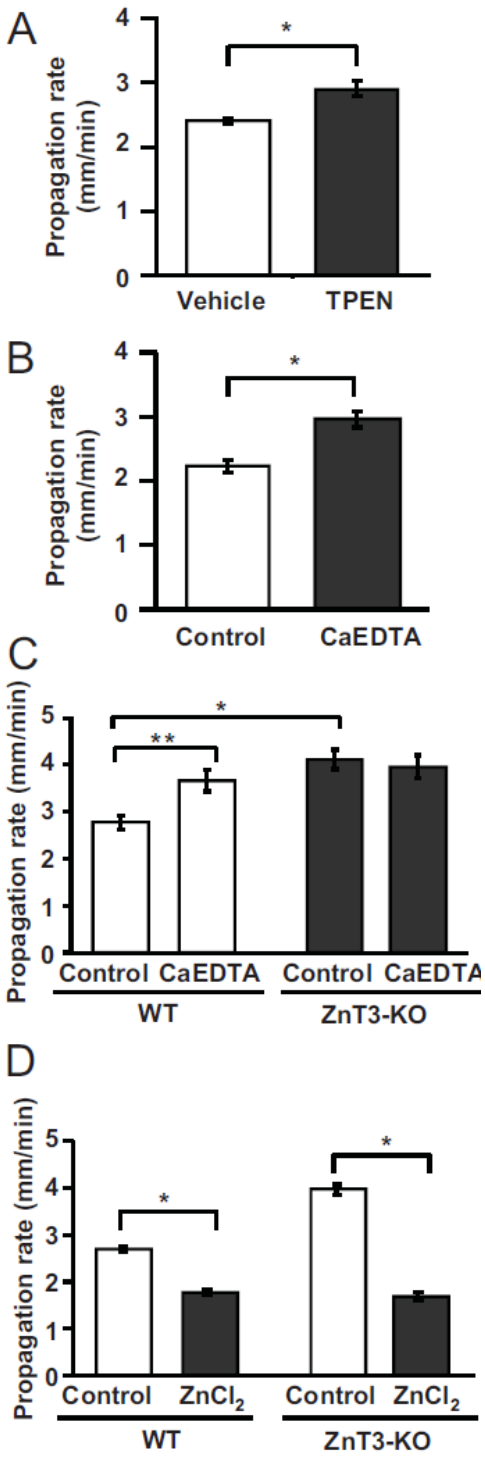
A
Propagation rate (mm/min)
0
1
2
3
4
*
Vehicle
TPEN
B
Propagation rate (mm/min)
0
1
2
3
4
*
Control
CaEDTA
C
Propagation rate (mm/min)
0
1
2
3
4
5
*
**
Control
CaEDTA
Control
CaEDTA
WT
ZnT3-KO
D
Propagation rate (mm/min)
0
1
2
3
4
5
*
*
Control
ZnCl2
Control
ZnCl2
WT
ZnT3-KO

Figure 33

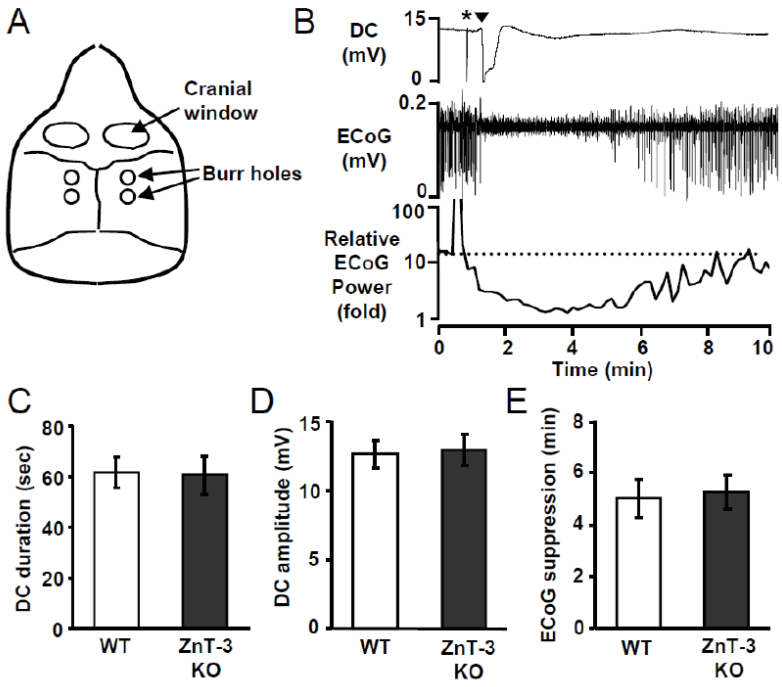
A
Cranial window
Burr holes
B
DC (mV)
15
0
*
0.2
ECoG (mV)
0
100
Relative ECoG Power (fold)
10
1
0
2
4
6
8
10
Time (min)
C
DC duration (sec)
80
60
40
20
0
WT
ZnT-3 KO
D
DC amplitude (mV)
15
10
5
0
WT
ZnT-3 KO
E
ECoG suppression (min)
8
6
4
2
0
WT
ZnT-3 KO

Figure 3.4

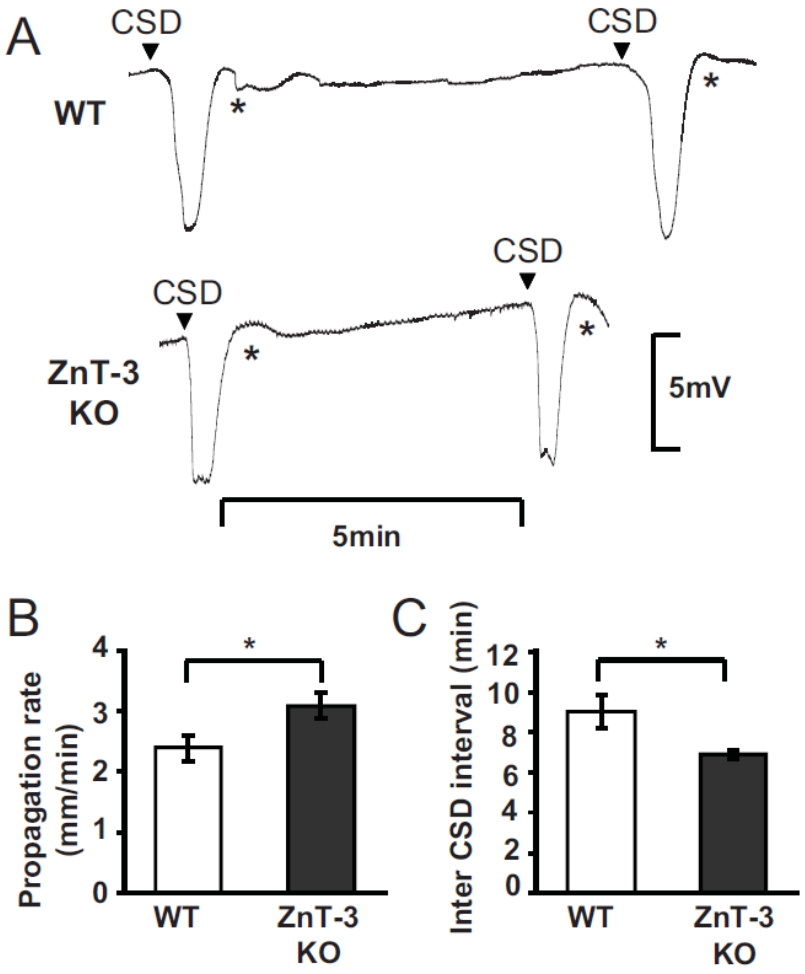
A
CSD
CSD
WT
*
*
CSD
CSD
ZnT-3
KO
*
*
5mV
5min
B
Propagation rate
(mm/min)
4
3
2
1
0
*
WT
ZnT-3
KO
C
Inter CSD interval (min)
12
10
8
6
4
2
0
*
WT
ZnT-3
KO

Figure 3.5

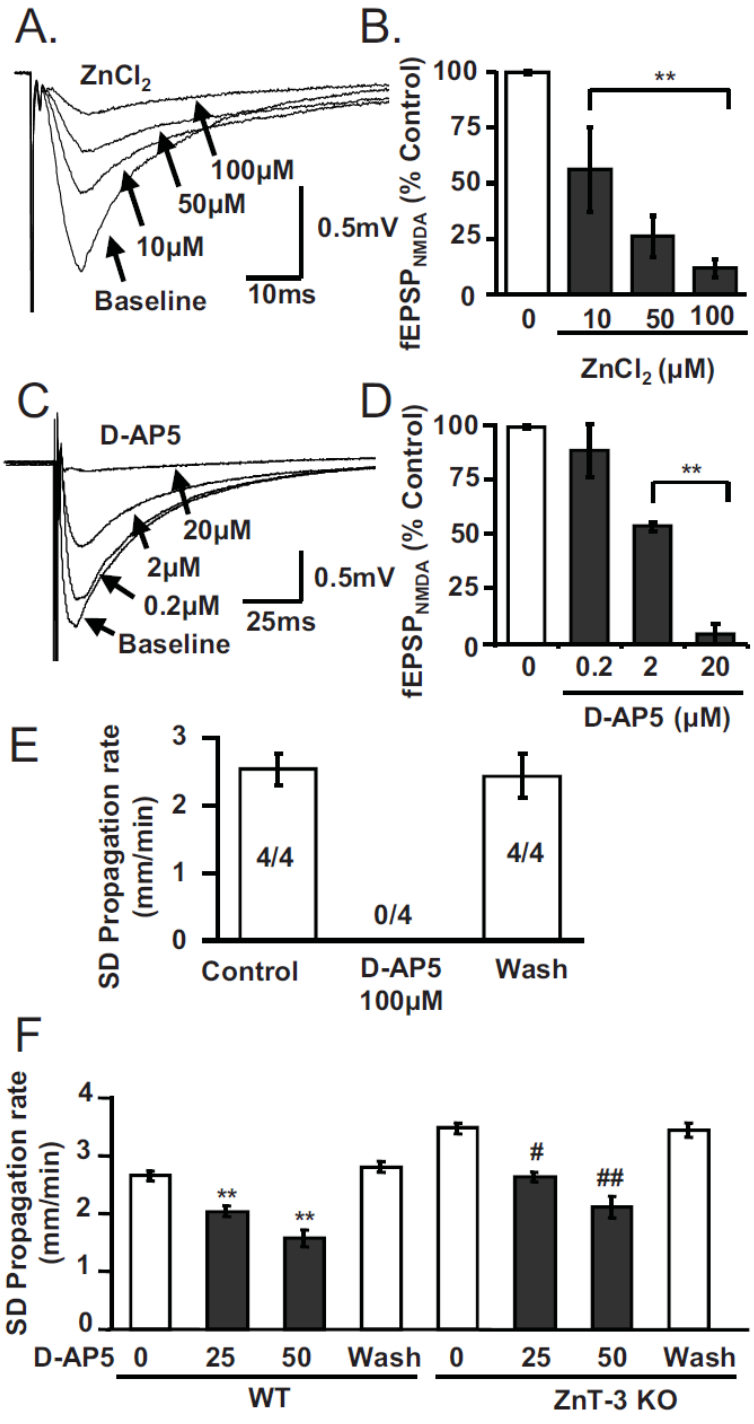
A.
ZnCl2
100μM
50μM
10μM
Baseline
0.5mV
10ms
B.
fEPSP NMDA (% Control)
100
75
50
25
0
**
0
10
50
100
ZnCl2 (μM)
C
D-AP5
20μM
2μM
0.2μM
Baseline
0.5mV
25ms
D
fEPSP NMDA (% Control)
100
75
50
25
0
**
0
0.2
2
20
D-AP5 (μM)
E
SD Propagation rate (mm/min)
3
2
1
0
4/4
0/4
4/4
Control
D-AP5 100μM
Wash
F
SD Propagation rate (mm/min)
4
3
2
1
0
**
**
#
##
D-AP5
0
25
50
Wash
0
25
50
Wash
WT
ZnT-3 KO

Figure 3.6

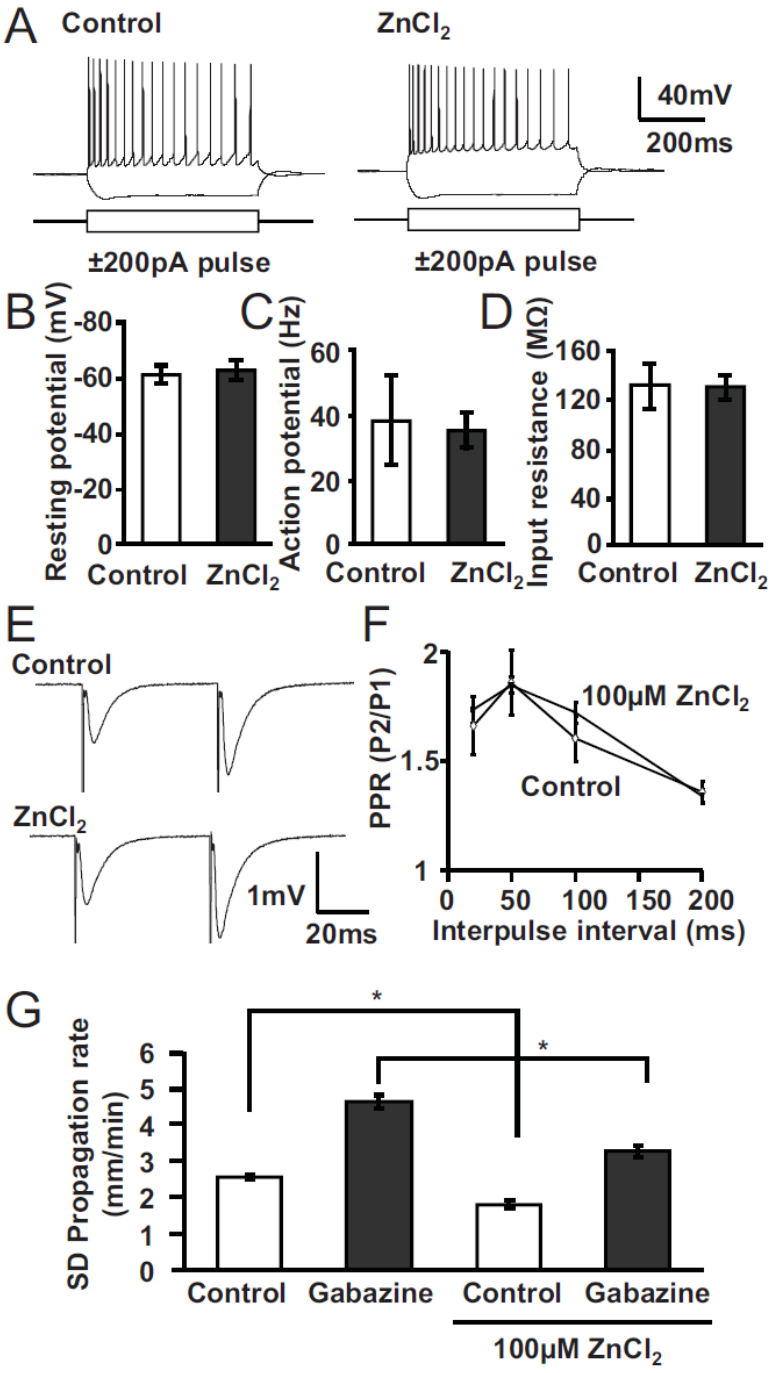
A
Control
ZnCl2
40mV
200ms
±200pA pulse
±200pA pulse
B
Resting potential (mV)
-80
-60
-40
-20
0
Control
ZnCl2
C
Action potential (Hz)
60
40
20
0
Control
ZnCl2
D
Input resistance (MΩ)
160
120
80
40
0
Control
ZnCl2
E
Control
ZnCl2
1mV
20ms
F
PPR (P2/P1)
2
1.5
1
100μM ZnCl2
Control
0
50
100
150
200
Interpulse interval (ms)
G
SD Propagation rate (mm/min)
6
5
4
3
2
1
0
*
*
Control
Gabazine
Control
Gabazine
100μM ZnCl2

4. Hypoxia Limits Inhibitory Effects of Zn^{2+} on Spreading Depolarizations

Isamu Aiba and C. William Shuttleworth

Department of Neurosciences, University of New Mexico, Albuquerque, NM, USA

Prepared for submission to "Neuroscience"

4.1 ABSTRACT

Spreading depolarizations (SDs) are coordinated depolarizations of brain tissue that are implicated in the progression of stroke injury. We have recently shown that extracellular Zn^{2+} accumulation can inhibit the propagation of SD events. In that prior work, Zn^{2+} was tested in normoxic conditions, where SD was generated by localized KCl pulses in oxygenated tissue. The current study examined the extent to which Zn^{2+} effects are modified by hypoxia, to assess potential implications for stroke studies. All studies examined SD generated in brain slices acutely prepared from mice and recordings were made from the hippocampal CA1 region. SDs were generated by either local potassium injection (K-SD), exposure to the Na^+/K^+ -ATPase inhibitor ouabain (ouabain-SD) or superfusion with modified ACSF with reduced oxygen and glucose (oxygen glucose deprivation: OGD-SD). Extracellular Zn^{2+} exposures (100μM $ZnCl_2$) effectively decreased SD propagation rate and significantly increased the initiation threshold for K-SD generated in oxygenated ACSF (95% O_2). In contrast, when SD was generated by either OGD, or ouabain in hypoxic conditions (0% 0_2), $ZnCl_2$ no longer inhibited SD propagation. In both these conditions, Zn^{2+} sensitivity was restored by exposure to the protein oxidizer DTNB, suggesting that redox modulation may contribute to resistance to Zn^{2+} in hypoxic conditions. DTNB pretreatment also significantly potentiated inhibitory efficacies of competitive (D-AP5) or allosteric (Ro25-6981) NMDA receptor antagonists on OGD-SD. Finally, Zn^{2+} inhibition of isolated NMDAR currents were greatly potentiated by DTNB. Together, these results demonstrate that

hypoxia-induced redox modulation can modulate sensitivity of SD to Zn^{2+} as well as other NMDAR antagonists, and this feature may limit the protective effects of endogenous Zn^{2+} accumulation in hypoxic regions close to ischemic infarcts.

4.2 INTRODUCTION

Many preclinical studies have accumulated evidence suggesting that slowly-propagating waves of coordinated neuronal and glial depolarization can contribute to expansion of stroke injury (Dreier, 2011; Lauritzen et al., 2011). The events initiate from depolarization of a volume of tissue and consequent elevations of extracellular potassium and glutamate concentration drive near complete depolarization of surrounding tissue, generate a slowly propagating (2-4 mm/min) feed-forward event (Somjen, 2001). These events are termed spreading depolarizations (SD), and underlie the well-recognized phenomenon of spreading depression of cortical activity (Leao, 1944), as well as spreading ischemia and other related consequences that depend on the physiological state of the brain tissue (Dreier, 2011). The cumulative metabolic burden of repetitive SDs that occur in the hours and days following injury appears to increase the volume of tissue involved in an infarct, and there is considerable interest in finding effective approaches to limit the spread of SDs (Marrannes et al., 1988; Lauritzen et al., 2011).

Antagonists of NMDA subtype glutamate receptors (NMDARs) are amongst the most well-studied inhibitors of SD. While NMDAR antagonists are very effective at blocking SDs under some conditions, in other SD models, the same agents can be completely ineffective. Thus SDs triggered by localized KCl pulses in well-oxygenated brain slices can reliably be blocked by NMDAR antagonists (Mody et al., 1987; Avoli et al., 1991; Kruger et al., 1999), and similar

effectiveness has been observed with NMDARs tested against SDs generated in vivo, in otherwise healthy brain (Marrannes et al., 1988). In contrast, SDs triggered by simulated ischemia (oxygen glucose deprivation) in brain slices were quite resistant to NMDAR blockers (Jarvis et al., 2001). Likewise the SDs generated by global ischemia *in vivo* (or anoxic depolarization) were not prevented by NMDAR antagonists and contribute to significant damage (Hernandez-Caceres et al., 1987; Lauritzen and Hansen, 1992; Murphy et al., 2008). In contrast, SD (or periinfarct depolarization) generated with focal ischemia by middle cerebral artery occlusion models showed significant sensitivity to NMDAR antagonists and decreased numbers of SD associated with infarct volume (Gill et al., 1992; Hartings et al., 2003). It is possible that part of the lack of antagonist efficacy in some circumstances is due to a lack of contribution of NMDARs in carrying SDs under ischemic conditions, and a larger role for K^+ or other mediators (Somjen, 2001). However, it is also known that the effectiveness of NMDAR block can be influenced by oxygen-dependent redox modulation (Pringle et al., 2000b), raising the possibility that similar mechanism could contribute to differential pharmacosensitivity of SD.

We have recently shown that Zn^{2+} can limit the progression of some forms of SD (Aiba et al., 2012). Thus for SDs generated by microinjection of KCl in brain slices, exogenous applications of $ZnCl_2$ significantly slowed the progression rate of SD. These actions were likely due to an extracellular action of Zn^{2+}. Large amounts of vesicular Zn^{2+} release also occurs during SD (Carter et al., 2011a), and release of endogenous Zn^{2+} from this source appeared to

contribute significantly to setting the rate and threshold of SD generated by KCl *in vivo* (Aiba et al., 2012). These observations may be significant for understanding the complex roles of Zn^{2+} in ischemic injury, since intracellular Zn^{2+} accumulation is implicated in the progression of stroke injury (Koh et al., 1996; Sensi et al., 2009), but appears to provide a protective effect under some circumstances (Zhao et al., 1996; Kitamura et al., 2006). A potentially protective role of vesicular Zn^{2+} is also consistent with reports on seizure and brain trauma where removal of an endogenous Zn^{2+} source facilitated injurious events or consequences (Cole et al., 2000; Dominguez et al., 2003; Doering et al., 2010; , but see also Qian et al., 2011). It is possible that inhibitory actions of Zn^{2+} on SD and/or other NMDA dependent injury could contribute to these complex results.

In the present study, we examined whether inhibitory effects of Zn^{2+} on SD were influenced by hypoxia, similar to the effects that have been described previously for synthetic NMDA receptor antagonists (described above). Such information should be helpful for determining the potential protective inhibitory effects of extracellular Zn^{2+} on SD in the stroke-injured brain. The results show a dependence of Zn^{2+} inhibition on oxygen availability, attributed to redox modulation. These effects were paralleled by effects on isolated NMDA receptor currents. In addition, the sensitivity of OGD-SD to some synthetic NMDA receptor antagonists was sensitized by redox modulation with some degree, suggesting a contribution of similar or identical mechanism to pharmacoresistance of SD.

4.3 EXPERIMENTAL PROCEURES

4.3.1 Animals and slice preparation

All experimental procedures were approved by the Institutional Animal Care and Use Committee (IACUC) at the University of New Mexico. Bain slices were prepared from 4-10 week old C57BL/6 or FVB/N mice of both sexes. In order to minimize experimental variables resulting from the variability of animals, effects of inhibitors were tested only on interleaved slices obtained from the same experimental animals.

Brain slices were prepared as previously described (Aiba et al. 2012). Briefly, mice were deeply anesthetized with subcutaneous injection of a ketamine/xylazine mixture (85 mg/ml and 15 mg/ml, respectively, total 150 µl) and decapitated. Brains were then extracted into ice cold cutting solution (mM: 220 Sucrose, 6 $MgSO_4$, 3 KCl, 1.25 Na_2HPO_4, 25 $NaHCO_3$, 10 glucose, 0.2 $CaCl_2$) and sliced with a vibratome at 350 µm thickness. Slices were then allowed for recover in ACSF (mM: 130 NaCl, 1 $MgSO_4$, 3 KCl, 1.25 Na_2HPO_4, 25 $NaHCO_3$, 10 glucose, 2 $CaCl_2$, equilibrated with 95% O_2/5% CO_2) at 35^oC for 1 hour, and then transferred to room temperature ACSF and held until transfer to the recording chamber.

4.3.2 SD generation and detection

SD was detected simultaneously with extracellular DC recording electrodes and optical detection of intrinsic optical signals. In order to decrease

variability, the condition of slices was visually inspected based on morphology of soma, and slices with local damage were not used. Electrical signals were recorded with a low resistance glass electrode (0.5-1 MΩ, filled with ACSF) placed in the CA1 dendritic subfield. Signals were amplified with a Multiclamp 700A amplifier, digitized (Digidata 1322A) and analyzed with pClamp9.2 software (Molecular Devices, CA). Changes in transmittance of light through slices (hereafter termed intrinsic optical signals; IOS) were also used to visualize the propagation of SD events. Light transmission (>575 nm high-pass filtered light) was acquired at 0.5-1 Hz using a charge-coupled device controlled by Till Vision software (Version 4.0) which allowed the velocity of traveling waves of IOS to be calculated. The region of interest (ROI) for IOS measurements was placed at the electrical recording site and optical data were expressed as light transmission changes with respect to basal levels ($\Delta T/T_0$).

SD was generated by one of three stimuli: 1) local injection of 1 M KCl (K-SD), 2) exposure of slices to a moderate concentration of the Na^+/K^+/ATPase inhibitor ouabain (ouabain-SD), 3) exposure of slices to oxygen-glucose deprivation (OGD-SD). All SDs were recorded with low resistance electrodes (0.5-1 MΩ) placed in the CA1 dendritic subfield. K-SD was induced by local ejection of 1 M KCl via glass micropipette (~1 µm tip diameter, 40 psi). The ejection volume was estimated to be ~10nl, based on the comparison between the diameter of droplet from 10-20 ejection and a reference volume (see Aiba et al., 2012). KCl ejection pipettes were placed in hippocampal CA1 dendritic subfield >300 µm distant from the recording sites at 50 µm from the slice surface.

The threshold for K-SD was determined with escalating duration of KCl microinjections. Threshold testing began with a 10 ms pulse, and then doubling of stimulus duration every 5 minutes, until a propagating event was generated. Ouabain SD was generated by superfusion of 30 µM ouabain containing ACSF, equilibrated with varying concentrations of O_2, as indicated in the text. OGD-SD was generated by superfusion with a modified ACSF, prepared by substitution of 95% O_2 with 95% N_2, and 10 mM glucose with 1.5mM glucose and 8.5mM sucrose.

Figure 1 shows representative SDs generated by the three test stimuli in this study (KCl microinjection, ouabain exposure or OGD). In each case, SD was demonstrated as spreading wave of intrinsic optical signal (IOS) increases, accompanied by a characteristic biphasic DC potential change recorded with the extracellular recording electrode. K-SD was generated from a local KCl microinjection site and propagating through CA1 region. This propagation was electrically detected as a characteristic biphasic extracellular DC shift (Fig. 1A). Following the passage of SD, IOS showed a long lasting (~10 min) increase, which returned to baseline level without any evidence of tissue damage.

K-SD was generated from a local KCl microinjection site and propagating through CA1 region. This propagation was electrically detected as a characteristic biphasic extracellular DC shift (Fig. 1A). Following the passage of SD, IOS showed a long lasting (~10 min) increase, which returned to baseline level without any evidence of tissue damage. Similar to K-SD, ouabain- and OGD exposures resulted in the propagating SD waves were detected as IOS

increases (Joshi and Andrew, 2001). Unlike K-SD, ouabain- and OGD exposures spontaneously generated SD. passage of SDs were followed by irrecoverable IOS decreases in dendritic fields (Fig. 1C-F), attributable to the formation of granular structure in dendrites (dendritic beading) that inhibits passage of visible light through the tissue (Jarvis et al., 1999). Electrical responses of ouabain- and OGD-SD were typically monophasic, likely reflecting a lack of transmembrane ion flux in the irrecoverably damaged tissue.

As presented in Figures 1B&C, initiation and propagation phases of ouabain- and OGD-SD could be reliably resolved with these imaging methods. Thus SD usually initiated on either side of the CA1 subfield with gradual increase of IOS signal, followed by a stable propagation phase. SD propagation rates were analyzed at least 8 s after SD, and rates were averaged from at least 3 consecutive images.

4.3.3 Drugs

D-AP5, MK801 and Ro256981 were obtained from Sigma. D-AP5 was dissolved in water at a stock concentration of 10 mM. MK801 and Ro25-6981 were dissolved in DMSO at 100 mM and 10 mM, respectively. Matched final DMSO concentrations were used in vehicle control experiments. In the experiments that included $ZnCl_2$, 200 µM histidine was always included in the ACSF. This method can effectively limit Zn^{2+} precipitation in phosphate containing solutions (Rumschik et al., 2009). Histidine supplementation was preferred for the present studies over phosphate removal, to avoid potential

negative effects on metabolism. As reported previously, (Aiba et al., 2012) no confounding effects of histidine alone on SD characteristics were detected.

4.3.4 NMDAR current recording

Whole-cell NMDAR currents were recorded from single CA1 pyramidal neurons. Whole-cell clamp was obtained with patch pipettes (2-3 MΩ) filled with internal solution containing (in mM): 130 Cs-methanesulfonate, 10 Hepes, 0.5 $CaCl_2$, 8 NaCl, 10 EGTA, 5 QX314, 2 Na_2ATP, 0.3 Na_3GTP, pH adjusted to 7.2. Neurons were dialyzed for at least 10 minutes prior to recordings. Excitatory postsynaptic NMDAR currents ($EPSC_{NMDA}$) were evoked by iontophoretic stimulations with high resistance electrodes (20-30 MΩ) filled with 1 M sodium glutamate. Glutamate electrodes were placed <30 µm from the putative locations of apical dendritic trees of whole-cell patched neurons. Recordings were made in the presence of 20 µM DNQX and 5 µM bicuculline, and evoked glutamate currents were initiated after stepping membrane voltage to +30 mV for 1 - 2 seconds, depending on the latency of the response. The duration and intensity of glutamate stimulation was adjusted for each recording in order to obtain evoked currents less than 1 nA in amplitude and 1 sec duration (typical stimuli: 10-30 µA, 0.5-3 ms). Control experiments utilizing the same parameters with 1 M NaCl-filled stimulation electrodes did not evoke postsynaptic currents (n=2). The Zn^{2+} sensitivity of NMDAR currents was measured by superfusing slices with ACSF containing 100 µM $ZnCl_2$. The effect of hypoxia and $ZnCl_2$ was evaluated by comparing the amplitudes of baseline responses (average of 9

traces) with the average of 4-6 responses obtained after 10-15 min exposure to the hypoxic solution containing $ZnCl_2$. Input resistance and series resistance was estimated ~500 ms prior to testing NMDA currents. Recordings in which series resistance changed by >20% were excluded from the analysis.

4.3.5 Statistics

Student *t*-tests or ANOVA with post hoc Turkey analysis were used for statistical analysis unless otherwise described. $P<0.05$ was considered to be statistically significant.

4.4 RESULTS

4.4.1 Differential sensitivity of K-SD and OGD-SD to extracellular Zn^{2+}

Figure 1 shows the general features of SD generated by the three stimuli used in the study: KCl microinjection, exposure of slices to the Na^+/K^+-ATPase inhibitor ouabain, or superfusion with modified ACSF with reduced oxygen and glucose. The sensitivity of these three types of SD to extracellular Zn^{2+} was examined by bath application of 100 µM $ZnCl_2$ (**Figure 2**), and experimental slices were interleaved with control slices throughout.

$ZnCl_2$ reliably inhibited the rate of propagation of K-SD, as reported previously and which was attributed to extracellular intracellular actions of Zn^{2+} in this model (Aiba et al., 2012). In addition, $ZnCl_2$ significantly increased the threshold

for K-SD initiation (Fig. 2A). This increased threshold is consistent with extracellular Zn^{2+} inhibition of SD frequency seen in an *in vivo* CSD model (Aiba et al., 2012).

Similar to K-SD, propagation of ouabain-SD (Fig. 2B) also showed a significant sensitivity to extracellular Zn^{2+}. The concentration of ouabain (30 µM) was determined to have significant sensitivity to NMDAR antagonists, and under these condition ouabain SD was reliably blocked with MK801 (n=5). In these experiments, slices were preincubated with 100 µM $ZnCl_2$ for 10 min and SD was then generated by further incubation with ouabain solution containing 100 µM $ZnCl_2$. $ZnCl_2$ showed significant inhibition of the SD propagation in this model (**Fig. 2C**). However except for propagation rate, SD was reliably generated in the presence of $ZnCl_2$, and SD threshold as evaluated by SD onset time was unaffected (**Fig. 2D**).

We next tested the sensitivity of OGD-SD to $ZnCl_2$. In the present study, the OGD solution lacked any added O2, but a small amount of glucose (1.5mM) was maintained in the modified ACSF, as these conditions proved effective for testing pharmacosensitivity of OGD-SD (see Methods, Figure 5 and Discussion). Similar to the test of ouabain SD, slices were preincubated with $ZnCl_2$ (100µM, 10min) and SD was then generated by OGD solution containing $ZnCl_2$. $ZnCl_2$ was without effect on propagation rate or onset of OGD-SD (**Fig. 2C**). Because of the poor solubility of $ZnCl_2$ in ACSF (see Methods), we could not did not test higher $ZnCl_2$ concentrations to determine whether resistance to Zn^{2+} was absolute. However these results reveal a large difference in Zn^{2+} sensitivities of OGD-SD,

compared with SD generated under conditions of abundant oxygen (K-SD and ouabain SD).

4.4.2 2. Oxygen concentration strongly influences Zn^{2+} sensitivity of SD propagation

We next examined whether the selective removal of oxygen and/or glucose could be sufficient to render KSD insensitive to Zn^{2+}. Ouabain was a suitable SD stimulus to test these possibilities, because ouabain exposure reliably generates SD in the absence of oxygen/glucose. We first examined the effects of different oxygen concentrations by equilibrating ACSF with either 0% or 21% O_2 with 5% CO_2. Unlike 95% O_2 condition and similar to OGD-SD, (see Fig 1C) significant tissue swelling (increased IOS) was observed prior to the onset of SD, when slices were exposed to hypoxic ouabain solutions (**Fig. 3A&B**). In addition, the propagation rate of ouabain-SD was significantly slower in 21% and 0% O_2, when compared with 95% O_2 ($n=5$, $p<0.05$). However, except for these differences, SD was reliably generated in these hypoxic conditions, and no differences in propagation rate or onset were observed between 21% and 0% O_2.

In contrast to these similarities, the $ZnCl_2$ sensitivities of ouabain SD generated with these lower O_2 concentrations SDs were quite different. Thus SD propagation in 21% O_2 was significantly inhibited by $ZnCl_2$ (**Fig. 3A**, similar to the 95% O_2 condition). However, no inhibitory effect of $ZnCl_2$ on the propagation of ouabain-SD was observed in 0% O_2 (**Fig. 3B**). These results suggest that O_2 concentration alone can significantly modify the sensitivity of SD to Zn^{2+}.

As shown in **Fig 3C**, both hypoxia solutions similarly inhibited synaptic transmission as measured by prompt inhibition fEPSP amplitude, likely via A_1 receptor dependent mechanism (Sebastiao et al., 2001). Mitochondrial respiration was also demonstrated to be effectively inhibited by these hypoxia solutions as evidenced by significant elevation of NAD(P)H autofluorescence (**Fig. 3D**). Since there was some trend towards a stronger synaptic depression under 0% O_2 than in 21% O_2, we considered the possibility that increased suppression of synaptic transmission could contribute to greater resistance of responses in 0% O_2 to $ZnCl_2$. This possibility was tested by blocking fully synaptic activity with the potent A_1-R agonist, N^6-cyclopentyladenosine (hereafter CPA, 300 nM in 95% O_2 superfusate). Exposure to CPA in 95% O_2 solution significantly decreased propagation rate, to a similar level as observed in 21% and 0% O_2. However CPA had no effect on the $ZnCl_2$ sensitivity (propagation rate, Control: 3.28 ± 0.20 mm/min, $ZnCl_2$: 2.09 ± 0.19 mm/min, n=5, p<0.01), indicating that basal synaptic strength did not influence the Zn^{2+} sensitivity.

In addition to testing effects on oxygen availability, we also examined the influence of glucose deprivation in the ouabain-SD model. SD was reliably generated by ouabain solutions that lacked all added glucose (in ACSF 95% O_2 and glucose substitution with sucrose). Under these conditions, SD propagation almost identical to control experiments (Figure 2C), and sensitivity to $ZnCl_2$ was unchanged (SD propagation rate, Control: 4.50 ± 0.44 mm/min, $ZnCl_2$: 2.71 ± 0.13 mm/min, n=5, p<0.01). These results argue against a potential role of glucose availability in the lack of $ZnCl_2$ sensitivities of OGD-SD.

4.4.3 Zn^{2+} sensitivity of OGD-SD reversed by the protein oxidizer DTNB

The results above suggested that O_2 concentration can be sufficient to affect the sensitivity of SD to extracellular Zn^{2+}. One potential mechanism that could explain these results is that severe hypoxia modulates Zn^{2+} sensitivities of target proteins by directly modifying extracellular redox potential. This possibility was tested by pre-exposure to the protein oxidizer DTNB. DTNB is a protein oxidizer with poor membrane permeability (Wagner et al., 1996) and has been used to modify redox modulation of many proteins, including extracellular domains of NMDAR (Pringle et al., 2000a; Choi et al., 2001; Herin et al., 2001). A previous study has shown that a high concentration of DTNB (2 mM) significantly inhibited SD triggered by hypoxia (Hepp et al., 2005), and consistent with this, 2 mM DTNB blocked OGD-SD in our recording conditions (data not shown). A lower concentration of DTNB (0.5mM) was found more appropriate for the current studies, since it did not prevent SD initiation, but likely retains an ability to prevent anoxia induced redox modulation (e.g. Gozlan et al., 1994). OGD-SD generated in control and the slices preincubated with DTNB (0.5 mM, 10 min, 95% O_2) showed similar propagation rates and onset times (**Figure 4A**). However DTNB pre-treatment significantly increased the sensitivity of OGD-SD to ZnCl2. Unlike control OGD-SD (Figure 2C), $ZnCl_2$ significantly decreased propagation rate and also delayed onset of OGD-SD DTNB preexposed slices (**Figure 4B**). Similarly, propagation of ouabain SD generated in 0% O_2 (which

was previously insensitive to $ZnCl_2$; see Figure 4G), became sensitive to $ZnCl_2$ in DTNB preexposed slices (**Figure 4C**). In addition to DTNB, oxidized glutathione (0.5mM 10min pre-exposure) also significantly reversed $ZnCl_2$ sensitivity of OGD-SD (propagation rate, Control: 2.26 ± 0.11 mm/min $ZnCl_2$: 1.55 ± 0.10 mm/min, n=5, p<0.01), supporting a role of redox modulation in the Zn^{2+} sensitivity of OGD-SD.

In contrast to significant effect on SD generated in anoxia, DTNB was without effect on the Zn^{2+} sensitivity of K-SD in normoxic conditions, in which little redox modulation was expected (**Figure 5D**). DTNB did not show any effect on Zn^{2+} sensitivity of threshold in these experiments (p>0.50, n=5). Therefore these results suggest that extracellular redox modulation under severe hypoxia is, at least in part, likely responsible for the lack of Zn^{2+} sensitivity of SD.

As an additional control, we examined whether intracellular Zn^{2+} accumulation could contribute to inhibitory effects of $ZnCl_2$ exposures, specifically in the conditions where a $ZnCl_2$ effect was revealed by DTNB. We examined this possibility by loading Zn^{2+} intracellularly by exposure to Zn^{2+}-ionophore complex (ZnPyr: 100 µM $ZnCl_2$ and 1 µM Pyrithione) for 10min. In order to exclude the effects of residual extracellular Zn^{2+} effect, slices were briefly washed with ACSF (3 min) and SD was generated with nomimnally Zn^{2+} free OGD solution. Intracellular Zn^{2+} loading did not affect propagation rate or onset of OGD-SD in DTNB (propagation rate, Control: 2.42 ± 0.15 mm/min, ZnPyr: 2.60 ± 0.24 mm/min, SD onset, Control: 7.24 ± 0.39 min, ZnPyr: 7.71 ± 0.44 min, n=5, p>0.5). These results argue against a possibility of intracellular Zn^{2+}

accumulation contributing to these effects, and support the idea that Zn^{2+} may inhibit OGD-SD in an anoxic redox modulation of an extracellular site.

4.4.4 Redox modulation in anoxic condition (0% O_2) can modulate Zn^{2+} sensitivity of NMDAR

We next tested whether the sensitivity of one potential target for Zn^{2+} (NMDAR) was modified by redox modulation by hypoxia and DTNB. For these analyses, NMDAR dependent whole-cell currents were evoked by local iontophoretic glutamate application at +30 mV in the presence of $GABA_A$ and AMPA receptor antagonists (see Methods). Under these conditions, the evoked whole-cell currents were detected as slow outward current (Figure 5A), and D-AP5 almost completely occluded these responses (10 μM AP5, 95.7 ± 5.0% inhibition, n=3).

We examined inhibitory effects of Zn^{2+} on these NMDAR currents in different O_2 concentration. After baseline responses were obtained, slices were exposed to 100 μM $ZnCl_2$ in various O_2 concentrations for 10 min and glutamate iontophoresis repeated. In contrast to synaptically-evoked responses (see Figure 3A above), glutamate iontophoresis reliably evoked NMDAR currents in 21% and 0% O_2 (NMDAR current in 95% O_2 vs. 21% or 0% O_2, $p>0.10$, paired t-test, **Fig. 6A&B**).

Effects of $ZnCl_2$ exposures were compared with time-control experiments. In 95% O_2, these NMDAR currents were strongly inhibited by Zn^{2+} (100 μM $ZnCl_2$, 79.7 ± 4.1%, n=3). Similarly, 100 μM $ZnCl_2$ significantly decreased the NMDAR

currents in 21% O_2, and similar inhibition was observed in DTNB pre-exposed slices (**Fig. 6B**). The current inhibition by $ZnCl_2$ in 21% O_2 was somewhat smaller than in 95% O_2, which may be due to modification of extracellular redox potential and/or due to other modification under hypoxia (see Discussion). In contrast to 95% or 21% O_2, addition of $ZnCl_2$ alone was almost without effect in 0% O_2, however significant Zn^{2+} inhibition was revealed when tested in 0% O_2 and DTNB preexposed slices. These results indicate that similar to SD, the Zn^{2+} sensitivity of NMDAR was attenuated by a mechanism involving hypoxia dependent redox modulation.

4.4.5 DTNB potentiated competitive NMDAR antagonist to inhibit SD

Finally, we examined whether the redox sensitivity of $ZnCl_2$ effects were matched by differences in sensitivity to synthetic NMDAR antagonists. This possibility was examined by testing effects of DTNB effect on the NMDAR antagonist sensitivities of OGD-SD, under the conditions as used above for probing differences in Zn^{2+} sensitivity (Figure 6). At high concentrations of these antagonists, no propagating SD wave was observed optically, and no sharp DC shift was recorded to indicate SD propagation. Slices degenerated progressively following ~15-20 minutes depletion of energy substrates under these conditions. Thus in order to evaluate additive effects of DTNB to the antagonist inhibition of OGD-SD, antagonist concentrations were chosen to obtain partial inhibitory effect (i.e. slower propagation rate or delayed SD onset) under control conditions,

before evaluating additive effects of DTNB. For the experiments below, slices were pre-incubated with either MK801 (20 µM), D-AP5 (25 µM) or Ro25-6981 (10 µM) for 10 min and then challenged with OGD.

Exposure to MK801 consistently delayed SD onset and decreased propagation rate of OGD-SD in control slices (**Figure 6A**) and the inhibitory effects were not significantly different in the DTNB pretreated slices. Similar to MK801, D-AP5 delayed the onset of OGD-SD, but was without effect on SD propagation rate. In DTNB pretreated slices, D-AP5 further delayed SD onset time and prevented SD generation in 1 of 5 DTNB slices. D-AP5 also decreased SD propagation rate in DTNB pretreated, but not in control slices. Ro25-6981 also delayed SD onset in control slices, and SD onset was further delayed in 4 out of 6 slices and in 2 DTNB pretreated slices SD was not generated. Unlike other antagonists, Ro25-6981 was without effect on the propagation rate of SD in both control and DTNB treated slices. These results imply that anoxic redox modulation can significantly affect efficacies of some NMDAR antagonists on OGD-SD.

4.5 DISCUSSION

4.5.1 General

We have previously shown that SD generated by local KCl application was inhibited by extracellular Zn^{2+}, and the present study extended the findings to other forms of SDs that may be relevant for acute brain injury. The initial

comparison revealed quite different $ZnCl_2$ sensitivities between normoxic SD (K-SD and ouabain SD in 21% and 0%) and anoxic SD (OGD-SD, ouabain SD in 0% O_2). The subsequent analysis suggested that the hypoxia effect was, at least in part, mediated by oxygen dependent redox modulation, and could potentially involve modification of targets such as NMDA receptors. These findings were extended to inhibitory effects of synthetic NMDAR antagonists and collectively indicate that anoxia induced redox modulation can significantly reduce efficacy of a range of pharmacological inhibitors of SD.

4.5.2 Zn^{2+} sensitivity of SD propagation and initiation

The present study evaluated the possibility that extracellular Zn^{2+} can act as an inhibitor of SD under conditions relevant to ischemia. The results showed that Zn^{2+} inhibition of SD seems to be abolished by anoxic redox modulation. Thus extracellular Zn^{2+} accumulation is likely no longer protective by limiting the numbers of SDs propagating through vulnerable ischemic tissues, and in contrast, may contribute to toxicity by increasing intracellular Zn^{2+} accumulation after transporter-mediated uptake (Qian et al., 2011).

The present study indicated that Zn^{2+} is not universally inhibitory to SD and that inhibitory effects are limited to SD propagating in oxygenated tissue. Mechanistic studies revealed that this is due to hypoxia dependent redox modulation and reversal of redox reduction by DTNB revealed Zn^{2+} sensitivity of SD propagating in hypoxic (0% O_2) tissue. Thus Zn^{2+} is intrinsically inhibitory for SD, but the efficacy is significantly modified by local tissue oxygenation. This

suggests that a SD generated at a single site can propagate differently depending on the degree of tissue oxygenation. The significance of extracellular Zn^{2+} accumulation and inhibition of SD propagation for stroke damage is not yet known. While a number of influential studies suggest a toxic role for intracellular Zn^{2+} accumulation in ischemic brain injury (Koh et al., 1996; Calderone et al., 2004), some studies have suggested protective roles of Zn^{2+} in similar focal ischemia models (Zhao et al., 1996; Kitamura et al., 2006). These protective effects raise the possibility that extracellular sites of Zn^{2+} action could provide some neuroprotection during ischemic brain injury. Some of the controversial roles of Zn^{2+} in ischemic brain injury could be due to variability in the volume of ischemia, reperfusion rate and effectiveness of recurrent supply which may modulate protective role of extracellular Zn^{2+} by affecting local tissue oxygenation. A recent study has demonstrated that SD generated following focal stroke in rodents can circularly propagate around the infarct core (Nakamura et al., 2010). Extracellular actions of Zn^{2+} released during SD (Carter et al., 2011a) may partly contribute to such a propagation pattern. Thus by preventing SD propagation in healthy tissue, elevation of extracellular Zn^{2+} concentration may confine SD propagation in the metabolically compromised vulnerable tissue.

4.5.3 Pharmacoresistance of SD

In general, acute ischemia first generates anoxic depolarization (AD), which is followed by recurrent periinfarct depolarizations (PIDs) that propagate around

hypoperfused penumbral tissue and contribute to damage of vulnerable neurons (Dreier, 2011; Lauritzen et al., 2011). Because of the extended time window in which PIDs are seen, it is likely that these events are primarily involved in the progression of delayed neuronal death. Complete oxygen and glucose deprivation has commonly been used to generate SD in brain slice models, but these events resemble to AD rather than PIDs, due to the complete lack of energy supply during these SD events, and their high resistance to NMDAR antagonists (see Introduction). As described in the Introduction, PIDs generated by focal ischemia models show significant sensitivities to NMDAR antagonists (Gill et al., 1992; Iijima et al., 1992; Hartings et al., 2003). However an *in vitro* PID model with similar NMDAR sensitivity has not previously been established. The present studies utilized an OGD model with a reduced metabolic stress by using only 85% glucose deprivation. While this model will not reproduce many aspects of PIDs occurring in vivo, OGD-SD in our study showed significant sensitivity to NMDAR antagonists (see Introduction, Figure 5) and allowed us to identify a redox dependent mechanism that reduced phrmacosensitivity to SD under anoxic condition. Similarly, the concentration of ouabain used here (30uM) generated an event that was reliably prevented by NMDAR antagonists, whereas NMDAR antagonist did not prevent SD when generated with 100 µM ouabain (Balestrino et al., 1999). Thus the data obtained here are not directly comparable to previous studies that showed insensitivity to NMDAR antagonist in similar brain slice preparations (Balestrino et al., 1999; Jarvis et al., 2001; Joshi and Andrew, 2001). SD propagation is contributed to by NMDAR activation and other

factors, such as extracellular potassium concentration While the increased NMDAR antagonist sensitivity by reduced stimuli was not a main subject of the present study, extracellular potassium clearance by residual Na^+/K^+-ATPase activity could contribute to reduced potassium concentration (Xiong and Stringer, 2000; D'Ambrosio et al., 2002) and enhanced reliance of SD propagation on NMDAR-dependent mechanisms.

4.5.4 Redox modulation of ion channel activities by anoxia

In the present study, we have shown that the oxidizer DTNB can significantly sensitize NMDAR to the Zn^{2+} in 0% O_2. Because only a single high $ZnCl_2$ concentration was tested in the present study, the mechanism(s) underlying the inhibitory effect of Zn^{2+} are not fully delineated. However recordings of NMDAR current at +30 mV suggest that the inhibition is not mediated by voltage dependent block, but is rather based on allosteric modulation (Paoletti et al., 1997). Redox modulation of NMDARs has been long been known, and it was concluded that reducing conditions potentiates NMDAR currents in neuronal cultures (Aizenman et al., 1989). The relevance for pathological conditions was subsequently examined, and found a deleterious role of NMDAR redox modulation in seizures and ischemic damage (Gozlan et al., 1994; Sanchez et al., 2000). Owing to the high oxygen consumption rates of acute brain slices (Galeffi et al., 2011; Hall et al., 2012), the brain tissue could have experienced severe tissue hypoxia and resulted in anoxia dependent redox modification.

Such a mechanism could contribute to some controversial results associated with roles of Zn^{2+} in seizures (e.g. Cole et al., 2000; Qian et al., 2011). On the other hand, effects of oxidation are controversial, since the protein oxidizer DTNB decreased NMDAR currents in isolated neurons (Aizenman et al., 1989), whereas it was without effect on NMDAR currents in brain slices (Sanchez et al., 2000). It was suggested in the latter study that NMDARs in brain slice preparation are mostly present as oxidized status. The high content of oxidized conformation in brain slice might have facilitated detection of reduced conformational change in 0% O_2.

Previous studies have suggested the presence of oxygen sensor sites in NMDAR at the N-terminal region (Takahashi et al., 2007). The presence of Zn^{2+} binding sites in the N-terminal domain suggest that structural changes in this region affected Zn^{2+} binding or subsequent conformation changes. Thus our results likely suggest that decreased oxygen concentration modulated NMDAR structure and significantly decreased Zn^{2+} sensitivity of NMDAR current. A previous study has also suggested significantly higher Zn^{2+} sensitivity of the oxidized NMDAR (Tang and Aizenman, 1993). The reported change in Zn^{2+} sensitivity was smaller compared with the present study. This could be explained by differences in the redox modulation method used (alkylation vs. anoxia) and different GluN2 subunit contents between brain tissues from adults vs. embryos. Similar to Zn^{2+}, redox modulation has been shown to decrease the efficacy of competitive NMDAR antagonist to prevent excitotoxicity and ischemia-induced neuronal death (Pringle et al., 2000b). The mechanism(s) underlying redox

modulation of NMDAR antagonist sensitivity is not understood. However in both the present and the previous study,the open channel blocker MK801 was shown to be insensitive to the redox modulation (Pringle et al., 2000b). Open channel blockers such as memantine and ketamine are already used in clinical settings and could be useful for targeting SD occurring near the ischemic core where oxygen concentration is severely decreased and NMDARs may be significantly modified to their reduced structure.

Although the NMDAR was the primary interest in the present study, other ion channels are also susceptible to hypoxia dependent redox modulations. For example, one study showed that DTNB can postpone hypoxic SD onset by activation of BK channels (Hepp et al., 2005). Activation of BK channels may decrease rate of discharge prior to large depolarization of SD and may reduce potassium accumulation ahead of SD wave. The resultant decreased extracellular potassium accumulation may increase demand on NMDAR activation for generation of propagating wave and made SD propagation more sensitive to the Zn^{2+} inhibition of NMDAR.

4.5.5 Conclusion

The present study shows that inhibitory effect of Zn^{2+} on SD and NMDAR are significantly decreased by severe hypoxia. This effect likely hinders protective functions of Zn^{2+} to limit SD- dependent injurious mechanisms in ischemic brain injury. Because of the high oxygen consumption of mammalian brain, severe excitatory injury may also capable of inducing such redox

modification of NMDAR and affect Zn^{2+} sensitivity. These findings should be important for design of targeting SD and NMDAR dependent brain injury.

4.6 FIGURE LEGENDS

Figure 4.1: Representative SD responses generated by the three different stimuli.

A: SD generated by KCl microinjection. Left panels show a series of 6 images (2 second intervals) of intrinsic optical signals ($\Delta T/T_0$) following KCl microinjection ejected via a micropipette (location indicated by "KCl"). Intensity increases in these ratio images are indicated by brightening of the image, and the advancing wavefront of SD is marked by the arrowheads. Traces at right show IOS and electrical signals recorded from the same preparation. IOS signals were recorded from a region of interest indicated by the box, and simultaneously recorded field potential changes recorded with a microelectrode place at position "rec". The dotted vertical line shows the alignment between the large DC shift and the initial IOS signal that accompanies the spread of SD. Scale bar: 400 µm **B:** SD generated by exposure of slice to the Na^+/K^+/ATPase inhibitor ouabain (30 µM). Details of the figure are as described for A, with large DC shift being and propagating wavefront of SD being generated ~5 min after the onset of ouabain exposure. **C:** SD generated by exposure of slice to OGD. Similar to ouabain-SD, OGD-SD was initiated after a significantly delay and rates of SD propagation could be calculated by advancing wavefront of IOS signals.

Figure 4.2: Differential sensitivities of K-SD, ouabain-SD and OGD-SD to $ZnCl_2$.

Slices were pre-exposed to $ZnCl_2$ (100 µM, 10 min) before application of one of the three SD stimuli. **A:** Propagation rates of K-SD were significantly reduced, and the threshold for SD onset (see Methods) was significantly increased in the same preparations (n=6, **p<0.01, ***p<0.005). **B:** $ZnCl_2$ significantly reduced propagation rates of outbain-SD, with no significant decrease in the time to SD onset (n=5, **p<0.01). **C:** In contrast to the two other stimuli, $ZnCl_2$ exposures were without effect on the propagation rates of OGD-SD (n=5).

Figure 4.3: Changing O_2 availability dictates sensitivity to $ZnCl_2$.

A&B: Evidence for effectiveness of experimental hypoxia. Slices were first exposed to ACSF equilibrated with 95% O_2, and then challenged with modified ACSF equilibrated with either 21% or 0% O_2 (replaced with N_2, see Methods). Consequences of tissue hypoxia were evaluated based on reductions in field excitatory postsynaptic potentials (fEPSP) (**A**) and increases in tissue NAD(P)H autofluorescence (**B** in the same preparations). **C&D:** Zn^{2+} sensitivity of ouabain SD generated under these reduced oxygen conditions. Left panels show representative traces of ouabain-SD and right panels show effects on propagation rate and SD onset. A significant decrease in SD propagation was observed in 21% by $ZnCl_2$ application but inhibitory effects ~~of $ZnCl_2$~~ were abolished in 0% O_2 (n=5 each, **p<0.01).

Figure 4.4: The protein oxidizer DTNB was sufficient to confer $ZnCl_2$ sensitivities to SDs in anoxic conditions.

A: DTNB pre-exposure (0.5 mM, 10 min) by itself had no effect on OGD-SD propagation rate (*left*) or onset (right). **B:** In the presence of DNTB, $ZnCl_2$ effectively inhibited OGD-SD propagation rate, and delayed OGD-SD onset (n=5, *p<0.05, **p<0.01). **C:** Similarly, ouabain-SD generated in 0% O_2 was also inhibited by ZnCl2 in DTNB pre-treated slices. **D:** Under conditions where $ZnCl_2$ was already effective, DTNB did not further enhance $ZnCl_2$ sensitivity. Illustrated here is a lack of effect of DTNB alone on K-SD, and a lack of effect on the inhibition of K-SD by $ZnCl_2$ (n=5).

Figure 4.5: Zn^{2+} inhibition of NMDAR current was sensitive to hypoxic redox modulation.

A: Whole-cell NMDAR currents were evoked by local glutamate iontophoresis pulses and examined in hypoxic conditions (0% O_2 ACSF). The top pair of traces shows a response in 95% O_2 (solid trace) and a small amount of rundown of the response in the same neuron obtained after 10min exposure to 0% O2 (dashed trace). The middle pair of traces show that $ZnCl_2$ exposure caused little additional run-down of evoked NMDAR current, when tested in 0% O_2. However when slices were exposed to DTNB in 0% O_2, $ZnCl_2$ caused a large decrease in current amplitude. **B:** Summary data from sets of data illustrated in A, and also similar experiments conducted in 21%O_2 ACSF (**p<0.01).

Figure 4.6: Augmentation of NMDA receptor antagonist efficacy by DTNB.

OGD-SD was generated in control (vehicle: 0.1% DMSO), in the presence of antagonist and with antagonist in DTNB treated slice. **A:** The NMDAR open channel blocker MK801 (20 μM) significantly delayed SD onset and inhibited propagation rate, but the inhibitory effect was not modified in DTNB pretreated slices. **B:** The competitive NMDAR antagonist D-AP5 (25 μM) also significantly delayed SD onset and inhibited propagation, and the inhibitory effect was significantly larger in the DTNB pretreated slices. In one experiment with D-AP5 and DTNB, SD was not detected. **C:** The GluN2B subunit selective allosteric inhibitor Ro25-6981 (10 μM) significantly delayed SD onset and the inhibitory effect was larger in the DTNB treated slices. Unlike other NMDA antagonists, Ro25-6981 was without effect on SD propagation in control and DTNSB treated slices. In two experiments with Ro25-6981 and DTNB, SD was not detected. Numbers in the bars indicate incidences of SD. Statistical tests were conducted by using values obtained from successfully generated SD. * $p<0.05$, ** $p<0.01$

Figure 4.1

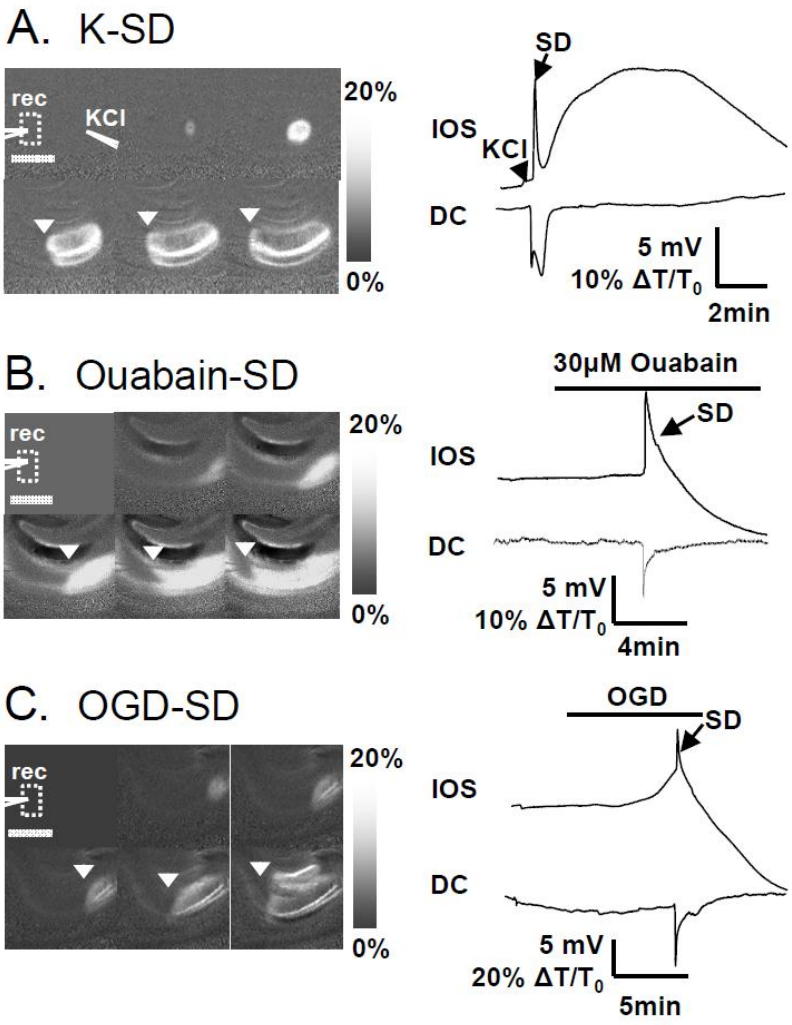
A. K-SD
rec
KCl
20%
0%
SD
IOS
KCl
DC
5 mV
10% ΔT/T0
2min
B. Ouabain-SD
rec
20%
0%
30μM Ouabain
SD
IOS
DC
5 mV
10% ΔT/T0
4min
C. OGD-SD
rec
20%
0%
OGD
SD
IOS
DC
5 mV
20% ΔT/T0
5min

Figure 4.2

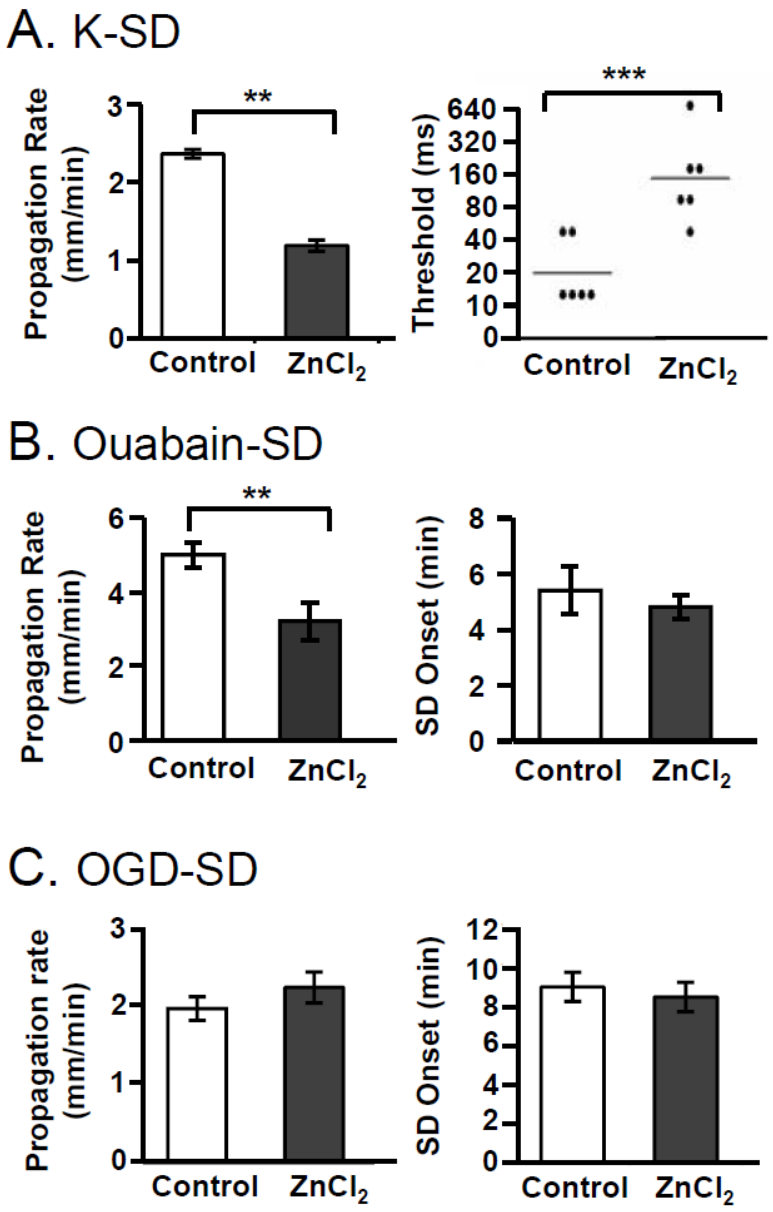
A. K-SD
Propagation Rate (mm/min)
3
2
1
0
**
Control
ZnCl2
Threshold (ms)
640
320
160
80
40
20
10
0
***
Control
ZnCl2
B. Ouabain-SD
Propagation Rate (mm/min)
6
4
2
0
**
Control
ZnCl2
SD Onset (min)
8
6
4
2
0
Control
ZnCl2
C. OGD-SD
Propagation rate (mm/min)
3
2
1
0
Control
ZnCl2
SD Onset (min)
12
10
8
6
4
2
0
Control
ZnCl2

Figure 4.3

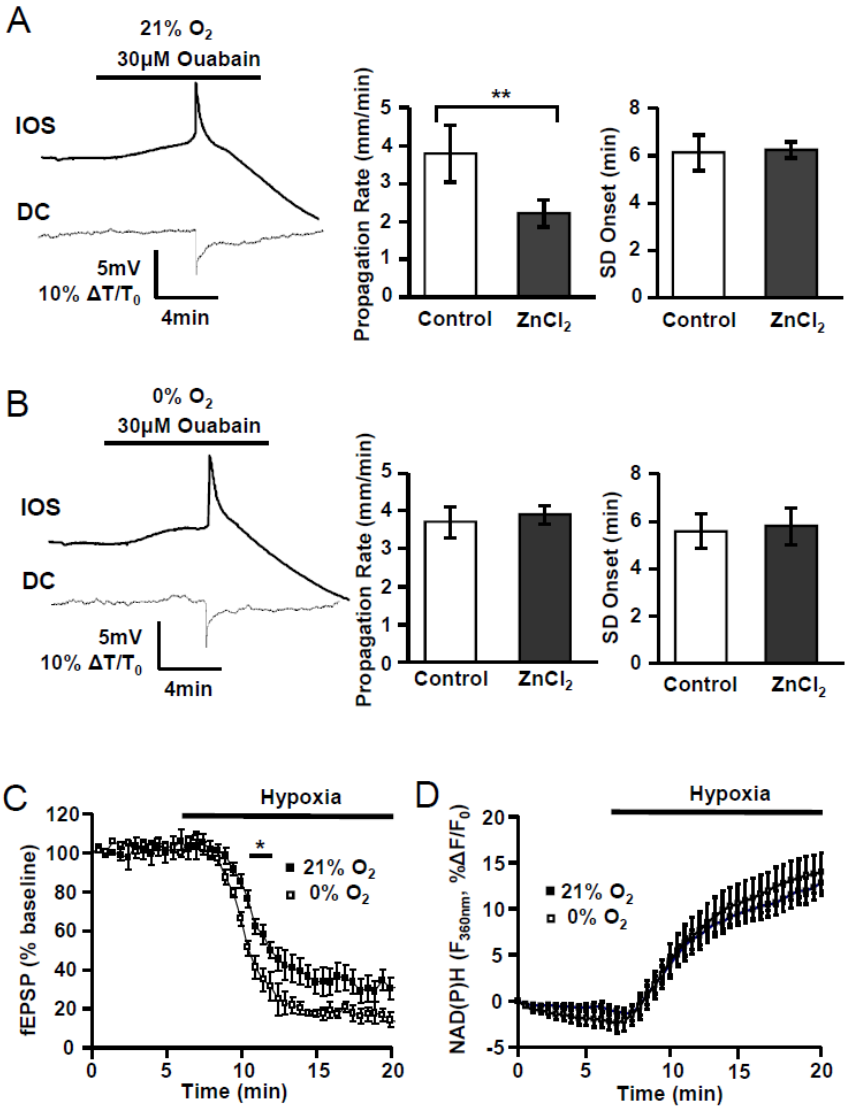
A
21% O2
30μM Ouabain
IOS
DC
5mV
10% ΔT/T0
4min
Propagation Rate (mm/min)
**
Control
ZnCl2
SD Onset (min)
Control
ZnCl2
B
0% O2
30μM Ouabain
IOS
DC
5mV
10% ΔT/T0
4min
Propagation Rate (mm/min)
Control
ZnCl2
SD Onset (min)
Control
ZnCl2
C
Hypoxia
fEPSP (% baseline)
*
21% O2
0% O2
Time (min)
D
Hypoxia
NAD(P)H (F360nm, %ΔF/F0)
21% O2
0% O2
Time (min)

Figure 4.4

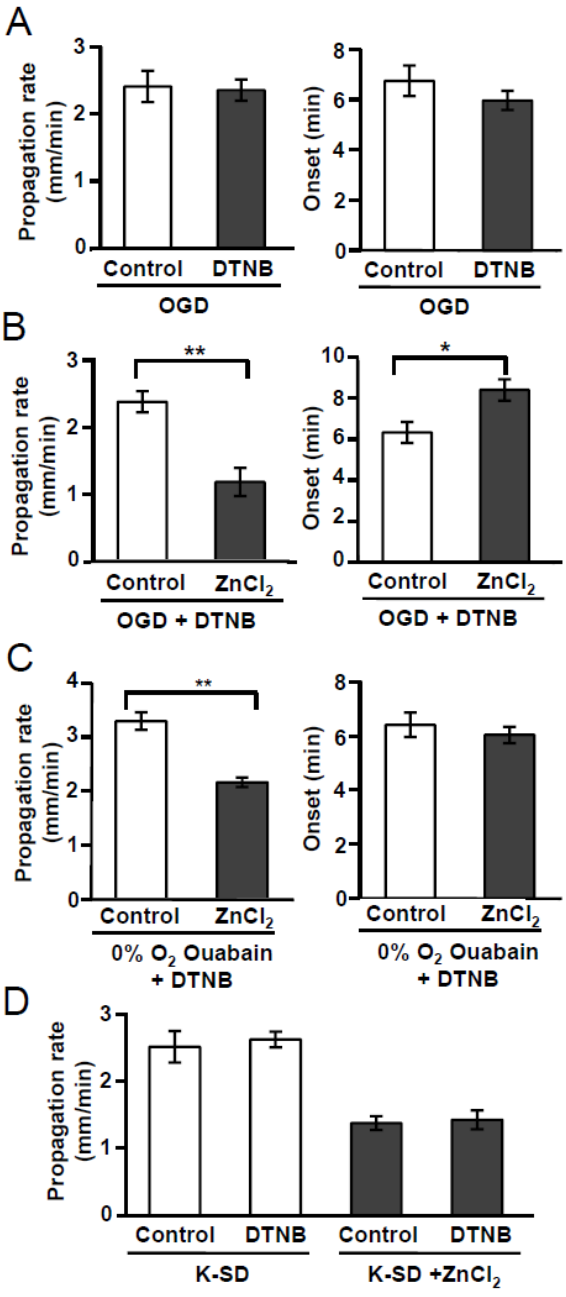
A
Propagation rate (mm/min)
Onset (min)
Control
DTNB
OGD
B
**
*
ZnCl2
OGD + DTNB
C
0% O2 Ouabain + DTNB
D
K-SD
K-SD +ZnCl2

Figure 4.5

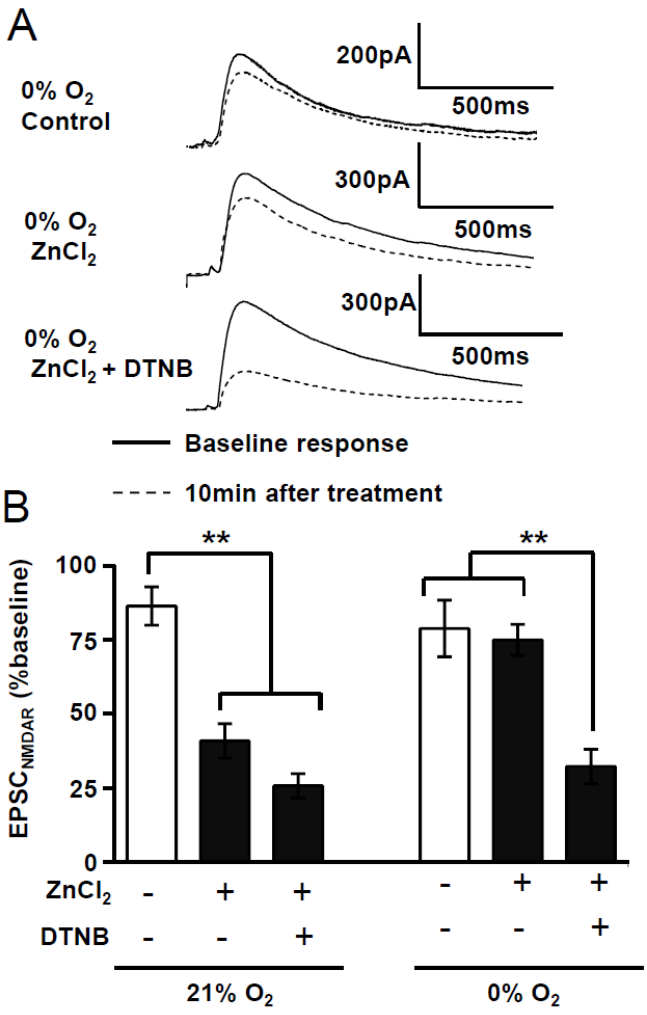
A
200pA
500ms
0% O2
Control
300pA
500ms
0% O2
ZnCl2
300pA
500ms
0% O2
ZnCl2 + DTNB
Baseline response
10min after treatment
B
**
**
EPSCNMDAR (%baseline)
100
75
50
25
0
ZnCl2 - + + - + +
DTNB - - + - - +
21% O2
0% O2

Figure 4.6

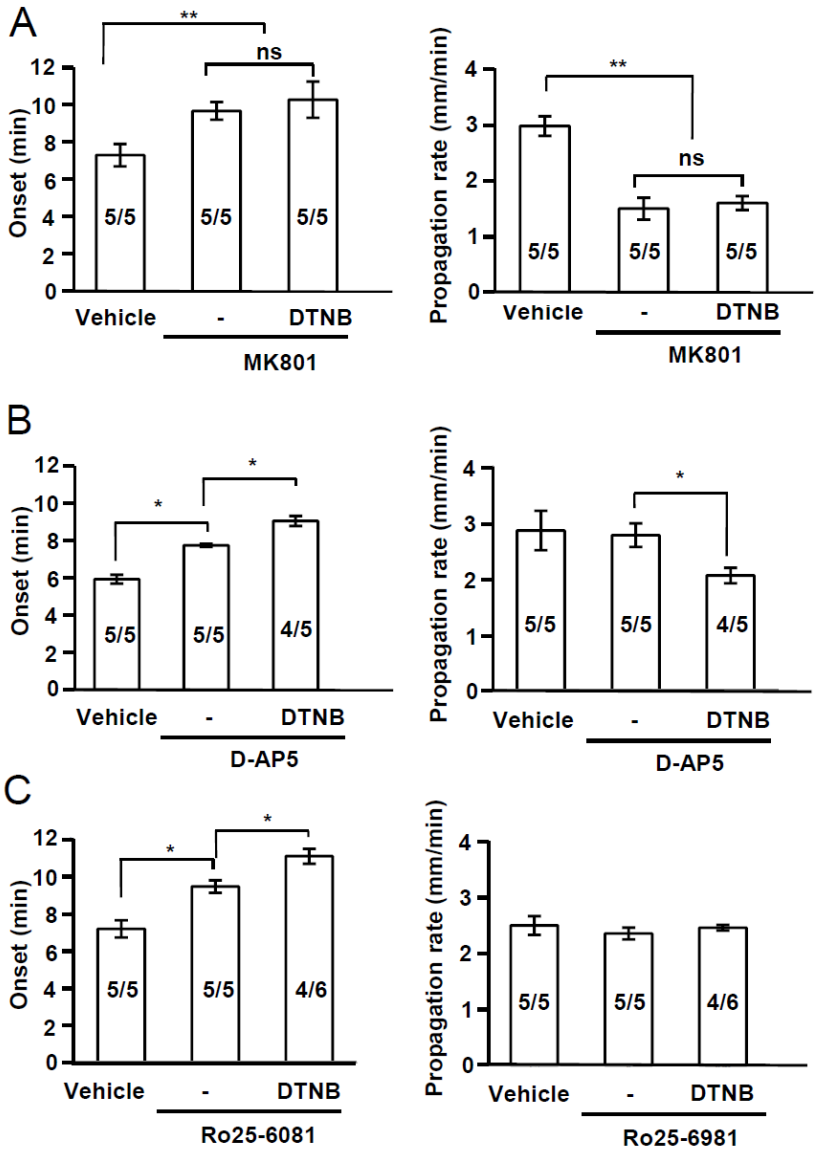
A
**
ns
Onset (min)
12
10
8
6
4
2
0
5/5
5/5
5/5
Vehicle
-
DTNB
MK801
**
ns
Propagation rate (mm/min)
4
3
2
1
0
5/5
5/5
5/5
Vehicle
-
DTNB
MK801
B
*
*
Onset (min)
5/5
5/5
4/5
Vehicle
-
DTNB
D-AP5
*
*
Propagation rate (mm/min)
5/5
5/5
4/5
Vehicle
-
DTNB
D-AP5
C
*
*
Onset (min)
5/5
5/5
4/6
Vehicle
-
DTNB
Ro25-6081
*
Propagation rate (mm/min)
5/5
5/5
4/6
Vehicle
-
DTNB
Ro25-6981

5. Intracellular Dialysis Disrupts Zn^{2+} Dynamics and Enables Selective Detection of Zn^{2+} Influx in Brain Slice Preparations

Isamu Aiba[1], Adrian West[2], Christian T Sheline[3] and C. William Shuttleworth[1]

[1] Department of Neurosciences, University of New Mexico, Albuquerque, NM, USA

[2]NeuroRepair Group, Menzies Research Institute, University of Tasmania, Hobart, Australia

[3]Department of Ophthalmology and the Neuroscience Center of Excellence LSU Health Sciences Center, New Orleans, LA, USA

Prepared for submission to "Journal of Neurochemistry"

5.1 ABSTRACT

Intracellular Zn^{2+} accumulation has been implicated in regulation of neuronal excitability and neuronal injury, and multiple sources of Zn^{2+} can contribute to this signaling. In addition to release from synaptic vesicles and transmembrane flux, significant amounts of Zn^{2+} can be sequestered by diffusible intracellular binding proteins and released following cytosolic acidification or change in redox state. Neuronal excitability is often recorded using whole-cell methods, that involve significant dialysis of intracellular contents. The present study evaluated whether intracellular dialysis significantly disrupts neuronal Zn^{2+} dynamics, by depleting intracellular buffering mechanisms. Intracellular Zn^{2+} was assessed in CA1 neurons in acutely-prepared brain slices. Single neurons were loaded with the Zn^{2+} indicator FluoZin3, using intracellular dialysis with conventional patch pipettes. Comparison between standard intracellular dialysis (20 minutes) and very brief dialysis (2 minutes) revealed large differences in intracellular FluoZin3 signals. Thus low concentrations of Zinc Pyrithione (ZnPyr) generated robust responses in neurons with standard dialysis, but signals were virtually absent in neurons with short dialysis. Supplementation with recombinant metallothionein 3 was sufficient to abolish ZnPyr responses in neurons with standard dialysis. Release from oxidation-sensitive Zn^{2+} pools also appeared reduced with standard dialysis, based on the lack of response to the oxidizer DTDP, when compared with large responses in neurons with brief dialysis. Different dialysis conditions were then used to probe responses to synaptic stimulation. Under standard dialysis conditions, trains of synaptic stimuli (20 Hz,

10 s) generated slow FluorZin3 signals which lasted for 2-3 minutes in wild-type (WT) preparations and such responses were not observed in the preparations lacking vesicular Zn^{2+} (ZnT3 KO). In contrast, under brief dialysis conditions, intracellular Zn^{2+} transients were very similar in WT and ZnT3 KO preparations. These results indicate that intracellular dialysis can be an important confound for studying intracellular Zn^{2+} signaling. However these effects may also be exploited for discriminating between contributions from different Zn^{2+} sources (i.e.

5.2 INTRODUCTION

Zn^{2+} is an essential heavy metal ion required for a wide range of functions in mammalian cells. While total intracellular Zn^{2+} content is quite high (>200 µM), cytoplasmic free Zn^{2+} concentrations are maintained at extremely low levels (<1 nM), due to the fact that much is bound in structural proteins and also the high activities of intracellular buffer and transporter systems (Colvin et al., 2008; Sensi et al., 2011). Recent Zn^{2+} studies have revealed diverse roles for cytosolic Zn^{2+} transients in physiological and pathophysiological. For example, elevated cytoplasmic free Zn^{2+} levels in neurons have been implicated to modulation of neuronal circuit activity (Manzerra et al., 2001; Hershfinkel et al., 2009; Huang and McNamara, 2010), and activation of neurotoxic pathways when intracellular Zn^{2+} levels become excessively high (Sensi et al., 2011).

In the mammalian brain, Zn^{2+} is highly concentrated in synaptic vesicles of glutamergic neurons, due to the activity of vesicular Zn^{2+} transporter ZnT3 (Cole et al., 1999). Vesicular Zn^{2+} can be released as a neuromodulator and can

directly modify the function of ion channels and receptors via direct interactions. In addition to extracellular actions, released Zn^{2+} can also translocate into postsynaptic neurons and potentially contribute to plasticity of some synapses (Li et al., 2001a; Huang et al., 2008). Glutamate exposures have been widely used to study neuronal intracellular Zn^{2+} homeostasis (Sensi et al., 2002; Colvin et al., 2008; Dineley et al., 2008; Kiedrowski, 2011). In these cases, activation of NMDA-type glutamate receptors (NMDARs) have been shown to release Zn^{2+} from intracellular pools. Therefore it seems likely that synaptic Zn^{2+} release and influx can contribute to postsynaptic Zn^{2+} concentration, in some combination with intracellular liberation from intracellular stores. The relative contributions of these two pathways remain to be clarified, as does the impact of standard electrophysiological recording methods on these Zn^{2+} signals.

Whole-cell clamp recording in acute brain slice preparation is a very widely used method for studying pre- and postsynaptic activities of single neurons. Whole-cell clamp technique involves substantial dialysis of the intracellular compartment due to the small intracellular volume ($10^{-10\sim12}$ litter) compared with the pipette solution volume (>10^{-6} litter). Due to effective washout of some intracellular components, intracellular dialysis can mask important neurophysiological responses such as long term potentiation (Malinow and Tsien, 1990), some Ca^{2+} currents (Belles et al., 1988) and intracellular signaling-dependent channel modifications (Manzerra et al., 2001). On the other hand, intracellular dialysis has been also exploited as a valuable method to manipulate intracellular constituents (Blatow et al., 2003; Eggermann and Jonas, 2012).

Whether or not whole-cell recording depletes neurons of important Zn^{2+} buffers and/or otherwise modifies detection of intracellular Zn^{2+} responses has not been explicitly tested.

In the present study, we demonstrate a significant vulnerability of intracellular Zn^{2+} buffers and/or pools to intracellular dialysis. While these dialysis methods may be a significant technical confound, we also demonstrate that they can be exploited to evaluate contributions of both synaptic and intracellular Zn^{2+} release, following synaptic stimulation.

5.3 METHODS

5.3.1 Slice preparation

All procedures using experimental animals were approved by the Institutional Animal Care and Use Committee of the University of New Mexico. Brain slices were prepared from 4-10 week old WT and ZnT3 KO C57BL/6 animals of both sexes. Data in each specific experiment were collected from matched numbers of each sex, within an age range of 2 weeks. ZnT3 KO animals were originally developed by (Cole et al., 1999) and backcrossed onto the C57BL/6 line for at least 13 generations. Both WT and ZnT3 KO homozygote colonies were established and maintained at the University of New Mexico.

Mice were deeply anesthetized with a subcutaneous injection (0.2 ml) of ketamine/xylazine mix (85 mg/ml and 15 mg/ml, respectively) and decapitated. Brains were carefully extracted into ice-cold cutting solution (in mM: 220 sucrose, 1.25 Na_3PO_4, 25 $NaHCO_3$, 3 KCl, 10 glucose equilibrated with 95% O_2/5% CO_2 gas), hemisected and sliced at 350 µm thickness with a vibratome. Slices were allowed to recovered in ACSF (in mM: 130 NaCl, 1.25 NaH_2PO_4, 25 $NaHCO_3$, 3 KCl, 10 glucose equilibrated with 95% O_2/5% CO_2 mix-gas) for 1 hour at 35^oC, and were subsequently maintained at room temperature in ACSF. Slices were transferred to a recording chamber (RC-27, Warner Instruments) and superfused with ACSF at 2 mm/min and 32^oC.

5.3.2 Zn^{2+} indicator loading into single CA1 neurons

Intracellular Zn^{2+} dynamics were evaluated by using the high affinity indicator Fluo-Zin3, loaded via whole cell dialysis into single CA1 pyramidal neurons. Neurons were visually identified, and patch pipettes (3-5 MΩ) contained (in mM): 135 potassium gluconate, 8 NaCl, 1 $MgCl_2$, 2 Na_2ATP, 0.3 NaGTP, 10 Hepes, 0.05 EGTA. pH was adjusted to 7.2 with KOH and Fluo-Zin3 added to the pipette solution.

A central issue in this study was the influence that whole-cell dialysis had on intracellular Zn^{2+} dynamics. Therefore the duration of dialysis was carefully monitored, and the electrode withdrawn from the neuron at specified times after the initial establishment of the whole-cell configuration. Thus membrane rupture was determined as the time when initial access resistances dropped below 30 MΩ, and if this was not completed within 10 seconds of initial attempts, the neuron was discarded. During intracellular dialysis, neurons were voltage clamped at -65 mV (holding current range between -50 and +50 pA), and the quality of whole-cell configuration was monitored based on the holding current and membrane response to test pulse (-5 mV, 100 ms). Neurons were discarded when holding current exceeded -100 pA for more than 20 s without any sign of recovery, or when series resistance exceeded 30MΩ. Following intracellular dialysis, the loading pipette was carefully withdrawn. Successful electrode withdrawal was determined by formation of an out-side-out recording configuration, and could be achieved within 20 seconds. After successful

electrode withdrawal, neurons were allowed 20 minutes recovery, prior to onset of any stimulation.

The concentration of FluoZin-3 added to the pipette solution depended on the duration of dialysis, in order to approximately match the final FluoZin-3 concentration achieved in neurons (see Figure 1). The tested concentration ranged from 40-500 µM (see Results).

In some experiments, recombinant human metallothionein-3 (MT3) was added to the intracellular solution. This was supplied as lyophilized purified recombinant human MT3 in various Zn^{2+} binding forms (approximately 80% Zn_7MT3, 10% of Zn_6MT3 and 10% Zn_8MT3 (Bestenbalt LLC, Tallinn, Estonia)). 5 µM MT3 stock solution was prepared in 10-times concentrated pipette solution lacking ATP/GTP, and containing 10% chelex resin, and stored at -80 ˚C. MT3 and ATP/GTP were then added to the pipette solution immediately prior to experiments

5.3.3 Fluorescence imaging

FluoZin-3 fluorescence was excited with 495 nm light (120 ms) delivered from monochromator via a dichoric mirror (505 nm long pass). Emission signals were band-passed filtered (535/50 nm) and acquired using a CCD camera (Till Imago) controlled by Till Vision software (version 4.04). Intracellular fluorescence signals were calculated after subtracting background neuronal autofluorescence within the same images.

Because of the high signal to noise ratio achieved by single-cell loading with FluoZin-3, intracellular fluorescence values could be approximated by the maximum fluorescence values obtained from low-pass filtered images. In each set of experiments, both analysis methods yielded similar values when ROI was carefully adjusted on neurons in every frame, except that analyses with maximum fluorescence always resulted in less noise. The kinetics of responses were analyzed as changes relative to the basal fluorescence intensities. In some experiments (e.g. Figure 1 100μM ZnPyr exposure), significant tissue swelling occurred and focus adjustment was required.

5.3.4 Synaptic stimulation

Synaptic responses were evoked with a concentric bipolar stimulating electrode placed >100 μm from the imaging site. Glass recording electrodes filled with ACSF (0.5-1 MΩ) were placed adjacent to neurons being imaged in order to verify activation of postsynaptic neurons near the recording sites. In each experiment, input-output curve were generated based on field excitatory postsynaptic potentials (fEPSP) evoked with single current pulses (70 μs, 0.1 Hz). 70% maximum stimulation was used for test stimuli. In all experiments, input-output curves were determined at least 10 minutes after recovery of neurons from indicator loading, and subsequently no stimulation was applied until a train of electrical stimulation (20 Hz, 10sec) was applied to evoke intracellular Zn^{2+} responses.

5.3.5 Reagents

Unless otherwise noted, all chemicals were from Sigma Aldrich (St Louis MO). FluoZin3, Alexa 633 and TPEN (N,N,N′,N′-Tetrakis(2-pyridylmethyl)ethylenediamine) were obtained from Life Technologies (Carlsbad, CA)

5.3.6 Statistics

All statistical tests were performed by using Graph Pad Prism software (GraphPad Software, Inc., version 4.03). One-way ANOVA with post hoc Newman-Keuls multiple comparison tests were used throughout. Values are presented as mean +/- SEM. n values indicate numbers of slices tested. A p-value <0.05 was considered to be statistically significant.

5.4 RESULTS

5.4.1 Intracellular dialysis increased detection of intracellular Zn^{2+} increases.

We first examined the hypothesis that intracellular dialysis could reduce intracellular Zn^{2+} buffering capacity, and make cytosolic Zn^{2+} increases more readily detectable. The general experimental approach is shown in **Figure 1**, where single pyramidal neurons were dialyzed via a conventional whole-cell patch pipette containing the membrane-impermeable Zn^{2+} indicator FluoZin-3. Two different durations of dialysis were compared (2 minutes and 20 minutes), and the concentration of indicator added to the pipette solution adjusted (500 µM and 40 µM, respectively) so that the final neuronal indicator concentrations were approximately matched. This was confirmed by exposing the indicator-loaded neurons with saturating concentration of ZnPyr (100 µM $ZnCl_2$, 5 µM sodium pyrithione, 20 minutes exposure) and obtaining maximum fluorescence signals (Figure 1A&B). The approximate intracellular Zn^{2+} concentrations were estimated by using an equation described in (Grynkiewicz et al., 1985), and the calculation confirmed extremely resting intracellular Zn^{2+} concentrations. These initial experiments verified that initial FluoZin3 concentrations were closely matched in the neuronal populations, despite very different dialysis durations.

Figure 2 shows that the duration of dialysis had a substantial effect on the amplitude of Zn^{2+} increases detected by FluoZin-3, when neurons were challenged with a low concentration of zinc pyrithione (ZnPyr: 1 µM $ZnCl_2$ and 1 µM sodium pyrithione). Pyrithione serves to facilitate Zn^{2+} passage across the

plasma membrane, and thereby increase intracellular Zn^{2+} levels independent of active transport mechanisms. As shown in Figure 2A, the FluoZin3 response in the briefly dialyzed neurons was barely detectable, whereas large FluoZin-3 increases were detected in all neurons that were first subjected to standard (20 minutes) dialysis (Figure 2B). The increased signals with standard dialysis could be due to washout of an endogenous Zn^{2+} buffer into the dialysis pipette, and/or changes in transport mechanisms involved in accumulation and clearance.

Experiments in Figure 2C show that supplementation of the pipette solution with recombinant MT3 (0.5 µM) was sufficient to abolish the large Zn^{2+} signals seen with standard dialysis. We estimated relevant intracellular MT concentrations from previous publications (Hidalgo et al., 1994; Colvin et al., 2008) and examined effects of a range of MT3 concentrations (0.1-5 µM) in an initial set of pilot studies. 0.5 µM MT3 was then chosen for subsequent experiments, as this concentration showed significant effects on intracellular Zn^{2+} responses while having little deleterious effect on the quality of whole-cell recordings.

Although the difference in the amplitudes of response could be affect by initial fluorescence or Zn^{2+} concentration, our estimates of maximum fluorescence values as well as near zero minimum fluorescence values (after TPEN exposure) suggested it was not the case (see Figure 1B&C). These observations indicate a large increase in the net accumulation of Zn^{2+} that was detectable by FluoZin-3, was caused by intracellular dialysis. Supplementation with recombinant MT3 is consistent with the possibility that washout of

endogenous Zn^{2+} buffering proteins could underlie the effect, however it is emphasized that addition of excess endogenous buffer in these studies could mask other contributing mechanisms (see Discussion).

5.4.2 Intracellular dialysis also reduced oxidation dependent intracellular Zn^{2+} release

Previous work has shown that addition of a membrane-permeable oxidant effectively mobilizes Zn^{2+} from intracellular stores/binding proteins, and leads to increases in Zn^{2+} that can be detected by cytosolic indicators (Aizenman et al., 2000). We therefore examined whether dialysis leads to depletion of the size of the oxidation-sensitive intracellular Zn^{2+} pool. After a stable baseline was collected, neurons were exposed to 200 µM DTDP for 20 minutes. As shown in **Figure 3**, briefly dialyzed neurons showed a robust increase in FluoZin3 signals. In contrast, FluoZin-3 signal responses were very small in neurons with standard dialysis, suggesting much smaller oxidation sensitive Zn^{2+} pools in these preparations. Intermediate Fluozin-3 responses were observed in neurons with standard dialysis supplemented with recombinant MT3. These results suggest that intracellular dialysis may deplete oxidation-sensitive Zn^{2+} pools, which may be contributed in part by differences in availability of MT3 or other redox-sensitive Zn^{2+} binding stores.

5.4.3 Dialysis allows dissection of multiple sources of Zn^{2+} following synaptic stimulation.

The results above suggest that differences in dialysis conditions could be used experimentally to manipulate the ability to preferentially detect transmembrane Zn^{2+} influx (with standard dialysis) and liberation from intracellular binding sites (with short dialysis). We next examined whether these experimental approaches could be exploited to assess the contributions of different Zn^{2+} sources to intracellular Zn^{2+} accumulation following synaptic stimulation.

This was done using trains of synaptic stimulation (20 Hz for 10 s), as this was suggested to be a physiologically relevant stimulation intensity in a recent study of tissue metabolism in a similar preparation (Hall et al., 2012). As shown in **Figure 4**, these stimuli provided reliable detection of post-synaptic Zn^{2+} accumulation. For these experiments, the slow Zn^{2+} chelator CaEDTA (1 mM) was included in recording bath solution in order to prevent detection of contaminating Zn^{2+} (see (Qian and Noebels, 2005) and Discussion). Based on previous studies, exposure to 1 mM CaEDTA should have little effect on basal intracellular Zn^{2+} concentration (Lavoie et al., 2007), and leaves a significant fraction of rapidly released Zn^{2+} available at synaptic clefts (Vogt et al., 2000; Pan et al., 2011).

Figure 4 shows a summary of intracellular Zn^{2+} responses of postsynaptic neurons, indicator loaded with standard dialysis, brief dialysis and standard

dialysis with MT3. In order to evaluate contributions of synaptic Zn^{2+} release, experiments were compared between WT and ZnT3 KO preparations. Strong genotypic differences were seen in the standard dialysis preparations (Fig 4A&B). Thus WT preparations showed a robust FluoZin3 signal increase peaked during 1-2 minutes after stimulation and slowly decayed over next 5 minutes, while responses was virtually absent in ZnT3 KO preparation (Fig 4A&B). These data suggesting that the response observed in dialyzed WT preparations were largely contributed to by presynaptic Zn^{2+} release, and are consistent with the possibility that significant depletion of intracellular Zn^{2+} buffering by standard dialysis facilitated detection of the response.

A strong difference between WT and ZnT3 KO preparations was not seen in briefly dialyzed neurons. Thus both WT and ZnT3 KO preparation showed intracellular Zn^{2+} responses in these cells, following synaptic stimulation (Fig 4C&D). The responses in ZnT3 KO preparations raised the possibility that these responses were generated by liberation from intracellular sources.

Figures 4E&F show experiments to test whether artificial provision of an intracellular Zn^{2+} source, by inclusion of MT3 in the pipette solution, could reveal additional Zn^{2+} release signals in neurons that had been extensively dialyzed. MT3 addition had no additional effect in WT neurons, but did significantly increase detection of Zn^{2+} increases in ZnT3 KO neurons.

Taken together, these results suggest that synaptic stimulation leads to postsynaptic Zn^{2+} accumulation from at least two sources, which can be

preferentially demonstrated with different dialysis methods. Synaptic release can be readily demonstrated after standard dialysis, where a large portion of the Zn^{2+} buffering system is lost. In contrast, briefly-dialyzed neurons appear to retain a significant source of intracellular Zn^{2+}, which can generate postsynaptic FluoZin-3 signals, even in the absence of synaptically-released Zn^{2+}.

5.5 Discussion

5.5.1 General

The present study examined effects of intracellular dialysis on Zn^{2+} measurements in neurons whole-cell clamped in acute slice preparations. A major finding is that dialysis appears to effectively deplete intracellular Zn^{2+} buffering and decrease the size of oxidation-sensitive intracellular Zn^{2+} pools. Such disruption of intracellular Zn^{2+} homeostasis was shown to significantly modify detection of intracellular Zn^{2+} responses to a train of synaptic stimulation. Thus standard whole-cell dialysis facilitated detection of synaptic Zn^{2+} translocation, whereas in briefly-dialyzed preparations intracellular Zn^{2+} responses seem to be mediated mainly by intracellular Zn^{2+} liberation. Together, these findings indicate a high vulnerability of intracellular Zn^{2+} homeostasis to whole-cell dialysis, and demonstrate its potential use for selective detection of intracellular Zn^{2+} signals arising from different mechanisms.

5.5.2 Dialysis effects

The present study compared effects of two different durations of intracellular dialysis; one standard (20 minutes) and one intentionally very brief (2 minutes). It is generally understood that intracellular dialysis is one of the most profound confounds of whole-cell clamp recordings. Washout of intracellular constituents and the imposition of a homogenous intracellular ionic composition improves the resolution of electrophysiological recordings, however dialysis of channel subunits or signaling molecules can prevent recording of significant physiological responses (see Introduction). The present demonstration of significant disruption of intracellular Zn^{2+} homeostasis is another example of the significant impact of dialysis. The 20 minutes dialysis conditions tested here are relatively common for studies of synaptic physiology or pathophysiology. The current results suggest that loss of Zn^{2+} buffering and/or intracellular release could be a significant variable in a range of whole-cell studies.

One of the most striking dialysis effects was the response to low concentrations of the Zn^{2+} carrier ZnPyrithione. As noted above, pyrithione serves to facilitate Zn^{2+} passage across the plasma membrane, and thereby increases intracellular Zn^{2+} levels independent of active transport mechanisms. The fact that standard intracellular dialysis significantly increased intracellular accumulation following ZnPyrithione could be due to washout of intracellular buffers, or possibly due to some other factors that decrease Zn^{2+} extrusion rates. Reversal of the dialysis effect with recombinant MT3 is consistent with the possibility that washout of endogenous Zn^{2+} buffering proteins could underlie the

effect, however as noted above (Results) addition of excess endogenous buffer in these studies could mask other contributing mechanisms. Likewise, the loss of intracellular Zn^{2+} accumulation following exposure of the oxidant DTDP is consistent with the hypothesis that dialysis washes out an oxidation-sensitive, diffusible Zn^{2+}-binding source, such as MT3. A similar role for metallothionein in intracellular Zn^{2+} buffering and regulating the oxidation sensitive pool size have previously been demonstrated with overexpression of metallothionein in astrocytes (Malaiyandi et al., 2004).

It is noted that even extensively dialyzed neurons maintained extremely low resting intracellular Zn^{2+} concentrations (estimated ~500pM) which were not different from cells loaded with brief dialysis (see Figure 1). This suggests that mechanisms required for maintaining resting Zn^{2+} concentrations are different from those that prevent excessive intracellular Zn^{2+} accumulation. Thus while Zn^{2+} binding molecules such as thionein and metallothioneins) are likely important defense molecules against severe Zn^{2+} influx (Hourez et al., 2005) resting Zn^{2+} concentrations may not be under control of these molecules. It was previously suggested that function of the membrane Zn^{2+} transporters ZIP1and ZIP3 and mitochondrial membrane potential seem to be resistant to intracellular dialysis (Zhou et al., 2010a; Qian et al., 2011). Thus mechanisms such as Zn^{2+} extrusion or sequestration into organelle alone could be sufficient for maintaining extremely low Zn^{2+} concentrations at rest (Sensi et al., 2011).

In addition to depletion of buffer molecules, the concentrations of small signaling molecules such as inositol phosphate can be modified by intracellular

dialysis (Hourez et al., 2005). Because we did not replenish these small molecules, intracellular dialysis could have significantly impaired intracellular signaling pathways. These effects certainly could have contributed to reduced detection of intracellular Zn^{2+} release in the dialyzed neurons, and facilitated selective detection of synaptic Zn^{2+} translocation in the dialyzed neurons.

Even though the mechanisms underlying dialysis effects are not yet definitively identified, the results from Figures 2&3, together imply that dialyzed neurons have higher sensitivities to the detection of Zn^{2+} influx, whereas in briefly dialyzed neurons FluoZin3 responses more strongly reflect intracellular Zn^{2+} release.

5.5.3 Other neuronal intracellular Zn^{2+} buffer systems

While the present study revealed that inclusion of MT alone was sufficient to restore a large portion of intracellular Zn^{2+} homeostasis, it does not necessarily rule out important contributions of other Zn^{2+} buffers to intracellular Zn^{2+} homeostasis. In an early studies it was shown that Zn^{2+}-GSH provides an additional major cytoplasmic Zn^{2+} buffer in hippocampus (Sato et al., 1984). While GSH is contained in all cell types, GSH is less abundant in neurons (1 mM) compared with the glia (10 mM) (Rice and Russo-Menna, 1998). The GSH concentration in recorded neurons may be even lower because of the fact that intracellular GSH can be severely depleted during brain slice preparation (Rice, 1999). This factor might have made contributions of MT3 dialysis relatively more detectable in the brain slice preparations studied here.

5.5.4 Intracellular Zn^{2+} responses during synaptic stimulation

Previous studies have suggested that synaptic stimulation can elevate intracellular Zn^{2+} levels by two mechanisms; intracellular Zn^{2+} release and synaptic Zn^{2+} translocation (Frederickson et al., 2005; Sensi et al., 2011). Bulk loading of populations of CA1 neurons with a low affinity Zn^{2+} indicator Newport Green (K_D = 1~3 μM) (Li et al., 2001b; Suh, 2009) has shown intracellular Zn^{2+} increases in postsynaptic neurons (Li et al., 2001b; Suh, 2009) and the latter study showed that accumulation was abolished in ZnT3 KO tissues. While this argues for a role of synaptic Zn^{2+} release and translocation, the results of the present study suggest that both synaptic release and intracellular release can contribute to postsynaptic Zn^{2+} accumulation. Thus in briefly dialyzed preparations, postsynaptic Zn^{2+} responses were observed in both WT and ZnT3 KO preparations. The presence of responses in ZnT3 KO preparations suggest that, in our recording conditions, intracellular Zn^{2+} release can significantly contribute to the FluoZin3 signal changes following synaptic stimulation Conversely, with standard dialysis, FluoZin-3 signals were abolished in ZnT3 KO tissues, implying preferential detection of Zn^{2+} that is released and taken up by postsynaptic neurons. Taken together, the preferential detection of intracellular Zn^{2+} release in the briefly dialyzed neurons is likely contributed to by the presence of intracellular buffers, which bind with Zn^{2+} with significantly higher affinity and masked a large part of fluxed Zn^{2+} from detection by FluoZin3. While it has been previously shown that glutamate can evoke intracellular Zn^{2+} release in neuronal culture models (Dineley et al., 2008; Kiedrowski, 2011), the present

study appears to be the first to suggest intracellular Zn^{2+} release during physiological synaptic activity.

5.5.5 Kinetics of Zn^{2+} responses

One of the remarkable features of intracellular Zn^{2+} responses following synaptic stimulation was their very slow kinetics. Both in standard dialysis and briefly dialyzed preparations, similar slow monophasic responses were detected. Such responses were much slower than intracellular Ca^{2+} transients observed with the same stimuli (data not shown). Previous single cell Zn^{2+} imaging during different stimuli (exposures to ouabain, oxygen glucose deprivation and NMDA) have also shown relatively slow changes in intracellular FluoZIn3 signals (Dietz et al., 2008; Medvedeva et al., 2009; Vander Jagt et al., 2009). One possibility is that high affinity endogenous intracellular Zn^{2+} buffers limit mobility of Zn^{2+} ions and contributed to sluggish responses. However our dialysis studies suggest this may not the case. In fact, similarly slow responses were also observed in the dialyzed neurons in which large fraction of intracellular Zn^{2+} buffer is likely to be significantly depleted. Instead of large buffer molecules, these slow responses could be contributed by interactions with organic anions (e.g. HCO_3^-, PO_4^{3-}) which are abundantly present in the cytoplasm with high affinity (Rumschik et al., 2009). An interesting question is whether the observed responses may reflect true intracellular Zn^{2+} dynamics, or whether signals are distorted due to presence of fluorescence probes. Thus a high affinity Zn^{2+} binding molecule such as FluoZin-3 could have significant impact on the mobility of Zn^{2+}. Because of

extremely low intracellular Zn^{2+} concentrations at rest and even after stimulation, such a confound may be inevitable for imaging studies of intracellular Zn^{2+}.

5.5.6 Conclusion

The present study revealed significant effects on intracellular Zn^{2+} homeostasis by conditions used in standard electrophysiological experiments. The present results also show that modifying whole cell indicator loading conditions can be valuable tool to help discriminate between different sources of Zn^{2+} that contribute to intracellular neuronal Zn^{2+} signals in adult brain slice preparations.

5.6 Figure Legends

Figure 5.1 Experimental approach for FluoZin-3 loading. The high affinity Zn^{2+} indicator FluoZin3 was loaded in hippocampal CA1 pyramidal neurons in acute brain slices via patch-pipettes. **A:** Three different intracellular dialyses effects were compared; short dialysis (top), standard dialysis (middle) and standard dialysis supplemented with 0.5 µM MT3 (bottom). In order to achieve similar intracellular indicator concentrations, different concentration of indicator concentrations were used. Detailed methods are provided described in Method and Results. **B:** Initial intracellular Zn^{2+} concentrations were compared based on their maximum fluorescence obtained by exposure to saturating concentration of ZnPyr (100 µM $ZnCl_2$ and 5 µM pyrithione, 20 minutes). A briefly dialyzed neuron is shown, after recovery (basal level) and then following ZnPyr exposure. **C:** Comparisons of maximum fluorescence obtained from 5 neurons differently indicator loaded in each condition. Results are transformed to the estimated FluoZin3-Zn^{2+} concentration (see Methods). No significant differences were in estimated resting levels ($p<0.5$). n=5 each.

Figure 5.2 Intracellular Zn^{2+} concentration changes following exposure to 1 µM ZnPyr. FluoZin-3-loaded neurons were exposed to 1 µM ZnPyr (1 µM $ZnCl_2$ and 1 µM sodium pyrithione, 20 minutes), followed by 20 µM TPEN. **A-C** Plots of responses from 5 individual neurons. **D.** Quantitative analysis of peak FluoZin3 responses. ***$p<0.005$,

Figure 5.3 Intracellular dialysis effect on oxidation dependent intracellular Zn^{2+} release. FluoZin-3-loaded loaded neurons were challenged with ACSF containing 200 µM DTDP. After significant Zn^{2+} responses were obtained, neurons were exposed to 20 µM TPEN. **A-C** shows responses from 5 individual neurons and **D** shows a quantitative analysis of peak responses. ***p<0.005

Figure 5.4 Intracellular dialysis effects on intracellular Zn^{2+} accumulation following synaptic stimulation. FluoZin3-loaded neurons from WT and ZnT3 KO slices are shown, with three different intracellular dialysis methods. Following recovery slices were challenged with Schaffer collateral synaptic stimulation (20 Hz, 10 s). Panels **A-F** shows individual responses obtained from 5 neurons in each preparation. Peak responses were obtained following data reduced traces and are compared in **G**. ***p<0.005

Figure 5.1

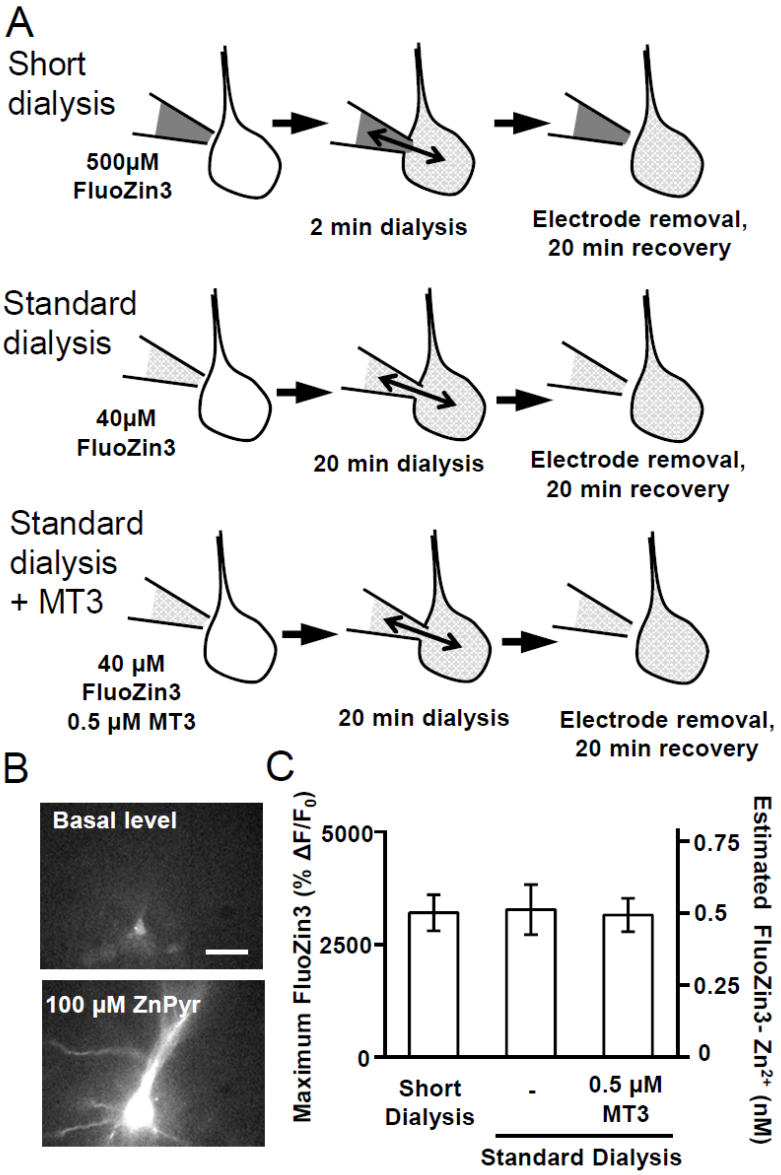
A
Short dialysis
500μM FluoZin3
2 min dialysis
Electrode removal, 20 min recovery
Standard dialysis
40μM FluoZin3
20 min dialysis
Electrode removal, 20 min recovery
Standard dialysis + MT3
40 μM FluoZin3
0.5 μM MT3
20 min dialysis
Electrode removal, 20 min recovery
B
Basal level
100 μM ZnPyr
C
Maximum FluoZin3 (% ΔF/F0)
5000
2500
0
Estimated FluoZin3- Zn2+ (nM)
0.75
0.5
0.25
0
Short Dialysis
-
0.5 μM MT3
Standard Dialysis

Figure 5.2

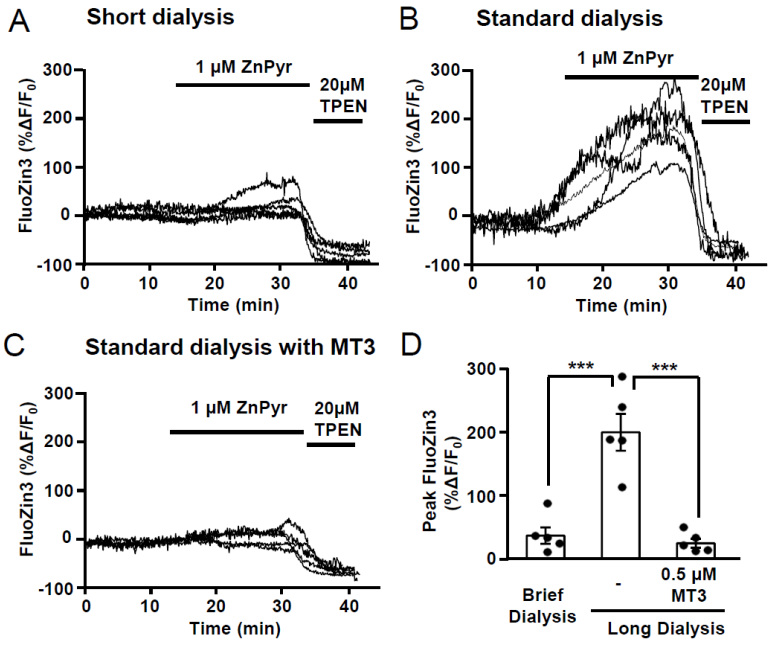
A
Short dialysis
1 μM ZnPyr
20μM TPEN
FluoZin3 (%ΔF/F0)
Time (min)
B
Standard dialysis
1 μM ZnPyr
20μM TPEN
FluoZin3 (%ΔF/F0)
Time (min)
C
Standard dialysis with MT3
1 μM ZnPyr
20μM TPEN
FluoZin3 (%ΔF/F0)
Time (min)
D
Peak FluoZin3 (%ΔF/F0)
***
***
Brief Dialysis
-
0.5 μM MT3
Long Dialysis

Figure 5.3

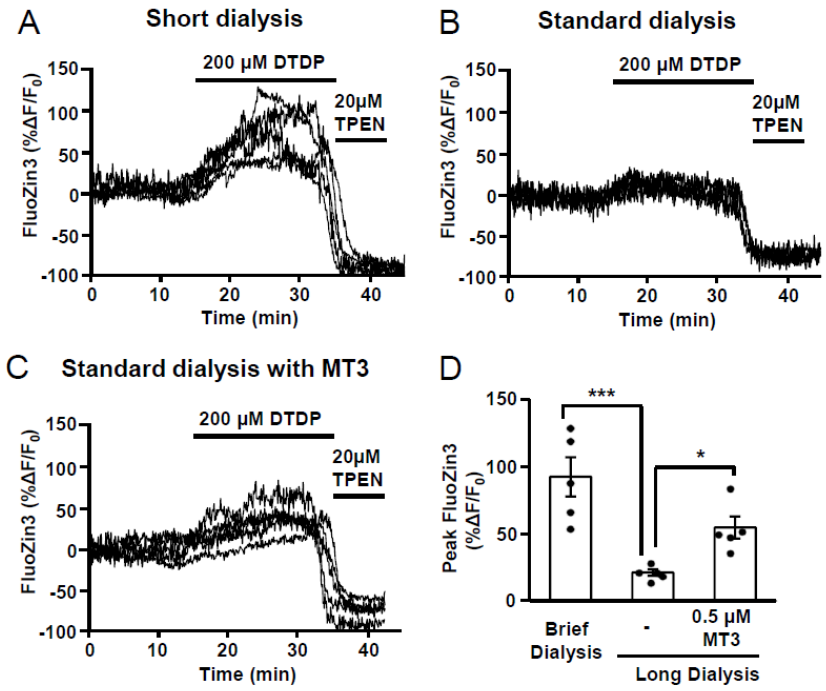
A
Short dialysis
200 μM DTDP
20μM
TPEN
FluoZin3 (%ΔF/F0)
Time (min)
B
Standard dialysis
200 μM DTDP
20μM
TPEN
FluoZin3 (%ΔF/F0)
Time (min)
C
Standard dialysis with MT3
200 μM DTDP
20μM
TPEN
FluoZin3 (%ΔF/F0)
Time (min)
D
Peak FluoZin3 (%ΔF/F0)
***
*
Brief Dialysis
-
0.5 μM MT3
Long Dialysis

Figure 5.4

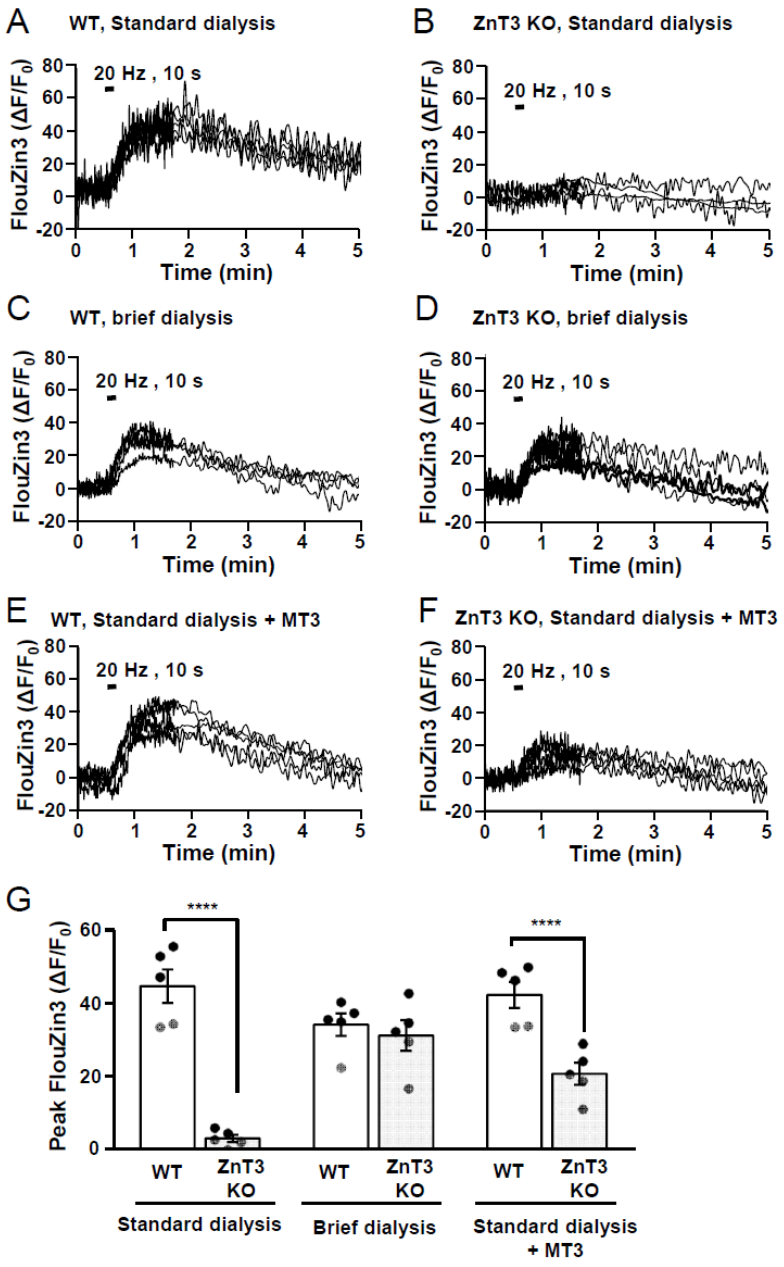
A
WT, Standard dialysis
B
ZnT3 KO, Standard dialysis
C
WT, brief dialysis
D
ZnT3 KO, brief dialysis
E
WT, Standard dialysis + MT3
F
ZnT3 KO, Standard dialysis + MT3
20 Hz , 10 s
FlouZin3 (ΔF/F0)
Time (min)
G
Peak FlouZin3 (ΔF/F0)
****
WT
ZnT3 KO
Standard dialysis
Brief dialysis
Standard dialysis + MT3

6. Discussion

6.1 Summary of the present studies

The present dissertation studies addressed how tissue metabolism can influence consequences of SD and synaptic Zn^{2+} release. Experiments in Chapter 2 suggested a critical role of an excitatory phase during the late-SD phase in determining recoverability of SD when energy metabolism was limited. Injurious consequences of SD were reliably reversed by an NMDAR antagonist, applied specifically in the late-SD phase. These results suggest a significant contribution of glutamate toxicity to SD-dependent injury.

Studies in Chapters 3&4 evaluated inhibitory effects of Zn^{2+} on SD propagation and initiation. These studies revealed different Zn^{2+} sensitivities of SD, depending on local oxygen concentrations. Mechanistic studies suggested that this was due in part to redox modulation of extracellular sites under conditions of severe hypoxia. In fact redox modulation alone significantly reversed the Zn^{2+} sensitivity of NMDARs and SD under hypoxia. These studies not only provided new insights into the roles of synaptic Zn^{2+} release in SD regulation, but also revealed an important influence of local tissue metabolism on NMDAR pharmacology.

Experiments in Chapter 4 did not directly test roles of Zn^{2+}, but provided a technical advance to evaluation of neuronal intracellular Zn^{2+} homeostasis. The experiments revealed a vulnerability of intracellular Zn^{2+} homeostasis to

intracellular dialysis, and demonstrated the use of different recording conditions to selectively detect synaptic Zn^{2+} influx in acute brain slice preparations. This recording technique should provide a useful approach for evaluating intracellular Zn^{2+} buffering capacity and contributions of synaptic influx in ischemia relevant conditions.

6.2 Excitotoxicity

6.2.1 Contributions of SD to delayed ischemic neuronal death

One of the important conclusions of the present work is that NMDAR activation during SD can trigger excitotoxic neuronal death. The result in Chapter 2 revealed that KCl-induced SD, which is normally fully recoverable in healthy tissues, became highly injurious when it involved metabolically compromised neurons. This was due to a brief period of NMDAR activation during the late phase of SD, as demonstrated by the finding that preventing NMDAR activation specifically during the late-SD period was sufficient to prevent neuronal injury. The presence of injurious NMDAR activation during the late-SD phase is consistent with the clinical observations that prolonged DC potential shifts were observed during SD in compromised tissue (Oliveira-Ferreira et al., 2010; Hartings et al., 2011b). Thus the duration of extracellular potential shifts could be an important clinical parameter to indicate the intensity of injurious NMDAR activation. This hypothesis deserves further validation in experimental stroke models as well as in clinical observations.

As described earlier, the term “excitotoxicity” was originally defined by Olney, who revealed that excessive excitatory neurotransmitter can cause neuronal degeneration (Olney, 1969; Olney and Sharpe, 1969). The increased glutamate release, NMDAR activation and NMDAR-dependent Ca^{2+} overload seen in the present work suggest that SD-dependent neuronal injury can be categorized as excitotoxicity. The similarity between SD-induced injury and excitotoxicity may provide a significant new insight to motivate selectively targeting of NMDAR dependent injury during SD and may help explain previous clinical failures in NMDAR antagonists. While there appear to be many similarities between SD-induced injury and excitotoxicity induced by glutamate applications, because of unique features of SD, the intensity of stimulation during SD may be much more profound, and it is important to further understand SD dependent injury processes to help identify relevant therapeutic targets.

SD-induced neuronal injury was characterized by Ca^{2+} deregulation and membrane dysfunction and in this respect was similar to necrotic cell death seen following intense NMDAR activation. Thus acute cell death induced by acute glutamate exposure (500 µM glutamate for 5 minutes) was characterized by Ca^{2+} overload, significant cell swelling and subsequent membrane rupture (Choi et al., 1987). Excitotoxicity is often considered to be an event contributing to only during the early phase of ischemic injury (Dirnagl et al., 1999). However because of the persistence of SD for long periods (even days) after initial stroke injury (Dohmen et al., 2008), the present study significantly extends the contribution of excitotoxic necrotic neuronal death following acute stroke injury.

6.2.2 Aberrantly increased presynaptic activity in metabolically compromised tissue

The studies in Chapter 2 revealed an important contribution of a brief period of excitation during SD, and provided evidence that this involved increased glutamate release. Thus presynaptic activity was significantly enhanced during the late SD phase and concomitant NMDAR activation was critical for determining injurious consequences of SD. While the contribution of glutamate release to injurious NMDAR activation was not directly confirmed, the aberrant release during the late SD phase could be a potential target to prevent SD induced injury in metabolically compromised tissue. Some of the potential mechanisms underlying increased presynaptic activity during SD were already speculated upon in Chapter 2 and will not be repeated here. Instead, the general discussion here will focus mainly on potential links between aberrant glutamate release and tissue metabolism.

In severe hypoxia, action potential-dependent presynaptic glutamate release is suppressed by an adenosine-dependent mechanism (Rudolphi et al., 1992; Tanaka et al., 2001). Such a mechanism may underlie the rapid loss of consciousness observed following cerebral arterial occlusion in humans mentioned in the Introduction (Rossen et al., 1943). However under extreme metabolic stress, such as produced by oxygen and glucose deprivation *in vitro*, the frequency of spontaneous glutamate release was significantly increased (Hershkowitz et al., 1993; Katchman and Hershkowitz, 1993; Andrade and Rossi, 2010; Ye et al., 2010). This aberrant excitatory synaptic activity may underlie the

important discovery made by Rothman concerning the basis of excitotoxicity in ischemic brain injury (see Introduction 1.4.2). An increase of synaptic activity can also be seen following oxygen glucose deprivation in the preparations used in the present studies (Supplementary Figures A1&2). Recording of spontaneous EPSCs reliably revealed high frequency EPSCs prior to the onset of OGD-SD (Appendix Figure A1). A similar observation was made when recording evoked fEPSPs (Appendix Figure A2). While action potential dependent release was suppressed following OGD, sustained exposure to OGD resulted in a transient recovery of action potential-dependent evoked response ~ 1minute before SD onset. During this phase, the paired pulse ratio was always reduced, indicating that action potential dependent release recovered and was actually enhanced just before the arrival of OGD-SD. The enhanced sEPSC and action potential-dependent release are quite similar to the excitatory phase seen during the late phase of SDs generated by localized KCl microinjections (K-SD, Chapter 2). In both situations, increased release was observed when tissue energy metabolism was expected to be severely compromised (i.e. continuous depletion of energy substrate in OGD, and increased energy demand during the late phase of K-SD). Thus it is possible that severe metabolic stress generally elevates presynaptic release probability and contributes to the excitatory phases with both stimuli. A prior study has examined underlying mechanisms of OGD-induced increased synaptic release (Andrade and Rossi, 2010). The increase is not Ca^{2+} dependent, as removal of extracellular Ca^{2+} did not prevent EPSC

frequency increases. Instead, presynaptic actin depolymerization has been suggested as a potential contributor (Andrade and Rossi, 2010).

An excitatory phase characterized by increased presynaptic release probability seems to be important for both K-SD and OGD-SD models. As discussed in Chapter 2, this excitatory phase seems to be critical for determining consequences of K-SD in metabolically compromised neurons. In the OGD-SD model, such an excitatory phase occurs prior to the wavefront of SD and increased discharge may contribute to elevation of extracellular potassium concentrations ahead of SD. Based on Grafstein's potassium hypothesis (Grafstein, 1956), such an increased potassium concentration may allow SD to propagate independently of NMDAR activation and thus reduce the therapeutic values of NMDAR antagonists. Thus understanding and block of aberrant glutamate release in K-SD may significantly ameliorate injurious consequences of SD, and in the OGD model, block of prodromal excitation could significantly enhance NMDAR antagonist to block SD propagation.

The studies presented in Chapter 2 concentrated on excitatory transmission, but additional studies were conducted to also evaluate inhibitory synaptic activity (IPSC) during SD generated by KCl microinjection (Appendix Figure A3). These experiments highlight different effects on transmission, comparing glutamate and GABA during SD. Isolated IPSCs showed a rapid increase in frequency prior to SD onset, followed by a large outward current. Unlike EPSCs, IPSC frequency did not change following SD. The increased IPSC frequency prior to SD also correlated with the discharge pattern of

interneurons (Figure A4). Thus interneurons showed extremely high frequency action potential trains ahead of SD onset, which were likely responsible for GABA release prior to SD onset. These results highlight different regulation of excitatory and inhibitory neurotransmitter release during K-SD. During the late-SD phase, glutamate release was enhanced however GABA release was not. Thus in the late SD phase there seems to be significant imbalance in glutamate-GABA balance, which may contribute to the sustained dendritic Ca^{2+} elevations described in Chapter 2.

6.3 Pharmacological intervention of SD

6.3.1 Subpopulations of NMDARs and their activation during in SD

The studies in Chapters 3&4 determined the NMDAR antagonist sensitivity of different forms of SDs. The results generally confirmed the efficacy of NMDAR antagonist to prevent SD. As described in Introduction, NMDAR antagonism is currently one of the most attractive approaches being considered to limit the incidence of SD. In addition to complete prevention of SD, the present work also suggests that NMDAR activation is critical for determining injurious consequences of SD, including following stroke. However the well-recognized failures of NMDAR antagonists in clinical trials have indicated that simple administration of NMDAR antagonists is not effective for stroke (Introduction 1.3.2). These failures may be due in part to the fact that NMDAR activation during SD may have unique features, and require targeting of selective receptor subtypes and/or timing of antagonist application. The following

discussion will examine different NMDAR populations identified previously and their potential contribution to SD and SD induced injury.

The simplest distinction between NMDAR subtypes can be made based on their composition, or different GluN1 splicing variants and GluN2 subunit content. Such subunit composition can strongly modulate the biophysical properties of NMDAR channels. GluN1 mRNA can be spliced in at least 8 variants and the presence of exon-5 can influence the deactivation kinetics of some NMDAR currents by as much as 300% (Vance et al., 2012). The GluN2 subunit also affects the desensitization kinetics of NMDARs such that GluN2A containing receptors deactivate faster than GluN2B containing receptors (Erreger et al., 2005). In addition to different biophysical properties, the cytoplasmic tails of GluN2 subunits significantly differ in their interaction with postsynaptic density proteins, and the GluN2 subunit composition significantly influences the degree of excitotoxic insult following NMDAR activation (Martel et al., 2012). It was suggested that selectively targeting different GluN2 subunits, may be beneficial for blocking excitotoxicity (Nikam and Meltzer, 2002; Liu et al., 2004). The sensitivities of OGD-SD to NMDAR antagonists were tested in Chapter 4 and revealed that most of antagonists had some inhibitory effect on OGD-SD. Of the antagonists used, Zn^{2+} and Ro25-6981 had some subunit selectivity. Thus Zn^{2+} preferentially inhibits GluN2A while Ro25-6981 blocks GluN2B containing receptors (Paoletti and Neyton, 2007). The results indicated that Zn^{2+} could inhibit both SD propagation and initiation, while Ro25-6981 only inhibited SD onset and did not affect propagation rate. While Zn^{2+} at this concentration likely

inhibited some of GluN2B containing receptors (Paoletti and Neyton, 2007), the data suggest that activation of both GluN2A and GluN2B containing receptors are important for SD initiation, while SD propagation can be conducted mainly by GluN2A containing receptors. A similar conclusion was obtained in an additional experiment, testing the sensitivity of ouabain SD to Zn^{2+} and ifenprodil, another GluN2B selective antagonist (Appendix Figure A5). The results was similar to OGD-SD, thus SD propagation was more sensitive to Zn^{2+}, whereas ifenprodil was without effect on ouabain-SD. The onset of ouabain-SD was not influenced by either antagonist alone, but was significantly delayed when both Zn^{2+} and ouabain were co-applied. GluN2A containing receptors have relatively faster activation kinetics compared with GluN2B containing receptors and it is possible that at the propagating SD wavefront, GluN2A containing receptors may be more important for driving depolarization in adjacent tissue. In contrast to propagation, the initiation of SD appears more insensitive to receptor kinetics, and the amount of charge transfer mediated by NMDARs may be more important. However Zn^{2+} at 100 µM should have inhibited some fraction of GluN2B as well as GluN2A receptor populations (Paoletti and Neyton, 2007). In addition, results from Chapter 4 indicate that the efficacies of antagonists can be significantly modulated by the extracellular environment. Thus it is possible that efficacy of the NR2B blockers was been reduced by pH, redox or local ionic strength. At this point, the present study cannot make a strong conclusion to support or reject the benefit of targeting specific GluN2 populations for SD. In the absence of receptor antagonists with higher subunit specificity, future tests for GluN2 subunit

selectivity could be conducted using preparations where specific GluN2 subunits have been genetically ablated.

NMDARs can also be classified into different populations based on their cellular localization. One major and potentially relevant classification is based on synaptic and extrasynaptic sites. While synaptic NMDARs are coupled tightly with signaling molecules present at postsynaptic densities, extrasynaptic NMDAR are not, and Ca^{2+} influx from these different populations can activate different or sometimes opposing signaling pathways (Hardingham and Bading, 2010). Because of the high glutamate concentrations in ischemic brain regions, activation of extrasynaptic receptors can occur in ischemic brain tissue. Activation of specific downstream signaling pathways linked to extrasynaptic receptors has therefore been considered an important neurodegenerative signal (Stark and Bazan, 2011) (but see also Wroge et al., 2012). In addition to cellular signaling pathways, extrasynaptic receptors may be less inhibited by synaptically released Zn^{2+} and thus may contribute more to charge transfer and Ca^{2+} influx during SD. Selectively targeting extrasynaptic NMDARs has therefore long been considered for selectively targeting neurodegenerative signaling. Memantine is an NMDAR open channel blocker with a high off rate (Lipton, 2006). Some studies claim that memantine is more selective for extrasynaptic receptors at specific test concentrations (Lipton, 2006; Hardingham and Bading, 2010). However there seems very little rationale for this conclusion and recent paper has challenged claims of selectivity (Wroge et al., 2012). Thus there are currently limited approaches for selectively targeting extrasynaptic receptors. In

this context, it is interesting that a very recent study demonstrated that synaptic NMDAR utilize D-serine as a coagonist while extrasynaptic NMDARs appear to use glycine for their activation (Papouin et al., 2012). While it is not known whether such selectively may persist during SD, this study raises the possibility of selectively inhibiting synaptic and extrasynaptic NMDAR population, to modify SD.

There is a study suggesting that different pools of NMDARs are present even at synaptic sites (Atasoy et al., 2008). This study showed that spontaneous glutamate release (contributing to sEPSCs) and evoked glutamate release activates distinct pools of NMDARs. In addition, NMDARs are expressed at silent synapses (Kerchner and Nicoll, 2008). Silent synapses either do not have sufficient glutamate release, or do not express sufficient AMPA receptors to generate significant postsynaptic current. Thus even in the presence of NMDAR surface expression they do not yield NMDAR currents. During SD, massive glutamate waves and depolarization throughout entire postsynaptic neurons could be sufficient to generate additional NMDAR current, which would then seem to be difficult to target with an open channel blocker. Because of the massive NMDAR activation during SD, the heterogeneity in synaptic NMDARs may not be significant for determining SD initiation or propagation. However these different populations of NMDAR may be important when considering cellular signaling pathways.

In addition to postsynaptic NMDARs several studies have proposed the presence of NMDARs at presynaptic terminals in cerebellar interneurons (e.g.

Glitsch and Marty, 1999) and recently in hippocampal pyramidal neurons (McGuinness et al., 2010; Larsen et al., 2011). In the latter studies, presynaptic NMDARs are expected to be activated by glutamate release from the same terminals and amplify Ca^{2+}-dependent glutamate release processes. Such a mechanism may amplify postsynaptic ionic loading in ischemia (Zhou et al., 2010b). However the contribution of presynaptic NMDARs seems to be very difficult to unequivocally prove. The NMDAR antagonist ifenprodil has been shown to decrease presynaptic release probability by inhibiting P/Q type Ca^{2+} channels in the basolateral amygdala (Delaney et al., 2012). In addition NMDAR currents in dendrites can propagate and directly activate axonal Ca^{2+} channels (Christie and Jahr, 2008). As described in the Chapter 2, significant NMDAR activation occurs after SD. Such dendritic NMDAR activation may increase presynaptic glutamate release and contribute to the glutamate release in the tissue where SD is propagating. However the massive NMDAR activation throughout SD makes it difficult to selectively determine a contribution of presynaptic NMDARs to SD propagation.

6.3.2 Pharmacology of NMDAR antagonists during SD

The present study mainly used the competitive NMDAR antagonist AP5 to evaluate contributions of NMDAR to SD and SD dependent injury. However as will be discussed later, this compound is not ideal for therapeutic purposes. The following discussion in this section will examine advantages and disadvantages

of different NMDAR antagonists for targeting SD initiation/propagation as well as SD dependent excitotoxic injury.

NMDAR channel blockers are often considered to be most potent antagonists because of their slow dissociation kinetics. In addition, use dependent inhibition may be useful to preferentially target brain tissue where NMDARs are severely over activated. This class of antagonists includes chemical analogues of PCP and includes MK801, memantine and ketamine. Because of current clinical use of memantine and ketamine, open channel blockers are likely the most feasible antagonist to be tested for SD in clinical settings. A confound to the use of open-channel blockers is the fact that most NMDAR open channel blockers (except for memantine) have significant psychotomimetic activity. Thus PCP is used experimentally to induce schizophrenia (Murray, 2002). One hypothesis for this effect is that open channel NMDAR blockers shift the excitatory–inhibitory balance in the neocortex. This effect is partly due to the fact that MK801 preferentially inhibits NMDAR expressed in interneurons *in vivo* (Homayoun and Moghaddam, 2007; Wang and Gao, 2012), and thus systemic injection of MK801 decreases the activity of inhibitory neurons and increases the firing rate of pyramidal neurons. This preferential block is likely due to a high discharge rate of interneurons which increases the probability of channel block. In injured brain, GABA tone is elevated (Clarkson et al., 2010) and NMDAR block rate by MK801 in interneurons could be even higher. Thus the acute effect of open channel NMDAR blocker in the neocortex may be a disinhibition of glutamergic neurons

and the resultant increased excitability could decrease threshold for SD, an effect that would obviously be undesirable in the injured brain.

Binding and dissociation kinetics of open channel blockers are often measured at resting potential, however these kinetics are significantly reduced when measured at severely depolarized membranes (MacDonald et al., 1991). This is likely because actions of channel blockers are partly based on the cation current, as is seen with voltage dependent Mg^{2+} block of NMDAR. Appendix Figure A6, adapted from previous literature (MacDonald et al., 1991) and presented in the appendix, shows an example of this phenomenon. At resting potential (-60 mV) the open channel blocker PCP moves into the channel and inhibits NMDAR current. However at +40mV, NMDAR current recovered from channel block by PCP in a use-dependent manner, due to loss of charge attraction of the blocker to the channel domain. Binding properties of open channel blockers can be quite variable and use-dependent recovery seen in this reference paper utilized unphysiological recording conditions (+40 mV). However these findings raise the possibility that even when NMDAR channels are preblocked by MK801, some NMDARs recover during depolarization and a significant amount of NMDAR may be available during the post-SD excitation phase. Thus open channel blockers may be useful for preventing SD, but may not be effective at preventing the excitatory phase critical for determining injurious consequence of SD described in Chapter 2.

As noted above, NMDAR antagonist competitive for glutamate sites (e.g. AP5) were used in the most of the present studies. This choice was made

mainly because of the high selectivity of this agent, and the fact that AP5 could be effectively washed out, thereby providing a useful for test for the specificity of the drug effect. However in most experiments, high AP5 concentrations were required to obtain reliable inhibitory effects on SD. Synaptically-evoked NMDAR currents were usually blocked with 1-2 μM AP5, however full block of SD required >100 μM and inhibition of post-SD excitation also required ~20 μM AP5. Based on mechanisms of competitive action, these differences in concentration could be simply be a reflection of the much higher glutamate concentrations achieved during SD, compared with synaptic stimulation. This also suggests that high concentrations of competitive antagonists will be required for prevention of SD in various clinical settings. Competitive antagonists (both at glutamate and glycine binding sites) generally do not have selectivity for different NMDAR subpopulations (Paoletti and Neyton, 2007). Nonselective inhibition of NMDAR activation required for block of SD would hinder physiological NMDAR activities as well as NMDAR dependent regeneration process (Lo, 2008; Murphy and Corbett, 2009). Thus the use of competitive antagonists could have significant unfavorable side effects in clinical setting.

Another class of NMDAR antagonists includes allosteric modulators. Ifenprodil, Ro25-6981 and Zn^{2+} belong to this category. Recent clinical studies showed that a member of this class (Ro25-6981) is potentially useful as a novel class of antidepressant (Pittenger et al., 2007) and some clinical studies have confirmed this is safe to administer to human patients (Pittenger et al., 2007). One of the characteristic features of this class is that most agents do not fully

block NMDAR currents. Zn^{2+} inhibition of NMDAR (GluN1/GluN2A) produces ~70% block of maximum currents and ifenprodil-like compounds inhibit ~90% (Paoletti and Neyton, 2007). In addition, the experiments in Chapter 3 suggest that the binding sites of these antagonists could be sensitive to the extracellular redox environment and protective effects may be limited in the context of severe brain injury. Ifenprodil and Ro25-6981 were shown to reduce SD (Faria and Mody, 2004; Peeters et al., 2007), and these compounds are potentially useful for preventing SD, in such cases as brain trauma and subarachnoid hemorrhage.

6.3.3 Strategies to enhance efficacy of NMDAR antagonists

The studies in Chapter 4 revealed that hypoxia-dependent redox modulation can be a confound for targeting NMDAR activation. In fact addition of DTNB significantly increased pharmacosensitivities of OGD-SD to zinc, D-AP5 and Ro25-6981. In addition to oxygen concentration, SD involves massive changes in other extracellular environment such as pH and ionic strength. It is not known whether these factors can modulate pharmacological compounds as well as their targets. Evaluation of these extracellular modifications on pharmacosensitivity should be important for designing pharmacologically targeting of SD occurring in severely injured brain.

In addition to modulation of the extracellular environment, studies in Chapter 4 briefly discussed the observation that decreasing the intensity of SD stimuli can significantly increase sensitivity of SD to NMDAR antagonists. For example, the use of modified oxygen glucose deprivation (OGD) which retained

15% glucose was necessary for revealing NMDAR sensitivity of OGD-SD. Because of significant sensitivity of periinfarct depolarizations to NMDAR antagonists, it is likely that such reduced SD stimuli are useful for evaluating pharmacosensitivity of SD occurring in periinfarct tissue.

The increased NMDAR antagonist sensitivity seen with more moderate stimuli could be explained by a reduced contribution of potassium ion concentration to SD initiation/propagation. While speculative, it seems possible that if SD initiation and propagation are regulated by additive contributions from potassium and glutamate, decreasing potassium contribution should thereby enhance the relative efficacy of NMDAR antagonists to prevent SD propagation. Extracellular potassium clearance is regulated by the activities of Na^+/K^+ ATPase activity and inward rectifier potassium channels, and support for cellular energy metabolism may help these processes. This issue was addressed in additional experiments (Appendix Figures A7, 8). OGD-SD is known to be highly resistant to NMDAR antagonists however experiments in Figure A7 showed that addition of glucose dramatically increased the sensitivity to NMDAR antagonist MK801. Thus when the glucose concentration was elevated to 1.5 mM in OGD solutions, the onset and propagation rates of OGD-SD did not change but became significantly more sensitive to MK801. In order to test whether increased capacity for glycolysis decreased potassium and sensitized SD to NMDAR antagonists, additional experiments were also conducted. Contributions of potassium were tested by adding additional KCl in OGD-solution. Under this condition MK801 was ineffective at inhibiting SD. Similarly when glycolysis was

inhibited by supplementation of iodoacetate (an inhibitor of glycolysis) MK801 sensitivity was also lost. While further experiments will be needed to verify mechanisms, these results suggest that approaches to enhance tissue metabolism could enhance efficacy of NMDAR antagonists.

6.3.4 Targets downstream of NMDAR activation in ischemic brain injury

The excitotoxic pathways revealed in the present study involve Ca^{2+} deregulation and associated membrane compromise. As described earlier, these are common features of excitoxic neuronal injury and the underlying mechanisms have been extensively studied in prior work. Because of the diverse function of NMDARs, NMDAR antagonists may not be ideal therapeutic compounds to limit excitotoxicity. However the toxic downstream pathways of NMDAR activation are very well studied in *in vitro* excitotoxicity models and several studies suggest the value of targeting downstream of NMDAR activation, without targeting NMDARs themselves. Direct evidence for a contribution of NMDAR-dependent signaling pathways to neuronal death came from the neuroprotection produced by disruption of NMDAR interaction with targets in rodent cortical neurons (Aarts et al., 2002) and very recently in non-human primates (Cook et al., 2012). As discussed earlier, cellular signaling pathways activated by SD could be unique and identification and selective block of these pathways may identify therapeutic approaches to prevent acute brain injury with less unwanted off-target effects.

One of the most interesting classes of compounds is protein kinase inhibitors. As seen in the present study, NMDAR activation significantly

prolonged neuronal depolarization and resultant depolarization should further activate NMDAR by preventing voltage-dependent Mg^{2+} block. Thus preventing persistent depolarization without affecting NMDAR should be beneficial for decreasing injurious NMDAR activation. Interestingly PKC and PKA inhibitors have been shown to enhance recoverability of neurons from cellular depolarization following oxygen glucose deprivation (OGD) (Liu et al., 2005; Murai et al., 2012). As described in the Introduction, OGD is a model of irrecoverable anoxic depolarization and is very difficult to prevent. Furthermore, once neurons were completely depolarized during OGD, neurons did not spontaneously recover even after superfusion with oxygenated saline. However in the presence of kinase inhibitors, neurons promptly recovered from OGD challenges (Liu et al., 2005; Murai et al., 2012). Similar protective effects of protein kinase inhibitors were observed in an excitotoxicity model. As discussed in the Chapter 2, SD induced Ca^{2+} deregulation resembles closely those observed in excitotoxicity models. Interestingly previous studies showed that prolonged Ca^{2+} deregulation induced by NMDA or glutamate applications was reliably prevented by a nonspecific kinase C inhibitor (Connor et al., 1988; Wadman and Connor, 1992). These findings suggest that Ca^{2+} deregulation and prolonged depolarization may not be simple loss of intracellular energy, but rather is a consequence of activation of injurious signaling pathways.

In addition to Ca^{2+} deregulation, membrane compromise has been observed in previous studies and several contributors have been identified. Another pathway potentially relevant to the present studies is opening of hemichannels. It

was previously shown that anoxic depolarization can effectively open hemichannels (Thompson et al., 2006). In that work, opening of hemichannels was a downstream event of NMDAR activation and this pathway was augmented by intracellular ATP depletion (Thompson et al., 2006; Thompson et al., 2008), which is quite similar to the conditions in the current studies, where SD triggered irrecoverable Ca^{2+} deregulation and membrane compromise. In several settings, hemichannels are regulated by protein kinases (Bao et al., 2007; Liu et al., 2011) but the significance of this regulation for neuronal injury has not been confirmed. In the present studies, the contribution of hemichannels was evaluated in some additional experiments evaluating the pharmacology of lucifer yellow leak in metabolically compromised neurons. However carbenoxolone, a nonspecific blocker for hemichannels did not prevent intracellular Lucifer yellow leak (n=2, data not shown). While not conclusive, the present studies could not verify an involvement of hemichannel activation in SD induced neuronal damage. Another potential mechanism is activation of volume regulated anion channels (VRAC) (Zhang et al., 2011). VRAC are activated by volume increases and allow permeation not only of small anions (Cl^-, SO_4^-), but also large molecules such as ATP (MW: 507.18). As seen in my studies, SD involves significant tissue swelling responses and it is feasible that SD opens VRAC. Interestingly, PKC was shown to be involved in activation of VRAC in some cell types (Rudkouskaya et al., 2008), while the significance of this observation is not yet confirmed for neurons. In addition to these possibilities, it is also possible that loss of membrane integrity reflected membrane damage. It has been shown

previously that NMDARs activate NADPH oxidase and generation of reactive oxygen species caused lipid oxidation and potential damage plasma membrane (Brennan et al., 2009). Interestingly this pathway also involves PKC activity and some of the protective effect provided by kinase inhibitor could involve this pathway.

6.3.5 Potential differences in cell signaling pathways in excitotoxicity and SD

Because of technical limitations, the present study focused mainly on acute phases of injury. However it is possible that SD can also trigger cytotoxic signaling pathways involved in progressive cell death pathways such as apoptosis, especially with milder insults. While necrotic cell death is prominent in most excitotoxic models, apoptotic cell death can also be induced in by milder stimuli in excitotoxicity models (Wang et al., 2009; Concannon et al., 2010; Carlsson et al., 2011; D'Orsi et al., 2012; Sibarov et al., 2012). For example, when neurons were exposed to a low concentration of NMDA (30-100 µM, 5 min), some fraction of neurons underwent rapid necrotic cell death, but a considerable remaining fraction of neurons survived for hours, and progressively died (D'Orsi et al., 2012). This delayed neuronal death was associated with activation of apoptosis-associated molecules. However the relevance of these pathways to SD dependent brain damage is not currently known. Understanding of cell signaling pathways activated by SD is currently very limited, but includes one report that SD in healthy tissue can upregulate MAPK activation, which in turn was implicated in preconditioning effects (Chow et al., 2002).

In order to evaluate contributions of SD to apoptotic pathways, future studies of intracellular signaling pathways seem essential. Studies of cellular signaling pathways associated with SD are currently very limited and further comparison between panoptic signaling pathways activated by excitotoxicity and SD becomes quite speculative. However because cell signaling pathways are amongst the most well studied topics in excitotoxicity, it seems appropriate to consider some key differences between these pathways for SD mechanisms. One of the differences between excitotoxicity and SD would be metabolic burdens involved in these events and, while speculative, it is possible that intracellular ATP depletion during SD can influence activities of some kinases not seen in classical excitotoxicity. Kinases generally transfer the γ-phosphate of ATP to target molecules and thus the activity is intrinsically ATP dependent. Intracellular ATP concentration was previously estimated to be within a range of 0.8-1.4 mM (Ainscow et al., 2002), and with intracellular 1 mM Mg^{2+}, free intracellular ATP concentration is estimated to be ~400 μM (calculation based on Maxchelator (http://www.stanford.edu/~cpatton/maxc.html)). The apparent affinities of relevant kinases for ATP are in the range of 10-30 μM (e.g. apparent K_D values for ATP: PKCα 20 μM, CaMKII 60 μM, ERK1 16 μM (values from Setyawan et al., 1999)). Na^+/K^+ ATPase are another important ATP consumer under conditions of ionic deregulation. The apparent affinity of Na^+/K^+ ATPase for ATP significantly changes depending on the Na^+/K^+ concentration. At high intracellular K^+ (at rest), K_D values for ATP are 200-400 μM, while at high intracellular Na^+ concentrations (e.g. during severe depolarization) K_D values

become ~30-100 nM (Jorgensen and Pedersen, 2001). If intracellular ATP is severely depleted and all reactions follow simple linear thermodynamic gradients, a large portion of the available ATP can be consumed by Na^+/K^+ ATPase, with little ATP then being available for kinases. Simultaneously, some phosphatases should be activated by Ca^{2+} flux through NMDAR and the ratio of protein phosphorylation and dephosphorylation may significantly decrease. Therefore, an intriguing possibility is that ATP availability could influence cell signaling being activated following SD. For example, when large NMDAR activation occurs, Ca^{2+} influx likely simultaneously activates protein kinases and phosphatases. In healthy brain tissue, high kinase activity is supported by normal intracellular ATP concentration and may overwhelm phosphatase activity and downstream effector molecules that are activated. However, during SD, ionic deregulation (involving high intracellular Na^+ concentration) strongly activates Na^+/K^+ ATPase activity, depletes intracellular ATP and may limit available ATP for kinases during the late SD phase. Under such conditions, simultaneously activated phosphatases could become dominant and silence signaling pathways. However as SD can be a physiologically occurring excitotoxic signal, intracellular ATP concentration may be an important factor and SD may potentially activate signaling cascades that are quite different from those activated by a simple glutamate exposures.

The real situation may not be as simple as described above, as some kinases are activated by decreased ATP/AMP ratio (e.g. AMP activated kinases (Ramamurthy and Ronnett, 2012)). In addition hemichannel opening by NMDAR activation was more pronounced when intracellular ATP concentrations were

decreased (Thompson et al., 2006). However intracellular ATP concentration changes may be a significant factor that influence the consequent kinase cascades, and may not be revealed by the classic excitotoxicity models in which stimulation would be accompanied by much milder metabolic stress.

Another important issue to consider is that most excitotoxic studies are conducted in culture models in which mature vesicular Zn^{2+} content is absent. As seen in Chapter 4, synaptic Zn^{2+} significantly contributes to intracellular Zn^{2+} accumulation of postsynaptic neurons. Some kinases such as Src kinase are upregulated by Zn^{2+} and may enhance NMDAR currents (Manzerra et al., 2001). Thus the absence of synaptic Zn^{2+} translocation mechanisms in excitotoxicity models of cultured neurons may also be quite different from signaling pathways following SD in more complex preparations.

6.4 Roles of synaptic Zn^{2+} release in the regulation of SD

6.4.1 Extracellular action of synaptic Zn^{2+} release

One of the aims of the present studies was to ask whether extracellular Zn^{2+} has any deleterious effect in the context of SD. The present study concluded that Zn^{2+} was actually inhibitory for some SD. While the sensitivity to hypoxia-dependent redox modulation suggested a limited protective effect in ischemic injury, such mechanism may be important in some injury such as brain trauma. While direct tests could not be achieved (see Discussion in Chapter 3),

the strong correlation between Zn^{2+} inhibition of NMDAR and SD suggested NMDAR as a relevant target of Zn^{2+} that contributes to SD inhibition.

Extracellular Zn^{2+} concentrations can reach 300 µM at the synaptic cleft (Howell et al., 1984) and extracellular Zn^{2+} at this concentration has been shown to inhibit many ion channels. The present studies showed that 100 µM of exogenously applied $ZnCl_2$ is sufficient to inhibit SD propagation (Chapter 3&4). Based on previous literature (Frederickson et al., 2005), it is likely that many channels were inhibited by extracellular Zn^{2+} at this concentration. However screening of potential Zn^{2+} targets in the present study did not show effects of $ZnCl_2$ on intrinsic excitability, or paired pulse facilitation. In addition to the data shown in Chapter 3, Zn^{2+} effects was tested on sEPSCs and sIPSCs in additional experiments (Appendix Figure A8). Interestingly sEPSC frequency (but not amplitude) was increased by bath application of 100 µM Zn^{2+}, whereas neither sIPSC frequency nor amplitude was significantly affected. While the sEPSC frequency increase was significant, based on Zn^{2+} effects on other neuronal functions, from these screening experiments it was concluded that 100 µM $ZnCl_2$ had relatively minor effects on overall excitability in the hippocampal slice model. The absence of a strong Zn^{2+} effect on GABA currents was unexpected because $GABA_A$ currents was one of the first identified Zn^{2+} sensitive targets (Westbrook and Mayer, 1987). The lack of effect here is likely because the system used to assess Zn^{2+} sensitivity is quite different. Thus Zn^{2+} sensitive $GABA_A$ receptors seen in prior work has been receptors lacking γ-subunits (Hosie et al., 2003). This effect may therefore be relevant for some brain subregion or in recordings

from immature preparations, but these sensitive channels are likely absent in cortex and hippocampus of adult animals where αβγ-containing $GABA_A$ receptors predominate (Moss and Smart, 2001; Smart et al., 2004). This emphasizes the importance of testing Zn^{2+} sensitivity of targets in comparable experimental conditions.

Zn^{2+} recently has been shown to upregulate KCC2 activity via interaction with the metabotropic receptor GPR39 (Chorin et al., 2011). The resultant increased Cl^- extrusion rate will increase charge transfer by $GABA_A$ channels and likely decrease excitability. The contribution of KCC2 upregulation could have been missed in the present studies because intracellular Cl^- concentrations were clamped by the pipette solution. While the discussion here did not cover all Zn^{2+} sensitive or responsive molecules, these studies illustrate that Zn^{2+} is not toxic as long as it is present in the extracellular space and Zn^{2+} can even be protective for neurons by decreasing excitability. These studies support the idea that selectively blocking intracellular Zn^{2+} accumulation, with minimally affecting extracellular Zn^{2+} concentration could be more beneficial for stroke injury (but see Discussion section of Chapter 4, regarding Zn^{2+} effects on SD propagation).

6.4.2 Intracellular Zn^{2+} accumulation following synaptically released Zn^{2+}

The present study identified a significant contribution of synaptic Zn^{2+} release to intracellular Zn^{2+} accumulation in postsynaptic neurons (Chapter 5, Supplemental Figure A10). This was done by comparison between intracellular Zn^{2+} responses in WT and ZnT3 KO preparations. Prior to the studies in Chapter

5, most single cell Zn^{2+} imaging study aimed to minimally-disrupt intracellular Zn^{2+} homeostasis by loading the Zn^{2+} indicator into neurons using either sharp microelectrodes electrode (Dietz et al., 2008) or very brief dialysis of intracellular component with conventional patch pipettes (Medvedeva et al., 2009; Vander Jagt et al., 2009). However under those recording conditions, it was not clarified whether or not synaptic Zn^{2+} translocation was detected.

The studies in Chapter 4 examined the effects of dialysis on intracellular Zn^{2+} accumulation, and concluded that standard electrophysiological recording methods (e.g. 20 min dialysis) markedly disrupted intracellular Zn^{2+} signals. This appears to be due to loss of intracellular Zn^{2+} buffering, and is matched by decreases in Zn^{2+} liberation from intracellular stores by oxidant exposure. These findings, together with the fact that supplementation with recombinant MT3 was sufficient to reverse this effect, suggests that washout of metallothionein 3 (or a related Zn^{2+} buffer) could underlie the observations. By comparison between responses seen with different dialysis conditions, in both WT and ZnT3 KO preparations, it was possible to conclude that both intracellular liberation of Zn^{2+}, and accumulation of synaptically-released Zn^{2+} contributes to intracellular increases after synaptic stimulation. Thus intracellular Zn^{2+} dialysis may be a very valuable method to accurately assess contributions from synaptic Zn^{2+} translocation. These methods may be applicable to other stimuli and be used to identify/evaluate contribution of synaptic Zn^{2+} translocation and intracellular Zn^{2+} release to, for example, intracellular Zn^{2+} accumulation contributing to ischemic neuronal brain injury.

Many Zn^{2+} studies have focused on neurotoxic roles of intracellular Zn^{2+} accumulation in the context of ischemic brain injury. Synaptic Zn^{2+} release is one potential source for intracellular Zn^{2+} accumulation. However most Zn^{2+} toxicity has been tested by exogenous Zn^{2+} applications (Koh and Choi, 1988; , but see Aizenman et al., 2000; Sheline et al., 2000; Bonanni et al., 2006), and the source(s) of toxic intracellular Zn^{2+} accumulation is not well studied. These sources are important for understanding the mechanism for neuroprotective effects of CaEDTA in stroke studies.

CaEDTA is a high affinity Zn^{2+} chelator, but its kinetics are limited by the need for dissociation of Ca^{2+} prior to stable interaction with Zn^{2+}. This restricts its ability to eliminate rapid extracellular Zn^{2+} concentration elevations. In brain slices, Zn^{2+} release following synaptic stimulation or SD results in a biphasic response, an initial sharp extracellular Zn^{2+} elevation and secondary slow accumulation response (Appendix Figure A10, (Qian and Noebels, 2005; Carter et al., 2011a). My studies of intracellular Zn^{2+} imaging suggest that CaEDTA cannot capture the fast component of Zn^{2+} release and this allows significant Zn^{2+} influx into postsynaptic neurons. Thus it is unlikely that neuroprotection provided with CaEDTA is due to prevention of fast synaptic Zn^{2+} translocation. My studies also indicate that a slow component of extracellular Zn^{2+} responses unlikely contributes to postsynaptic Zn^{2+} accumulation. When intracellular Zn^{2+} accumulation responses were compared between with or without CaEDTA, intracellular Zn^{2+} responses during SD were significantly decreased by CaEDTA but the effect on kinetics was very small compared with the CaEDTA effect on

extracellular Zn^{2+} response (Appendix Figure A10). In brain slice experiments, ACSF is contaminated by Zn^{2+} originating from the surface of glassware or in recording solutions (Kay, 2004), and this significantly contributed to Zn^{2+} responses in ZnT3 KO preparations. By considering the effects of removal of contaminating Zn^{2+} on the kinetics of intracellular FluoZin3 responses, it is likely that the contribution of slow components of extracellular Zn^{2+} release to intracellular accumulation is quite small. Therefore synaptic Zn^{2+} translocation appears mainly mediated by the rapid Zn^{2+} release following the SD stimulation and the slow component of the released Zn^{2+} is unlikely to contribute to acute Zn^{2+} accumulation.

In addition to acute Zn^{2+} accumulation by synaptic Zn^{2+} translocation, transmembrane Zn^{2+} flux can occur when extracellular Zn^{2+} concentration is elevated by exogenous application of $ZnCl_2$. In fact the studies with bath application of 100 μM $ZnCl_2$ revealed that a significant amount of Zn^{2+} can accumulate in the neurons (Figure 3.1E) likely via passive Zn^{2+} uptake by the activities of Zn^{2+} transporters. Studies of ZIP transporters suggest that neurotoxic intracellular Zn^{2+} accumulation is mediated by ZIP1 and ZIP3 transporters during seizures (Qian et al., 2011). This raises the possibility that during seizure or ischemia, Zn^{2+} accumulates in the extracellular space and neurons passively uptake Zn^{2+} in amounts sufficient to trigger neurotoxic pathways.

In contrast to uptake mechanisms, regulatory mechanisms for extracellular Zn^{2+} accumulation and clearance are not well under stood. This is partly

because regulation of extracellular Zn^{2+} concentrations *in vivo* has not been very actively studied. Early studies using radiolabeled Zn^{2+} showed that dietary administered Zn^{2+} was found mainly in the choroid plexus (CP), and some in brain tissue (Kasarskis, 1984). Among brain tissues, periventricular tissue contained relatively higher $^{65}Zn^{2+}$ levels. Although the evidence is very limited, the presence of high $^{65}Zn^{2+}$ concentrations in the CP suggests that most serum Zn^{2+} is filtered at the CP and this system first limits Zn^{2+} entry into brain tissue. In addition, the localization of $^{65}Zn^{2+}$ in the periventricular zone, and the absence of $^{65}Zn^{2+}$ in the CSF suggest that small amounts of Zn^{2+} are provided to CSF, but most can be effectively absorbed by brain tissues. Effective Zn^{2+} absorption by brain tissue does not necessarily mean uptake by neurons or glia (although cellular uptake is feasible). One of the interesting possibilities is that Zn^{2+} forms precipitates in the extracellular space. Zn^{2+} is very insoluble in phosphate-containing solutions. In ACSF containing 1.25 mM phosphate, Zn^{2+} above 10 µM immediately formed precipitates (unpublished observation, consistent with (Rumschik et al., 2009)). Thus it is possible that most Zn^{2+} actually forms precipitates and did not contribute to extracellular Zn^{2+} concentration *in vivo*. In addition to precipitation, there is evidence that metallothionein is expressed in the extracellular space and can chelate extracellular Zn^{2+} in brain tissue (Chung et al., 2008). This immobilized Zn^{2+} may be solubilized by acidification (e.g. after SD) and then may be slowly taken up by local neurons or glia.

A more complete understanding of extracellular Zn^{2+} homeostasis will be important for fully understanding of synaptic Zn^{2+} release, its contribution to

intracellular Zn^{2+} accumulation and extracellular actions. It is not known, for example, for how long Zn^{2+} may block NMDAR at synaptic sites. In addition, little is known concerning how mobilized or immobilized extracellular Zn^{2+} can interact with Zn^{2+} influx proteins (ZIP) to internalize into postsynaptic neurons.

6.4.3 Tentative quantitative analysis of intracellular Zn^{2+} accumulation

Intracellular Zn^{2+} homeostasis was characterized in studies Chapter 5 and confirmed a strong intracellular Zn^{2+} buffer capacity of CA1 neurons in acute slice preparations. While that result was expected from prior experiments in neuronal cultures, the new results suggest that intracellular Zn^{2+} homeostasis can be studies even in acute rain slice preparations, which retain many important features of intact brain tissue. One of the interesting new findings data was that intracellular Zn^{2+} concentration of resting neurons is extremely low, regardless of the degree of neuronal dialysis. In fact indicator saturation seen after exposures to 100 μM ZnPyr was extremely large and revealed $\Delta F/F_0$: 4000%. Following exposure to the Zn^{2+} chelator TPEN, intracellular FluoZin3 signals were almost $\Delta F/F_0$: 0. A K_D value of FluoZin3 for Zn^{2+} was reported to be ~15 nM. By using an approach described in (Grynkiewicz et al., 1985) (while it may not be fully appropriate) the resting intracellular Zn^{2+} concentration was estimated to be ~500 pM. This result itself is not surprising as many papers report intracellular free Zn^{2+} that are extremely low, or even absent (Colvin et al., 2008; Sensi et al., 2011). However if this estimated value is true, or at least approximates true intracellular Zn^{2+} concentrations, it is possible that the magnitude of intracellular

Zn^{2+} responses described throughout this dissertation are actually very small, and may not be sufficient to trigger degenerative signaling.

To assess this possibility, the magnitude of intracellular Zn^{2+} responses during SD generated with KCl (K-SD) were assessed as part of an additional study conducted in collaboration during the time of this dissertation work (Carter et al., 2011a). Those experiments revealed that the intracellular FluoZin3 signal changes were between $\Delta F/F_0$:100-200% during SD. From a simple estimation based on initial resting Zn^{2+} concentrations discussed above, the intracellular Zn^{2+} concentration change was estimated to be <1 nM. Previously work has not determined the exact amount of Zn^{2+} required to exert its toxicity, but one of the lowest Zn^{2+} concentrations demonstrated to exert toxicity was about 10-100 nM, which can be sufficient to open mitochondrial permeability transition pores in isolated mitochondria (Jiang et al., 2001). Because of the low intracellular Zn^{2+} responses and relatively rapid recovery seen after SD (~1 minute, Figure A10), it unlikely that intracellular Zn^{2+} response during K-SD reached threshold concentrations required to trigger neurotoxic pathways. Such low intracellular Zn^{2+} concentrations achieved during K-SD may be reasonable, considering the full recoverability of brain tissue to this form of SD. .

It is important to consider that these values are estimated from soma, and dendritic Zn^{2+} concentrations have not been accurately determined. Because of the large surface to volume ratio and higher synaptic density in dendrites, intracellular Zn^{2+} concentrations are expected to be higher in these compartments. Dendritic imaging with FluoZin3 was technically challenging

because of the high background fluorescence and low FluoZin3 signal due to the low intracellular Zn^{2+} concentrations. While higher concentrations of FluoZin3 should improve visualization of dendrite, FluoZin3 will significantly disrupt endogenous Zn^{2+} buffering. For example, intracellular metallothionein concentration is estimated to be ~300 nM, and the Zn^{2+} affinity of the weakest Zn^{2+} binding sites in MT3 is lower than of FluoZin3. In my experimental setup, 40 µM FluoZin3 was required for detection, even in soma. With 40 µM intracellular FluoZin3, a substantial fraction of Zn^{2+} should be bound by FluoZin3. Higher concentrations should have a further impact on intracellular Zn^{2+} buffering and would likely compromise endogenous responses. Based on the low basal intracellular Zn^{2+} concentration and small Zn^{2+} responses, a fluorescence indicator quenched by Zn^{2+} (rather than activated by it) may be more beneficial for dendritic Zn^{2+} measurements.

Throughout the studies, toxicity of endogenous Zn^{2+} was not obvious in the acute toxicity models, while intracellular Zn^{2+} loading with ZnPyr showed some toxicity. Based on these intracellular Zn^{2+} measurements from soma, low intracellular Zn^{2+} concentrations achieved by endogenous Zn^{2+} release mechanisms seem to be the reason for the lack of acute Zn^{2+} toxicity. However based on excitotoxicity studies, dendrites are the most vulnerable neuronal compartment. Visualization of dendritic Zn^{2+} concentration may be necessary to examine whether endogenous Zn^{2+} can reach toxic concentrations in those compartments.

6.4.4 Tissue metabolism and intracellular Zn^{2+}homeostasis

One interesting question is whether intracellular Zn^{2+} homeostasis can be modulated by tissue metabolism. Intracellular Zn^{2+} buffer capacity could be a particularly important component of intracellular Zn^{2+} homeostasis in the context of metabolic compromise because, as discussed earlier, presynaptic activity is aberrantly increased under conditions of metabolic stress (section 5.2.2.). Thus neurons are expected to be exposed to synaptically released Zn^{2+} under metabolically compromised tissue and without significant intracellular buffering, intracellular Zn^{2+} concentrations could readily elevate.

There are reports suggesting that endogenous Zn^{2+} buffer systems, especially MT, can be sensitive to intracellular ATP concentrations (Jiang et al., 1998). While MT is generally a short peptide, MT directly bind with glutathione and ATP, and such interactions can significantly change MT's ability to transfer Zn^{2+} to high affinity binding sites (Jiang et al., 1998). Thus ATP binding can increase transfer of MT3 bound Zn^{2+} to higher affinity sites. ATP binding to MT is also modulated by the ratio of reduced/oxidized glutathione (GSH/GSSG). The presence of GSH decreases MT3-ATP binding whereas GSSG promotes MT-ATP interactions. An important consideration is the low affinity of MT for ATP, and this was estimated to be ~170 µM (Jiang et al., 1998). These values were obtained in the absence of Mg^{2+} and the apparent affinity *in vivo* will likely be lower. Under ischemic conditions, intracellular ATP can drop to ~12% (Mies and Paschen, 1984), and potentially saturate intracellular MT with Zn^{2+}, thereby decreasing buffering capacity. In the present study, this was tested by imaging

intracellular Zn^{2+} in briefly dialyzed neurons during OGD (Supplementary Figure A11). OGD significantly elevated intracellular Zn^{2+} prior to SD, but Zn^{2+} accumulation was absent or very small in ZnT3 KO preparations. During OGD, presynaptic activity significantly increased (Figure A1&2). The correlation with presynaptic activity suggests that significant synaptic Zn^{2+} translocation occurred during the exposure to OGD. It is noted that synaptic stimulation in some preparations resulted in almost equal intracellular Zn^{2+} accumulation in WT and ZnT3 KO preparations (Chapter 5). These preliminary results support the idea that metabolic stress significantly decreases intracellular Zn^{2+} buffering in neurons and makes neurons more sensitive to Zn^{2+} influx. Further studies will be needed to validate this possibility.

6.5 Confounds of the present study and future directions

6.5.1 Model to test neuronal injury following SD

Ischemic brain injury is usually studied in one of three different preparations; neuronal cultures, acute brain slices or *in vivo*. These three preparations are quite different and data obtained from different system should be carefully compared.

One of the important differences is their thresholds for metabolic inhibition. This seems to be attributable to differences in energy metabolism between these preparations; however this aspect is rarely addressed. The most significant difference would be their oxygen demands. Neuronal cultures are

successfully maintained in mixed gas containing 21% O_2, which is higher than *in vivo* oxygen concentrations in vivo, which in turn is usually considered to be ~10% (Ndubuizu and LaManna, 2007). However such a difference is much smaller when compared with the fact that acute brain slices are generally maintained in 95% O_2. It is noted here that the experiments in chapter 4 revealed that 21% is already hypoxic for neurons and evoked synaptic transmission was severely suppressed at this O_2 concentration. The high sensitivity of brain slices to oxygen concentration is due to the extremely high oxygen demand of these preparations. There are several studies of tissue oxygenation of brain slices and these studies generally report a remarkably high oxygen consumption of brain slice even at rest (Hall and Attwell, 2008; Galeffi et al., 2011; Hall et al., 2012). A study using O_2 sensitive electrode and 300 µm thick hippocampal slices revealed an O_2 concentration drop from 550 µM (95% O_2/5% CO_2 mix gas) to ~400 µM (or 70% saturation) at the slice surface, and further decreased to 220 µM O_2 (or >50% saturation) at 100 µm below the surface of the slice (Hall et al., 2012). It is important note that O_2 concentration in brain slices is purely determined by diffusion from superfusate and thus the low tissue O_2 concentrations is mainly due to consumption by brain tissue. Neuronal cell bodies are usually ~20 µm in diameter and thus in a 300 µm slice there are at least 15 layers of neurons. This is quite different from neurons in culture medium, which are often maintained as a single layer at much lower densities. Because of the lower local O_2 consumption rate and direct exposure to O_2 containing media, 21% O_2 should be sufficient for maintaining cultured

neurons. In brain, O_2 may be even more effectively delivered to local tissue with capillary delivery. Functional neurovascular coupling should be also effective for providing O_2 on demand after SD.

In brain slice experiments, the steep O_2 gradient may not be a problem as long as neuronal activities are recorded from the slice surface; however SD propagation involves a volume of tissue, including the surface, center and possibly also bottom of the brain slice. The metabolic burden during SD will increase oxygen consumption rate and generate tissue hypoxia (Galeffi et al., 2011). Because of poor supply to center part of the slice, brain slices may be experiencing more severe hypoxic stress during SD than neurons *in vivo,* despite the fact that brain slice is oxygenated with 95% O_2 and O_2 concentrations *in vivo* are often assumed to be much lower. A previous study *in vivo* showed that decreased tissue oxygenation can significantly prolong DC shift (Takano et al., 2007). Thus the low oxygenation of brain slice may explain why saddle-like DC shifts are reliably detected in brain slices, whereas monophasic DC shifts are common in the SD generated by KCl in healthy tissue. Most single cell recordings in the present studies were conducted from neurons present >100 µm distant from the surface the brain surface. Given the exposure to high oxygen concentration, these single cell responses may not represent average tissue responses to SD.

One of the other confounds in the present studies is that all experiments were conducted in healthy brain slices or animals. As described in the Introduction, a significant recent finding is the fact that SD can contribute to

secondary injury. While metabolic inhibition was used to model partially metabolically compromised tissue in the present study, differences in brain tissue after injury is not limited to differences in cellular metabolism. One of the most important possibilities is that of modified channel expression and neuronal excitability in injured brain tissue. There is evidence that injured brain initiates regenerative processes and these include enhanced synaptic plasticity (Lo, 2008; Murphy and Corbett, 2009). Importantly, such modulation can occur when secondary injury processes are still ongoing (Lo, 2008). Among the multiple possibilities, one of the potentially most important processes is the down regulation of the AMPA-type glutamate receptor subunit GluA2. AMPARs in adult brain usually contain GluA2. GluA2 AMPAR subunits are important for determining selective permeability, and receptors lacking GluR2 are highly permeable to Ca^{2+} and Zn^{2+} (Weiss and Sensi, 2000; Jia et al., 2002). It has been shown that there is a significant reduction in GluR2 following ischemic injury (Gorter et al., 1997; Calderone et al., 2004). Such increased Ca^{2+} and Zn^{2+} permeability of AMPAR should be important for promoting synaptic reorganization in the injured brain however this would significantly increase vulnerability to SD. It is obviously possible that such increases in Ca^{2+} and potentially Zn^{2+} permeability of neurons should increase their vulnerability. Thus experiments in preparations from post-ischemic animals could reveal significantly different sensitivities to SD as well as Zn^{2+} toxicity, when compared with studies here in slices prepared from healthy animals.

In addition to neuronal modulation, astrocytes are generally activated in the injured brain (Chen and Swanson, 2003; Escartin and Bonvento, 2008). These astrocytes are activated by inflammatory cytokines and plays important roles in tissue remodeling following CNS injury (Escartin and Bonvento, 2008). However reactive astrocytes are also important for their capacity for glutamate uptake. From earlier studies from our laboratory (conducted by Jessica Seidel Ph.D.), it was shown that astrocyte activity can limit SD in brain slices. One of the interesting possibilities is whether increased activities of astrocytes modify sensitivity of SD to NMDAR antagonists. Reactive astrocytes usually occupy a large volume of tissue and potentially have a higher capacity to prevent extracellular potassium accumulation (Escartin and Bonvento, 2008). If potassium concentrations are reduced, NMDAR antagonists are expected to more effectively block SD.

Importantly there is a model to test these possibilities. In the gerbil, bilateral common carotid occlusion induces global ischemia and selectively damages hippocampus CA1. Previous studies have shown that GluR2 downregulation in this model and brain slices prepared from these gerbils showed some alternation in Ca^{2+} signaling (Gorter et al., 1997; Connor et al., 1999; Shuttleworth et al., 2000). Comparisons of sensitivities between healthy and once metabolically compromised tissues to the injurious stimulus in vitro could provide important insights into roles of tissue remodeling and vulnerability to injurious stimuli. These experiments could potentially identify important insights into the toxicity of SD in secondary injury.

Appendix: Supplemental Data

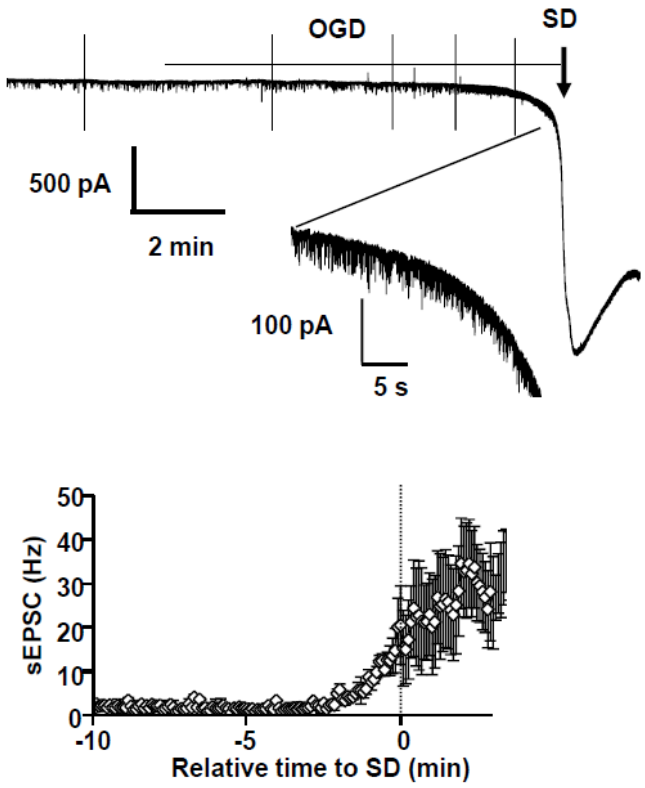

Figure A1. Increased spontaneous EPSC frequency prior to OGD-SD onset.

Top: A representative recording of whole cell current recorded from a CA1 pyramidal neurons during OGD exposure. Recording was made at -55 mV with a potassium gluconate based internal solution. High frequency spontaneous EPSCs were reliably detected. Bottom panel shows a mean plot of sEPSC frequency change (mean ± S.E., n=5). The time was adjusted to SD onset.

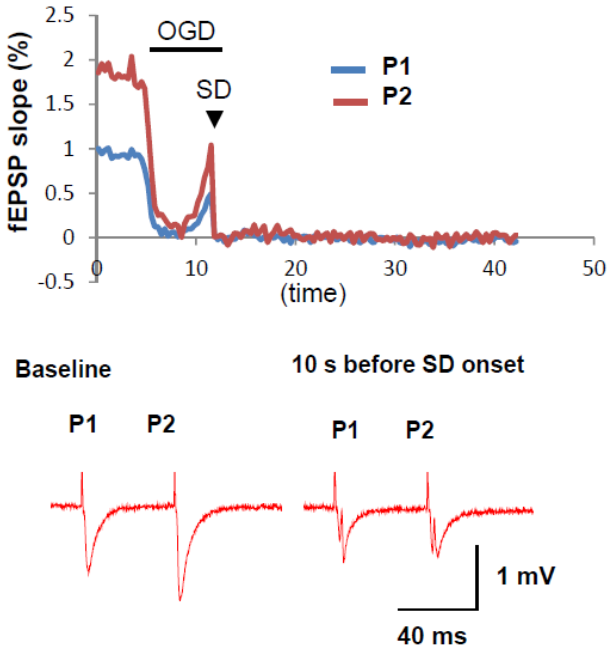

Figure A2. Detection of transient excitatory phase prior to OGD-SD by fEPSP recording.

Top panel shows an example trace of fEPSP responses during OGD exposure. Paired pulse bipolar stimulation (50ms interpulse interval) was applied throughout, and changes in release probability were evaluated based on fEPSP ratio. At baseline, paired-pulse ratio (P2/P1; PPR) was around 2 suggesting low release probability. Following OGD exposure, fEPSP was usually suppressed by adenosine receptor dependent mechanism, but recovered with greatly reduced PPR prior to SD onset. The results also indicate a high release probability just prior to SD onset.

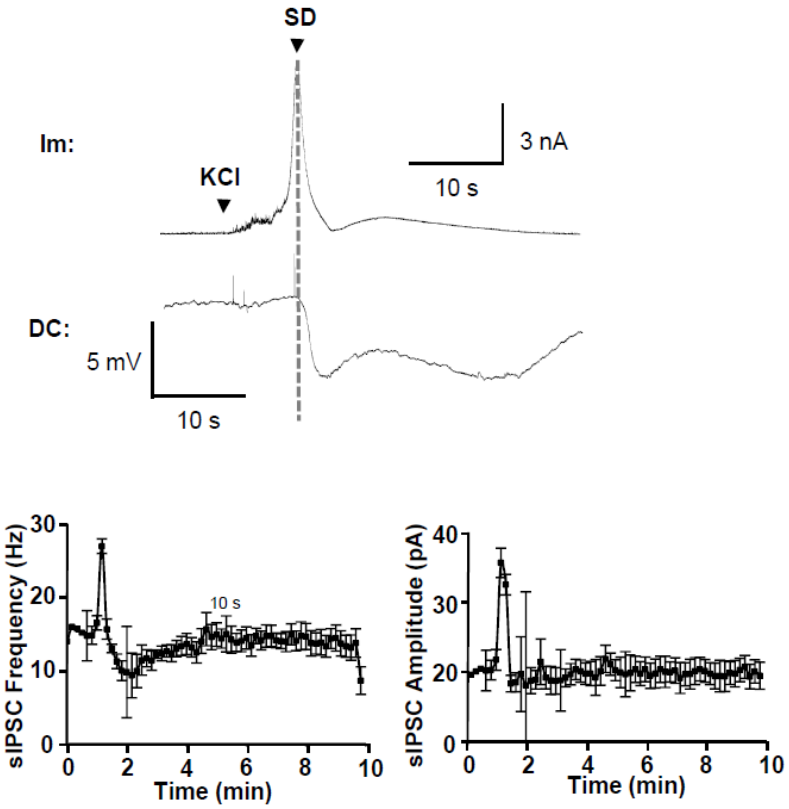

Figure A3. spontaneous IPSCs during KCl induced SD.

Top: Representative recording of whole cell current and extracellular potential shift associated with KCl-induced SD. Recording was made from CA1 pyramidal neurons. Membrane potential was held at 0mV to selectively detect spontaneous IPSCs (outward currents). IPSC frequency was increased immediately after KCl microinjection. A large outward current of unknown origin was reproducibly detected just prior to SD onset. Bottom panels show mean data from 4 such experiments, demonstrating increased sIPSC frequency (left) and amplitude (right)

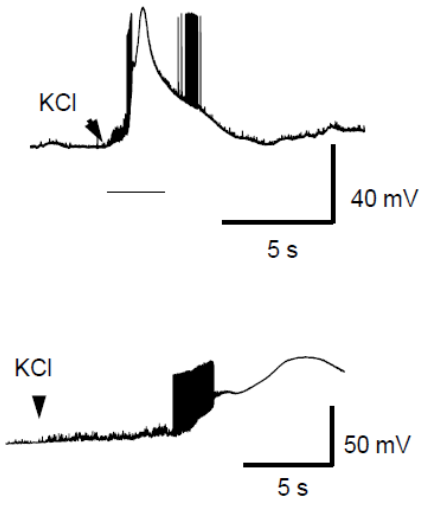

Figure A4. Depolarization of putative interneurons during KCl-induced SD.

Interneurons in the pyramidal cell layer were identified based on their small capacitance (>30pF) and high frequency firing rate (data not shown). The top trace shows neuronal depolarization during SD generated by KCl microinjection. Note the high frequency train of action potentials prior to, and after the large depolarization. The bottom panel shows the same trace, expanding the early phase of SD. KCl injection immediately increased EPSP frequency in this and other putative interneurons recorded throughout these studies.

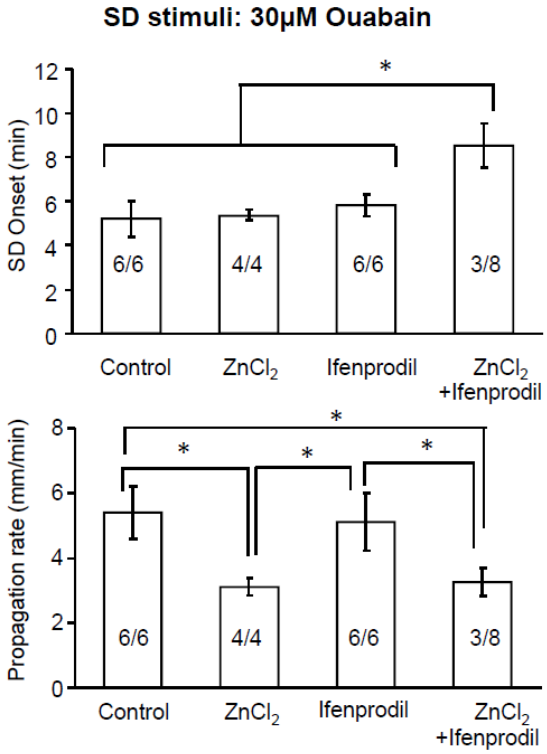

Figure A5. Effect of Zn^{2+} and/or Ifenprodil on ouabain SD.

SD was generated by ouabain exposures in the presence of either 100 μM $ZnCl_2$, 10 μM Ifenprodil, or a combination of 100 μM $ZnCl_2$ and10 μM Ifenprodil. $ZnCl_2$ did not affect SD onset, but significantly decreased propagation rate. Ifenprodil was without effect on both onset and propagation rate. The combination of $ZnCl_2$ and Ifenprodil prevented SD onset in 5 out of 8 experiments and delayed onset of SD in the remainder. The number of SDs generated and the total number of slices tested are indicated by numbers in the bars. *$p<0.05$ one-way ANOVA with post hoc *t*-test

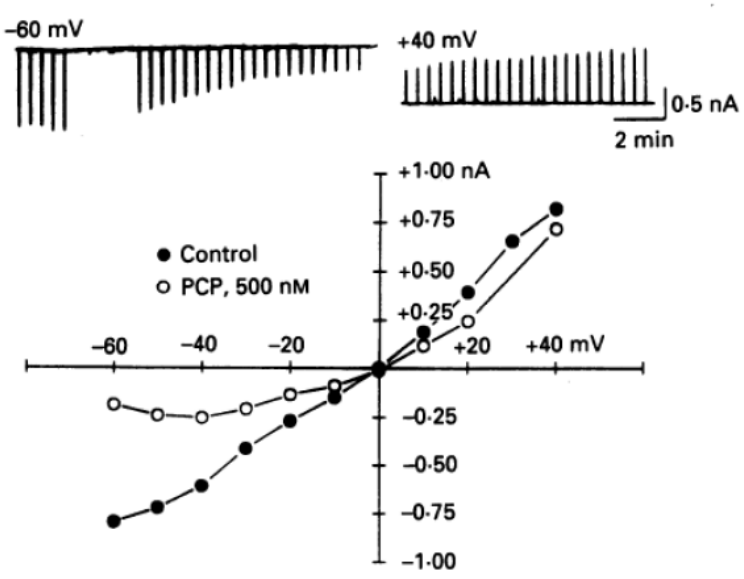

Figure A6 voltage dependency of NMDAR channel block by PCP.

This figure is adapted from MacDonald et al., 1991. J Physiology)

PCP, a NMDAR open channel blocker, use dependently blocked NMDAR current at -60 mV (top left), but use dependent recovery was seen at +40 mV (top right). The I-V curve at bottom illustrates voltage sensitivity of PCP block of NMDAR channel.

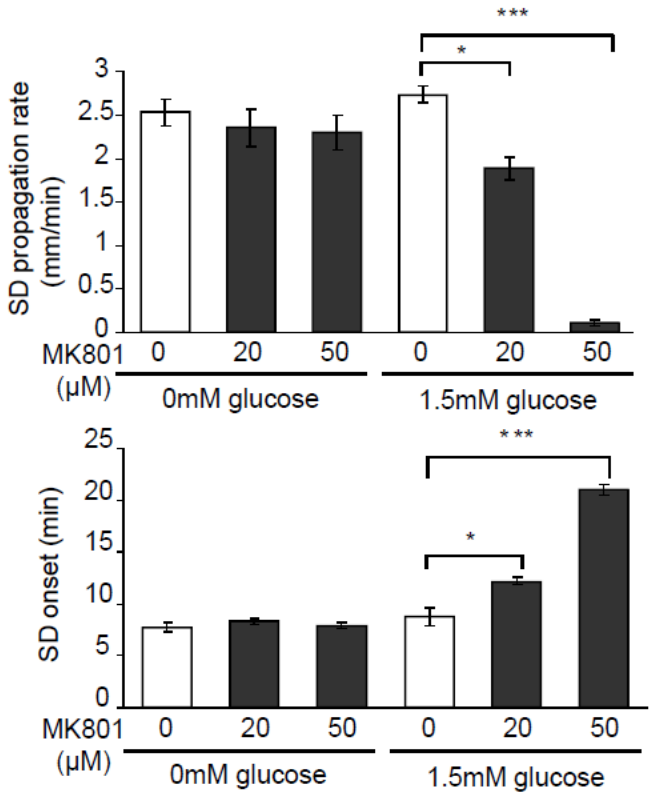

Figure A7 Glucose availability significantly enhanced sensitivity of OGD-SD to MK801 .

Hippocampal slices were exposed to different OGD solutions: either 100% oxygen glucose deprivation or 100% oxygen and 85% glucose deprivation. SDs were reliably detected in both conditions, but showed a remarkable difference in their sensitivity to MK801. n=5, *p<0.05, **p<0.001, ***p<0.0001 one-way ANOVA with post hoc *t*-test

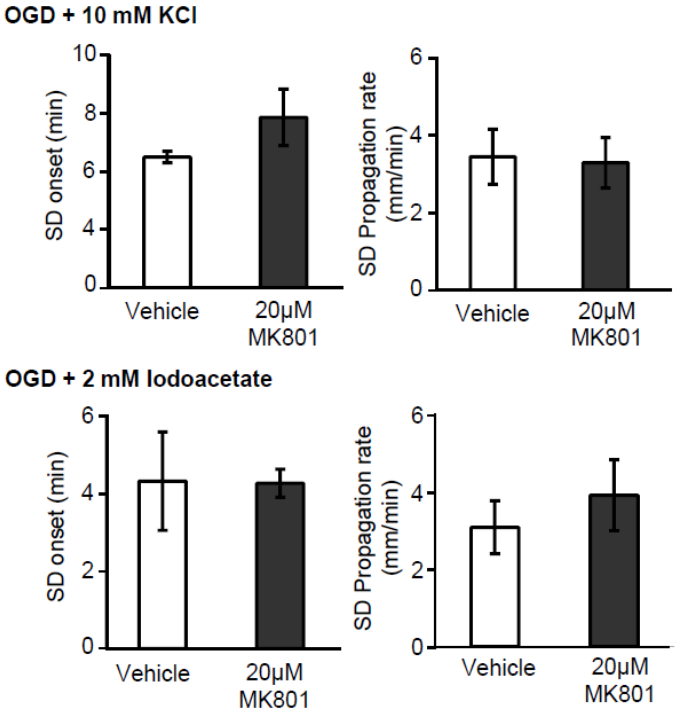

Figure A8 Elevation of K^+ concentration or addition of a glycolysis inhibitor diminished MK801 sensitivity.

The effects of either 1) 10mM KCl (top panels) or 2) 2 mM Iodoacetate (bottom panels) were tested on OGD-SD (100% oxygen and 85% glucose deprivation). Under these conditions, MK801 showed no inhibitory effect on OGD-SD. n=5

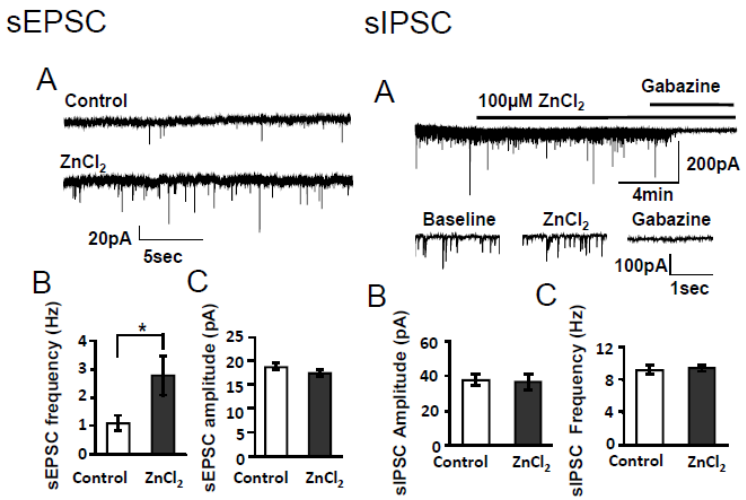

Figure A9 $ZnCl_2$ significantly increased sEPSC frequency buy was without effect on the sIPSC.

Left: sEPSCs were recorded from CA1 pyramidal neurons at -60 mV using a K-gluconate based internal solution. 100 μM $ZnCl_2$ significantly increased sEPSC frequency. A representative traces, B: mean sEPSC frequency, C: mean sEPSC amplitudes.

Right: sIPSCs were recorded by using a cesium chloride based internal solution. 2 mM kynureic acid and 10 μM AP5 were supplemented to the extracellular medium to block sEPSC. Unlike sEPSC, 100 μM $ZnCl_2$ did not affect IPSC.

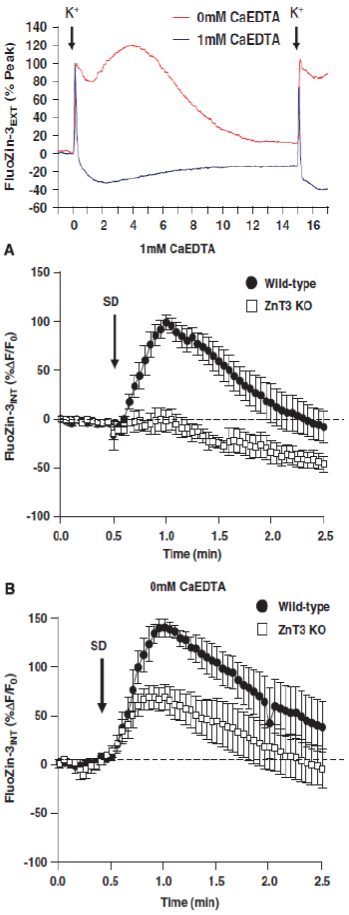

Figure A10 Synaptic Zn^{2+} release and intracellular Zn^{2+} accumulation during KCl induced SD (K-SD).

This work was performed by the candidate during the course of the dissertation studies, and published in collaboration (Carter et al., 2010).

Top: Extracellular Zn^{2+} responses during K-SD were analyzed based on bath applied of 2 μM FluoZin3 in control and in the presence of 1 mM CaEDTA.
Middle: Intracellular Zn^{2+} response recorded from CA1 pyramidal neurons in WT and ZnT3 KO preparations. Neurons were loaded with FluoZin3 via sharp electrodes and intracellular Zn^{2+} responses were monitored during K-SD. induced in the presence of CaEDTA (n=5)
Bottom: same experiment as middle panel but without CaEDTA. Note significant intracellular Zn^{2+} response in ZnT3 KO preparations which were absent in the presence of 1mM CaEDTA (middle panel).

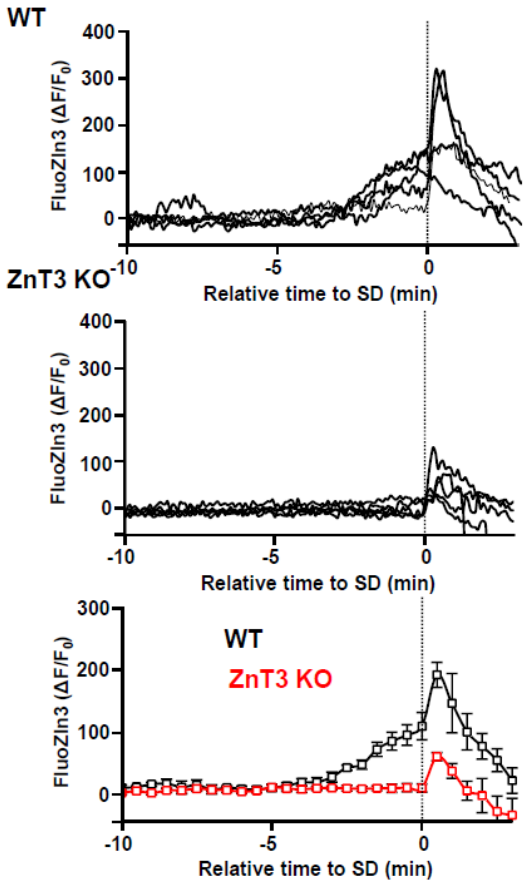

Figure A11. Intracellular Zn^{2+} accumulation during OGD exposure.

CA1 pyramidal neurons in WT and ZnT3 KO preparations were loaded with FuloZin3 via a patch pipette using the brief (2min) dialysis technique. WT neurons showed significantly larger intracellular Zn^{2+} accumulation when compared with ZnT3 KO preparations. Individual traces (WT: top and ZnT3 KO: middle) and average traces (bottom) are presented (n=5). Reponses are aligned to SD onset.

Abbreviations Used

ACSF	artificial cerebral spinal fluid
AMPA	α-amino-3-hydroxy-5-methylsozazole-4-propionic acid
DC	direct current
DTNB	5,5′-Dithiobis(2-nitrobenzoic acid)
EDTA	ethylenediaminetetraacetic acid
EPSC	excitatory postsynaptic current
EPSP	excitatory postsynaptic potential
FAD	flavoprotein
GABA	gamma-aminobutyric acid
I_m	whole-cell current
IPSC	inhibitory postsynaptic current
NMDA	N-methyl-D-asparate
NADH	nicotinamide adenine dinucleotide
NADPH	nicotinamide adenine dinucleotide phosphate
OGD	oxygen glucose deprivation
PCP	phencyclidine
SD	spreading depolarization
SEM	standard error of th emean
tPA	tissue plasminogen activator
V_m	membrane potential
WT	wild-type
ZnT3	zinc transpoter 3

References

Aarts, M., Liu, Y., Liu, L., Besshoh, S., Arundine, M., Gurd, J. W., Wang, Y. T., Salter, M. W. and Tymianski, M. (2002) Treatment of ischemic brain damage by perturbing NMDA receptor- PSD-95 protein interactions. *Science,* **298,** 846-850.

Abele, A. E., Scholz, K. P., Scholz, W. K. and Miller, R. J. (1990) Excitotoxicity induced by enhanced excitatory neurotransmission in cultured hippocampal pyramidal neurons. *Neuron,* **4,** 413-419.

Adlard, P. A., Parncutt, J. M., Finkelstein, D. I. and Bush, A. I. (2010) Cognitive loss in zinc transporter-3 knock-out mice: a phenocopy for the synaptic and memory deficits of Alzheimer's disease? *The Journal of neuroscience : the official journal of the Society for Neuroscience,* **30,** 1631-1636.

Aiba, I., Carlson, A. P., Sheline, C. T. and Shuttleworth, C. W. (2012) Synaptic release and extracellular actions of Zn^{2+} limit propagation of spreading depression and related events in vitro and in vivo. *Journal of neurophysiology,* **107,** 1032-1041.

Ainscow, E. K., Mirshamsi, S., Tang, T., Ashford, M. L. and Rutter, G. A. (2002) Dynamic imaging of free cytosolic ATP concentration during fuel sensing by rat hypothalamic neurones: evidence for ATP-independent control of ATP-sensitive K(+) channels. *The Journal of physiology,* **544,** 429-445.

Aizenman, E., Lipton, S. A. and Loring, R. H. (1989) Selective modulation of NMDA responses by reduction and oxidation. *Neuron,* **2,** 1257-1263.

Aizenman, E., Stout, A. K., Hartnett, K. A., Dineley, K. E., McLaughlin, B. and Reynolds, I. J. (2000) Induction of neuronal apoptosis by thiol oxidation: putative role of intracellular zinc release. *Journal of neurochemistry,* **75,** 1878-1888.

Anderson, T. R. and Andrew, R. D. (2002) Spreading depression: imaging and blockade in the rat neocortical brain slice. *Journal of neurophysiology,* **88,** 2713-2725.

Andrade, A. L. and Rossi, D. J. (2010) Simulated ischaemia induces Ca^{2+}-independent glutamatergic vesicle release through actin filament depolymerization in area CA1 of the hippocampus. *The Journal of physiology,* **588,** 1499-1514.

Aras, M. A. and Aizenman, E. (2011) Redox regulation of intracellular zinc: molecular signaling in the life and death of neurons. *Antioxidants & redox signaling,* **15,** 2249-2263.

Aronowski, J. and Zhao, X. (2011) Molecular pathophysiology of cerebral hemorrhage: secondary brain injury. *Stroke; a journal of cerebral circulation,* **42,** 1781-1786.

Assaf, S. Y. and Chung, S. H. (1984) Release of endogenous Zn^{2+} from brain tissue during activity. *Nature,* **308,** 734-736.

Atasoy, D., Ertunc, M., Moulder, K. L., Blackwell, J., Chung, C., Su, J. and

Kavalali, E. T. (2008) Spontaneous and evoked glutamate release activates two populations of NMDA receptors with limited overlap. *The Journal of neuroscience : the official journal of the Society for Neuroscience,* **28,** 10151-10166.

Avoli, M., Drapeau, C., Louvel, J., Pumain, R., Olivier, A. and Villemure, J. G. (1991) Epileptiform activity induced by low extracellular magnesium in the human cortex maintained in vitro. *Annals of neurology,* **30,** 589-596.

Azevedo, F. A., Carvalho, L. R., Grinberg, L. T., Farfel, J. M., Ferretti, R. E., Leite, R. E., Jacob Filho, W., Lent, R. and Herculano-Houzel, S. (2009) Equal numbers of neuronal and nonneuronal cells make the human brain an isometrically scaled-up primate brain. *The Journal of comparative neurology,* **513,** 532-541.

Balestrino, M., Young, J. and Aitken, P. (1999) Block of (Na+,K+)ATPase with ouabain induces spreading depression-like depolarization in hippocampal slices. *Brain research,* **838,** 37-44.

Bano, D., Young, K. W., Guerin, C. J., Lefeuvre, R., Rothwell, N. J., Naldini, L., Rizzuto, R., Carafoli, E. and Nicotera, P. (2005) Cleavage of the plasma membrane Na+/Ca^{2+} exchanger in excitotoxicity. *Cell,* **120,** 275-285.

Bao, X., Lee, S. C., Reuss, L. and Altenberg, G. A. (2007) Change in permeant size selectivity by phosphorylation of connexin 43 gap-junctional hemichannels by PKC. *Proceedings of the National Academy of Sciences of the United States of America,* **104,** 4919-4924.

Basarsky, T. A., Feighan, D. and MacVicar, B. A. (1999) Glutamate release through volume-activated channels during spreading depression. *The Journal of neuroscience : the official journal of the Society for Neuroscience,* **19,** 6439-6445.

Beal, M. F. (1992) Mechanisms of excitotoxicity in neurologic diseases. *FASEB journal : official publication of the Federation of American Societies for Experimental Biology,* **6,** 3338-3344.

Benveniste, H., Drejer, J., Schousboe, A. and Diemer, N. H. (1984) Elevation of the extracellular concentrations of glutamate and aspartate in rat hippocampus during transient cerebral ischemia monitored by intracerebral microdialysis. *Journal of neurochemistry,* **43,** 1369-1374.

Blatow, M., Caputi, A., Burnashev, N., Monyer, H. and Rozov, A. (2003) Ca^{2+} buffer saturation underlies paired pulse facilitation in calbindin-D28k-containing terminals. *Neuron,* **38,** 79-88.

Bonanni, L., Chachar, M., Jover-Mengual, T. et al. (2006) Zinc-dependent multi-conductance channel activity in mitochondria isolated from ischemic brain. *The Journal of neuroscience : the official journal of the Society for Neuroscience,* **26,** 6851-6862.

Bosche, B., Graf, R., Ernestus, R. I., Dohmen, C., Reithmeier, T., Brinker, G., Strong, A. J., Dreier, J. P. and Woitzik, J. (2010) Recurrent

spreading depolarizations after subarachnoid hemorrhage decreases oxygen availability in human cerebral cortex. *Annals of neurology,* **67,** 607-617.

Busija, D. W., Bari, F., Domoki, F., Horiguchi, T. and Shimizu, K. (2008) Mechanisms involved in the cerebrovascular dilator effects of cortical spreading depression. *Prog Neurobiol,* **86,** 379-395.

Calderone, A., Jover, T., Mashiko, T., Noh, K. M., Tanaka, H., Bennett, M. V. and Zukin, R. S. (2004) Late calcium EDTA rescues hippocampal CA1 neurons from global ischemia-induced death. *The Journal of neuroscience : the official journal of the Society for Neuroscience,* **24,** 9903-9913.

Carlsson, Y., Schwendimann, L., Vontell, R. et al. (2011) Genetic inhibition of caspase-2 reduces hypoxic-ischemic and excitotoxic neonatal brain injury. *Annals of neurology,* **70,** 781-789.

Carter, R. E., Aiba, I., Dietz, R. M., Sheline, C. T. and Shuttleworth, C. W. (2011) Spreading depression and related events are significant sources of neuronal Zn^{2+} release and accumulation. *Journal of cerebral blood flow and metabolism : official journal of the International Society of Cerebral Blood Flow and Metabolism,* **31,** 1073-1084.

Chatterton, J. E., Awobuluyi, M., Premkumar, L. S. et al. (2002) Excitatory glycine receptors containing the NR3 family of NMDA receptor subunits. *Nature,* **415,** 793-798.

Chen, Y. and Swanson, R. A. (2003) Astrocytes and brain injury. *Journal of cerebral blood flow and metabolism : official journal of the International Society of Cerebral Blood Flow and Metabolism,* **23,** 137-149.

Choi, D. W., Maulucci-Gedde, M. and Kriegstein, A. R. (1987) Glutamate neurotoxicity in cortical cell culture. *The Journal of neuroscience : the official journal of the Society for Neuroscience,* **7,** 357-368.

Choi, D. W. and Rothman, S. M. (1990) The role of glutamate neurotoxicity in hypoxic-ischemic neuronal death. *Annual review of neuroscience,* **13,** 171-182.

Choi, Y., Chen, H. V. and Lipton, S. A. (2001) Three pairs of cysteine residues mediate both redox and zn^{2+} modulation of the nmda receptor. *The Journal of neuroscience : the official journal of the Society for Neuroscience,* **21,** 392-400.

Chorin, E., Vinograd, O., Fleidervish, I., Gilad, D., Herrmann, S., Sekler, I., Aizenman, E. and Hershfinkel, M. (2011) Upregulation of KCC2 activity by zinc-mediated neurotransmission via the mZnR/GPR39 receptor. *The Journal of neuroscience : the official journal of the Society for Neuroscience,* **31,** 12916-12926.

Christie, J. M. and Jahr, C. E. (2008) Dendritic NMDA receptors activate axonal calcium channels. *Neuron,* **60,** 298-307.

Chung, R. S., Penkowa, M., Dittmann, J. et al. (2008) Redefining the role of metallothionein within the injured brain: extracellular

metallothioneins play an important role in the astrocyte-neuron response to injury. *The Journal of biological chemistry,* **283,** 15349-15358.

Ciabarra, A. M., Sullivan, J. M., Gahn, L. G., Pecht, G., Heinemann, S. and Sevarino, K. A. (1995) Cloning and characterization of chi-1: a developmentally regulated member of a novel class of the ionotropic glutamate receptor family. *The Journal of neuroscience : the official journal of the Society for Neuroscience,* **15,** 6498-6508.

Clarkson, A. N., Huang, B. S., Macisaac, S. E., Mody, I. and Carmichael, S. T. (2010) Reducing excessive GABA-mediated tonic inhibition promotes functional recovery after stroke. *Nature,* **468,** 305-309.

Cole, S. L. and Corday, E. (1956) Four-minute limit for cardiac resuscitation. *Journal of the American Medical Association,* **161,** 1454-1458.

Cole, T. B., Martyanova, A. and Palmiter, R. D. (2001) Removing zinc from synaptic vesicles does not impair spatial learning, memory, or sensorimotor functions in the mouse. *Brain research,* **891,** 253-265.

Cole, T. B., Robbins, C. A., Wenzel, H. J., Schwartzkroin, P. A. and Palmiter, R. D. (2000) Seizures and neuronal damage in mice lacking vesicular zinc. *Epilepsy research,* **39,** 153-169.

Cole, T. B., Wenzel, H. J., Kafer, K. E., Schwartzkroin, P. A. and Palmiter, R. D. (1999) Elimination of zinc from synaptic vesicles in the intact mouse brain by disruption of the ZnT3 gene. *Proceedings of the National Academy of Sciences of the United States of America,* **96,** 1716-1721.

Colvin, R. A., Holmes, W. R., Fontaine, C. P. and Maret, W. (2010) Cytosolic zinc buffering and muffling: their role in intracellular zinc homeostasis. *Metallomics : integrated biometal science,* **2,** 306-317.

Concannon, C. G., Tuffy, L. P., Weisova, P. et al. (2010) AMP kinase-mediated activation of the BH3-only protein Bim couples energy depletion to stress-induced apoptosis. *The Journal of cell biology,* **189,** 83-94.

Connor, J. A. and Cormier, R. J. (2000) Cumulative effects of glutamate microstimulation on Ca($^{2+}$) responses of CA1 hippocampal pyramidal neurons in slice. *Journal of neurophysiology,* **83,** 90-98.

Connor, J. A., Razani-Boroujerdi, S., Greenwood, A. C., Cormier, R. J., Petrozzino, J. J. and Lin, R. C. (1999) Reduced voltage-dependent Ca^{2+} signaling in CA1 neurons after brief ischemia in gerbils. *Journal of neurophysiology,* **81,** 299-306.

Connor, J. A., Wadman, W. J., Hockberger, P. E. and Wong, R. K. (1988) Sustained dendritic gradients of Ca^{2+} induced by excitatory amino acids in CA1 hippocampal neurons. *Science,* **240,** 649-653.

Cook, D. J., Teves, L. and Tymianski, M. (2012) Treatment of stroke with a PSD-95 inhibitor in the gyrencephalic primate brain. *Nature,* **483,** 213-217.

Czeh, G., Aitken, P. G. and Somjen, G. G. (1993) Membrane currents in CA1 pyramidal cells during spreading depression (SD) and SD-like hypoxic depolarization. *Brain research,* **632,** 195-208.

D'Ambrosio, R., Gordon, D. S. and Winn, H. R. (2002) Differential role of KIR channel and Na(+)/K(+)-pump in the regulation of extracellular K(+) in rat hippocampus. *Journal of neurophysiology,* **87,** 87-102.

Delaney, A. J., Power, J. M. and Sah, P. (2012) Ifenprodil reduces excitatory synaptic transmission by blocking presynaptic P/Q type calcium channels. *Journal of neurophysiology,* **107,** 1571-1575.

Dietz, R. M., Weiss, J. H. and Shuttleworth, C. W. (2008) Zn^{2+} influx is critical for some forms of spreading depression in brain slices. *The Journal of neuroscience : the official journal of the Society for Neuroscience,* **28,** 8014-8024.

Dirnagl, U., Iadecola, C. and Moskowitz, M. A. (1999) Pathobiology of ischaemic stroke: an integrated view. *Trends in neurosciences,* **22,** 391-397.

Doering, P., Stoltenberg, M., Penkowa, M., Rungby, J., Larsen, A. and Danscher, G. (2010) Chemical blocking of zinc ions in CNS increases neuronal damage following traumatic brain injury (TBI) in mice. *PloS one,* **5,** e10131.

Dohmen, C., Sakowitz, O. W., Fabricius, M. et al. (2008) Spreading depolarizations occur in human ischemic stroke with high incidence. *Annals of neurology,* **63,** 720-728.

Dominguez, M. I., Blasco-Ibanez, J. M., Crespo, C., Marques-Mari, A. I. and Martinez-Guijarro, F. J. (2003) Zinc chelation during non-lesioning overexcitation results in neuronal death in the mouse hippocampus. *Neuroscience,* **116,** 791-806.

D'Orsi, B., Bonner, H., Tuffy, L. P., Dussmann, H., Woods, I., Courtney, M. J., Ward, M. W. and Prehn, J. H. (2012) Calpains are downstream effectors of bax-dependent excitotoxic apoptosis. *The Journal of neuroscience : the official journal of the Society for Neuroscience,* **32,** 1847-1858.

Dreier, J. P. (2011) The role of spreading depression, spreading depolarization and spreading ischemia in neurological disease. *Nat Med,* **17,** 439-447.

Dreier, J. P., Korner, K., Ebert, N. et al. (1998) Nitric oxide scavenging by hemoglobin or nitric oxide synthase inhibition by N-nitro-L-arginine induces cortical spreading ischemia when K+ is increased in the subarachnoid space. *Journal of cerebral blood flow and metabolism : official journal of the International Society of Cerebral Blood Flow and Metabolism,* **18,** 978-990.

Dreier, J. P., Major, S., Manning, A. et al. (2009) Cortical spreading ischaemia is a novel process involved in ischaemic damage in patients with aneurysmal subarachnoid haemorrhage. *Brain : a journal of neurology,* **132,** 1866-1881.

Dreier, J. P., Major, S., Pannek, H. W. et al. (2012) Spreading

convulsions, spreading depolarization and epileptogenesis in human cerebral cortex. *Brain : a journal of neurology,* **135,** 259-275.

Drenckhahn, C., Winkler, M. K., Major, S. et al. (2012) Correlates of spreading depolarization in human scalp electroencephalography. *Brain : a journal of neurology,* **135,** 853-868.

Eikermann-Haerter, K., Lee, J. H., Yuzawa, I. et al. (2012) Migraine mutations increase stroke vulnerability by facilitating ischemic depolarizations. *Circulation,* **125,** 335-345.

Erreger, K., Dravid, S. M., Banke, T. G., Wyllie, D. J. and Traynelis, S. F. (2005) Subunit-specific gating controls rat NR1/NR2A and NR1/NR2B NMDA channel kinetics and synaptic signalling profiles. *The Journal of physiology,* **563,** 345-358.

Escartin, C. and Bonvento, G. (2008) Targeted activation of astrocytes: a potential neuroprotective strategy. *Molecular neurobiology,* **38,** 231-241.

Fabricius, M., Fuhr, S., Bhatia, R., Boutelle, M., Hashemi, P., Strong, A. J. and Lauritzen, M. (2006) Cortical spreading depression and peri-infarct depolarization in acutely injured human cerebral cortex. *Brain : a journal of neurology,* **129,** 778-790.

Fabricius, M., Jensen, L. H. and Lauritzen, M. (1993) Microdialysis of interstitial amino acids during spreading depression and anoxic depolarization in rat neocortex. *Brain research,* **612,** 61-69.

Faden, A. I., Demediuk, P., Panter, S. S. and Vink, R. (1989) The role of excitatory amino acids and NMDA receptors in traumatic brain injury. *Science,* **244,** 798-800.

Faller, P. and Vasak, M. (1997) Distinct metal-thiolate clusters in the N-terminal domain of neuronal growth inhibitory factor. *Biochemistry,* **36,** 13341-13348.

Faria, L. C. and Mody, I. (2004) Protective effect of ifenprodil against spreading depression in the mouse entorhinal cortex. *Journal of neurophysiology,* **92,** 2610-2614.

Fernandez-Klett, F., Offenhauser, N., Dirnagl, U., Priller, J. and Lindauer, U. (2010) Pericytes in capillaries are contractile in vivo, but arterioles mediate functional hyperemia in the mouse brain. *Proceedings of the National Academy of Sciences of the United States of America,* **107,** 22290-22295.

Frederickson, C. J., Koh, J. Y. and Bush, A. I. (2005) The neurobiology of zinc in health and disease. *Nature reviews. Neuroscience,* **6,** 449-462.

Frederickson, C. J., Rampy, B. A., Reamy-Rampy, S. and Howell, G. A. (1992) Distribution of histochemically reactive zinc in the forebrain of the rat. *Journal of chemical neuroanatomy,* **5,** 521-530.

Frederickson, C. J., Suh, S. W., Koh, J. Y., Cha, Y. K., Thompson, R. B., LaBuda, C. J., Balaji, R. V. and Cuajungco, M. P. (2002) Depletion of intracellular zinc from neurons by use of an extracellular chelator

in vivo and in vitro. *The journal of histochemistry and cytochemistry : official journal of the Histochemistry Society,* **50,** 1659-1662.

Galeffi, F., Somjen, G. G., Foster, K. A. and Turner, D. A. (2011) Simultaneous monitoring of tissue PO2 and NADH fluorescence during synaptic stimulation and spreading depression reveals a transient dissociation between oxygen utilization and mitochondrial redox state in rat hippocampal slices. *Journal of cerebral blood flow and metabolism : official journal of the International Society of Cerebral Blood Flow and Metabolism,* **31,** 626-639.

Gielen, M., Siegler Retchless, B., Mony, L., Johnson, J. W. and Paoletti, P. (2009) Mechanism of differential control of NMDA receptor activity by NR2 subunits. *Nature,* **459,** 703-707.

Gill, R., Andine, P., Hillered, L., Persson, L. and Hagberg, H. (1992) The effect of MK-801 on cortical spreading depression in the penumbral zone following focal ischaemia in the rat. *Journal of cerebral blood flow and metabolism : official journal of the International Society of Cerebral Blood Flow and Metabolism,* **12,** 371-379.

Glitsch, M. and Marty, A. (1999) Presynaptic effects of NMDA in cerebellar Purkinje cells and interneurons. *The Journal of neuroscience : the official journal of the Society for Neuroscience,* **19,** 511-519.

Gniel, H. M. and Martin, R. L. (2010) Changes in membrane potential and the intracellular calcium concentration during CSD and OGD in layer V and layer II/III mouse cortical neurons. *Journal of neurophysiology,* **104,** 3203-3212.

Goldberg, W. J., Kadingo, R. M. and Barrett, J. N. (1986) Effects of ischemia-like conditions on cultured neurons: protection by low Na+, low Ca^{2+} solutions. *The Journal of neuroscience : the official journal of the Society for Neuroscience,* **6,** 3144-3151.

Gorter, J. A., Petrozzino, J. J., Aronica, E. M., Rosenbaum, D. M., Opitz, T., Bennett, M. V., Connor, J. A. and Zukin, R. S. (1997) Global ischemia induces downregulation of Glur2 mRNA and increases AMPA receptor-mediated Ca^{2+} influx in hippocampal CA1 neurons of gerbil. *The Journal of neuroscience : the official journal of the Society for Neuroscience,* **17,** 6179-6188.

Grafstein, B. (1956) Mechanism of spreading cortical depression. *Journal of neurophysiology,* **19,** 154-171.

Grenell, R. G. (1946) Central nervous system resistance; the effects of temporary arrest of cerebral circulation for periods of two to ten minutes. *Journal of neuropathology and experimental neurology,* **5,** 131-154.

Grynkiewicz, G., Poenie, M. and Tsien, R. Y. (1985) A new generation of Ca^{2+} indicators with greatly improved fluorescence properties. *The Journal of biological chemistry,* **260,** 3440-3450.

Hablitz, J. J. and Heinemann, U. (1989) Alterations in the microenvironment during spreading depression associated with epileptiform activity in the immature neocortex. *Brain research.*

Developmental brain research, **46,** 243-252.
Hacke, W., Donnan, G., Fieschi, C. et al. (2004) Association of outcome with early stroke treatment: pooled analysis of ATLANTIS, ECASS, and NINDS rt-PA stroke trials. *Lancet,* **363,** 768-774.
Haddad, S. H. and Arabi, Y. M. (2012) Critical care management of severe traumatic brain injury in adults. *Scandinavian journal of trauma, resuscitation and emergency medicine,* **20,** 12.
Hagberg, H., Lehmann, A., Sandberg, M., Nystrom, B., Jacobson, I. and Hamberger, A. (1985) Ischemia-induced shift of inhibitory and excitatory amino acids from intra- to extracellular compartments. *Journal of cerebral blood flow and metabolism : official journal of the International Society of Cerebral Blood Flow and Metabolism,* **5,** 413-419.
Hall, C. N. and Attwell, D. (2008) Assessing the physiological concentration and targets of nitric oxide in brain tissue. *The Journal of physiology,* **586,** 3597-3615.
Hall, C. N., Klein-Flugge, M. C., Howarth, C. and Attwell, D. (2012) Oxidative phosphorylation, not glycolysis, powers presynaptic and postsynaptic mechanisms underlying brain information processing. *The Journal of neuroscience : the official journal of the Society for Neuroscience,* **32,** 8940-8951.
Hamann, M., Rossi, D. J., Marie, H. and Attwell, D. (2002) Knocking out the glial glutamate transporter GLT-1 reduces glutamate uptake but does not affect hippocampal glutamate dynamics in early simulated ischaemia. *The European journal of neuroscience,* **15,** 308-314.
Hammond, C., Crepel, V., Gozlan, H. and Ben-Ari, Y. (1994) Anoxic LTP sheds light on the multiple facets of NMDA receptors. *Trends in neurosciences,* **17,** 497-503.
Hardingham, G. E. and Bading, H. (2010) Synaptic versus extrasynaptic NMDA receptor signalling: implications for neurodegenerative disorders. *Nature reviews. Neuroscience,* **11,** 682-696.
Hartings, J. A., Bullock, M. R., Okonkwo, D. O. et al. (2011) Spreading depolarisations and outcome after traumatic brain injury: a prospective observational study. *Lancet neurology,* **10,** 1058-1064.
Hartings, J. A., Rolli, M. L., Lu, X. C. and Tortella, F. C. (2003) Delayed secondary phase of peri-infarct depolarizations after focal cerebral ischemia: relation to infarct growth and neuroprotection. *The Journal of neuroscience : the official journal of the Society for Neuroscience,* **23,** 11602-11610.
Hartings, J. A., Watanabe, T., Bullock, M. R. et al. (2011) Spreading depolarizations have prolonged direct current shifts and are associated with poor outcome in brain trauma. *Brain : a journal of neurology,* **134,** 1529-1540.
Herin, G. A., Du, S. and Aizenman, E. (2001) The neuroprotective agent ebselen modifies NMDA receptor function via the redox modulatory site. *Journal of neurochemistry,* **78,** 1307-1314.

Hernandez-Caceres, J., Macias-Gonzalez, R., Brozek, G. and Bures, J. (1987) Systemic ketamine blocks cortical spreading depression but does not delay the onset of terminal anoxic depolarization in rats. *Brain research,* **437,** 360-364.

Herreras, O., Largo, C., Ibarz, J. M., Somjen, G. G. and Martin del Rio, R. (1994) Role of neuronal synchronizing mechanisms in the propagation of spreading depression in the in vivo hippocampus. *The Journal of neuroscience : the official journal of the Society for Neuroscience,* **14,** 7087-7098.

Herreras, O. and Somjen, G. G. (1993) Analysis of potential shifts associated with recurrent spreading depression and prolonged unstable spreading depression induced by microdialysis of elevated K+ in hippocampus of anesthetized rats. *Brain research,* **610,** 283-294.

Herreras, O. and Somjen, G. G. (1993) Propagation of spreading depression among dendrites and somata of the same cell population. *Brain research,* **610,** 276-282.

Hershkowitz, N., Katchman, A. N. and Veregge, S. (1993) Site of synaptic depression during hypoxia: a patch-clamp analysis. *Journal of neurophysiology,* **69,** 432-441.

Hertle, D. N., Dreier, J. P., Woitzik, J. et al. (2012) Effect of analgesics and sedatives on the occurrence of spreading depolarizations accompanying acute brain injury. *Brain : a journal of neurology*.

Heuchel, R., Radtke, F., Georgiev, O., Stark, G., Aguet, M. and Schaffner, W. (1994) The transcription factor MTF-1 is essential for basal and heavy metal-induced metallothionein gene expression. *The EMBO journal,* **13,** 2870-2875.

Homayoun, H. and Moghaddam, B. (2007) NMDA receptor hypofunction produces opposite effects on prefrontal cortex interneurons and pyramidal neurons. *The Journal of neuroscience : the official journal of the Society for Neuroscience,* **27,** 11496-11500.

Hosie, A. M., Dunne, E. L., Harvey, R. J. and Smart, T. G. (2003) Zinc-mediated inhibition of GABA(A) receptors: discrete binding sites underlie subtype specificity. *Nature neuroscience,* **6,** 362-369.

Howell, G. A., Welch, M. G. and Frederickson, C. J. (1984) Stimulation-induced uptake and release of zinc in hippocampal slices. *Nature,* **308,** 736-738.

Hoyte, L., Barber, P. A., Buchan, A. M. and Hill, M. D. (2004) The rise and fall of NMDA antagonists for ischemic stroke. *Current molecular medicine,* **4,** 131-136.

Huang, Y. Z., Pan, E., Xiong, Z. Q. and McNamara, J. O. (2008) Zinc-mediated transactivation of TrkB potentiates the hippocampal mossy fiber-CA3 pyramid synapse. *Neuron,* **57,** 546-558.

Hwang, J. J., Lee, S. J., Kim, T. Y., Cho, J. H. and Koh, J. Y. (2008) Zinc and 4-hydroxy-2-nonenal mediate lysosomal membrane permeabilization induced by H2O2 in cultured hippocampal

neurons. *The Journal of neuroscience : the official journal of the Society for Neuroscience,* **28,** 3114-3122.

Hyun, H. J., Sohn, J., Ahn, Y. H., Shin, H. C., Koh, J. Y. and Yoon, Y. H. (2000) Depletion of intracellular zinc induces macromolecule synthesis- and caspase-dependent apoptosis of cultured retinal cells. *Brain research,* **869,** 39-48.

Iijima, T., Mies, G. and Hossmann, K. A. (1992) Repeated negative DC deflections in rat cortex following middle cerebral artery occlusion are abolished by MK-801: effect on volume of ischemic injury. *Journal of cerebral blood flow and metabolism : official journal of the International Society of Cerebral Blood Flow and Metabolism,* **12,** 727-733.

Iijima, T., Shimase, C., Iwao, Y. and Sankawa, H. (1998) Relationships between glutamate release, blood flow and spreading depression: real-time monitoring using an electroenzymatic dialysis electrode. *Neuroscience research,* **32,** 201-207.

Ikonomidou, C. and Turski, L. (2002) Why did NMDA receptor antagonists fail clinical trials for stroke and traumatic brain injury? *Lancet neurology,* **1,** 383-386.

Investigators, C. A. S. P. R. C. (2005) Prioritizing interventions to improve rates of thrombolysis for ischemic stroke. *Neurology,* **64,** 654-659.

Izumi, Y., Auberson, Y. P. and Zorumski, C. F. (2006) Zinc modulates bidirectional hippocampal plasticity by effects on NMDA receptors. *The Journal of neuroscience : the official journal of the Society for Neuroscience,* **26,** 7181-7188.

Jaiswal, B. S. and Conti, M. (2003) Calcium regulation of the soluble adenylyl cyclase expressed in mammalian spermatozoa. *Proceedings of the National Academy of Sciences of the United States of America,* **100,** 10676-10681.

Jarvis, C. R., Anderson, T. R. and Andrew, R. D. (2001) Anoxic depolarization mediates acute damage independent of glutamate in neocortical brain slices. *Cereb Cortex,* **11,** 249-259.

Jarvis, C. R., Lilge, L., Vipond, G. J. and Andrew, R. D. (1999) Interpretation of intrinsic optical signals and calcein fluorescence during acute excitotoxic insult in the hippocampal slice. *NeuroImage,* **10,** 357-372.

Jia, Y., Jeng, J. M., Sensi, S. L. and Weiss, J. H. (2002) Zn^{2+} currents are mediated by calcium-permeable AMPA/kainate channels in cultured murine hippocampal neurones. *The Journal of physiology,* **543,** 35-48.

Jiang, D., Sullivan, P. G., Sensi, S. L., Steward, O. and Weiss, J. H. (2001) $Zn(^{2+})$ induces permeability transition pore opening and release of pro-apoptotic peptides from neuronal mitochondria. *The Journal of biological chemistry,* **276,** 47524-47529.

Jiang, L. J., Maret, W. and Vallee, B. L. (1998) The ATP-metallothionein complex. *Proceedings of the National Academy of Sciences of the*

United States of America, **95,** 9146-9149.

Jorgensen, P. L. and Pedersen, P. A. (2001) Structure-function relationships of Na(+), K(+), ATP, or $Mg^{(2+)}$ binding and energy transduction in Na,K-ATPase. *Biochimica et biophysica acta,* **1505,** 57-74.

Joshi, I. and Andrew, R. D. (2001) Imaging anoxic depolarization during ischemia-like conditions in the mouse hemi-brain slice. *Journal of neurophysiology,* **85,** 414-424.

Kasarskis, E. J. (1984) Zinc metabolism in normal and zinc-deficient rat brain. *Experimental neurology,* **85,** 114-127.

Katchman, A. N. and Hershkowitz, N. (1993) Early anoxia-induced vesicular glutamate release results from mobilization of calcium from intracellular stores. *Journal of neurophysiology,* **70,** 1-7.

Kerchner, G. A. and Nicoll, R. A. (2008) Silent synapses and the emergence of a postsynaptic mechanism for LTP. *Nature reviews. Neuroscience,* **9,** 813-825.

Kitamura, Y., Iida, Y., Abe, J. et al. (2006) Protective effect of zinc against ischemic neuronal injury in a middle cerebral artery occlusion model. *Journal of pharmacological sciences,* **100,** 142-148.

Koh, J. Y. (2001) Zinc and disease of the brain. *Molecular neurobiology,* **24,** 99-106.

Koh, J. Y. and Choi, D. W. (1988) Zinc alters excitatory amino acid neurotoxicity on cortical neurons. *The Journal of neuroscience : the official journal of the Society for Neuroscience,* **8,** 2164-2171.

Koh, J. Y., Suh, S. W., Gwag, B. J., He, Y. Y., Hsu, C. Y. and Choi, D. W. (1996) The role of zinc in selective neuronal death after transient global cerebral ischemia. *Science,* **272,** 1013-1016.

Kohout, S. C., Corbalan-Garcia, S., Torrecillas, A., Gomez-Fernandez, J. C. and Falke, J. J. (2002) C2 domains of protein kinase C isoforms alpha, beta, and gamma: activation parameters and calcium stoichiometries of the membrane-bound state. *Biochemistry,* **41,** 11411-11424.

Kohr, G., Eckardt, S., Luddens, H., Monyer, H. and Seeburg, P. H. (1994) NMDA receptor channels: subunit-specific potentiation by reducing agents. *Neuron,* **12,** 1031-1040.

Koumura, A., Kakefuda, K., Honda, A. et al. (2009) Metallothionein-3 deficient mice exhibit abnormalities of psychological behaviors. *Neuroscience letters,* **467,** 11-14.

Krezel, A. and Maret, W. (2007) Dual nanomolar and picomolar Zn(II) binding properties of metallothionein. *Journal of the American Chemical Society,* **129,** 10911-10921.

Kruger, H., Heinemann, U. and Luhmann, H. J. (1999) Effects of ionotropic glutamate receptor blockade and 5-HT1A receptor activation on spreading depression in rat neocortical slices. *Neuroreport,* **10,** 2651-2656.

Kunkler, P. E. and Kraig, R. P. (2004) P/Q Ca^{2+} channel blockade stops

spreading depression and related pyramidal neuronal Ca^{2+} rise in hippocampal organ culture. *Hippocampus,* **14,** 356-367.

Langmade, S. J., Ravindra, R., Daniels, P. J. and Andrews, G. K. (2000) The transcription factor MTF-1 mediates metal regulation of the mouse ZnT1 gene. *The Journal of biological chemistry,* **275,** 34803-34809.

Larrosa, B., Pastor, J., Lopez-Aguado, L. and Herreras, O. (2006) A role for glutamate and glia in the fast network oscillations preceding spreading depression. *Neuroscience,* **141,** 1057-1068.

Larsen, R. S., Corlew, R. J., Henson, M. A. et al. (2011) NR3A-containing NMDARs promote neurotransmitter release and spike timing-dependent plasticity. *Nature neuroscience,* **14,** 338-344.

Lauritzen, M., Dreier, J. P., Fabricius, M., Hartings, J. A., Graf, R. and Strong, A. J. (2011) Clinical relevance of cortical spreading depression in neurological disorders: migraine, malignant stroke, subarachnoid and intracranial hemorrhage, and traumatic brain injury. *Journal of cerebral blood flow and metabolism : official journal of the International Society of Cerebral Blood Flow and Metabolism,* **31,** 17-35.

Lauritzen, M. and Hansen, A. J. (1992) The effect of glutamate receptor blockade on anoxic depolarization and cortical spreading depression. *Journal of cerebral blood flow and metabolism : official journal of the International Society of Cerebral Blood Flow and Metabolism,* **12,** 223-229.

Lavoie, N., Peralta, M. R., 3rd, Chiasson, M., Lafortune, K., Pellegrini, L., Seress, L. and Toth, K. (2007) Extracellular chelation of zinc does not affect hippocampal excitability and seizure-induced cell death in rats. *The Journal of physiology,* **578,** 275-289.

Leao (1944) Spreading depression of activity in the cerebral cortex. *Journal of Neurophysiology,* **7,** 359–390.

Lee, J. M., Zipfel, G. J., Park, K. H., He, Y. Y., Hsu, C. Y. and Choi, D. W. (2002) Zinc translocation accelerates infarction after mild transient focal ischemia. *Neuroscience,* **115,** 871-878.

Lee, J. Y., Cole, T. B., Palmiter, R. D. and Koh, J. Y. (2000) Accumulation of zinc in degenerating hippocampal neurons of ZnT3-null mice after seizures: evidence against synaptic vesicle origin. *The Journal of neuroscience : the official journal of the Society for Neuroscience,* **20,** RC79.

Lee, J. Y., Kim, J. S., Byun, H. R., Palmiter, R. D. and Koh, J. Y. (2011) Dependence of the histofluorescently reactive zinc pool on zinc transporter-3 in the normal brain. *Brain research,* **1418,** 12-22.

Leonard, W. R., Snodgrass, J. J. and Robertson, M. L. (2007) Effects of brain evolution on human nutrition and metabolism. *Annual review of nutrition,* **27,** 311-327.

Li, J., Henman, M. C., Doyle, K. M., Strbian, D., Kirby, B. P., Tatlisumak, T. and Shaw, G. G. (2004) The pre-ischaemic neuroprotective

effect of a novel polyamine antagonist, N1-dansyl-spermine in a permanent focal cerebral ischaemia model in mice. *Brain research,* **1029,** 84-92.

Li, Y., Hough, C. J., Frederickson, C. J. and Sarvey, J. M. (2001) Induction of mossy fiber --> Ca3 long-term potentiation requires translocation of synaptically released Zn^{2+}. *The Journal of neuroscience : the official journal of the Society for Neuroscience,* **21,** 8015-8025.

Lindquist, B. S. and Shuttleworth, C. W. (2011) Adenosine activation of A_1 receptors depresses synaptic activity after spreading depolarization *Annual meeting of Society for Neuroscience abstract*.

Lipton, S. A. (2006) Paradigm shift in neuroprotection by NMDA receptor blockade: memantine and beyond. *Nature reviews. Drug discovery,* **5,** 160-170.

Liu, L., Wong, T. P., Pozza, M. F., Lingenhoehl, K., Wang, Y., Sheng, M., Auberson, Y. P. and Wang, Y. T. (2004) Role of NMDA receptor subtypes in governing the direction of hippocampal synaptic plasticity. *Science,* **304,** 1021-1024.

Liu, L. Y., Wei, E. Q., Zhao, Y. M., Chen, F. X., Wang, M. L., Zhang, W. P. and Chen, Z. (2005) Protective effects of baicalin on oxygen/glucose deprivation- and NMDA-induced injuries in rat hippocampal slices. *The Journal of pharmacy and pharmacology,* **57,** 1019-1026.

Liu, S. J. and Zukin, R. S. (2007) Ca^{2+}-permeable AMPA receptors in synaptic plasticity and neuronal death. *Trends in neurosciences,* **30,** 126-134.

Lo, E. H. (2008) A new penumbra: transitioning from injury into repair after stroke. *Nat Med,* **14,** 497-500.

Lu, X. C., Williams, A. J., Wagstaff, J. D., Tortella, F. C. and Hartings, J. A. (2005) Effects of delayed intrathecal infusion of an NMDA receptor antagonist on ischemic injury and peri-infarct depolarizations. *Brain research,* **1056,** 200-208.

MacDonald, J. F., Bartlett, M. C., Mody, I., Pahapill, P., Reynolds, J. N., Salter, M. W., Schneiderman, J. H. and Pennefather, P. S. (1991) Actions of ketamine, phencyclidine and MK-801 on NMDA receptor currents in cultured mouse hippocampal neurones. *The Journal of physiology,* **432,** 483-508.

Maclean, D. M. and Bowie, D. (2011) Transmembrane AMPA receptor regulatory protein regulation of competitive antagonism: a problem of interpretation. *The Journal of physiology,* **589,** 5383-5390.

Maclean, K. H., Cleveland, J. L. and Porter, J. B. (2001) Cellular zinc content is a major determinant of iron chelator-induced apoptosis of thymocytes. *Blood,* **98,** 3831-3839.

Manev, H., Favaron, M., Guidotti, A. and Costa, E. (1989) Delayed increase of Ca^{2+} influx elicited by glutamate: role in neuronal death. *Molecular pharmacology,* **36,** 106-112.

Manzerra, P., Behrens, M. M., Canzoniero, L. M., Wang, X. Q., Heidinger,

V., Ichinose, T., Yu, S. P. and Choi, D. W. (2001) Zinc induces a Src family kinase-mediated up-regulation of NMDA receptor activity and excitotoxicity. *Proceedings of the National Academy of Sciences of the United States of America,* **98,** 11055-11061.

Marrannes, R., Willems, R., De Prins, E. and Wauquier, A. (1988) Evidence for a role of the N-methyl-D-aspartate (NMDA) receptor in cortical spreading depression in the rat. *Brain research,* **457,** 226-240.

Martel, M. A., Ryan, T. J., Bell, K. F. et al. (2012) The subtype of GluN2 C-terminal domain determines the response to excitotoxic insults. *Neuron,* **74,** 543-556.

Martins-Ferreira, H., Nedergaard, M. and Nicholson, C. (2000) Perspectives on spreading depression. *Brain research. Brain research reviews,* **32,** 215-234.

McGuinness, L., Taylor, C., Taylor, R. D. et al. (2010) Presynaptic NMDARs in the hippocampus facilitate transmitter release at theta frequency. *Neuron,* **68,** 1109-1127.

McGuinness, L., Taylor, C., Taylor, R. D. et al. (2011) Presynaptic NMDARs in the hippocampus facilitate transmitter release at theta frequency. *Neuron,* **68,** 1109-1127.

Medvedeva, Y. V., Lin, B., Shuttleworth, C. W. and Weiss, J. H. (2009) Intracellular Zn^{2+} accumulation contributes to synaptic failure, mitochondrial depolarization, and cell death in an acute slice oxygen-glucose deprivation model of ischemia. *The Journal of neuroscience : the official journal of the Society for Neuroscience,* **29,** 1105-1114.

Mies, G. and Paschen, W. (1984) Regional changes of blood flow, glucose, and ATP content determined on brain sections during a single passage of spreading depression in rat brain cortex. *Experimental neurology,* **84,** 249-258.

Mody, I., Lambert, J. D. and Heinemann, U. (1987) Low extracellular magnesium induces epileptiform activity and spreading depression in rat hippocampal slices. *Journal of neurophysiology,* **57,** 869-888.

Moleirinho, A., Carneiro, J., Matthiesen, R., Silva, R. M., Amorim, A. and Azevedo, L. (2011) Gains, losses and changes of function after gene duplication: study of the metallothionein family. *PloS one,* **6,** e18487.

Moss, S. J. and Smart, T. G. (2001) Constructing inhibitory synapses. *Nature reviews. Neuroscience,* **2,** 240-250.

Murai, Y., Okabe, Y. and Tanaka, E. (2012) Activation of protein kinase A and C prevents recovery from persistent depolarization produced by oxygen and glucose deprivation in rat hippocampal neurons. *Journal of neurophysiology,* **107,** 2517-2525.

Murphy, T. H. and Corbett, D. (2009) Plasticity during stroke recovery: from synapse to behaviour. *Nature reviews. Neuroscience,* **10,** 861-872.

Murphy, T. H., Li, P., Betts, K. and Liu, R. (2008) Two-photon imaging of stroke onset in vivo reveals that NMDA-receptor independent ischemic depolarization is the major cause of rapid reversible damage to dendrites and spines. *The Journal of neuroscience : the official journal of the Society for Neuroscience,* **28,** 1756-1772.

Murray, J. B. (2002) Phencyclidine (PCP): a dangerous drug, but useful in schizophrenia research. *The Journal of psychology,* **136,** 319-327.

Nakamura, H., Strong, A. J., Dohmen, C. et al. (2010) Spreading depolarizations cycle around and enlarge focal ischaemic brain lesions. *Brain : a journal of neurology,* **133,** 1994-2006.

Ndubuizu, O. and LaManna, J. C. (2007) Brain tissue oxygen concentration measurements. *Antioxidants & redox signaling,* **9,** 1207-1219.

Nedergaard, M. and Hansen, A. J. (1993) Characterization of cortical depolarizations evoked in focal cerebral ischemia. *Journal of cerebral blood flow and metabolism : official journal of the International Society of Cerebral Blood Flow and Metabolism,* **13,** 568-574.

Neher, E. (1995) The use of fura-2 for estimating Ca buffers and Ca fluxes. *Neuropharmacology,* **34,** 1423-1442.

Nicoll, R. A., Tomita, S. and Bredt, D. S. (2006) Auxiliary subunits assist AMPA-type glutamate receptors. *Science,* **311,** 1253-1256.

Nikam, S. S. and Meltzer, L. T. (2002) NR2B selective NMDA receptor antagonists. *Current pharmaceutical design,* **8,** 845-855.

Ohta, K., Graf, R., Rosner, G. and Heiss, W. D. (2001) Calcium ion transients in peri-infarct depolarizations may deteriorate ion homeostasis and expand infarction in focal cerebral ischemia in cats. *Stroke; a journal of cerebral circulation,* **32,** 535-543.

Oliveira-Ferreira, A. I., Milakara, D., Alam, M. et al. (2010) Experimental and preliminary clinical evidence of an ischemic zone with prolonged negative DC shifts surrounded by a normally perfused tissue belt with persistent electrocorticographic depression. *Journal of cerebral blood flow and metabolism : official journal of the International Society of Cerebral Blood Flow and Metabolism,* **30,** 1504-1519.

Olney, J. W. (1969) Brain lesions, obesity, and other disturbances in mice treated with monosodium glutamate. *Science,* **164,** 719-721.

Olney, J. W. and Sharpe, L. G. (1969) Brain lesions in an infant rhesus monkey treated with monsodium glutamate. *Science,* **166,** 386-388.

Pachernegg, S., Strutz-Seebohm, N. and Hollmann, M. (2012) GluN3 subunit-containing NMDA receptors: not just one-trick ponies. *Trends in neurosciences,* **35,** 240-249.

Palumaa, P., Tammiste, I., Kruusel, K., Kangur, L., Jornvall, H. and Sillard, R. (2005) Metal binding of metallothionein-3 versus metallothionein-2: lower affinity and higher plasticity. *Biochimica et biophysica acta,* **1747,** 205-211.

Pan, E., Zhang, X. A., Huang, Z., Krezel, A., Zhao, M., Tinberg, C. E., Lippard, S. J. and McNamara, J. O. (2011) Vesicular zinc promotes presynaptic and inhibits postsynaptic long-term potentiation of mossy fiber-CA3 synapse. *Neuron,* **71,** 1116-1126.

Paoletti, P., Ascher, P. and Neyton, J. (1997) High-affinity zinc inhibition of NMDA NR1-NR2A receptors. *The Journal of neuroscience : the official journal of the Society for Neuroscience,* **17,** 5711-5725.

Paoletti, P. and Neyton, J. (2007) NMDA receptor subunits: function and pharmacology. *Current opinion in pharmacology,* **7,** 39-47.

Paoletti, P., Vergnano, A. M., Barbour, B. and Casado, M. (2009) Zinc at glutamatergic synapses. *Neuroscience,* **158,** 126-136.

Papouin, T., Ladepeche, L., Ruel, J. et al. (2012) Synaptic and Extrasynaptic NMDA Receptors Are Gated by Different Endogenous Coagonists. *Cell,* **150,** 633-646.

Park, J. S., Bateman, M. C. and Goldberg, M. P. (1996) Rapid alterations in dendrite morphology during sublethal hypoxia or glutamate receptor activation. *Neurobiology of disease,* **3,** 215-227.

Pedarzani, P., Mosbacher, J., Rivard, A., Cingolani, L. A., Oliver, D., Stocker, M., Adelman, J. P. and Fakler, B. (2001) Control of electrical activity in central neurons by modulating the gating of small conductance Ca^{2+}-activated K+ channels. *The Journal of biological chemistry,* **276,** 9762-9769.

Peeters, M., Gunthorpe, M. J., Strijbos, P. J., Goldsmith, P., Upton, N. and James, M. F. (2007) Effects of pan- and subtype-selective N-methyl-D-aspartate receptor antagonists on cortical spreading depression in the rat: therapeutic potential for migraine. *J Pharmacol Exp Ther,* **321,** 564-572.

Perrais, D., Veran, J. and Mulle, C. (2010) Gating and permeation of kainate receptors: differences unveiled. *Trends Pharmacol Sci,* **31,** 516-522.

Petrozzino, J. J., Pozzo Miller, L. D. and Connor, J. A. (1995) Micromolar Ca^{2+} transients in dendritic spines of hippocampal pyramidal neurons in brain slice. *Neuron,* **14,** 1223-1231.

Pittenger, C., Sanacora, G. and Krystal, J. H. (2007) The NMDA receptor as a therapeutic target in major depressive disorder. *CNS & neurological disorders drug targets,* **6,** 101-115.

Pomper, J. K., Haack, S., Petzold, G. C., Buchheim, K., Gabriel, S., Hoffmann, U. and Heinemann, U. (2006) Repetitive spreading depression-like events result in cell damage in juvenile hippocampal slice cultures maintained in normoxia. *Journal of neurophysiology,* **95,** 355-368.

Pringle, A. K., Self, J., Eshak, M. and Iannotti, F. (2000) Reducing conditions significantly attenuate the neuroprotective efficacy of competitive, but not other NMDA receptor antagonists in vitro. *The European journal of neuroscience,* **12,** 3833-3842.

Qian, J. and Noebels, J. L. (2005) Visualization of transmitter release with

zinc fluorescence detection at the mouse hippocampal mossy fibre synapse. *The Journal of physiology,* **566,** 747-758.

Qian, J. and Noebels, J. L. (2006) Exocytosis of vesicular zinc reveals persistent depression of neurotransmitter release during metabotropic glutamate receptor long-term depression at the hippocampal CA3-CA1 synapse. *The Journal of neuroscience : the official journal of the Society for Neuroscience,* **26,** 6089-6095.

Qian, J., Xu, K., Yoo, J., Chen, T. T., Andrews, G. and Noebels, J. L. (2011) Knockout of Zn transporters Zip-1 and Zip-3 attenuates seizure-induced CA1 neurodegeneration. *The Journal of neuroscience : the official journal of the Society for Neuroscience,* **31,** 97-104.

Ramamurthy, S. and Ronnett, G. (2012) AMP-Activated Protein Kinase (AMPK) and Energy-Sensing in the Brain. *Experimental neurobiology,* **21,** 52-60.

Reynolds, I. J., Rush, E. A. and Aizenman, E. (1990) Reduction of NMDA receptors with dithiothreitol increases [3H]-MK-801 binding and NMDA-induced Ca^{2+} fluxes. *British journal of pharmacology,* **101,** 178-182.

Rossen, L., Kabat, H. and Anderson, J. (1943) Acute arrest of cerebral circulation in man. *Archives of Neurology and Psychiatry,* **50,** 510-528.

Rossi, D. J., Brady, J. D. and Mohr, C. (2007) Astrocyte metabolism and signaling during brain ischemia. *Nature neuroscience,* **10,** 1377-1386.

Rossi, D. J., Oshima, T. and Attwell, D. (2000) Glutamate release in severe brain ischaemia is mainly by reversed uptake. *Nature,* **403,** 316-321.

Rothman, S. (1984) Synaptic release of excitatory amino acid neurotransmitter mediates anoxic neuronal death. *The Journal of neuroscience : the official journal of the Society for Neuroscience,* **4,** 1884-1891.

Rothman, S. M. (1983) Synaptic activity mediates death of hypoxic neurons. *Science,* **220,** 536-537.

Rudkouskaya, A., Chernoguz, A., Haskew-Layton, R. E. and Mongin, A. A. (2008) Two conventional protein kinase C isoforms, alpha and beta I, are involved in the ATP-induced activation of volume-regulated anion channel and glutamate release in cultured astrocytes. *Journal of neurochemistry,* **105,** 2260-2270.

Rudolphi, K. A., Schubert, P., Parkinson, F. E. and Fredholm, B. B. (1992) Neuroprotective role of adenosine in cerebral ischaemia. *Trends Pharmacol Sci,* **13,** 439-445.

Rumschik, S. M., Nydegger, I., Zhao, J. and Kay, A. R. (2009) The interplay between inorganic phosphate and amino acids determines zinc solubility in brain slices. *Journal of neurochemistry,* **108,** 1300-1308.

Sakowitz, O. W., Kiening, K. L., Krajewski, K. L., Sarrafzadeh, A. S., Fabricius, M., Strong, A. J., Unterberg, A. W. and Dreier, J. P. (2009) Preliminary evidence that ketamine inhibits spreading depolarizations in acute human brain injury. *Stroke; a journal of cerebral circulation,* **40,** e519-522.

Sanchez, R. M., Wang, C., Gardner, G., Orlando, L., Tauck, D. L., Rosenberg, P. A., Aizenman, E. and Jensen, F. E. (2000) Novel role for the NMDA receptor redox modulatory site in the pathophysiology of seizures. *The Journal of neuroscience : the official journal of the Society for Neuroscience,* **20,** 2409-2417.

Sara, Y., Mozhayeva, M. G., Liu, X. and Kavalali, E. T. (2002) Fast vesicle recycling supports neurotransmission during sustained stimulation at hippocampal synapses. *The Journal of neuroscience : the official journal of the Society for Neuroscience,* **22,** 1608-1617.

Sebastiao, A. M., de Mendonca, A., Moreira, T. and Ribeiro, J. A. (2001) Activation of synaptic NMDA receptors by action potential-dependent release of transmitter during hypoxia impairs recovery of synaptic transmission on reoxygenation. *The Journal of neuroscience : the official journal of the Society for Neuroscience,* **21,** 8564-8571.

Sensi, S. L., Paoletti, P., Bush, A. I. and Sekler, I. (2009) Zinc in the physiology and pathology of the CNS. *Nature reviews. Neuroscience,* **10,** 780-791.

Setyawan, J., Koide, K., Diller, T. C., Bunnage, M. E., Taylor, S. S., Nicolaou, K. C. and Brunton, L. L. (1999) Inhibition of protein kinases by balanol: specificity within the serine/threonine protein kinase subfamily. *Molecular pharmacology,* **56,** 370-376.

Sheline, C. T., Behrens, M. M. and Choi, D. W. (2000) Zinc-induced cortical neuronal death: contribution of energy failure attributable to loss of NAD(+) and inhibition of glycolysis. *The Journal of neuroscience : the official journal of the Society for Neuroscience,* **20,** 3139-3146.

Shin, H. K., Dunn, A. K., Jones, P. B., Boas, D. A., Moskowitz, M. A. and Ayata, C. (2006) Vasoconstrictive neurovascular coupling during focal ischemic depolarizations. *Journal of cerebral blood flow and metabolism : official journal of the International Society of Cerebral Blood Flow and Metabolism,* **26,** 1018-1030.

Shuttleworth, C. W. and Connor, J. A. (2001) Strain-dependent differences in calcium signaling predict excitotoxicity in murine hippocampal neurons. *The Journal of neuroscience : the official journal of the Society for Neuroscience,* **21,** 4225-4236.

Shuttleworth, C. W., Greenwood, A. C. and Connor, J. A. (2000) Ca^{2+} signaling in gerbil CA3 hippocampal neurons following transient in vivo ischemia. *Neuroscience letters,* **286,** 75-78.

Sibarov, D. A., Bolshakov, A. E., Abushik, P. A., Krivoi, II and Antonov, S. M. (2012) The Na+,K+-ATPase Functionally Interacts with the

Plasma Membrane Na+,Ca^{2+}-Exchanger to Prevent Ca^{2+} Overload and Neuronal Apoptosis in Excitotoxic Stress. *J Pharmacol Exp Ther*.

Simon, R. P., Swan, J. H., Griffiths, T. and Meldrum, B. S. (1984) Blockade of N-methyl-D-aspartate receptors may protect against ischemic damage in the brain. *Science,* **226,** 850-852.

Sinner, B. and Graf, B. M. (2008) Ketamine. *Handbook of experimental pharmacology***,** 313-333.

Smart, T. G., Hosie, A. M. and Miller, P. S. (2004) Zn^{2+} ions: modulators of excitatory and inhibitory synaptic activity. *The Neuroscientist : a review journal bringing neurobiology, neurology and psychiatry,* **10,** 432-442.

Somjen, G. G. (2001) Mechanisms of spreading depression and hypoxic spreading depression-like depolarization. *Physiol Rev,* **81,** 1065-1096.

Somjen, G. G. (2002) Ion regulation in the brain: implications for pathophysiology. *The Neuroscientist : a review journal bringing neurobiology, neurology and psychiatry,* **8,** 254-267.

Spruston, N., Jonas, P. and Sakmann, B. (1995) Dendritic glutamate receptor channels in rat hippocampal CA3 and CA1 pyramidal neurons. *The Journal of physiology,* **482 (Pt 2),** 325-352.

Stark, D. T. and Bazan, N. G. (2011) Synaptic and extrasynaptic NMDA receptors differentially modulate neuronal cyclooxygenase-2 function, lipid peroxidation, and neuroprotection. *The Journal of neuroscience : the official journal of the Society for Neuroscience,* **31,** 13710-13721.

Stemer, A. and Lyden, P. (2010) Evolution of the thrombolytic treatment window for acute ischemic stroke. *Current neurology and neuroscience reports,* **10,** 29-33.

Straub, C., Hunt, D. L., Yamasaki, M., Kim, K. S., Watanabe, M., Castillo, P. E. and Tomita, S. (2011) Distinct functions of kainate receptors in the brain are determined by the auxiliary subunit Neto1. *Nature neuroscience,* **14,** 866-873.

Strong, A. J., Fabricius, M., Boutelle, M. G., Hibbins, S. J., Hopwood, S. E., Jones, R., Parkin, M. C. and Lauritzen, M. (2002) Spreading and synchronous depressions of cortical activity in acutely injured human brain. *Stroke; a journal of cerebral circulation,* **33,** 2738-2743.

Strong, A. J., Hartings, J. A. and Dreier, J. P. (2007) Cortical spreading depression: an adverse but treatable factor in intensive care? *Current opinion in critical care,* **13,** 126-133.

Strong, A. J. and Macdonald, R. L. (2012) Cortical spreading ischemia in the absence of proximal vasospasm after aneurysmal subarachnoid hemorrhage: evidence for a dual mechanism of delayed cerebral ischemia. *Journal of cerebral blood flow and metabolism : official journal of the International Society of Cerebral Blood Flow and*

Metabolism, **32,** 201-202.
Strong, A. J., Smith, S. E., Whittington, D. J., Meldrum, B. S., Parsons, A. A., Krupinski, J., Hunter, A. J., Patel, S. and Robertson, C. (2000) Factors influencing the frequency of fluorescence transients as markers of peri-infarct depolarizations in focal cerebral ischemia. *Stroke; a journal of cerebral circulation,* **31,** 214-222.
Suh, S. W. (2009) Detection of zinc translocation into apical dendrite of CA1 pyramidal neuron after electrical stimulation. *Journal of neuroscience methods,* **177,** 1-13.
Sun, H. S., Feng, Z. P., Miki, T., Seino, S. and French, R. J. (2006) Enhanced neuronal damage after ischemic insults in mice lacking Kir6.2-containing ATP-sensitive K+ channels. *Journal of neurophysiology,* **95,** 2590-2601.
Sykova, E. and Nicholson, C. (2008) Diffusion in brain extracellular space. *Physiol Rev,* **88,** 1277-1340.
Takahashi, H., Shin, Y., Cho, S. J. et al. (2007) Hypoxia enhances S-nitrosylation-mediated NMDA receptor inhibition via a thiol oxygen sensor motif. *Neuron,* **53,** 53-64.
Takamatsu, H., Kondo, K., Ikeda, Y. and Umemura, K. (1998) Neuroprotective effects depend on the model of focal ischemia following middle cerebral artery occlusion. *European journal of pharmacology,* **362,** 137-142.
Takano, T., Tian, G. F., Peng, W., Lou, N., Lovatt, D., Hansen, A. J., Kasischke, K. A. and Nedergaard, M. (2007) Cortical spreading depression causes and coincides with tissue hypoxia. *Nature neuroscience,* **10,** 754-762.
Takeda, A., Hirate, M., Tamano, H., Nisibaba, D. and Oku, N. (2003) Susceptibility to kainate-induced seizures under dietary zinc deficiency. *Journal of neurochemistry,* **85,** 1575-1580.
Takeda, Y., Zhao, L., Jacewicz, M., Pulsinelli, W. A. and Nowak, T. S., Jr. (2011) Metabolic and perfusion responses to recurrent peri-infarct depolarization during focal ischemia in the Spontaneously Hypertensive Rat: dominant contribution of sporadic CBF decrements to infarct expansion. *Journal of cerebral blood flow and metabolism : official journal of the International Society of Cerebral Blood Flow and Metabolism,* **31,** 1863-1873.
Tanaka, E., Yasumoto, S., Hattori, G., Niiyama, S., Matsuyama, S. and Higashi, H. (2001) Mechanisms underlying the depression of evoked fast EPSCs following in vitro ischemia in rat hippocampal CA1 neurons. *Journal of neurophysiology,* **86,** 1095-1103.
Tang, L. H. and Aizenman, E. (1993) Allosteric modulation of the NMDA receptor by dihydrolipoic and lipoic acid in rat cortical neurons in vitro. *Neuron,* **11,** 857-863.
Tauck, D. L. (1992) Redox modulation of NMDA receptor-mediated synaptic activity in the hippocampus. *Neuroreport,* **3,** 781-784.
Thompson, R. J., Jackson, M. F., Olah, M. E., Rungta, R. L., Hines, D. J.,

Beazely, M. A., MacDonald, J. F. and MacVicar, B. A. (2008) Activation of pannexin-1 hemichannels augments aberrant bursting in the hippocampus. *Science,* **322,** 1555-1559.

Thompson, R. J., Zhou, N. and MacVicar, B. A. (2006) Ischemia opens neuronal gap junction hemichannels. *Science,* **312,** 924-927.

Toriumi, S., Saito, T., Hosokawa, T., Takahashi, Y., Numata, T. and Kurasaki, M. (2005) Metal binding ability of metallothionein-3 expressed in Escherichia coli. *Basic & clinical pharmacology & toxicology,* **96,** 295-301.

Tottene, A., Conti, R., Fabbro, A., Vecchia, D., Shapovalova, M., Santello, M., van den Maagdenberg, A. M., Ferrari, M. D. and Pietrobon, D. (2009) Enhanced excitatory transmission at cortical synapses as the basis for facilitated spreading depression in Ca(v)2.1 knockin migraine mice. *Neuron,* **61,** 762-773.

Tsien, R. Y. (1980) New calcium indicators and buffers with high selectivity against magnesium and protons: design, synthesis, and properties of prototype structures. *Biochemistry,* **19,** 2396-2404.

Tsuda, M., Imaizumi, K., Katayama, T., Kitagawa, K., Wanaka, A., Tohyama, M. and Takagi, T. (1997) Expression of zinc transporter gene, ZnT-1, is induced after transient forebrain ischemia in the gerbil. *The Journal of neuroscience : the official journal of the Society for Neuroscience,* **17,** 6678-6684.

Tymianski, M., Charlton, M. P., Carlen, P. L. and Tator, C. H. (1993) Secondary Ca^{2+} overload indicates early neuronal injury which precedes staining with viability indicators. *Brain research,* **607,** 319-323.

Tymianski, M., Wallace, M. C., Spigelman, I., Uno, M., Carlen, P. L., Tator, C. H. and Charlton, M. P. (1993) Cell-permeant Ca^{2+} chelators reduce early excitotoxic and ischemic neuronal injury in vitro and in vivo. *Neuron,* **11,** 221-235.

Uchida, Y., Takio, K., Titani, K., Ihara, Y. and Tomonaga, M. (1991) The growth inhibitory factor that is deficient in the Alzheimer's disease brain is a 68 amino acid metallothionein-like protein. *Neuron,* **7,** 337-347.

Van Harreveld, A. (1959) Compounds in brain extracts causing spreading depression of cerebral cortical activity and contraction of crustacean muscle. *Journal of neurochemistry,* **3,** 300-315.

Van Harreveld, A. and Stamm, J. S. (1953) Spreading cortical convulsions and depressions. *Journal of neurophysiology,* **16,** 352-366.

Vance, K. M., Hansen, K. B. and Traynelis, S. F. (2012) GluN1 splice variant control of GluN1/GluN2D NMDA receptors. *The Journal of physiology*.

Vander Jagt, T. A., Connor, J. A. and Shuttleworth, C. W. (2008) Localized loss of Ca^{2+} homeostasis in neuronal dendrites is a downstream consequence of metabolic compromise during extended NMDA exposures. *The Journal of neuroscience : the official journal of the*

Society for Neuroscience, **28,** 5029-5039.
Vander Jagt, T. A., Connor, J. A., Weiss, J. H. and Shuttleworth, C. W. (2009) Intracellular Zn^{2+} increases contribute to the progression of excitotoxic Ca^{2+} increases in apical dendrites of CA1 pyramidal neurons. *Neuroscience,* **159,** 104-114.
Vergara, C., Latorre, R., Marrion, N. V. and Adelman, J. P. (1998) Calcium-activated potassium channels. *Current opinion in neurobiology,* **8,** 321-329.
Vogt, K., Mellor, J., Tong, G. and Nicoll, R. (2000) The actions of synaptically released zinc at hippocampal mossy fiber synapses. *Neuron,* **26,** 187-196.
Wadman, W. J. and Connor, J. A. (1992) Persisting modification of dendritic calcium influx by excitatory amino acid stimulation in isolated Ca1 neurons. *Neuroscience,* **48,** 293-305.
Wagner, C. A., Waldegger, S., Osswald, H., Biber, J., Murer, H., Busch, A. E. and Lang, F. (1996) Heavy metals inhibit Pi-induced currents through human brush-border NaPi-3 cotransporter in Xenopus oocytes. *The American journal of physiology,* **271,** F926-930.
Walter, S., Kostopoulos, P., Haass, A. et al. (2012) Diagnosis and treatment of patients with stroke in a mobile stroke unit versus in hospital: a randomised controlled trial. *Lancet neurology,* **11,** 397-404.
Wang, H. X. and Gao, W. J. (2012) Prolonged exposure to NMDAR antagonist induces cell-type specific changes of glutamatergic receptors in rat prefrontal cortex. *Neuropharmacology,* **62,** 1808-1822.
Wang, Y., Dong, X. X., Cao, Y., Liang, Z. Q., Han, R., Wu, J. C., Gu, Z. L. and Qin, Z. H. (2009) p53 induction contributes to excitotoxic neuronal death in rat striatum through apoptotic and autophagic mechanisms. *The European journal of neuroscience,* **30,** 2258-2270.
Weiss, J. H., Hartley, D. M., Koh, J. Y. and Choi, D. W. (1993) AMPA receptor activation potentiates zinc neurotoxicity. *Neuron,* **10,** 43-49.
Weiss, J. H. and Sensi, S. L. (2000) Ca^{2+}-Zn^{2+} permeable AMPA or kainate receptors: possible key factors in selective neurodegeneration. *Trends in neurosciences,* **23,** 365-371.
Westbrook, G. L. and Mayer, M. L. (1987) Micromolar concentrations of Zn^{2+} antagonize NMDA and GABA responses of hippocampal neurons. *Nature,* **328,** 640-643.
Woitzik, J., Dreier, J. P., Hecht, N. et al. (2012) Delayed cerebral ischemia and spreading depolarization in absence of angiographic vasospasm after subarachnoid hemorrhage. *Journal of cerebral blood flow and metabolism : official journal of the International Society of Cerebral Blood Flow and Metabolism,* **32,** 203-212.
Woitzik, J. and Schilling, L. (2007) A new method for superselective

middle cerebral artery infusion in the rat. *Journal of neurosurgery,* **106,** 872-878.

Wroge, C. M., Hogins, J., Eisenman, L. and Mennerick, S. (2012) Synaptic NMDA receptors mediate hypoxic excitotoxic death. *The Journal of neuroscience : the official journal of the Society for Neuroscience,* **32,** 6732-6742.

Xiong, Z. Q. and Stringer, J. L. (2000) Sodium pump activity, not glial spatial buffering, clears potassium after epileptiform activity induced in the dentate gyrus. *Journal of neurophysiology,* **83,** 1443-1451.

Ye, H., Jalini, S., Zhang, L., Charlton, M. and Carlen, P. L. (2010) Early ischemia enhances action potential-dependent, spontaneous glutamatergic responses in CA1 neurons. *Journal of cerebral blood flow and metabolism : official journal of the International Society of Cerebral Blood Flow and Metabolism,* **30,** 555-565.

Yu, S. P., Yeh, C., Strasser, U., Tian, M. and Choi, D. W. (1999) NMDA receptor-mediated K+ efflux and neuronal apoptosis. *Science,* **284,** 336-339.

Zeng, L. H., Xu, L., Rensing, N. R., Sinatra, P. M., Rothman, S. M. and Wong, M. (2007) Kainate seizures cause acute dendritic injury and actin depolymerization in vivo. *The Journal of neuroscience : the official journal of the Society for Neuroscience,* **27,** 11604-11613.

Zhang, H., Cao, H. J., Kimelberg, H. K. and Zhou, M. (2011) Volume regulated anion channel currents of rat hippocampal neurons and their contribution to oxygen-and-glucose deprivation induced neuronal death. *PloS one,* **6,** e16803.

Zhao, Y. J., Yang, G. Y. and Domino, E. F. (1996) Zinc protoporphyrin, zinc ion, and protoporphyrin reduce focal cerebral ischemia. *Stroke; a journal of cerebral circulation,* **27,** 2299-2303.

Zhou, N., Gordon, G. R., Feighan, D. and MacVicar, B. A. (2010) Transient swelling, acidification, and mitochondrial depolarization occurs in neurons but not astrocytes during spreading depression. *Cereb Cortex,* **20,** 2614-2624.

Zhou, N., Rungta, R. L., Feighan, D. and MacVicar, B. A. (2010) A novel form of regenerative glutamate release causes spreading depression *Annual meeting of Society for Neuroscience abstract*.